Université catholique de Louvain

Faculty of Medicine

ONE STEP TNM STAGING OF PATIENTS WITH HIGH RISK PROSTATE CANCER USING MRI

Vassiliki-Parthena Pasoglou, MD

A dissertation for the degree of Doctor of Philosophy (PhD) in Medical Sciences

February 2016

Promoter

Prof. Frédéric Lecouvet

Jury Members

Prof. Bertrand Tombal

Prof. Jean-Pascal Machiels

Prof. François Jamar

Prof. Nicolas Michoux

Prof. Laurence Annet

External Members

Prof. Catherine Cyteval

Prof. Geert Villeirs

TABLE OF CONTENTS

I. AKNOWLEDGEMENTS

First of all, I would like to express my sincere gratitude to my promoter Prof. Lecouvet for his inspirational ideas and continuous support throughout my PhD study and related research, for his patience, motivation, hard work and immense knowledge. My sincere thanks also go to my co-promoter Prof. Tombal. I am extremely thankful and indebted to him for sharing expertise and valuable guidance. I could not have imagined having better advisors and mentors for my PhD.

I place on record, my sincere thank you to Nicolas Michoux, for the continuous encouragement. His guidance helped me during all the time of research and writing of this thesis. I would also like to thank the rest of my thesis Committee Members: Prof. Machiels, Prof. Jamar, Prof. Annet, Prof. Cyteval and Prof. Villeirs for their insightful comments and encouragement, but also for their critical questions which motivated me to widen my research from various perspectives.

I am grateful to “FNRS Télévie” and the non-profit organisation “Fondation Contre le Cancer” for their - not only - financial support. It has been a great honour for me to have been given the chance to conduct my research with the support of the prestigious FRS-FNRS / Télévie Grant.

I would like to thank Prof. Vande Berg, my “maître de stage”, for giving me the opportunity to study MSK Radiology amongst the best and for the advice he has provided throughout my time as a resident. I have been extremely lucky to have had a supervisor who responded to my questions and queries so promptly.

My sincere thanks also go to all the people of the Radiology Department of Cliniques Universitaires Saint Luc. Prof. Malghem, and Prof. Maldague, Ahmed Larbi, Patrick Omoumi and Vicky Perlepe who provided me an opportunity to join their team as intern and for all the precious clinical knowledge and support. A big thank you goes to Prof. Coche, Prof. Danse, Dr. Dragean, Sandy, Xavier, Latifa Fellah, Isabelle Leconte, Mariem Sy.

Through it all I would like to express my gratitude to my friends and colleagues for the stimulating discussions, their help, their encouragement and for always being there… Ilias, Alexia, Korina,

Vassilis, Manolis, Ioanna, Florence, Julie, Audrey, Raphael, Hanan, Yousra, Marta, Thomas, Pierre. Tom, Quentin and Pascal for helping us develop the new sequence and protocol… The MRI team of our hospital… Sabine, Seb, Eric, Souad, Patrick, Frank Peeters… Francoise Martin for her help since the beginning.

I thank my friends and supervisors in CHR Citadelle de Liège. In particular, I am grateful to Dr. Tebache and Dr. Collignon for enlightening me the first glance of research and for their words of encouragement and untiring support; a big thank you to Dr. Kuta, Dr. Bostem and Dr. Rausin. I also want to thank all my new colleagues in Centre Hospitalier de Jolimont for their help, encouragement and understanding; Dr. Everarts, Dr. Goddart, Dr. Bitar, Dr Compère...

Last but not the least, I would like to thank my family, ''my safety net''. My parents-in-law George and Katerina. Chrysostomos for sharing expertise, sincere and valuable guidance throughout my life and studies and for always encouraging me. My grandmother Maria for her love. My brothers Vassilis and Philip. My mother Kyparissia for the ceaseless encouragement, support, love and attention. You were, are and always will be my inspiration. My husband Vangelis for his love, encouragement, help, patience and for always being there for me, even through the most difficult of times… I could not make it without your support. Finally I would like to thank my son Odysseas for bringing us joy and fulfilling our lives.

II. LIST OF PUBLICATIONS

- **wbMRI to detect bone metastases: critical review on diagnostic accuracy and comparison to other imaging modalities.**
  Pasoglou V, Michoux N, Tombal B, Jamar F, Lecouvet FE.
  Clin Transl Imaging (2015) 3:141–157.

- **Whole body 3D T1 MR imaging: feasibility and evaluation in metastatic screening, taking PCa as a model.**
  Pasoglou V, Michoux N, Peeters F, Larbi A, Tombal B, Selleslagh T, Omoumi P, Vande Berg BC, Lecouvet FE.
  Radiology. 2014 Dec 15:141242.

- **One-step TNM staging of high-risk prostate cancer using magnetic resonance imaging (MRI): Toward an upfront simplified "all-in-one" imaging approach?**
  Pasoglou V, Larbi A, Collette L, Annet L, Jamar F, Machiels JP, Michoux N, Vande Berg BC, Tombal B, Lecouvet FE.
  Prostate. 2014 May;74(5):469-77.

- **Novel imaging techniques reshape the landscape in high-risk prostate cancers.**
  Lecouvet FE, Lhommel R, **Pasoglou V**, Larbi A, Jamar F, Tombal B.
  Curr Opin Urol. 2013 Jul;23(4):323-30.

- **MRI for response assessment in metastatic bone disease.**
  Lecouvet FE, Larbi A, **Pasoglou V**, Omoumi P, Tombal B, Michoux N, Malghem J, Lhommel R, Vande Berg BC.
  Eur Radiol. 2013 Jul;23(7):1986-97.

III. ABBREVIATIONS

BM: Bone Metastasis

BS: Bone Scintigraphy

BVC: Best Valuable Comparator

CNR: Contrast to Noise Ratio

CT: Computed Tomography

LN: Lymph Node

LNM: Lymph Node Metastasis

mpMRI: Multiparametric MRI of the Prostate

NPV: Negative Predictive Value

PCa: Prostate cancer

PPV: Positive Predictive Value

PSA: Prostate Serum Antigen

SNR: Signal-to-Noise Ratio

TXR: Targeted XRays

WBMRI: Whole Body Magnetic Resonance Imaging

99m Tc BS: Technetium 99m bone scintigraphy

IV. ABSTRACT

WBMRI and PET-CT are emerging as powerful tools for the staging of oncologic patients. The Prostate cancer (PCa) area is no exception, with the dissemination of multiparametric prostate MRI (mpMRI) as cornerstone tool for the diagnosis, local staging, and local treatment of patients with localized disease. In contrast, the implementation of MRI in the distant staging of PCa is much slower. Even though there is compelling evidence for the low sensitivity and specificity of Technetium Bone Scanning (BS) for the detection of bone metastases (BM) and of Thoraco-Abdominal CT for the detection of lymph nodes metastases (LNM), these techniques are routinely used in - current - clinical practice. The introduction of Whole Body Diffusion Weighted MRI (WBDWI) with background body signal suppression challenges this approach.

At first, we conducted an in-depth review of the literature to evaluate the role of WBMRI in the detection of BM in oncologic patients. We effectuated a comparison of techniques that are used in the clinical practice (BS, WBMRI, PET, CT) and synthesized the results of the individual studies into an integrated review. Interestingly, we came across substantial differences between teams regarding the anatomic sequences and planes used. The need for homogenization of the WBMRI protocols relating to their anatomic component led us to the second step.

We then developed a three-dimensional (3D) WB T1 sequence, which could potentially replace the variable anatomic components of WBMRI protocols for the bone and node staging of PCa patients. This new sequence can be reconstructed in any plane, is of millimetric resolution, requires only 18 minutes to complete and demonstrates enhanced image quality, compared to the two dimensional sequences utilized until now.

Thirdly, we combined this new 3D sequence of the WB with an mpMRI of the prostate, in order to attain the complete TNM staging of PCa patients in a single step MRI protocol.

The findings of our studies are expected to aid in the improvement of clinical management of patients with PCa.

V.INTRODUCTION

A. Prostate Cancer

A.1. Incidence/ Prevalence

Prostate cancer is one of the most commonly diagnosed male tumours and is the second leading cause of death from cancer in men [1,2]. According to the American Cancer Society, PCa will affect one in five American men; there are currently more than two million men living with PCa in the United States and there is a notable global variation of PCa incidence [3]. Asian countries, especially China, have the lowest rates, while the USA, Scandinavia and Western Europe have the highest (**Figures 1** and **2**). The relative incidence of PCa in African American men is higher than in Caucasians (1.6 times higher in the USA). Regarding the lifetime risk, one in six Caucasians (17.6%) and 1 in 5 African Americans (20.6%) men will be diagnosed with PCa at some point of their lives.

Various factors such as genetic susceptibility, exposure to unknown risk factors, or differences in quality of health care and the accuracy of cancer registers can explain these differences [3]. Nevertheless, an increase in the incidence of PCa is lately observed in some Asian countries, maybe due to greater awareness [4,5].

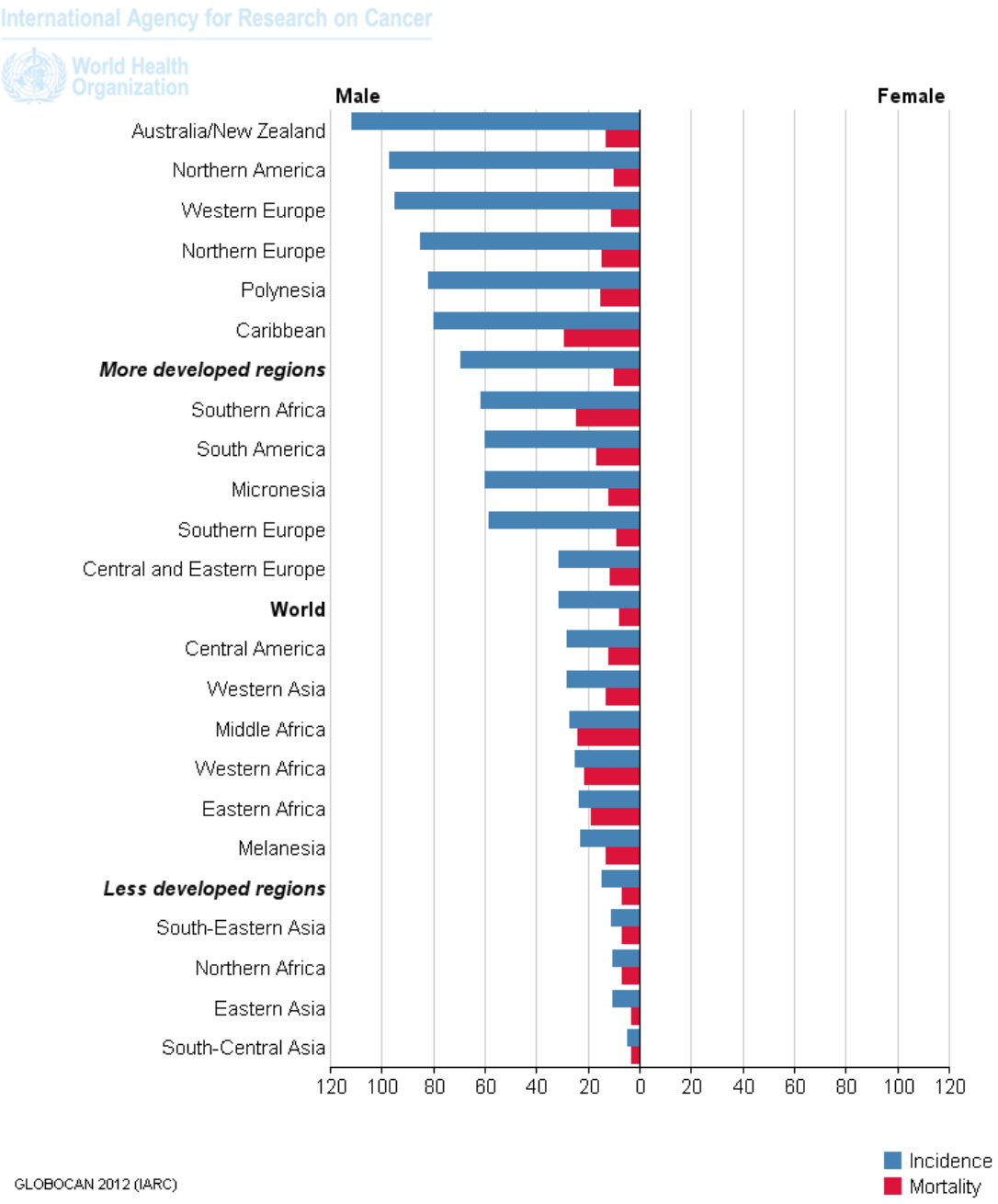

Figure 1. Bar graph of the worldwide PCa incidence. Rates are estimated as cases per 100,000 [6].

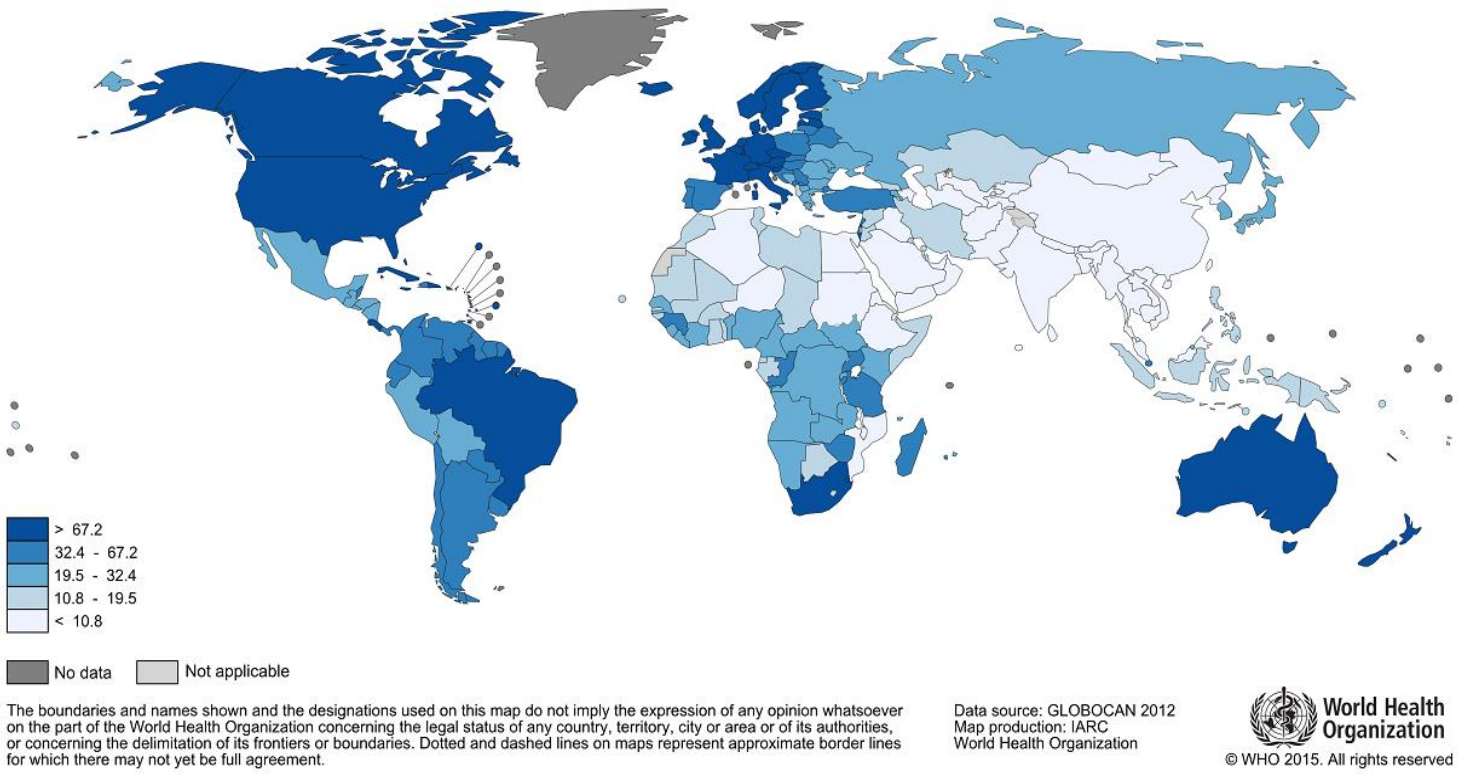

Figure 2. World map with the estimated incidence of PCa. Rates are estimated per 100,000 [6].

A.2. Mortality

According to SEER (Surveillance, Epidemiology and End Results), PCa is the fifth leading cause of death in men with an estimated 307,000 deaths in 2012 [7]. The mortality from 1987 to 1991 statistically increased. From 1991 the observed mortality rate started to decrease: first at a slow rate of 0.5% per year through 1994 and then at a more rapid decline of 4.1% per year from 1994 to 2005.

A.3. Genetics

Several highly penetrating genes associated with PCa have been identified. 10-15% of patients with PCa (white, African, or Asian) have at least one relative who is also affected. There is an increased risk for developing the disease in first-degree relatives of patients with PCa [8]. Furthermore, there is an excess risk of PCa in men with affected brothers compared to those with affected fathers, which is consistent with the hypothesis of an X-linked, or recessive, model of inheritance [9].

A.4. Symptoms

The grand majority of PCa are and will stay asymptomatic. Early PCa usually does not cause any symptoms. The appearance of symptoms is due to the local extension of the tumour. The symptoms exhibit no difference depending on the benign or malignant nature of the tumour and can include:

- Dysuria
- Haematuria
- Erectile dysfunction

Furthermore, the PCa growth can compress the urethra, invade the bladder and the ureters, causing ureterohydronephrosis. On the other hand, PCa can be detected after a complication caused by metastatic disease such as pain or pathologic fracture. Occasionally, some patients can be presented with nodal enlargement.

A.5. Screening

The aim of screening is to identify a disease at an early stage where it can be treated, in order to reduce mortality from that disease. The screening of PCa remains a source of debate and has divided the opinion of the international medical community and the regulatory bodies of the USA, Europe and the UK.

Two tests are currently widely used for the screening of PCa:

-Digital rectal examination (DRE)

-Blood PSA levels testing (>4 ng/ml).

PSA is a serine protease produced exclusively by prostatic epithelial cells [10]. It is known that blood level of PSA is elevated in men with PCa. The risk of PCa for PSA values <0.5 ng/ml is 6,6% and it increases to 26,9% for PSA values between 3.1 and 4.0 ng/ml [11]. It has to be highlighted that a number of benign conditions, such as prostatitis and benign prostate hyperplasia, can cause an increase in PSA values (and lead to false positive results).

Currently 4 ng/ml is used as the highest normal value. For men in their fifties or younger, PSA level should be lower than 2.5 ng/ml in most cases. Nevertheless, PCa, including high grade cancers, is not rare in patients with PSA <4 ng/ml. Thomson et al. demonstrated that as many as 15% of men with PSA <4 ng/ml had PCa [12] (**Table 1**). It has to be noted that various factors can cause a man's PSA level to increase, such as prostatitis and urinary tract infections, prostate biopsies and surgery.

The European Randomized Study of Screening for PCa (ERSPC) which was initiated in order to assess the effect of screening with PSA testing on death rates from PCa, concluded that PSA-based screening reduced the rate of PCa-related death by 20% [13].

PSA level, ng/ml	Risk of PCa, %
0–0.5	6.6
0.6–1	10.1
1.1–2	17.0
2.1–3	23.9
3.1–4	26.9

Table 1. Risk of PCa in patients with low PSA levels according to Thompson et al [12].

On the other hand, this testing was associated with a high risk of over-diagnosis. According to the ERSPC study, 1,410 men would have to be screened and 48 would have to be treated in order to prevent one death by PCa.

On the contrary, Andriole et al. in the first report from Prostate, Lung, Colorectal, and Ovarian (PLCO) Cancer Screening Trial on prostate-cancer mortality, reported that PCa screening provided no reduction in death rates and that there was no indication of an actual benefit [14].

A recent meta-analysis demonstrated that existing evidence from randomised controlled trials failed to show a significant impact of PCa screening on overall mortality or death from PCa [15].

It has been reported that thanks to the PCa screening there is a decrease in PCa mortality in the USA and Austria, the United Kingdom and France [16] and a reduction of the risk of being diagnosed with metastatic PCa [17].

A.6. Diagnosis

An elevated PSA level with a suspicious DRE should initiate medical investigation (**Table 2**) [18]. When an infective or inflammatory disease is suspected as the source of the abnormal PSA levels, the blood test has to be repeated after appropriate antibiotic treatment (4-6weeks).

A positive DRE in patients with a PSA level of <2 ng/ml has a PPV of 5-30% [19].

The specificity of PSA can be improved by several modifications, such as PSA density, PSA density of the transition zone, age-specific ranges and PSA molecular zones [20]. If a malignancy is suspected by the DRE, further tests are required, such as a transrectal ultrasound (TRUS) with a biopsy if necessary. An immediate biopsy should not be prompted by first time-elevated levels of PSA, except when PSA levels are >20 ng/ml after prostatitis has been excluded [20].

Only a histopathologist can confirm the diagnosis of PCa. TRUS-guided prostate biopsy is the gold standard to obtain pathological specimens for the histologic diagnosis of PCa. Random systematic sextant biopsy [21] is no longer considered adequate, although it is still superior compared to biopsies directed only at specific hypo-echoic areas. Studies have suggested that standard sextant biopsy may underestimate the incidence of cancer, with reported false-negative rates of 20-30% [22,23]. There have been several alterations of the biopsy scheme in an effort to enhance the detection rates[24,24,25] (**Figure 3**). Presti et al., demonstrated that 6 systematic biopsies of the peripheral zone are inadequate and a minimum of 8, including the apex, mid lobar mid gland, lateral mid gland and lateral base, should routinely be performed [26]. At a glandular volume of 30-40 mL, at least 8 cores should be sampled. The British Prostate Testing for Cancer and Treatment Study recommended 10 core biopsies, with >12 cores being not significantly more conclusive [27,28]. Eskew et al. introduced the “5-region” technique of prostate biopsy, in order to increase the diagnostic yield of prostate biopsy [29]. They found this technique to be safe, and superior to sextant biopsies in diagnosing PCa in patients with a PSA level of less than 10.

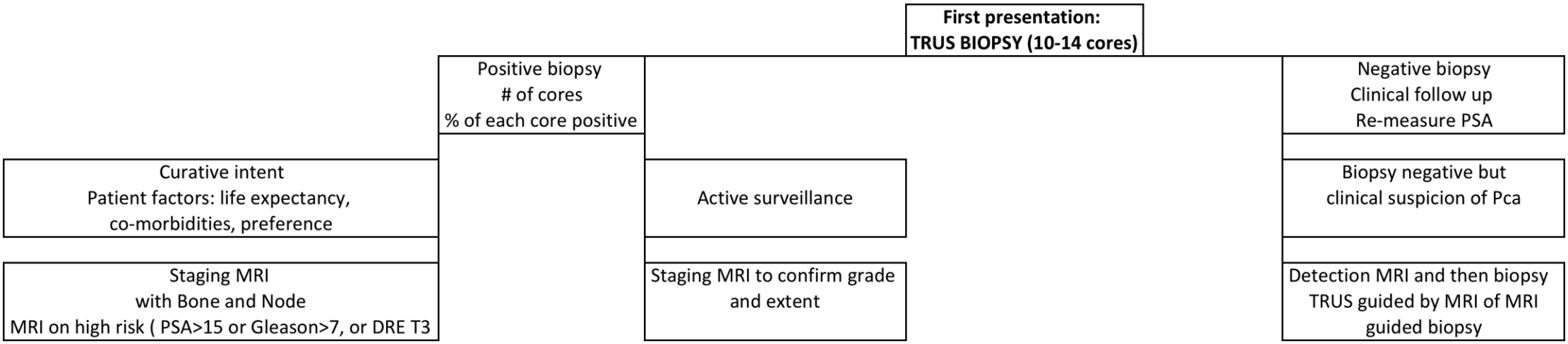

Table 2. Algorithm in imaging men referred with elevated PSA according to Barentsz et al. [18].

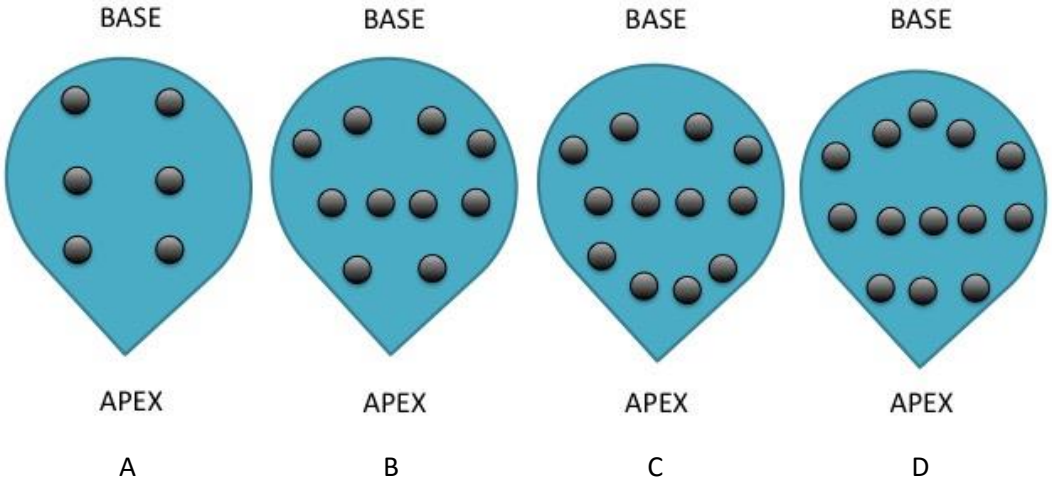

Figure 3.

A: Classic sextant biopsy scheme proposed by Hodges et al. [21]

B: The 10-core biopsy proposed by Presti et al. [26]

C: The 12-core or double sextant biopsy

D: The 13-core ''5-region biopsy'' of Eskew et al. [29]

A.7. Metastasis

The most frequent sites of metastasis in patients with PCa are LNs, bone, lung and liver [30]. Bubendorf et al., carried out 19,316 autopsies in men older than 40 years old and PCa was found in 8.2% of them [30]. Lymphatic or haematogenous metastases were seen in 39.7% of all patients, and in 65.8% in the 837 patients with clinically known cancer. Regarding distant metastases, 90.1% of patients had bone involvement, 45.7% had lung and 25% liver metastasis (**Figure 4**). 90% of the patients with BM had spine involvement.

According to Bubendorf et al., there is a strong association between lymphatic and haematogenous metastasis. Simultaneous haematogenous dissemination is significantly more frequent in tumours with para-aortic LNM than in those with pelvic LNM (88.9% v 63.9%, $P < 0.0001$).

According to the same study, the prevalence of haematogenous metastasis is associated with the grade and the local stage of the tumour.

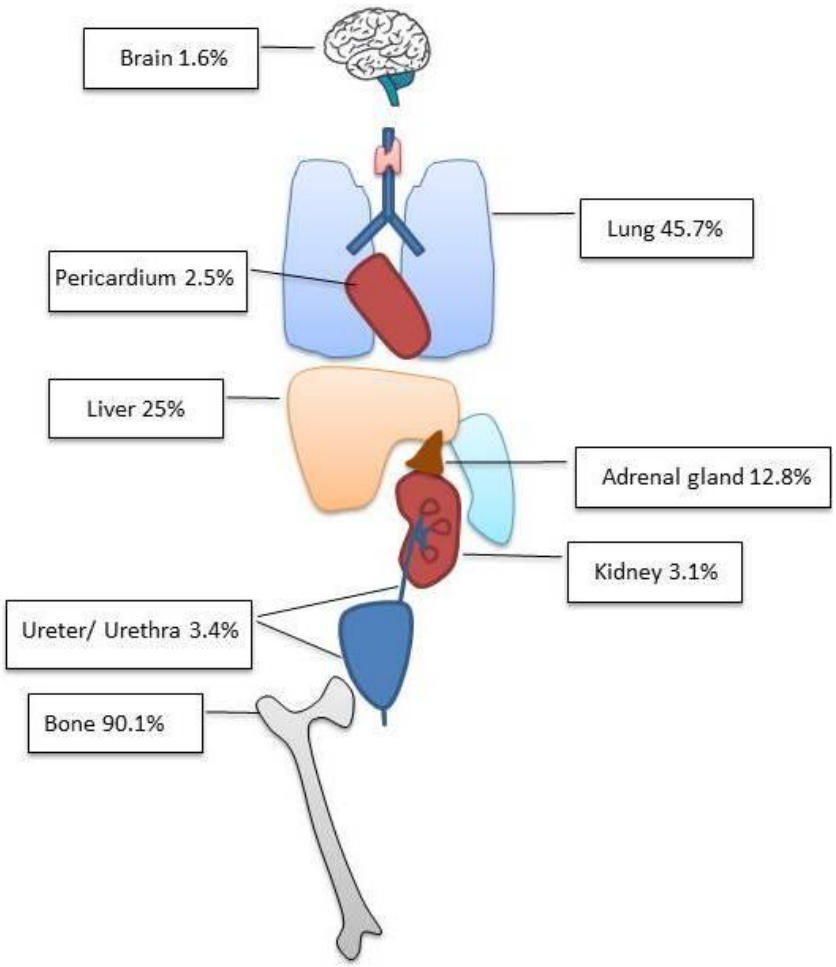

Figure 4. Distribution of haematogenous metastasis according to Bubendorf et al. (n=556 patients).

A.8. TNM (Tumour Node Metastasis) Staging

Even though there are several staging systems, the most widely used is the TNM system. For PCa, T1 refers to organ-confined tumours that are clinically and radiologically occult. T2 refers to organ-confined tumours that are clinically or radiologically apparent. T3 refers to tumours that extend outside the prostatic capsule in the form of extracapsular extension or seminal vesicle invasion. T4 refers to tumours that invade the adjacent structures. Lastly, N1 indicates the presence of locoregional LNM and M1 indicates the presence of distant metastases.

Extracapsular extension is associated with a greater risk of a positive surgical margin and decreases the possibility of long-term cancer control [31]. Seminal vesicle invasion is associated with an increased incidence of positive LNs and a poor prognosis [32].

a. Local (T)

a.1. General

Local staging (T) of PCa is based on findings from digital rectal exam and MRI (**Figure 5**). The number and sites of positive prostate biopsies, the percentage of core involvement, tumour grade, and level of serum PSA provide further information [33,34].

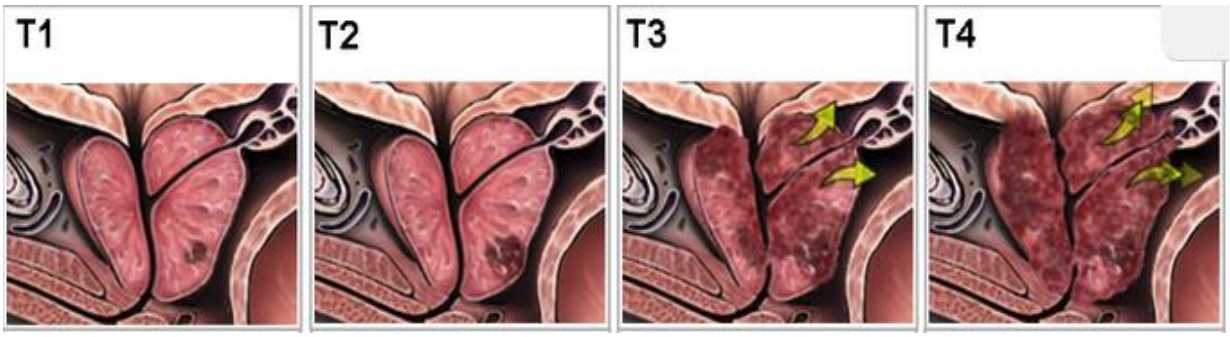

Figure 5. (www.prostatehealth.org)

TX	Primary tumour cannot be assessed
T0	No evidence of primary tumour
T1	Clinically inapparent tumour not palpable or visible by imaging
T1a	Tumour incidental histologic finding in ≤5% of tissue resected
T1b	Tumour incidental histologic finding in >5% of tissue resected
T1c	Tumour identified by needle biopsy (because of elevated prostate specific antigen [PSA] level)
T2	Tumour confined within prostate; tumours found in 1 or both lobes by needle biopsy but not palpable or reliably visible by imaging
T2a	Tumour involves one-half of 1 lobe or less
T2b	Tumour involves more than one-half of 1 lobe but not both lobes
T2c	Tumour involves both lobes
T3	Tumour extends through the prostatic capsule; invasion into the prostatic apex, or the prostatic capsule is classified not as T3 but as T2
T3a	Extracapsular extension (unilateral or bilateral)
T3b	Tumour invading seminal vesicle(s)
T4	Tumour fixed or invades adjacent structures other than seminal vesicles (e.g. bladder, levator muscles, and/or pelvic wall)

a.2. Gleason score

Donald Gleason described the "Gleason score" in 1966 and since then it is the cornerstone for the diagnosis and management of PCa. The grading is based on the histologic pattern of arrangement of the PCa cells in a haematoxylin-eosin stained section (**Figure 6**).

The overall Gleason score is calculated by adding together two Gleason grades from the performed biopsies. The grading ranges from 2 to 10 and indicates the possibility that a tumour will spread. A high Gleason score means the cancer tissue is very aggressive and the PCa is more likely to spread.

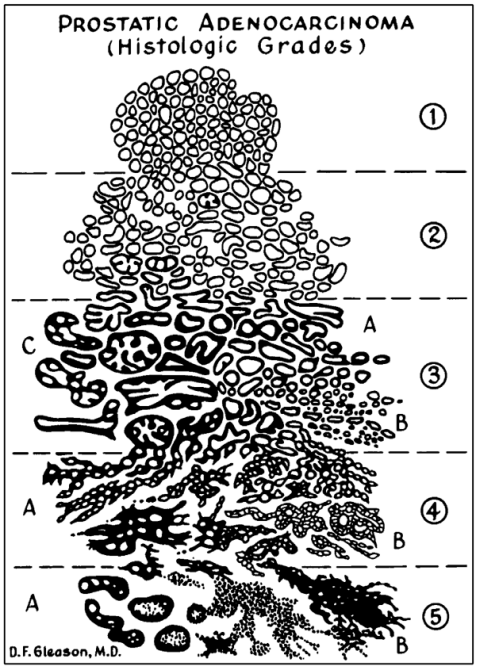

Figure 6. Gleason drawing sought to assign a number (1-5) to the differentiation of the cells in the biopsy specimen. 1: small uniform glands, 2: more stroma between glands, 3: distinctly infiltrative margins, 4: irregular masses of neoplastic glands, 5: only occasional gland formation.

a.3. Assessment of the risk

In order to assess the risk of metastasis there are many risk assessment methods including the D'Amico classification, a variety of nomograms and the UCSF-CAPRA score.

The D'Amico classification was originally developed in order to estimate the risk of biochemical recurrence after treatment for localised PCa [35]. The ability of this risk

stratification to predict disease progression and patient survival was validated in 2007 by Boorjian et al. [36].

The D'Amico classification uses PSA level, Gleason grade, and T stage in order to classify men as low-, intermediate-, or high-risk (**Table 3**).

Low Risk	Diagnostic PSA < 10 ng/ml and highest biopsy Gleason score ≤6 and clinical stage T1c or T2a
Intermediate risk	Diagnostic PSA ≥ but < 20 ng/ml or highest biopsy Gleason score =7 or clinical stage T2b
High risk	Diagnostic PSA ≥ 20ng/ml or highest biopsy Gleason score ≥8 or clinical T2c/T3

Table 3. D'Amico risk stratification for clinically localized PCa [35].

By current estimates, high-risk disease accounts for 15% of all prostate cancer diagnoses [37]. Here, it has to be highlighted that there are various definitions of high risk PCa:

American Urological Association

• Preoperative PSA >20 ng/ml, and/or preoperative Gleason score of 8–10, and/or clinical stage ≥ T2c [35,38]

European Association of Urology

• Preoperative PSA >20 ng/ml, and/or preoperative Gleason score of 8–10, and/or clinical stage ≥T3a [39]

Radiation Therapy Oncology Group

• High risk: T1–2 and Gleason 8–10, or T3 or N1 with Gleason 7

• Very high risk: T3 or N1 with Gleason 8–10 [40]

National Comprehensive Cancer Network

• High risk: Preoperative PSA >20 ng/ml, preoperative Gleason score of 8–10, or clinical stage T3a

• Very high risk: T3b–T4

Cancer of the Prostate Risk Assessment (CAPRA)

• Includes age, PSA, clinical stage, Gleason score and percentage of positive biopsy cores [41]

a.4. Prostate MRI

Although prostate MRI has been available for over 3 decades, it has not been routinely integrated into clinical care until the last few years. Nowadays, advances in MRI improve the detection and characterization of PCa by using a multiparametric approach, which combines anatomical and functional information [42]. MRI is considered as the most accurate imaging modality for the staging of PCa, even though there is an important variation in its performance [43], due to variations in technique and interpretation of the MR images.

In order to resolve this problem a group of prostate MRI experts from the European Society of Urogenital Radiology (ESUR) have developed a consensus regarding the conduct, interpretation and reporting of mpMRI, based on literature evidence and expert opinion [42]. True evidence-based guidelines were not defined, but a compromise, reflected by "minimal" and "optimal" requirements has been made. In addition to instructions regarding the MR protocols, a structured reporting system is described (PI-RADS). PI-RADS is a scoring system similar to that employed on breast imaging (BI-RADS) and it is now used in order to detect a lesion and determine the possibility that this lesion is malignant [18] (**Table 4**).

The multiparametric MRI protocol consists of high resolution T2 weighted images (T2WI) in three planes (axial, sagittal and coronal) for the analysis of the prostate's zonal anatomy and capsule, dynamic contrast-enhanced MRI (DCE MRI) for the analysis of the vascular

characteristics of the tumour, diffusion weighted imaging (DWI) and apparent diffusion coefficient (ADC) maps for the study of the cellularity and aggressiveness of the lesion and finally, magnetic resonance spectroscopic imaging (MRSI) which is able to show the lower levels of citrate and higher levels of choline in PCa compared with benign tissue. The value of MR spectroscopy is uncertain.

The assessment of PCa by MRI has certain limitations. One of the main problems is the inaccurate volume measurement [44,45, 46]. Two other disadvantages are the limited ability of MRI to distinguish tumours from other causes of hypointense T2 zones signal in the peripheral zone - such as scars or areas of prostatitis - and to detect early macroscopic capsular penetration.

Score Criteria

A1. T2WI for the peripheral zone (PZ)

1 Uniform high signal intensity (SI)
2 Linear, wedge shaped, or geographic areas of lower SI, usually not well demarcated
3 Intermediate appearances not in categories 1/2 or 4/5
4 Discrete, homogeneous low signal focus/mass confined to the prostate
5 Discrete, homogeneous low signal intensity focus with extra-capsular extension/invasive behaviour or mass effect on the capsule (bulging), or broad (>1.5 cm) contact with the surface

A2. T2WI for the transition zone (TZ)

1 Heterogeneous TZ adenoma with well-defined margins: "organised chaos"
2 Areas of more homogeneous low SI, however well marginated, originating from the TZ/BPH
3 Intermediate appearances not in categories 1/2 or 4/5
4 Areas of more homogeneous low SI, ill defined: "erased charcoal sign"
5 Same as 4, but involving the anterior fibromuscular stroma or the anterior horn of the PZ, usually lenticular or water-drop shaped.

B. Diffusion weighted imaging (DWI)

1 No reduction in ADC compared with normal glandular tissue. No increase in SI on any high b-value image (≥b800)
2 Diffuse, hyper SI on ≥b800 image with low ADC; no focal features, however, linear, triangular or geographical features are allowed
3 Intermediate appearances not in categories 1/2 or 4/5
4 Focal area(s) of reduced ADC but iso-intense SI on high b-value images (≥b800)
5 Focal area/mass of hyper SI on the high b-value images (≥b800) with reduced ADC

C. Dynamic contrast enhanced (DCE)-MRI

1 Type 1 enhancement curve
2 Type 2 enhancement curve
3 Type 3 enhancement curve

+1 For focal enhancing lesion with curve type 2–3
+1 For asymmetric lesion or lesion at an unusual place with curve type 2–3

D1. Quantitative MRS for 1.5 T. Diagram

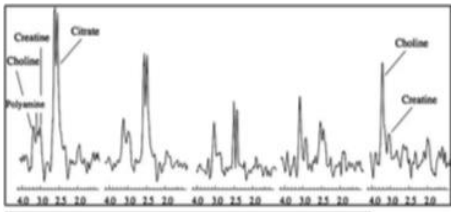

Choline + Creatine/Citrate Ratios for the Different Tissues in the Prostate on a 5-Point Scale

Rating	Peripheral Zone	Central Gland
1. Definitely benign tissue	≤0.44	≤0.52
2. Probably benign tissue	0.44–0.58	0.52–0.66
3. Possible malignant tissue	0.58–0.72	0.66–0.80
4. Probably malignant tissue	0.72–0.86	0.80–0.94
5. Definitely malignant tissue	>0.86	>0.94

D2. Qualitative magnetic resonance spectroscopic imaging (MRSI)

1 Citrate peak height exceeds choline peak height >2 times
2 Citrate peak height exceeds choline peak height times >1, <2 times
3 Choline peak height equals citrate peak height
4 Choline peak height exceeds citrate peak height >1, <2 times
5 Choline peak height exceeds citrate peak height >2 times

In qualitative analysis, the relative peak heights of citrate and choline are visually compared (pattern analysis), rather than quantified.
The criteria apply for 1.5: for at least three adjacent voxels
Score 1 0 Clinically significant disease is highly unlikely to be present Score 2 0 Clinically significant cancer is unlikely to be present
Score 3 0 Clinically significant cancer is equivocal
Score 4 0 Clinically significant cancer is likely to be present
Score 5 0 Clinically significant cancer is highly likely to be present

Table 4. PI-RADS score according to Barentsz et al. [18].

b. Distant disease

It is widely known that the most common sites of metastatic spread of PCa are LNs and bone marrow. With a high Gleason score at diagnosis or a rapid PSA progression during follow-up, guidelines recommend technetium Tc 99m BS and contrast-enhanced CT or MRI of the abdomen for the screening of BM and LM respectively.

b.1. N Staging

Accurate detection of LNM in PCa is of major significance. Patients with local disease have the options of radical prostatectomy, watchful waiting, and radiotherapy. LN disease is associated with poor prognosis and significantly decreased biochemical recurrence-free survival rates [47]. Regarding N staging:

NX	Regional lymph nodes were not assessed
N0	No regional lymph node metastasis
N1	Metastasis in regional lymph node(s)

The prostate lymphatics drain into the obturator/internal iliac, external iliac, presacral/perirectal nodes and, less frequently, into the common iliac nodes [48] (**Figure 7**). Regional LNM has been observed in 5-12% of PCa patients with clinically organ-confined cancer [47].

Cheng et al. demonstrated that the 10-year cancer-specific survival was significantly worse in PCa patients with positive LNs after pelvic lymphadenectomy [49].

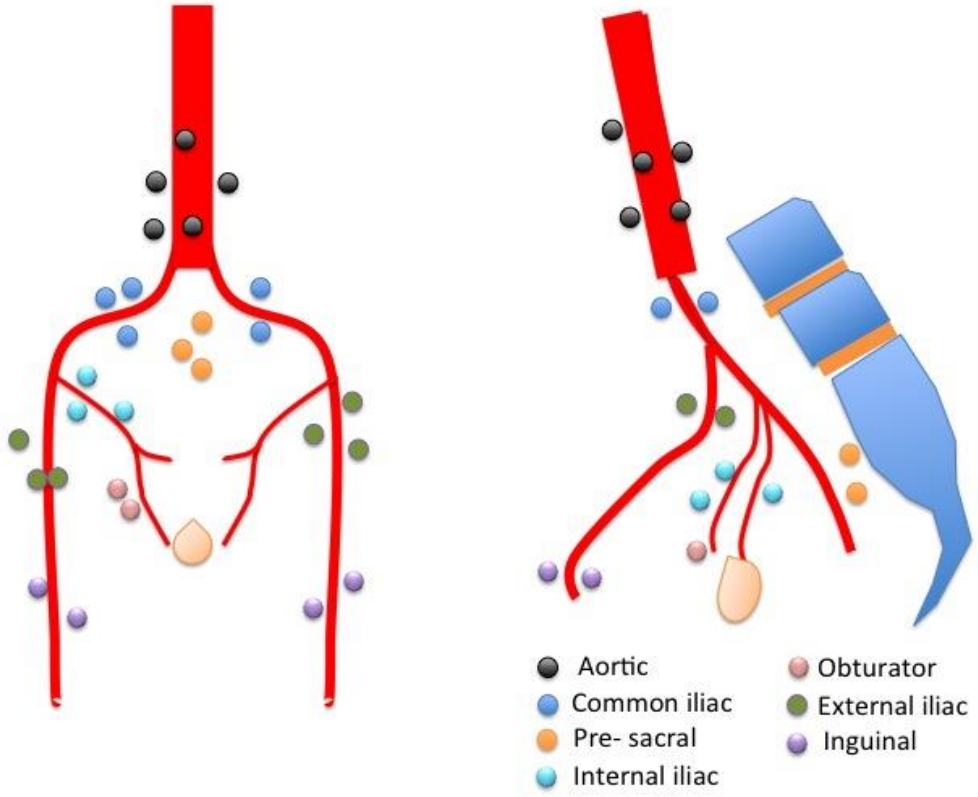

Figure 7. Prostate lymphatic drainage

In patients with intermediate or high risk of having nodal metastases, diagnostic pelvic lymph-node dissection (PLND) is the gold standard for the detection of nodal disease. Non-invasive imaging with CT and MRI can be used for N staging, but the sensitivity of these techniques is only 36% [50] and the specificity about 82% [51]. An important challenge is to avoid PLND and replace it by new, more sophisticated, sensitive and specific imaging techniques for the N staging.

The imaging techniques that are currently used for N staging are CT, PET- CT and MRI.

i. CT, MRI and MRL

State-of-the-art CT scanners offer excellent resolution, resulting in visualisation of normal abdominal LNs. Normal LNs are ovoid in shape and display soft tissue density on CT.

In MR imaging, LNs are best demonstrated on T1-weighted images as they are typically isointense to muscles and surrounded by hyperintense fat. Short tau inversion time (STIR) sequences may be useful as malignant nodes can be of high signal, but this aspect is not specific for malignancy.

The most widely used CT and MR criteria to determine whether a node is benign or malignant are:

The size: The sole widely accepted criterion for discriminating between normal and pathologic nodes on CT and MRI is the size. The short axis diameter of a LN should be measured, in order to minimize errors due to node orientation. The short axis diameter is measured perpendicularly to the longest diameter of the LN. It has been demonstrated that this is consistent despite orientation because it is likely to become rounder before it elongates [52,53].

Retrocrural and portohepatic nodes should not exceed 6 mm, while the upper limit of gastro-hepatic ligament nodes is 8 mm. Retroperitoneal, celiac, mesenteric and pelvic nodes greater than 10 mm are considered abnormal [54]. It has to be noted that multiple,

slightly smaller (8-10 mm) nodes in these regions should be cautiously interpreted. For peri-rectal nodes, 3 mm has been recommended as a size threshold for indicating malignancy [55].

The sensitivity and specificity of LN staging based on the size of the LN is a subject of considerable controversy, as the frequency of metastasis in normal sized LN is substantial. In general, the smaller the nodal diameter criterion used to separate malignant from benign nodes, the higher the sensitivity and the lower the specificity are [56]. It has been demonstrated that 10-20% of normal-sized locoregional nodes will contain tumour deposits [57,58]. On the other hand, 30% of enlarged nodes are benign [56, 58].

The shape and contour: Normal LNs are reniform with regular contours. Irregular LN borders suggest malignancy due to extra-capsular expansion. Rounded nodes without any internal fat are also highly suspicious for malignancy.

The number: A group of normal-appearing nodes can suggest malignancy, even though this sign can lead to false positive interpretations [59].

The morphology: Large metastatic nodes frequently appear heterogeneous on contrast-enhanced CT and MRI. Large low density on CT and hyper-intense on T2 MR imaging nodes may be suggesting necrosis, which is particularly common in primary squamous cell cancers.

Heesakkers et al. compared the diagnostic accuracy of MR lymphoangiography (MRL) with a new lymph-node-specific MR contrast agent (ferumoxtran-10) to multidetector CT in a prospective, multicentre cohort study [60]. The results suggested that MRL had significantly higher sensitivity and NPV than CT for patients with PCa who had intermediate or high risk of having lymph-node metastases. As a result, after a negative MRL, the probability of having lymph-node metastases is low enough (less than 4%) to omit a PLND. The new imaging MRL technique could change current practice by eliminating the need for PLND in patients with a negative MRL. Unfortunately, the evaluation tests of this new contrast agent are currently withdrawn.

ii. PET-CT

PET-CT, which provides both functional and anatomical information, has been proven useful for the concurrent detection of N and M metastasis in various cancers [61]. There are many radiopharmaceuticals that can be used and each of them has different characteristics. The most widely used is ^{18}F-FDG (18-Fluoro-D-deoxyglucose), which is a non-specific tumour-seeking radiopharmaceutical. The use of ^{18}F-FDG is based on the heightened glycolysis in tumour cells, which provokes a high uptake of ^{18}F-FDG from the tumour. It has to be noted that kidneys excrete ^{18}F-FDG resulting to a physiological uptake by urinary tract and a suboptimal analysis of these organs (kidneys, ureters, bladder, prostate). On the other hand, not all kinds of neoplasms demonstrate high glycolysis. For example neuroendocrine neoplasms, prostate, kidney, stomach and gastrointestinal tract cancers can have low glycolysis levels. There are many new and promising radiopharmaceuticals for the detection of PCa metastasis.

b.2. M Staging

M0	No distant metastasis
M1	Distant metastasis
M1a	Non-regional lymph nodes(s)
M1b	Bone(s)
M1c	Other site(s) with or without bone disease

The most common metastatic site of PCa is the bone. BMs represent the initial metastatic site in more than 80% of PCa patients. The main site of BM is the axial skeleton (skull, vertebra, ribs and collar bone, scapula, and proximal femur) [62,63]. Wang et al., studied 102 patients with BM and they detected 2,000 lesions, 28.9% of which were distributed in the ribs, 14.8% in thoracic vertebrae, 13.8% in the ilium and 8.0% in the lumbar vertebrae [63]. According to Bubendorf et al., there is a gradual decrease in spine involvement from the

lumbar to the cervical level (97% v 38%), which is consistent with a subsequent upward metastatic spread along spinal veins after initial lumbar metastasis [30]. It has been suggested that the distribution of BMs is correlated with the total number of metastatic bone lesions of patients (**Figure 8**). With an increase in the metastatic bone lesion numbers, the distribution of metastatic lesions changes. For example, as the number of metastatic lesions increases, the proportion of rib metastasis increases from 8.6% for few metastasis to 30.9% for extensive bone disease [63].

PCa patients with bone disease cannot have local treatment (surgery or radiation therapy), hence accurate detection of bone disease is an essential component in the discussion relating to the treatment approach.

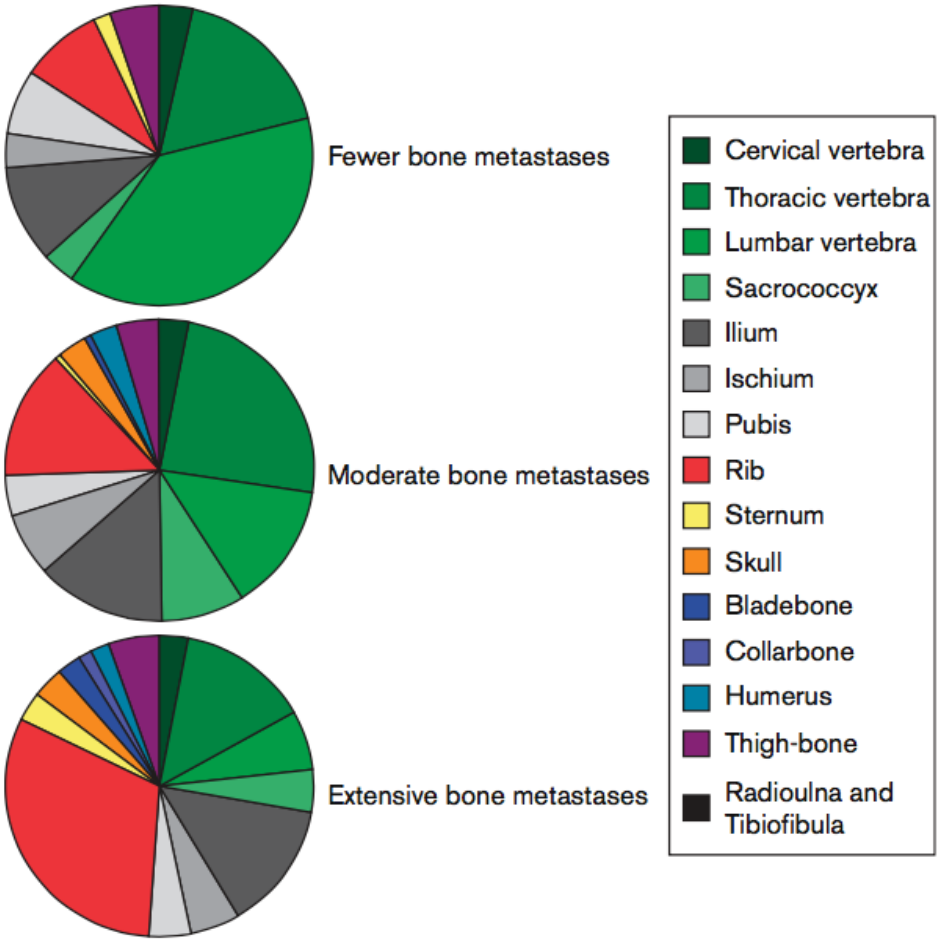

Figure 8. Distribution of BMs in the different disease load.

Reprinted from ''Study on the distribution features of bone metastases in PCa'' by Wang C. Shen Y [63]. With the permission of Lippincott Williams.

i. XRays

XRays are considered a relatively insensitive technique, which cannot be used as a screening method for asymptomatic patients. The detection of lytic bone disease is usually delayed as well before any radiographic change becomes noticeable, up to 30-50 % of the trabecular bone has to be destroyed or a lesion must be greater than 1.5 cm.

Detection of trabecular bone metastases is difficult, especially at the level of the spine where XRays cannot rule out metastatic disease. Even though rare, cortical bone metastases might be easier to detect even if they are only a few millimetres wide [64].

ii. **Computed Tomography**

CT is widely used in some cancers for localizing the primary tumour and assessment for metastatic disease. This technique is used for LNM detection in PCa patients, although the sensitivity is low, as discussed earlier. On the other hand, CT is not used for T or M screening in PCa, although bone disease may be present in a significant proportion of patients.

It is evident that CT is more sensitive than XRays for the detection of BM, due to its high spatial and temporal resolution. The extent and the pattern of BM can be demonstrated by CT. Helms et al. provided evidence for the capability of CT to quantify medullary density and asymmetry in order to detect bone disease [65]. Asymmetry of marrow density greater than 20 Hounsfield Units (HU) is likely to represent a pathologic process, although the disease is not specific.

iii. Bone Scintigraphy

BS is one of the most frequently performed nuclear medicine procedures, as it is a brief, relatively inexpensive and widely available technique. The radionuclide used is Tc 99m bound to a bisphosphonate.

Tc 99m accumulates rapidly in the skeletal system even though the uptake mechanisms have not been completely clarified. The degree of radiotracer uptake depends on the blood flow and the osteoblastic activity [66,67]. Imaging is usually performed 2-6 hours after administration of the radionuclide.

BS has played a crucial role in tumour staging for years, but its reliability has been repeatedly questioned, firstly because of the high incidence of false positive results. Wu et al., studied the clinical significance of solitary rib hot spots on bone scans in patients with extra skeletal cancer and demonstrated that most solitary rib hot spots on bone scans were benign

[68]. There are sites of increased symmetric activity such as acromial and coracoid processes, costochondral junctions and the angle of Louis of the sternum. Most importantly, false positive results are frequently observed in osteoarthritis, Paget's disease and fractures. Very frequently a positive BS will lead to another modality (XRay, CT, MRI) in order to clarify the diagnosis.

Secondly, despite its lack of sensitivity and specificity which have been demonstrated by various studies [69,70,71,], the sequential work up for the detection of BM in PCa patients still relies on BS. Targeted XRays should elucidate regions of increased uptake in order to distinguish a benign (fracture, Paget's disease, degenerative disease, angioma) from a malignant etiology. This Tc 99mBS and targeted XRays association is imperfect, and the use of CT or MRI is often necessary in order to clarify the diagnosis.

iv. SPECT CT (Single Photon Emission Computed Tomography)

SPECT (Single Photon Emission Computed Tomography) consists of a gamma camera - or a set of gamma cameras - mounted on a gantry and as a result multiple angle imaging is obtained. The use of SPECT or SPECT-CT has been shown to improve both sensitivity and specificity of BS for the detection of bone metastases [72,73,74] but its sensitivity and specificity remain suboptimal.

v. PET (Positron Emission Tomography) **CT**

Interpretation of CT findings is based solely on morphologic changes and contrast enhancement patterns. PET-CT is the fusion of functional and anatomic information and arises as an "all organ staging method" for the N and M staging of cancer patients.

The method of PET-CT is based on the phenomenon of spontaneous positron emission by the nuclei of some unstable ultra-short-lived radionuclides (USLRs). Two gamma-photons having the same amount of energy (511 keV) are released after the positron annihilates with an electron. The gamma-photons are moving to opposite directions at almost 180° apart

(close to collinearly) [75]. The length of the flight of the positron from the emission point to the annihilation point depends on its own energy and on the density of the environment. In the muscle it varies from 1 to 8 mm. This is one of the reasons why PET has a smaller resolving capacity than some other imaging methods (MRI, CT).

There is a great variety of radiotracers that can be used (**Table 7**). In order to obtain ultra-short-lived positron-emitting radionuclides, a cyclotron complex and a radiochemical laboratory are necessary.

Radionuclide	**Substance**	**Description**	**Purpose of the indicator and its range of applications**
[11C]	Thymidine	^{11}C-thymidine	Proliferative activity in tumour cells
[11C]	Choline	^{11}C-choline	Speed of phospholipid synthesis – marker of membrane-forming (PCa)
[18F]	Fluorine desoxyglucose	2-[^{18}F]-fluorine-2- desoxy-d-glucose (^{18}F-FDG)	Speed of the metabolism of (transmembrane transfer) of glucose

[18F]	DOPA	^{18}F-fluorine-dihydroxyphenylalanine (^{18}F-DOPA)	Concentration of dopamine receptors in brain and in some tumours (medullary thyroid cancer, pancreas tumours, GIST, brain tumours)
[18F]	Thyrosine	^{18}F-fluoro-ethyl-tyrosine (^{18}F-FET)	Speed of transmembrane transfer of amino acids (in tumours)
[18F]	Fluoride	^{18}F-ion (fluoride) ^{18}-F-NaF	Speed of calcium metabolism (revealing bone metastases)
[18F]	Thymidine	3-deoxy-3-[^{18}F]-fluorothymidine (^{18}F-FLT)	Speed of proliferative activity in tumour cells
[18F]	Choline	^{18}F-choline	Speed of phospholipid synthesis – membrane-forming (PCa)

Table 7. The main radiotracers for PET-CT

The procedure of the whole-body PET examination includes three stages: the injection of the radiopharmaceutical, patient positioning, transmission and emission scanning. The examination is performed on a patient on an empty stomach. The patient should be in a comfortable position with their eyes closed no less than 20-30 min before and 15 min after the injection of ^{18}F-FDG in order to preclude hypermetabolism of glucose in muscles. The patient should drink a minimum of 0.7 L of water before the exam in order to reduce background activity.

For example, ^{18}F-FDG is slowly introduced intravenously in a volume of no less than 5-10 mL physiological saline at 200–220 MBq/m^2 of the body surface. The diagnostic dose of the radiotracer in whole-body examination amounts to 300-500 MBq and the effective dose is 8.1-13.5 mSv. The optimal time to begin scanning varies between 60 and 120 min after the introduction of ^{18}F-FDG [76,77].

Promising new radiotracers have been developed for the staging of PCa: ^{18}F- and ^{11}C-Choline [78,79]. Choline is an essential constituent of the phospholipid cell membrane. As a result, there is a substantial uptake of the radiotracer by regions with rapid cellular proliferation, such as tumours. ^{11}C-Choline is excreted by the bowel and is a very promising technique for the imaging of urinary tract tumours such as PCa, as well as hepatocellular carcinoma and gliomas [79]. Hara et al. evaluated ^{11}C-choline PET in few patients with PCa and compared results with ^{18}F-FDG PET and concluded that the advantage of ^{11}C-cholinePET over ^{18}F-FDG PET in patients with PCa involved not only the absence of ^{11}C-choline activity in the urine but also the high uptake of ^{11}C-choline in the PCa itself [78]. Unfortunately, ^{11}C-Choline has a short half-life and as a result can only be used by hospitals with cyclotron. On the other hand, ^{18}F-Choline is excreted by the kidneys, it has a longer half-life compared to ^{11}Choline and thus a cyclotron is not necessary.

A new and very up-and-coming technique for PCa detection is Prostate-specific membrane antigen (PSMA) PET-CT. PSMA is a cell surface protein overexpressed by PCa cells. Ligands of PSMA are labelled with ^{68}Ga, Tc 99m and $^{123/124/131}$I for the detection of PCa metastases or

local relapse [80,81,82,83.]. Afshar-Oromieh et al. demonstrated that suspicious PCa lesions present excellent contrast as early as 1 h post-injection of PSMA. In a retrospective analysis of 319 patients who underwent ^{68}Ga-PSMA-ligand PET-CT, the same team found that PSMA is highly specific for PCa and detects the disease in a high percentage of patients (82.8%) [84,85].

vi. MRI

MRI plays a crucial role in the detection, characterization and follow-up of BMs. It possesses the unique advantage of directly exploring the bone marrow and as a result allows early detection of bone involvement.

Until now, MRI has been used for the imaging of the complications of metastatic disease (fractures, neurologic compression) or as a second-line imaging technique if an anomaly is detected in BS, XRays or CT and there is residual doubt regarding its either benign or malignant origin.

Numerous studies have demonstrated that MRI of the axial skeleton and, later, WBMRI is superior to the current multistep BS based staging protocol [86,87,88,89,90,91].

The usual protocols include the following sequences:

T1 weighted spin echo images:

Bone marrow contains 80% fat, which explains its high signal on T1; hence any malignant lesion showing a lower signal is easy to detect. As a result T1 is the first sequence used, in order to detect bone involvement.

The haematopoietic marrow, containing water but also fat, is hypointense to subcutaneous fat, but hyperintense to normal muscles. If the marrow signal becomes hypointense to the muscles and vertebral discs, this indicates marrow infiltration [92].

T2 weighted spin echo images:

Due to the high signal of fatty bone marrow on fast T2 sequences, and similar signal intensity of some bone metastases (due to water content), the latter may be missed. Fat suppression is thus mandatory [92].

Fat-suppression techniques:

Fat-suppressed MRI sequences demonstrate potential advantages over conventional spin-echo images for the detection of bone marrow disease. The reduction of the background signal intensity of fat containing marrow makes high-signal intensity lesions more obvious.

Two of the most widely available methods of fat suppression are short-TI inversion recovery (STIR) and frequency selective fat saturation. A 180 - inversion pulse is used initially for short tau inversion recovery (STIR) sequences [93]. The inversion time is chosen to cancel the signal of fat. Although the conspicuousness of lesions is more important with fat saturation sequences, these acquisitions demonstrate some limitations. Because of the suppression of the signal of lipid protons, the signal-to-noise ratio is reduced resulting in a grainy image appearance [94]. Lower signal-to-noise ratio also makes these sequences susceptible to motion artefacts caused by vascular, peristaltic, respiratory movement or body movement of the patient. T2 fat saturation sequences are very time-consuming and demonstrate field inhomogeneities. STIR sequence is less affected by field inhomogeneity and is very sensitive in detecting bone marrow abnormalities. However, it is less specific as it tends to suppress anything that has a T1 relaxation time similar to that of fat [93].

Chemical shift imaging

Chemical shift sequences use the signal-cancelling effect between fat and water protons on opposed phase imaging, in order to highlight bone marrow replacement. The difference in resonance frequency between water and fat protons has no impact on the contrast of conventional spin-echo sequences as the 180-pulse cancels the difference. On the in phase image, the readout gradient is centered on the echo, which appears symmetrically on the

90-pulse with respect to the 180-pulse and as a result the signal is proportional to the sum of water and fat protons. By shifting the readout window, it is possible to obtain images the contrast of which is related to the difference between the quantities of water and fat protons (opposed-phase images) [95]. The signals of gradient-echo sequences in which fat and water protons are in phase, are added; if they are opposed-phase, they are subtracted. At 1.5 T, water and fat protons are in-phase if TR = (2 n) 2.4 ms, and opposed-phase if TR = (2n + 1) 2.4 ms. No subtraction will occur if the fatty bone marrow is pathologic. Opposed-phase images will highlight the difference between fat and water containing bone marrow and bone tumour.

Diffusion Weighted Imaging (DWI):

Diffusion of water molecules is the basis of diffusion-weighted imaging (DW-MRI), although water mobility in biological tissues is an exceptionally complex process. Even though various mathematical models of water mobility have been proposed in order to describe empiric observations, the true nature of water movement in biological tissues is not entirely understood.

The random movement of particles in a fluid or gas is referred to as “Brownian motion”, in honour of the botanist Robert Brown who first commented on the motion of pollen grains in fluid in 1827. In 1905, Albert Einstein constructed a mathematical framework of Brownian motion, where he established a statistical relationship between the average distance that particles move over a time interval, as well as functional dependencies on particle size, medium viscosity and temperature. DWI explores the random motion of water molecules in the body. Water molecules outside the body are in constant random Brownian motion. For example, in a glass of water, the motion of the water molecules is completely random and is limited only by the boundaries of the container [96,97]. This unrestricted motion of water molecules is called free diffusion. In biologic tissues, the movement of water is restricted, as its motion is limited by interaction with cell membranes and macromolecules (**Figure 9**).

The tissue cellularity is inversely correlated to the degree of restriction to water diffusion. In tissues with high cellularity (such as tumour tissue), the movement of water molecules is deprived. The motion of the molecules is restricted by cell membranes, which act as barriers to molecule motion in both extra- and intracellular spaces. In contrast, in regions with low cellularity or where the membranes are damaged, the motion of the water molecules is less restricted.

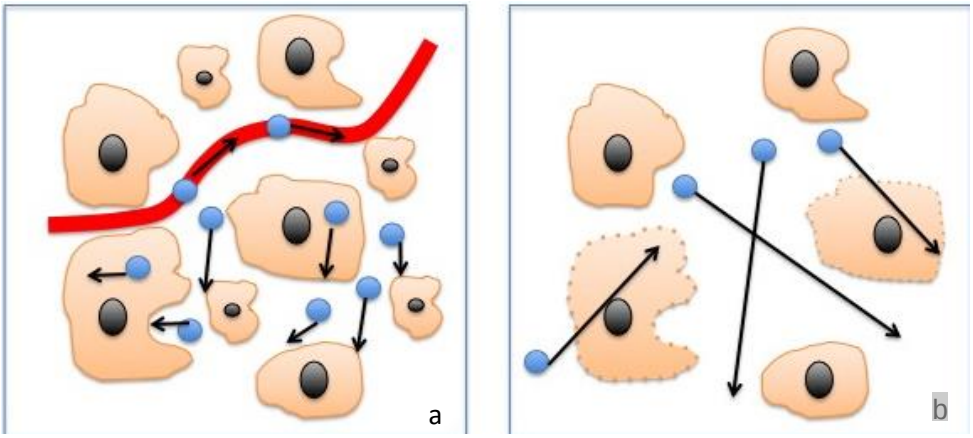

Figure 9.

a: Cellularity, intact cell membranes and vessels lead to restricted diffusion of the water molecules (blue circles) within extracellular, intracellular and intravascular space, all of which contribute to the signal.

b: Low cellularity and ruptured cell membranes leading to free diffusion.

It has to be noted that this figure is a simplified portrait of the Diffusion mechanism in the tissues. Cellularity is the first mechanism invoked to explain the restriction of diffusion, but this remains an oversimplified vision of diffusion in the tissues.

In a DW-MRI study, the amount of signal attenuation from each voxel after application of the MPGs is related to the strength of the motion probing gradients (MPG) and the diffusion coefficient.

$S0\ \exp(-\gamma^2 G^2 \delta^2 (\Delta - \delta/3) D$

(where S0 is the baseline signal without diffusion weighting; S the signal after applying diffusion weighting; γ, G, Δ and δ the gyromagnetic ratio, strength of the diffusion gradients, time interval between the diffusion gradients and duration of the gradient, respectively).

In the above equitation, the term $[-\gamma^2 G^2 \delta^2 (\Delta - \delta/3) D]$ can be replaced by the b-value. It is possible to quantify the diffusion coefficient by performing imaging using at least two b-values.

As mentioned above, water movement in tissues is influenced by various factors such as pressure gradient, ionic and osmotic gradients, capillary perfusion and bulk tissue movements. Cell membranes and macromolecules slow down the water motion. Thus, the measurement of diffusion coefficient D in tissues is only an estimation of pure water diffusivity and is termed "apparent diffusion coefficient" (ADC). By increasing the diffusion weighting, a signal loss is observed. The rate of the signal loss with increasing b-values represents the ADC.

Molecular water is the probe used in diffusion-sensitive MR imaging, but it is the non-water constituents that provide contrast by reducing water mobility relative to free diffusion. The term "restricted" diffusion may be used to refer to the intracellular water, even though this suggests that the water has to remain intracellularly. Certainly, cell membranes are at least semi-permeable to water, thus the term "impeded" diffusion is used to describe water mobility within the cellular matrix more accurately.

DWI using single-shot echo-planar imaging (EPI) is a well-established method to examine the brain. However extracranial DWI did not become a clinical standard until recently, because the use of EPI was complicated by magnetic susceptibility artefacts and severe image distortion in the body [98, 99]. This problem has been largely exceeded with the introduction of parallel imaging techniques, such as sensitivity encoding (SENSE) [100,101,102] and the development of stronger gradients and multichannel coils. Despite numerous breakthroughs in DWI, breath-hold or respiratory triggered scanning was still considered necessary until 2004 when Takahara et al. developed a unique sequence of WB DWI, called "diffusion-

weighted whole-body imaging with background body signal suppression" (DWIBS) [103]. This technique intentionally uses free breathing in order to visualize moving visceral organs and their lesions. The same team also observed that SNR of DWI during free-breathing was considerably superior to that of breath-hold scanning. The scanning time is no more a limitation (as in breath-hold scanning) and the acquisition time is no more confined to a particular phase of the breathing cycle (as in respiratory triggered scanning). Images with multiple b-values including high b-values around 1,000 s/mm^2 can be acquired, thin slices can be obtained, and multiple signal averaging is possible. Furthermore, these advances enable volumetric [three-dimensional (3D)] image processing, including maximum intensity projections (MIPs), volume rendering and multiplanar reformatting (MPR) in any plane.

It is recommended to obtain axial slices in DWIBS, in order to reduce image distortion. Thanks to thin axial slices (up to 4 mm), high quality reformatted images can subsequently be created in any plane [103].

The implementation of WB DWI is easier on 1.5-Tesla (1.5-T) than on 3-Tesla (3-T) systems. The minimization and control of artefacts is more challenging at 3-T but almost all difficulties raised by high fields have now been solved and DWI can be acquired on both 1.5 and 3T magnets. Some residual challenges must be addressed. Rapid switching of the magnetic gradient field with echo-planar imaging cause residual magnetization and results in geometric distortion and image shearing (**Figure 10A**) [1]. This distortion can make it more difficult to register and align DW images with corresponding morphologic T1- and T2-weighted images. On the other hand, because of the greater field inhomogeneity at 3 T, uniform fat suppression across large fields of view can be challenging, and the result is chemical-shift and ghosting artefacts (**Figure 10B**) [1]. Finally, due to the fact that the MR frequency offsets applied differ between anatomic stations, voxel shift occurs in the phase-encoding direction and cause misalignment of structures (e.g. the spinal cord) between imaging stations (**Figure 10C**) [1]. Coronal reformats are usually less affected because the phase-encoding direction is anteroposterior.

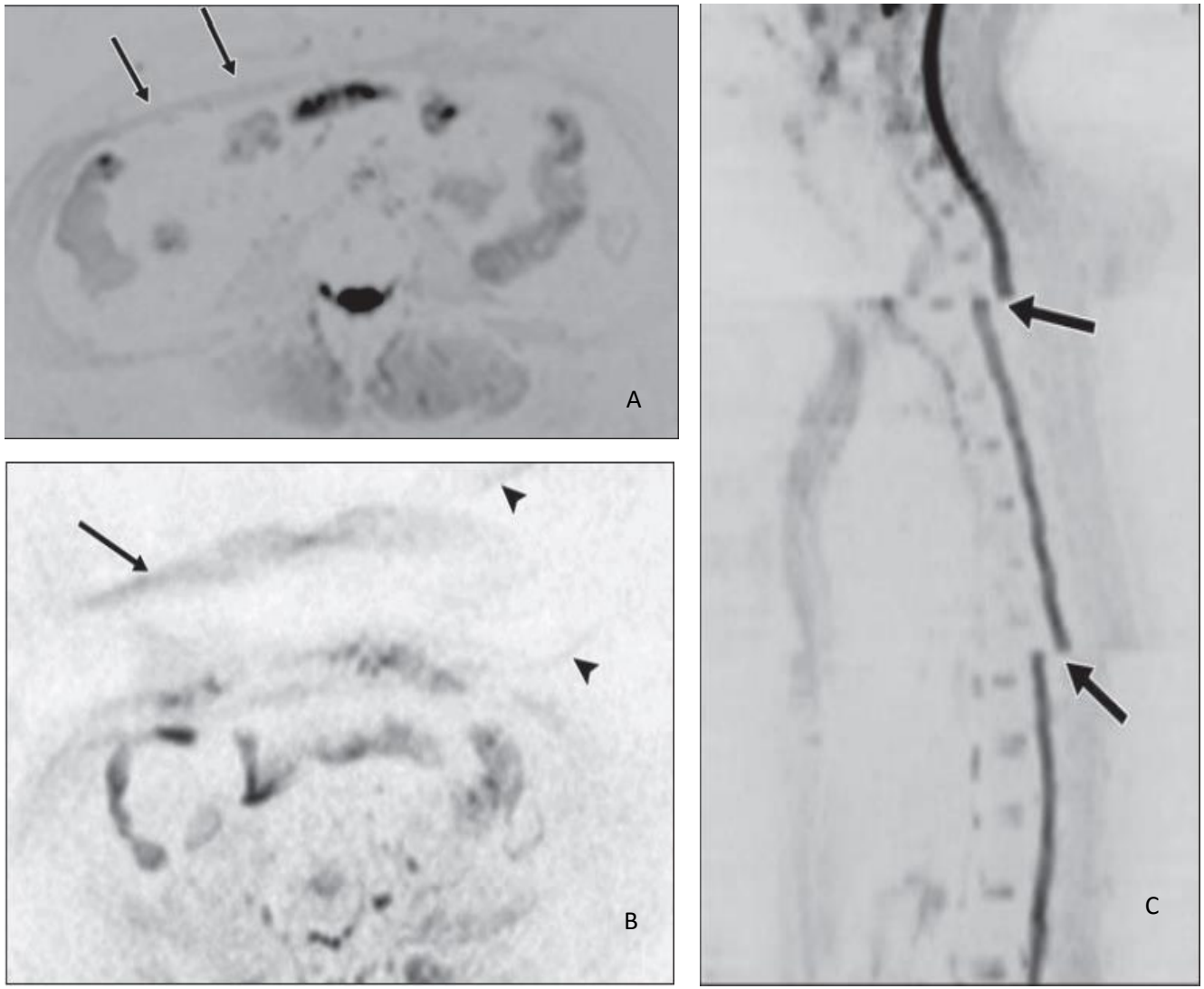

Figure 10.

Potential problems with DWI MRI at 3T.
A: shows geometric distortion with distorted appearance (arrows) of right anterior abdominal wall
B: ghosting artefact (arrowheads)
C: three image stacks with misalignment of the spine (arrows).

Reprinted from ''Whole-body diffusion-weighted MRI: tips, tricks, and pitfalls''. Koh et al. [1]
With permission from ARRS.

DWI provides functional information and DWI images obtained at high b-values can be used for the detection and characterization of pathologic processes, including malignant tumours as it enables an “at-a-glance” assessment; this reduces interpretation times of examination by driving the attention to abnormalities, which can then be evaluated on anatomic whole-body MR images. Whole-body DWI is considered a supplement to anatomic whole-body MR imaging, leading to improved reader performance of the latter [104,105].

Most importantly, concurrent bone and node staging become possible with the use of the WB DWI (**Figure 11**). WBMRI thus offers, along with PET-CT, this ability to globally assess cancer (N and M) in one step.

It has to be noted that tumour histologic type and grade, as well as the anatomic location, affect the ability of DWI to detect it. The detection ability of DWI is good for breast cancers, myeloma, and lymphoma and for tumours with tightly-packed small cancer cells such as neuroendocrine tumours, small-cell cancers, and many childhood tumours [106,107,108,109]. On the contrary, primary tumours and metastases from renal cancers are sometimes less well seen [110,111].

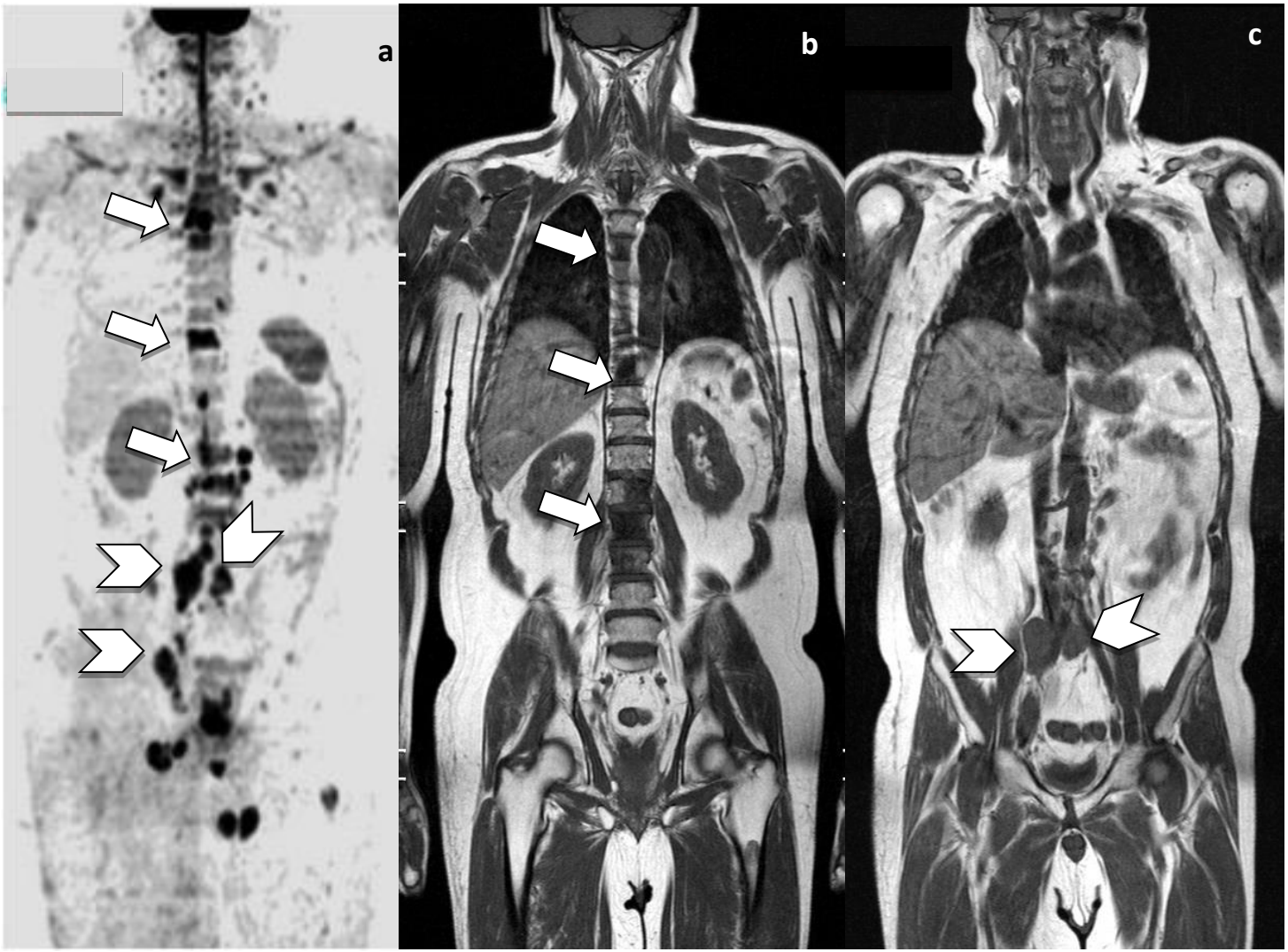

Figure 11.

a: Whole body DWI

b & c: Anatomic T1 sequence.

PCa patient with bone (arrows) and node metastasis (arrowheads) detected by DWI and confirmed by the anatomic sequences

A.9. Treatment

Not all PCa require treatment. The majority of tumours detected by screening are not aggressive and their evolution is slow. We abstain from an aggressive attitude when the disease is indolent or when the general condition of the patient is not good with short life expectancy, as the tumour will not have the time to progress.

The age is not a risk factor for the progression of the tumour. Aggressive cancers should be treated the same way in every patient, regardless of the age.

a. Radical prostatectomy:

The radical prostatectomy is the reference surgical treatment of PCa. During the surgery the prostate gland and the seminal vesicles are removed. When the tumour is aggressive, the regional lymph nodes are also removed.

The prostate can be removed with open surgery (open radical retropubic prostatectomy), or via laparoscopic and robot-assisted surgery [112].

The complications of this procedure include:

-Haemorrhage

- Infection

- Erectile dysfunction: one of the serious side effects of radical prostatectomy caused by the damage to the nerves. About half of men are able to regain some of their ability to have erections. It can take as little as 3 months, but for most men, it will be 6-12 months [112].

- Urinary incontinence: this complication is usually caused by damage to the external sphincter. Up to half of all men who have a radical prostatectomy develop urinary incontinence ranging from a need to wear pads to occasional dribbling.

- Sterility, vesico-urethral anastomotic stenosis: in 0.5-14.5% of patients.

- Bladder or rectal trauma

b. External Beam Radiotherapy:

External beam radiation therapy (EBRT) has a long-standing history in the treatment of PCa. However the technique of the therapy has dramatically evolved [113]. Conventional radiation therapy involves X-ray photons created by a linear accelerator. Ionizing radiation achieves tumour cell kill by creating double strand breaks in DNA. Cells with sufficient damage typically die a mitotic cell death during subsequent attempts at cell division. Tumour cells, compared to normal tissues, have a reduced capacity for repairing radiation damage because of acquired mutations in DNA repair genes. The daily radiation dose is an important determinant of cell death. Traditionally, daily fraction sizes of 1.8-2.0 Gy have been employed for most cancers, as this dose is thought to strike a favorable balance between tumour cell kill and allowance for normal tissue repair. Theoretical modeling has suggested that the use of fewer but larger fraction sizes, called hypofractionation, may enhance prostate tumour cell kill - relative to normal tissues - due to the slow proliferation of prostate cancer cells.

Side effects of radiation therapy are categorized into acute and late effects. Acute effects occur during treatment or in the immediate 3–6-month period following radiation treatment, while late effects generally develop a year or more following treatment [113,114].In general, acute effects following prostate radiotherapy are relatively common, transient and mild in nature. Acute urinary effects may consist of obstructive and irritative symptoms including frequency, nocturia, urgency, dysuria, intermittency, and hesitancy[113,114] but urinary retention is rare. Acute radiation effects on the bowel include rectal urgency, frequency, loose stools, tenesmus and proctitis.

The late complications may include bowel urgency, rectal bleeding, urinary urgency, urethral strictures, reduced bladder capacity, erectile dysfunction, hip fractures and secondary malignancies. Urinary or rectal incontinence are rare [114].

c. Brachytherapy

Within recent years, permanent interstitial brachytherapy of the prostate has become a widely accepted, attractive treatment approach, typically for the low-risk prostate cancers [115]. There are two types of brachytherapy: seed implantation (low dose rate therapy - LDR) and high dose rate therapy (HDR). Both types treat PCa with radiation from within the prostate gland. 80 to 120 very small radioactive seeds are implanted into the prostate gland via a fine needle inserted through the perineum [115].

The complications of brachytherapy include irritative and obstructive lower urinary tract symptoms that can develop immediately as a result of implant trauma or over the first weeks as a result of the radiation. Urinary retention is rare.

Late rectal complications, including proctitis with diarrhea, tenesmus, or rectal bleeding, may occur in 2-19% of patients [113].

d. Hormone therapy

Androgens are required for normal growth and function of the prostate. The tumour cells depend on the hormone testosterone to grow. Lowering the testosterone levels in the body can: a) lower the risk of an early PCa recurrence after treatment and b) diminish / minimize an advanced prostate tumour or impede its (re)growth.

The reduction of androgens can be achieved surgically or through the use of medications.
Surgically: orchiectomy
Medically: injection of luteinizing hormone releasing hormones (LH-RHs) which suppresses the body's natural production of testosterone. Non-steroidal anti-androgen - drugs can also be used in order to block testosterone from reaching cancer cells.

The side effects of hormone therapy are:
-Nausea and vomiting
-Hot flushes
-Anaemia

-Lethargy

-Osteoporosis

-Gynaecomastia (sometimes painful)

-Erectile dysfunction

B. Whole body MRI (WBMRI)

B.1. General

Between 1997 and 2001, the first studies about WBMRI were published [116,117,118.] The imaging quality of these early whole body protocols was reduced in comparison to dedicated examinations and as a result they were not introduced into the clinical routine. The patient had to be repositioned several times during one examination and the coils had to be frequently rearranged. Important improvements were the introduction of a rolling table platform mounted on top of the MRI table [119] and the application of parallel imaging techniques [120]. Parallel imaging has the advantage of a shorter acquisition time for the same spatial resolution or a higher spatial resolution within a reasonable acquisition time [121,122].

B.2. Components of an MRI system for WBMRI

The effective imaging region or field of view (FOV) of an MRI system depends crucially on three hardware components and their performance parameters: (1) the main magnet providing a uniform magnetic field over the whole imaging volume, (2) the gradient system providing linearity over the imaging volume and (3) the radiofrequency (RF) system providing RF signal homogeneity and sensitivity.

The field strength of the main magnet has to be high enough in order to provide adequate basic magnetization. The latter is mandatory for achieving a high signal-to-noise ratio (SNR) and a good image quality.

The image distortion is minimized and the signal homogeneity maximized by using a uniform main magnetic field over the patient. This is achieved by a cylindrical configuration of the main magnet.

A high-performance gradient system is required for WBMRI protocols. A fast slew rate (given in mT/m/ms) has to be combined with a high gradient amplitude (given in mT/m). These characteristics allow short repetition and echo times (TR and TE), which are indispensable for fast image acquisition and coverage of a large volume in a short period of time. A short TR is

also important to achieve maximum T1 contrast. The radiofrequency system should provide homogenous excitation of a large imaging volume. In order to overcome the limited signal readout due to the modest SNR, surface coils are used. These receive signal for nearby tissues and improve SNR and thus offer better image quality and spatial resolution.

B.3. From partial to global imaging

The FOV of the WB can be extended by moving the scanner table between acquisitions, so as to shift the position of the patient relative to the imaging field [123,124] . This technique allows the successive imaging of different parts of the patient's body. Moving tables with a range of approximately 200 cm with RF readout coils (that cover the whole body) are the prerequisites for multistation WB imaging. The maximum table range directly determines the imaging range or how much of the patient's body can be moved through the scanner's effective FOV.

B.4. WBMRI in oncology

MRI, with its lack of ionizing radiation, ability to image bone marrow, but also soft tissue, and spatial resolution is a precious tool for cancer detection and staging. A high sensitivity has been reported for the detection of metastatic disease notably for neoplasms that metastasize to the bone, LNs, brain and liver [12,125,126]. Dedicated assessment of individual organs can be combined in one whole-body study combining anatomic and functional DWI coverage, offering whole body tumour staging.

WBMRI is increasingly used for an ample variety of applications thanks to the improved accessibility and technological advances described above. Several studies have shown that MRI is a highly sensitive method for early detection of BM as it allows the identification of malignant cells in the bone marrow before bone remodelling [127,128]. Walker et al. support that WBMRI represents a convenient and cost-effective method for screening patients with breast cancer. The imaging protocol included coronal STIR images of the whole body and a dedicated MR brain protocol. Regarding to the skeleton evaluation, MRI permitted the same - or improved - evaluation compared to scintigraphy [127]. These results are in concordance

with an earlier study by Eustace et al., comparing whole body STIR with Tc 99m BS in 49 patients with suspected skeletal metastases [129]. The authors demonstrated that WBMRI is an effective method of examining patients with suspected skeletal metastasis with better sensitivity than Tc 99m BS.

Regarding to multi-organ screening, Antoch et al., studied 98 patients with various histologically proven malignancies and concluded that in overall TNM staging the performance of [^{18}F]-fluorodeoxyglucose-PET-CT was superior than WBMRI without DWI [130]. Studies have shown that in patients with lung cancer, WBMRI can be used for the M-stage assessment and may be considered at least as effective as FDG PET-CT [131].

In 2005, Schmidt et al. compared the accuracy of WBMRI and PET-CT in the staging of various malignant tumours [132]. Regarding to tumour assessment, WBMRI demonstrated a sensitivity of 86% as the recurrence of an oesophageal carcinoma was not identified by the technique. As regards to LN involvement, WBMRI had a sensitivity of 80% and specificity of 75%. Finally when it comes to metastatic disease, the sensitivity was 96% and specificity 82%. A study in patients with breast cancer from the same team, confirms that WBMRI is highly sensitive to distant metastatic disease while PET-CT is more sensitive in detecting LN involvement [133]. Regarding to N-staging, PET-CT achieved sensitivity 96% and equal specificity of 96% at a diagnostic accuracy of 96%, while WBMRI showed a sensitivity of 73% and a specificity of 77% with a diagnostic accuracy of 75%. Regarding to the M-staging PET-CT, demonstrated a sensitivity of 91% and specificity of 86% with a diagnostic accuracy of 90%. WBMRI showed a sensitivity of 95%, specificity of 92% and a diagnostic accuracy of 94%. WBMRI accurately detected more metastases of the bone (WBMRI *n* = 69 versus PET–CT *n* = 63), liver (*n* = 70 versus *n* = 67) and showed an equal performance for the detection of lung metastases.

The main disadvantages of WBMRI are its relatively long scanning times, artefacts from motion (requiring patient cooperation or general anaesthesia) and limited specificity. However, advances in hardware and imaging techniques, including additional sequences (are

reducing the impact of some of these challenges. Most importantly, the introduction of DWI radically improves the diagnostic effectiveness of WBMRI and promotes the technique as a tool of choice for PCa staging.

VI. Limits of current staging methods for PCa patients

As mentioned above, accurate staging of PCa patients is crucial in order to adapt treatment to the actual stage of the disease. A precise evaluation of the metastatic burden is essential, especially with the development of clinical trials evaluating novel compounds and local treatment in oligo-metastatic patients [134,135].

As regards to the local staging of PCa, it is essential for the surgical planning to evaluate the extracapsular extension and whether or not there is an invasion of seminal vesicles and adjacent organs (bladder, rectum etc) [136]. Recent studies have shown that the T staging accuracy increases with the use of multi-parametric magnetic resonance imaging (mpMRI) [39,137]. In addition, there is a significant improvement in the quality of radiotherapy treatment with the use of mpMRI [138].

Most guidelines recommend CT and/or abdominal MRI and Tc 99m BS with targeted XRays if necessary for N and M staging [39,137].

The aforementioned multimodality algorithm necessitates multiple hospital visits and appointments in different departments (Radiology and Nuclear Medicine), leading to additional times and discomfort for this group of patients (mostly elderly with multiple comorbidities). The delays for the interpretation of all these examinations also have to be considered.

Furthermore, the drawbacks of current staging methods are well-known. Concerning the bone staging, even though Tc 99m BS is still widely used for the detection of metastatic bone disease, various studies have underlined its poor sensitivity and specificity [73,90,118,128]. The lack of specificity implies the frequent use of additional targeted radiographs to distinguish

between malignant and benign causes of BS uptake [88,139]. BS suffers from limited spatial resolution. SPECT and CT can improve this resolution and the specificity, but their sensitivity remains low [140].

Concerning targeted XRays, Tudor et al., demonstrated that even skilled radiologists miss approximately 30% of signs that depict evidence of disease and are likely to over-interpret up to 2% of films that are negative for disease, even though mean accuracy was improved in the light of the clinical information [141].

Regarding to node staging, a meta-analysis by Hövels et al., reported that both CT and MRI perform equally poorly in the detection of LNM from PCa [51]. Normal structures and other pathologic processes can mimic nodal disease. Common pitfalls include small bowel loops in close proximity to the retroperitoneum that can mimic nodal disease, normal ovaries that can be misdiagnosed as external iliac nodal enlargement, aberrant vessels that can be mistaken for a LN especially on non-contrast-enhanced CT and normal anatomic variants such as a left-sided inferior vena cava or duplicated IVC. Finally peritoneal nodules can mimic mesenteric or pelvic LNs and lymphocoeles.

Multimodality algorithms would advantageously be replaced by one step modalities (WBMRI and PET) protocols which have suggested their superiority and allow the rapid assessment of total tumour and all organ evaluation.

Concerning PET-CT, the most commonly used and widely available radiotracer is ^{18}F-FDG that is a non-specific tumour-seeking radiopharmaceutical. The use of ^{18}F-FDG is based on the heightened glycolysis in tumour cells, which provokes a high uptake of ^{18}F-FDG from the tumour. It is known that PCa cells are not ^{18}F-FDG-avid as they have low glycolysis levels and as a result FDG PET modality is poorly efficient [142]. Moreover, kidneys secrete ^{18}F-FDG and as a result there is a physiological uptake by urinary tract. This explains a suboptimal analysis of these organs (kidneys, ureters, bladder, prostate). Choline and more recently PSMA have been developed and are currently the best tools amongst nuclear medicine techniques.

All of the methods mentioned above are irradiating and require the injection of a radioactive product. In rare occasions, as recent chemotherapy or radiotherapy, the interpretation of the PET-CT is difficult.

Regarding WBMRI, even though various studies demonstrated its superiority compared to the current staging methods, there is an important heterogeneity between different countries, centers, or even teams, regarding the anatomic sequences, acquisition planes and duration of the examination (**Table 8**). There is an urgent need for precision and standardization of the protocols, depending on the cancer type and the patient, which is discussed later.

STUDY		CANCER	SEQUENCES
Walker	J Magn Reson Imaging. 2000 Apr;11(4):343-50.	Breast	WB turbo STIR(coronal) Thoracic imaging with respiratory gating
Engelhard	Eur Radiol (2004) 14:99–105	Breast	WB STIR (coronal) Coronal WB STIR cranium: axial T2 TSE spine: T1 FLASH (sagittal)
Schmidt	Eur J Radiol. 2008 Jan;65(1):47-58.	Breast	WB T1 and STIR (coronal) T1 and STIR of the spine (sagittal) HASTE/STIR of the lung (coronal and axial) T2WI and 3Dvibe of the liver (axial) T1FS+C of the abdomen (axial)

Heusner	Eur J Nucl Med Mol Imaging. 2010 Jun;37(6):1077-86.	Breast	WBDWI HASTE with fat suppression of the spine (sagittal) DWI of the spine (sagittal) WB T2 SPAIR (axial and sagittal) WB T2 HASTE (axial) WB T1 in- and opposed-phase (FLASH) (axial) WB T1 volumetric interpolated breath- hold examination (VIBE) +C
Venkitaraman	J Med Imaging Radiat Oncol. 2009 Jun;53(3):241-7.	Prostate	WB T1 and STIR (coronal) Spine T1 and STIR (sagittal)
Gutzeit	Skeletal Radiol. 2010 Apr;39(4):333-43.	Prostate, Breast	WBDWI T1FS+C of the abdomen (axial)
Mosavi	AJR. 2012 Nov;199(5):1114-20.	Prostate	WB T1 and STIR (coronal) DWIBS

Takenaka	J Magn Reson Imaging. 2009 Aug;30(2):298-308.	NSCLC	WB in phase T1 gradient echo sequence -/+C WB opposed phase T1-gradient echo sequence WB sequentially reordered half Fourier multishot STIR
Ohno	Radiology. 2008 Aug;248(2):643-54.	NSCLC	WB in- phase T1-gradient echo sequence -/+contrast WB opposed-phase T1-gradient echo sequence WB sequentially-reordered half-Fourier multishot STIR TSE WB sequentially reordered half-Fourier single-shot STIR SE-planar
Ohno	J. Magn. Reson. Imaging 2007;26:498–509.	Lung	WB in- phase T1-gradient echo sequence -/+contrast WB opposed-phase T1-gradient echo sequence WB sequentially-reordered half-Fourier multishot STIR TSE brain:T1-weighted SE -/+C, T2-weighted fast SE,FLAIR
Squillaci	Abdom Imaging (2008) 33:676–688.	Colon	WB T1 FFE, T2 weighted TSE and STIR TSE, T1 weighted FFE+C (coronal) Thorax,abdomen and pelvis: Multiphasic 3D FFE T1 with fat supression -/+C

Schmidt	Eur Radiol (2009) Jun 19: 1366–1378.	Colorectal	WB T1 and STIR (coronal) T1 and STIR of the spine (sagittal) HASTE/STIR of the lung (coronal and axial) T2WI and 3Dvibe of the liver (axial)
Stecco	Radiol Med. 2013 Apr;118(3):465-75.	Solid tumours	DWIBS
Sohaib	Br J Radiol. 2009 Aug;82(980):632-9.	Renal CA	WB T1 and STIR (coronal)
Giraudet	J Clin Endocrinol Metab. 2007 Nov;92(11):4185-90.	Thyroid	WB STIR and T1(coronal)
Heusner	Eur J Radiol. 2011 Jun;78(3):430-5.	Melanoma, NSCLC	T1 gradient echo sequence and T2 HASTE with fat suppression of the thorax and upper abdomen 3D VIBE T1 +C

Michielsen	Eur Radiol. 2014 Apr;24(4):889-901.	Ovarian	DWIBS WB respiratory triggered T2 TSE (transverse and coronal) Thorax,abdomen,pelvis:3D T1-weighted gradient-echo +C
Eustace	AJR1997;169:1655-1661	Various	WB turbo STIR (coronal)
Steinborn	JCAT 1999;23:123-9.	Various	WB T1 GRE (coronal) Spine turbo STIR and T1 SE (sagittal)
Lauenstein	Eur Radiol. 2002 Aug;12(8):2091-9.	Various	T1 GRE (coronal) HASTE with fat suppression STIR Spine GRE and HASTE (sagittal)
Ghanem	In vivo (2006); 20: 173-182	Various	WB turbo STIR (coronal) Thorax and abdomen: breath-hold technique was used

Nakanishi	Magn Reson Med Sci. 2007;6(3):147-55.	Various	WB STIR and T1(coronal) STIR and T1 of the spine (sagittal) DWIBS
Balliu	Clin Radiol. 2010 Dec;65(12):989-96.	Various	WB T1 and STIR (coronal)
Daldrup-Link	AJR 2001 Jul;177(1):229-36.	Various	WB T1(coronal)
Antoch	JAMA. 2003;290:3199-3206	Various	Chest and abdomen: T1 and T2 T1+C:abdomen(arterialphase)/chest,abdomen(portal phase) /pelvis,thighs head (late venous phase)

Schmidt	Invest Radiol. 2005 Dec;40(12):743-53.	Various	WB T1 and STIR (coronal) T1 and STIR of the spine (sagittal) HASTE/STIR of the lung (coronal and axial) T2WI and 3Dvibe of the liver (axial) T1FS+C of the abdomen (axial)
Schmidt	Eur J Radiol. 2012 Mar;81(3):e269-76.	Various	WB T1 and STIR (coronal) T1 and STIR of the spine (sagittal) HASTE/STIR of the lung (coronal and axial) T2WI and 3Dvibe of the liver (axial) T1FS+C of the abdomen (axial)
Manenti	Eur J Radiol. 2012 Aug;81(8):1917-25.	Various	WB T1-weighted -C (coronal) sequences WB T2- weighted TFE (coronal) DWIBS WB 3D-CE-T1W sequences (THRIVE) (axial)

Akay	J Med Imaging Radiat Oncol. 2013 Jun;57(3):274-82.	Various	DWIBS WB STIR (coronal)
Krohmer	Eur J Radiol. 2010 Apr;74(1):256-61.	Various	WB T2- STIR (axial) WB T1-TSE (coronal)
Komori	Ann Nucl Med (2007) 21:209–215	Various	DWIBS

Table 8. Heterogeneity between teams, regarding WBMRI protocol evaluation for metastatic screening (anatomic sequences, acquisition planes, variety of primary cancers).

VI. SPECIFIC AIMS OF THE DOCTORAL THESIS

SNAPSHOT AT THE BEGINNING OF THE DOCTORAL THESIS

The in-depth literature analysis leads to 3 observations that resulted in the 3 questions addressed in this PhD thesis:
The 3 observations resulted from the in-depth literature analysis, each initiating one of the 3 hypotheses.

1. WBMRI emerges along with PET as a powerful all-organ screening tool, allowing T, N and M staging of cancer in one step. This also seems to be the case in PCa but there is a need for a large-scale review of the literature, in order to determine the value of the different techniques → STEP 1.

2. There is a wide variety of imaging protocols. This also deserves critical review and simplification. Anatomic and functional DWI sequence must be acquired for the N and M staging of oncologic patients. Some confusion exists concerning the choice of anatomic sequence and there is an urgent need for harmonisation → STEP 2.

3. mpMRI is the standard of care for T staging of PCa. Furthermore WBMRI appears very promising for the N and M staging of PCa. The combination of T, N, M staging into an MRI session is evaluated → STEP 3.

Based on the above and after detailed evaluation of the current situation, we built a three-step project to optimize the TNM staging of PCa based on the use of MRI.

Hypothesis 1:

To perform an in-depth investigation and confirm the value of WBMRI as a tool for BM screening by effectuating a critical review of the literature.

We reviewed recent progress on the subject of imaging of BM and investigated the diagnostic performance of WBMRI in comparison to other modalities used for the detection of BM. We synthesized the results of the individual studies into an integrated review. Our objective was to outline the overall picture of the topic, compare the results of different studies and sum up the problems that are currently addressed. Furthermore, we aimed to explain the basis of conflicts - if any-, in order to conclude regarding the best imaging tool for the detection of BM in different types of cancer, the sequences and planes used by the different teams and finally to support the further use of WBMRI in the staging of PCa.

Hypothesis 2:

To develop a fast and reliable anatomic MRI sequence for all organ (N+M) screening. Nowadays, the tendency is to use anatomic and functional DWI sequences for the staging of cancer. The heterogeneity between teams concerns the ‘’anatomic part’’ of the protocol: which are the sequences and the planes that should be used? In order to harmonize this situation

we decided to develop a three-dimensional whole body T1 sequence (3D T1) that can be reconstructed in any plane. We compared this new sequence with currently used MRI sequences (2D T1 WBMRI with or without sagittal proton density fat suppression sequence of the whole spine) for concurrent Bone and Node staging. We wanted to know if this new 3D T1 sequence could be a sufficient anatomic counterpart to WB functional DWI for the one step distant (N & M) staging of PCa.

Hypothesis 3:

To assess the feasibility of an all-in-one MRI session for T,N,M staging
We developed an ‘’All-in-one‘’ MRI protocol for Bone, Node and Local staging of patients with high risk PCa.

This protocol included:
- a 3D T1 anatomic WBMRI sequence for M and N staging
- a whole body diffusion weighted MR sequence (WBDWI) for M and N staging
- an mpMRI for T staging.

We compared the effectiveness to current separate T, N and M work-up, which consists of mpMRI, Thoraco-abdominal CT and BS +/- XRays.

VII. STEP 1

WBMRI and detection of Bone Metastasis: A critical review on diagnostic and comparison to other imaging modalities

A. Objective

Our objective was to provide a critical review concerning the performance of WBMRI for BM screening versus other nuclear medicine or radiologic modalities and derive conclusions from a classification tree and an evidence table. The STARD recommendations (STAndards for the Reporting of Diagnostic accuracy studies) were used for the quality assessment and the evidence tables[143, 144]. A plethora of imaging modalities is available to perform the staging of a cancer. There is an important heterogeneity between studies concerning the methodology, the gold standard and the sequences used and we tried to synthesize the results in order to investigate the diagnostic performance of WBMRI, in comparison to other modalities used for the detection of BM. The objective of the STARD initiative is to improve the accuracy and completeness of reporting of studies of diagnostic accuracy, to allow readers to assess the potential for bias in the study (internal validity) and to evaluate its generalizability (external validity). Five other reviews studying the diagnostic accuracy of MRI for BM detection were found.

B. Materials and methods

A systematic search of the literature was performed to identify studies on WBMRI associated to BM. A sequential search based on keywords under PubMed was performed, as indicated in **Table 9**.

Sequence of the search	Keywords	Number of PubMed References
1	MRI OR MR imaging OR magnetic resonance imaging	408,479
2	Search 1 AND Bone	51,448
3	Metastases OR Metastasis	320,240
4	Search 2 AND Search 3	3,084
5	Whole-body OR Whole Body OR wb OR WBMRI OR WBMRI	76,167
6	Search 4 AND Search 5	301

Table 9. Search performed with the PubMed Advanced Search Builder.

Abstracts of all articles that were identified were reviewed by two authors (V.P., F.L.). In case of disagreement on study eligibility, this was resolved by discussion and consensus. Eligibility criteria of a study were defined as follows: (a) report on the diagnostic value of WBMRI in the detection of BM, (ii) comparison of WBMRI (anatomical sequences) with or without DWI to BS and/or PET and/or PET-CT, (iii) explicit report on the comparison of imaging technique capabilities Se (sensitivity) and/or Sp (specificity) in the same group of subjects, (iv) study of subjects with known primary malignant solid tumours, (v) whole-body imaging study in which at least the area from the neck to the pelvis was imaged, (vi) study where the reference standard did not consist of only one of the tests under comparison, and (vii) study including at least 10 patients. Only English or French language studies were considered. Animal studies, opinion or update articles, case reports, feasibility studies, review studies and meta-analyses, and retrospective studies were excluded. Finally haematological cancers, particularly lymphoma and myeloma, were not included.

The remaining articles were independently reviewed by two authors (V.P., N.M.). A four-step assessment of the studies was undertaken.

A. Information on main study characteristics and results were extracted (listed in **Table 10**), in order to provide a fair overview before evaluation.

B. A review of the reference standard used in each study was performed, in order to identify potential bias in the estimation of techniques capabilities

Se/Sp and to determine whether heterogeneity across studies requires defining of study subsets.

C. A decision tree representing the present situation of studies on WBMRI was constructed (**Figure 12**).

D. The superiority of an imaging technique over its competitors in terms of Se and Sp was evaluated in computing 8 evidence tables (**Table 11**).

Because of the heterogeneity in the studies design and characteristics, methods of evaluation and key data reporting, as well as the limited number of available studies for Se and Sp comparison, no statistical meta-analysis was performed in this review. The criteria for the quality assessment and the evidence tables were based on the STARD recommendations for the amelioration of the quality of reporting of studies of diagnostic accuracy [143, 144].

Study	Cancer	Patients (PP/BM)	Analysis	Modality	Reference standards	Reported conclusions
Antoch[a]	Multiple origins	98 (11/87)	L	MRI PET-CT	Histology and clinical/radiological follow-up	PET CT > wbMRI for TNM staging
Balliu*	Multiple origins	38 (18/–)	P	MRI BS	Clinical follow-up, additional imaging tests and/or biopsy	wbMRI > BS (Se, Sp, Acc) Detects lesions in tissues other than bone
Costelloe	Breast 29 (29/862)		R	MRI BS	Biopsy or imaging studies other than wbMRI and BS	wbMRI > BS (Se) for BM Detects lesions of the liver
Daldrup-Link*	Multiple origins	39 (21/51)	P + L	MRI PET BS	Histopathology for 22 of the 51 BM All BM: clinical and imaging follow-up	WbMRI > BS (Se) for BM WBMRI < PET-CT (Se) for BM
Engelhard[a]	Breast	22 (12/–)	P	MRI BS	Unclear primary origin cross-checked by at least one follow-up study (MRI, BS, CT and X-Rays)	wbMRI tends to have a higher accuracy It should be preferred in patients with high suspicion of metastasis
Eustace	Multiple origins	25 (25/–)	R	MRI BS	Clinical outcome (≥12 months) Additional imaging (CT, 11 patients; MRI, 6 patients) Biopsy (13 patients), Autopsy (1 patient)	wbMRI > BS (Se) for BM
Gutzeit[a]	Prostate (11), breast (25)	36 (7/45)	L	$DWI^{0/1000}$ BS	Consensus reading of all available imaging (DWIBS, CT, MRI, Scintigraphy, PET, PET-CT,US, X-Rays) Oncological follow-up (≥6 months)	DWIBS is not superior to BS for staging More BM are detected with DWIBS
Heusner[a]	Breast	20 (7/268)	P	PET-CT $DWI^{50/600/800}$	BS + other MR sequences + DWI (all patients)	DWI sensitive but unspecific for locoregional or metastatic breast cancer staging
Heusner	Melanoma, NSCLC	109 (11/–)	P	MRI PET-CT	Radiological and clinical follow-up	PET-CT and MRI are equally effective for BM
Jouvet[a]	Melanoma	37 (16/–)	L	MRI + $DWI^{0/800}$ DWI PET-CT CT US	Histology or sequential imaging during clinical follow-up (≥9 months)	wbMRI equivalent to combined CT + PET-CT + lymph node US in diagnostic performance
Kembhavi[a]	Solid small round cell tumors	34 (6/124)	L	PET-CT MRI	Conventional staging and clinical evaluation For BM: PET-CT and BMA/B (30/34 patients) BS with biopsy (4/34 patients)	wbMRI has high diagnostic accuracy
Kumar	Multiple origins	26 (26/–)	R	MRI PET-CT BS	Discordant findings evaluated by Clinical outcome (≥11 months), MRI, Iliac crest biopsy	wbMRI and PET-CT>BS (Se, Sp) for BM
Laurent[a]	melanoma	35 (–/14)	L	MRI PET-CT	Histology or imaging or clinical follow-up	wbMRI with DWI is the most accurate method for detecting secondary lesions

Study	Cancer	Patients (PP/BM)	Analysis	Modality	Reference standards	Reported conclusions
Leboulleux	Multiple origins	79 (36/333)	P + R + L	MRI BS	Discordant findings evaluated by second examination and/or MRI with contrast focused on the skeletal segment involved	Bone staging is recommended with Somatostatin Receptor BS and spine MRI
Lecouvet*	Prostate	100 (100/–)	P	MRI + DWI$^{0/1000}$ BS BS/TXRBS/TXR/CT	Consensus review of available imaging tests (BS/TXR and wbMRI), follow-up ≥6 months	wbMRI outperforms BS and BS/TXR for BM wbMRI performs as well as CT for LM
Ohno*	NSCLC	90 (25/–)	P	MRI PET-CT	Standard imaging, Biopsy, follow-up (≥20 months)	wbMRI as effective as FDG-PET for M-staging of lung cancer patients
Pfannenberg[a]	Melanoma	64 (–/50)	L	MRI PET-CT PET CT	Histology Imaging follow-up (PET-CT, CT, dedicated MRI, US, BS or X-Rays) Clinical follow-up	Whole-body staging is most accurate by combining PET-CT and organ-specific wbMRI
Sakurai*	Thyroid	23 (20/–)	R	MRI + DWI$^{0/800}$ PET-CT MRI	Minimum of 2 imaging modalities (BS, wbMRI, PET, and CT)	Adding DWI improved sensitivity and the overall accuracy of wbMRI for BM
Schmidt	Multiple origins	30 (23/102)	P + L	MRI PET-CT	Radiological follow-up (≥6 months)	wbMRI and PET-CT may improve the detection of BM
Schraml*	Neuroendocrine tumors	51 (41/131)	P + L	PET-CT PET CT MRI	Correlation of radiological, histologic and surgical data Radiologic follow-up (≥12 months)	PET-CT and wbMRI have comparable overall lesion-based but different organ-based detection rates wbMRI > PET-CT (detection rate) for BM and liver M PET-CT > wbMRI (Se) for LM and lung M
Sohaib	renal	47 (15/34)	P + L	MRI BS	Consensus review by 2 radiologists, further imaging and follow-up	wbMRI > BS (Se) for BM
Takenaka*	NSCLC	115 (25/67)	P + L	MRI + DWI$^{0/1000}$ MRI DWI PET-CT BS	Results of initial and follow-up imaging (BS, FDG-PET/CT, wbMRI) Biopsy (n = 52 sites), follow-up	wbMRI with DWI is as accurate as BS and/or PET-CT for BM
Venkitaraman	Prostate	39 (10/–)	P	MRI BS	Initial study of the MRI and BS, other imaging (X-rays, CT) and follow-up	wbMRI did not show a significant advantage over BS

Table 10.

*Statistical significance assessed at p 0.05 with no adjustment for performing multiple comparisons

[a] Qualitative comparison (reported or performed) of techniques' capabilities

PP number of patients positive to bone metastases, BM number of bone metastases

C. Results

Literature search

Three hundred and one studies concerning WBMRI and BM were found following the systematic search on PubMed (**Table 9**). Twenty-four studies were eligible [88,90,117,129,130,131,145,146,147,148,149,150,151,152,153,154,155,156,157,158,159,160,161], while twenty-three presented sufficient data for statistical analysis.

Reference standard

The clinical and imaging follow-up of the patients was used as reference standard. Considering it included all of the studies under evaluation, the reference standard was not completely independent. Hence there were some potential bias for the definition of true negative and for the assessment of Sp. Certain authors did not use the same reference standard for all patients or/and lesions, or performed various additional examinations when disagreement was present between imaging modalities[117, 152, 161]. Confirmation of certain lesions by histologic analysis was present in five studies [117, 129, 146, 151]. The reference standards achieved by the 23 studies were considered as correctly classifying the target conditions (lesion or patient). The characteristics and conclusions of these studies are reported in **Table 10**.

Patient selection

All studies included cancer patients who underwent imaging for staging or evaluation of suspected BM due to symptoms, clinical findings or high levels of tumour markers. Patients with known BM were included in two studies. Engelhard et al. studied patients with suspected BM on XRays or inconclusive findings in BS [88]. Costelloe et al. studied only patients with known BM and hence admitted a favourable bias towards BS [145]. Balliu et al. specified that patients with known BM were excluded [146]. Five studies mention that the patients were newly diagnosed without specifying how [117, 149, 150, 152, 160]. The rest of the studies did not indicate whether the presence of BM was an exclusion criterion or if patient selection was made at the initial staging.

Study characteristics

Sample size

An important heterogeneity was observed concerning the sample size. This has to be highlighted as the strength of the statistical evaluation of the diagnostic performance of imaging techniques depends on the latter. The median number of patients recruited in performance studies was 38 [range: 22; 115]; the median number of patients with confirmed BM was 19 [range: 6; 41] and the median number of BM was 87 [range: 14; 862].

WBMRI planes and sequences

The majority of teams used a whole-body STIR- or T1-weighted imaging in the coronal plane (n = 12/23 for T1 [88, 90, 117, 145,152,156,159,162] and n = 13/23 for STIR [90,131,146,152,153,154,155,156,157,159,160] (**Table 11**). The oldest published study performed only coronal STIR sequences [129]. Seven teams added dedicated sagittal sequences [88,90,117,145,153,157,160]. Two teams did not use the same imaging protocol for all patients [117,152] . Daldrup-Link et al. did not perform STIR in all patients and Kembhavi et al added more sequences when a metastatic lesion was detected [117,152]. Lastly, eight studies included DWI in their MRI protocol [90,145,148,149,151,154,156,162].

Comparative evaluation of the imaging techniques

Repeatability

Out of the 23 studies, 4 reported inter-observer agreement analysis on a per-lesion basis [148,131,151,162]. 2 reported inter-observer agreement analysis on a per-patient basis, and 1 reported intra-observer agreement analysis [90]. The visual detection of BM was assessed according to different scoring scales, using either a 2-point scale (presence or absence of lesion) [151], a 3-point scale [148], a 4-point scale [146], or even a 5-point scale (1 = lesion definitely absent, 2 = lesion probably absent, 3 = lesion equivocal, 4 = lesion probably present, 5 = lesion definitely present) [131,162]. The pertinence of aggregating the results was limited by the complexity of the different scales. Inter-observer agreement was reported to be very good for WBMRI DWI (K = 0.87 [0.66; 1.00] based on three studies [90,151,162]); substantial for

PET-CT (K = 0.75, one study [162]); substantial for WBMRI (K = 0.73 [0.66; 0.90], three studies [146]); substantial for PET (K = 0.70, one study [131]); substantial for DWI (K = 0.66 [0.64; 0.80], three studies[148,151]); and moderate for BS (K = 0.60 [0.26; 0.78], three studies [146,162]).

STUDY	SEQUENCES					
	WB T1 (coronal)	WB STIR or T2 (coronal)	Spine T1 (sagittal)	Spine STIR or T2 (sagittal)	Spine GRE and HASTE	DWIBS
Eustace		x				
Steinborn	x		x			
Walker		x				
Lauenstein	x	x			x	
Engelhard		x	x			
Ghanem	x					
Nakanishi		x	x	x		x
Lecouvet	pelvis and femurs	pelvis and femurs	x	x		
Sohaib	x	x				
Venkitaraman	x	x	x	x		
Gutzeit						x
Balliu	x	x				
Stecco						x
Daldrup-Link	x		x	x (in ten patients)		
Takenaka	x					
Mosavi	x	x				x
Schmidt	x	x	x	x		
Komori						x
Giraudet	x	x				
Ohno	x					
Squillaci	x	x				
Ohno	x	x				
Schmidt (2005)	x	x	x	x		
Schmidt (2008)	x	x	x	x		
Krohmer	x	x				x
Heusner	x	x				
Schmidt (2009)	x	x	x	x		
Manenti	x	x				x
Akay		x				x
Michielsen		x				x

Table 11. Variability of MRI sequences used for bone staging amongst research teams

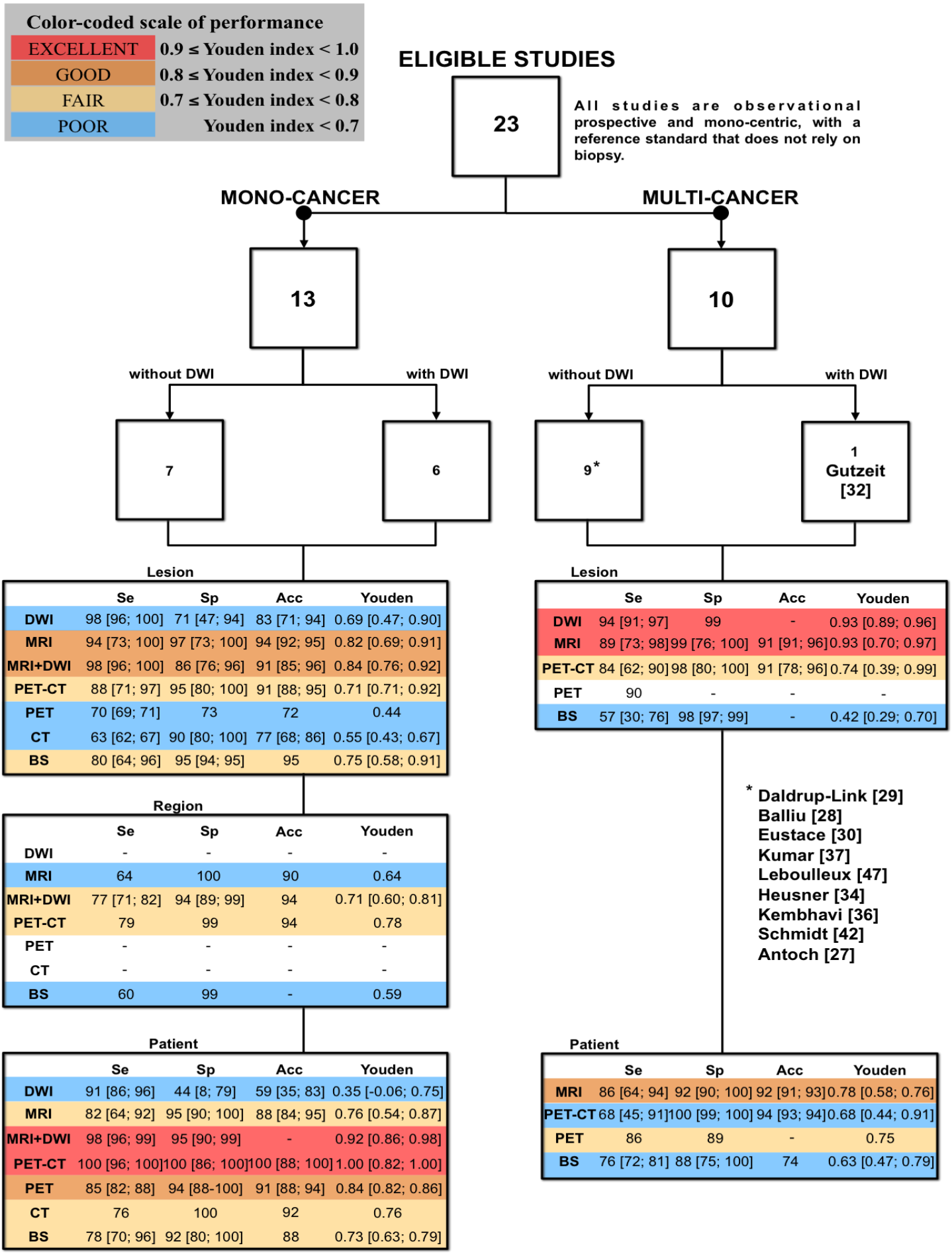

Figure 12 (a). Classification tree

Figure 12 (b). Classification tree

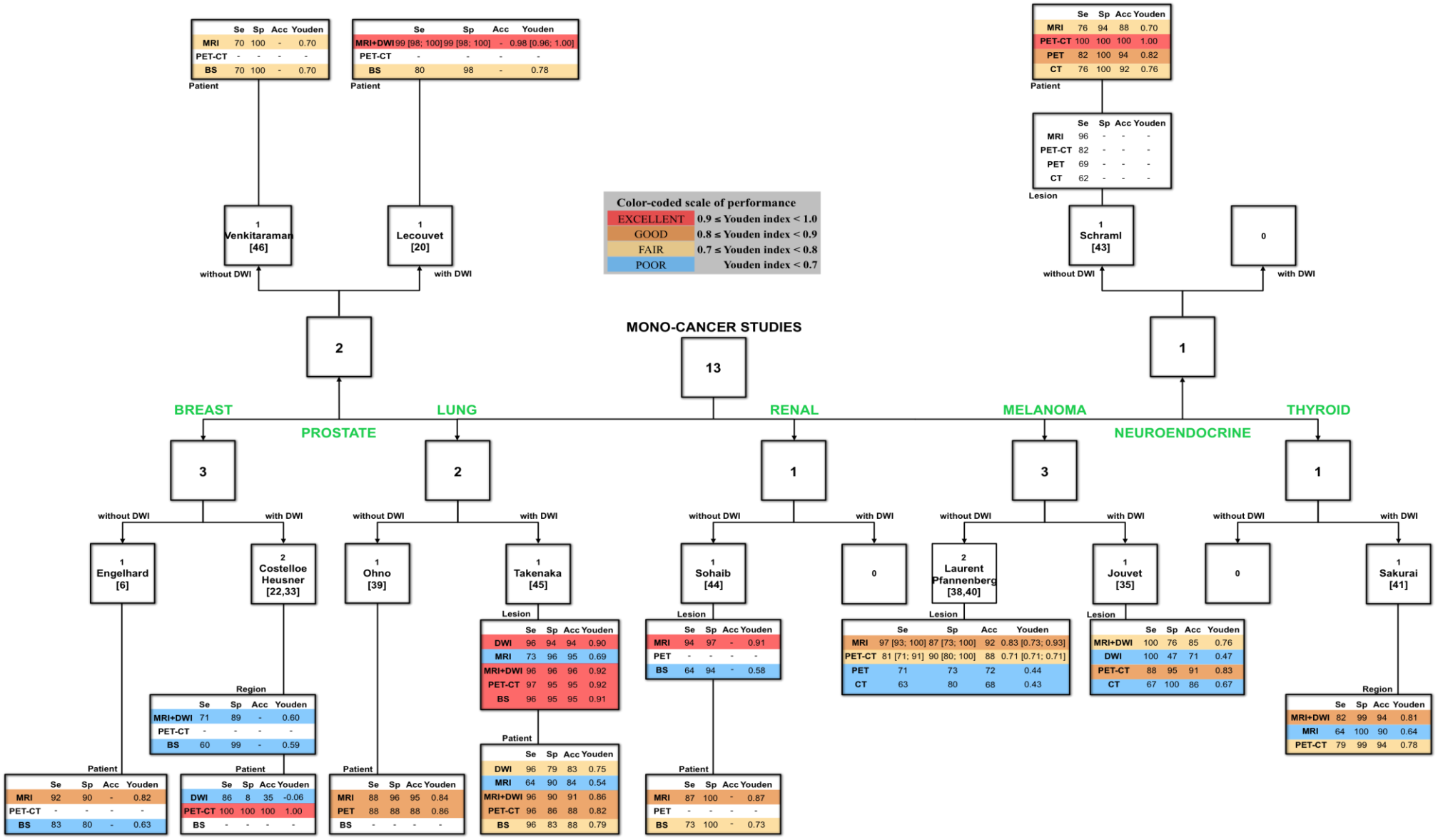

Context

A classification tree was constructed which provided a global overview of the diagnostic accuracy of WBMRI when compared with other imaging techniques used for BM screening (**Figure 12**).

All studies were observational prospective and mono-center studies. There were no multi-center studies. Histopathological confirmation was not used in all patients or all lesions. Half of the teams studied a single cancer and the remaining half addressed several primary cancers. In mono-cancer studies, the performance of the imaging techniques was assessed by three studies for breast cancer (three studies [88,145,149] and for melanoma [151,154,155] and two studies for prostate (two studies [90,160]) and NSCLC (two studies [131,162]). The performance was calculated either on a per-patient-basis, a per-region basis or on a per-lesion-basis. Only one study assessed the imaging techniques on the three bases [161]. Five studies assessed imaging techniques on both a per-patient and a per-lesion-basis [117,157,158,159,162].

<u>Diagnostic accuracy</u>

A color-coded scale of performance was added to the classification tree. Concerning mono-cancer studies, [^{68}Ga] DOTA- TOC PET-CT is the most accurate technique for neuroendocrine tumours [158], WBMRI +DWI or ^{18}FDG PET-CT in thyroid cancer [156], WBMRI in renal tumours [159], WBMRI or PET-CT in melanoma [151,154,155] and WBMRI+DWI or PET-CT or BS in lung cancer [131,162]. In prostate and breast cancers, trends differed for lesion, region and

patient-based analysis. In patient-based analysis of PCa, WBMRI+ DWI is more accurate [90] (**Figure 12**), while WBMRI and BS are reported to be equivalent [160]. In breast cancer, WBMRI+DWI is more accurate in region-based analysis [145], while PET-CT is more accurate in patient-based analysis [163].

When we sum up the information from the classification tree, WBMRI+DWI is superior or equal to other techniques in 5/6 analyses, PET-CT is superior or equal to other techniques in 5/8 analyses, WBMRI is superior or equal to other techniques in 7/11 analyses, DWI alone is superior or equal to BS or PET-CT in 3/6 analyses, BS is superior to WBMRI in 2/6 analyses, and BS is superior to WBMRI+DWI in 0/3 analyses.

Concerning performances in mono-cancer studies (**Figure 12**), the observation of the colour codes suggests that WBMRI+DWI and PET-CT have similar diagnostic accuracy in region and patient-based analysis, while WBMRI (with or without DWI) is superior to other imaging techniques in lesion-based analysis.

In multi-cancer studies (**Figure 12**), WBMRI is superior to other imaging techniques in lesion- and patient-based analysis. In prostate and breast cancers conjoint studies, DWI is more accurate than BS in lesion-based analysis [148].

Capabilities of Se and Sp

According to the evidence table, for the diagnostic value of imaging techniques (**Table 12**), there is strong evidence that WBMRI is more sensitive than BS (4 bSD among 5 SD) [129,153,159,161] but less evidence concerning the superiority of WBMRI in terms of Sp (3 SD against 6 Eq). The superiority of MRI compared to BS in terms of Se, is confirmed when DWI is added (1 bSD among 2 SD) [90,145], while evidence on Sp is balanced. There is strong evidence that DWI is less specific than PET-CT (3 SD) [151,162], while difference in Se is not evident [151].

There is some evidence that WBMRI is more sensitive than PET (1 bSD among 2 SD) [155,158] but limited evidence that WBMRI is more specific (1 SD). There is some evidence that WBMRI is more sensitive than PET-CT (2 bSD) [157,158] and little evidence that PET-CT is more specific than WBMRI (1 SD against 7 Eq). There is insufficient evidence that adding DWI to WBMRI improves its Se compared to PET-CT and very little evidence that it improves its Sp (1 SD against 1 nsSD +2 Eq). The results are consistent with the strong evidence that WBMRI+DWI is more sensitive than WBMRI alone (1 bSD among 3 SD) [156,162] and with the lack of improvement in Sp by adding DWI to WBMRI (1 nsSD against 3 Eq) [156,162].

	MRI superiority	PET superiority	Equivalence
Se	**2 (1)**	**1 + 1**	**1**
Sp	**1 + 1**	**1**	**1**

4 studies: Schraml et al., Pfannenberg et al., Daldrup et al., Ohno et al.

5 Se comparisons and 4 Sp comparisons.

	MRI superiority	PET-CT superiority	Equivalence
Se	**3 (2) + 7**	**3**	**_**
Sp	**_**	**1 + 3**	**7**

10 studies: Kumar et al., Heusner et al., Schmidt et al., Antoch et al., Sakurai et al., Schraml et al., Laurent et al., Kembhavi et al., Takenaka et al., Pfannenberg et al.

13 Se comparisons and 11 Sp comparisons.

	MRI+DWI superiority	PET-CT superiority	Equivalence
Se	**1**	**_**	**3**
Sp	**1**	**1**	**2**

3 studies: Jouvet et al., Sakurai et al., Takenaka et al.

4 Se comparisons and 4 Sp comparisons.

	MRI+DWI superiority	MRI superiority	Equivalence
Se	**3 (1)**	_	**1**
Sp	**1**	_	**3**

3 studies: Sakurai et al., Takenaka et al., Jouvet et al.

4 Se comparisons and 4 Sp comparisons.

	MRI superiority	BS superiority	Equivalence
Se	**5 (4) + 3**	**2**	**3**
Sp	**3 + 1**	_	**6**

9 studies: Balliu et al., Eustace et al., Kumar et al., Leboulleux et al., Engelhard et al., Sohaib et al., Daldrup et al., Venkitaraman et al., Takenaka et al.

13 Se comparisons and 10 Sp comparisons.

	MRI+DWI superiority	BS superiority	Equivalence
Se	**2 (1)**	_	**2**
Sp	**2**	**1 (1)**	**1**

3 studies: Takenaka et al., Costelloe et al., Lecouvet et al.

4 Se comparisons and 4 Sp comparisons.

	DWI superiority	PET-CT superiority	Equivalence
Se	**1**	**1**	**2**
Sp	**_**	**3 + 1**	**_**
3 studies: Jouvet et al., Takenaka et al., Heusner et al. *4 Se comparisons and 5 Sp comparisons.*			

	DWI superiority	BS superiority	Equivalence
Se	**1**	**_**	**2**
Sp	**_**	**1**	**2**
2 studies: Takenaka et al., Gutzeit et al. *3 Se comparisons and 3 Sp comparisons.*			

Table 12. Evidence table demonstrating:
(i) the number and references of comparative studies available, (ii) the number of comparisons of Se/Sp available (which can be different from the number of studies when a particular study includes multiple analyses, such as analyses on a per-patient and a per-lesion-basis of the diagnostic capability Se/Sp), (iii) the frequency of significance levels.

From superior to inferior quality ranking, a red level is given when differences between capability values are assessed at a p value compliant with Bonferroni's correction (bSD), a black level when differences between capability values are assessed at a standard p value <0.05 (SD), a green level when differences between capability values are superior or equal to 5% and are assessed qualitatively, or are reported to be statistically non-significant (nsSD), and a blue level when differences between capability

values are inferior to 5% and are assessed qualitatively, or are reported to be statistically non-significant (Eq). The table can be read as follows: when comparing WBMRI to PET, there is some evidence, based on one Bonferroni-corrected statistical difference (1 bSD, in red) among two statistical differences (2 SD, in black) against one SD plus one non-significant statistical difference (1 nsSD, in green) and one equivalence (1 Eq, in blue), that MRI is more sensitive than PET.

D. Discussion

Depending on the primary cancer, the recommendations for bone staging differ [164]. The most common method for BM detection in breast cancer is BS [165]. Targeted XRays should confirm a positive BS, unless multiple foci are detected. For PCa, staging BS is recommended in patients with a biopsy Gleason score ≥7 or with a PSA >10 ng/ml and palpable disease (cT2/T3) prior to treatment [166]. There are no guidelines concerning non-small cell lung cancer and the necessity of BS [164,167].

<u>Performance of WBMRI</u>

Our data suggest that WBMRI+DWI has a high repeatability and demonstrate high reproducibility, superior to that of PET-CT, WBMRI without DWI and BS. The latter tends to be the least reproducible imaging technique, also when compared to DWI alone.

In terms of diagnostic performance, there is some evidence that WBMRI is a more sensitive imaging technique compared to PET-CT, PET and BS. The

sensitivity of the whole-body examination is improved with the addition of DWI sequence, without improving its specificity. DWI is a very promising technique for the detection of BM [149,156], without being able to confirm this observation due to the limited number of studies assessing its Se and Sp. There is strong evidence that DWI alone is less specific than PET-CT, suggesting that the use of anatomical sequences remains essential in WBMRI protocols.

The review of ”mono-cancer” studies shows that WBMRI+DWI has higher or equal diagnostic accuracy to PET-CT in lesion, region and patient-based analyses. BS is found to be inferior or equal to these two techniques in the three analyses. Adding DWI to conventional WBMRI sequences improves the Se of WBMRI in region-based and patient-based analyses. DWI alone does not demonstrate a sufficiently high accuracy as false positive findings occur.

Multi-cancer studies represent a heterogeneous framework for assessing the capabilities of the different techniques and should be considered with caution if they are used for nuancing conclusions made from mono-cancer studies.

Comparison with other reviews

Five reviews studying the diagnostic accuracy of MRI for BM detection were identified. Three of them provide additional contextual information [105,168,169] and two may appear redundant. One includes studies discussed in this review [170] and the second may be considered redundant or potentially

biased (4/9 of elected studies coming from the same team on the same type of cancer) [171]. Yang et al. reported that ^{18}FDG PET and MRI were equivalent and both significantly more accurate than CT and BS for BM screening, based on 67 multi-cancer studies (before January 2010 and including 7 studies on MRI and 15 on WBMRI) [168]. Based on 16 PCa studies (anterior to November 2012 and including 3 studies on MRI, 1 on WBMRI and 2 on WBMRI+DWI), Shen et al. reported that MRI was superior to choline PET-CT and BS in patient-based analysis, although choline PET-CT had the highest specificity [169]. Based on 11 multi-cancer studies (anterior to September 2010 and including 5 WBMRI studies discussed in our review), Wu et al. reported that DWI had a high sensitivity but limited specificity for the detection of whole-body tumour involvement [105]. The latter is consistent with previous reviews showing that although DWI stands out at detecting bony lesions, it is less capable in soft tissue metastases [172].

It has to be noted that there is currently a lack of studies comparing diagnostic accuracies of WBMRI with PET-CT based on newer tracers such as ^{18}F sodium fluoride [173,174,] ^{11}C-Choline [79,172,175] or Prostate-Specific Membrane Antigen (PSMA) [80,84].

Luboldt et al. compared the effectiveness of a fast DWI to anatomic MR sequences and to ^{11}C-Choline PET- CT and suggested that DWI is equivalent to, if not more sensitive than, the STIR and T1-weighted SE MR sequences and as effective as ^{11}C-Choline PET-CT for the detection of PCa BM [176]. Mosavi et al. evaluated the accuracy of DWI versus NaF PET-CT for the

detection of BM in patients with PCa, concluding that DWI has higher Sp but lower Se [177]. Afshar-Oromieh et al. demonstrated that suspicious PCa lesions present excellent contrast as early as 1 h post-injection of PSMA. In a retrospective analysis of 319 patients who underwent ^{68}Ga-PSMA-ligand PET-CT, the same team found that PSMA is highly specific for PCa and detects the disease in a high percentage of patients (82.8%) [84,85] .

PET-MRI is an innovative diagnostic imaging modality that combines the anatomical information given by MRI and the functional data from PET. Even though there has been great progress in this field, there still remain some issues that need to be resolved. The main pitfalls relate to imaging bias and artefacts due to image distortion [178,179]. The technique is recently introduced and will hopefully help in the comparison of MRI and PET and in the identification of the necessary and sufficient images to obtain, which may differ according to the primary cancer.

Weakness of performance study

There were no multi-center studies, which are crucial before generalization. These studies allow enlarged and homogeneous enrolment of patients for each cancer type. Furthermore, the participation of investigators from different countries, regions, even hospitals offer the guarantee of an objective evaluation, not restricted by local habits and facilitates evaluation of the inter-center repeatability and reproducibility of the technique.

The reviewed studies present different sources of heterogeneity. First of all, the study design and the patients' inclusion criteria, which can affect Se and Sp. An important heterogeneity regarding the gold standard is found between studies and - sometimes - within the same study. When the gold standard does not represent the true disease status, Se/Sp and accuracy are biased [180]. On the other hand, in the context of clinical studies it is neither feasible nor ethical to biopsy all the metastatic lesions, in order to have a histopathological confirmation. As a result, it is acceptable to use the consensus reading of all clinical and imaging follow-up data as gold standard. At this point, the need of standardization of the gold standard has to be highlighted. This problem has to be addressed by a working group of independent clinicians and researchers with experience in the field of oncology, in order to construct a consensus document which could include a list of criteria that have to be fulfilled (minimum follow-up period, appropriate and necessary imaging modalities, scoring system, reading methodology, relevant clinical or/and biological information, etc).

There was substantial heterogeneity concerning WBMRI sequences that vary depending on the team, the hospital, the country as well as the primary cancer. There is an urgent need to determine which sequences are the most appropriate, ''necessary and sufficient'' and cost/time-effective, in order to set a global guideline. Combining whole-body anatomic 3D sequences to DWI is a potential solution [181] .

Limitations of the review

Our work is a “snapshot” of the current situation with conclusions that may change very soon as there are many studies published every month on the topic.

Only a PubMed search based on English and French language was undertaken. The search was updated until mid-November 2014 and a publication bias is possible. Funnel plot analysis was not performed but a crosscheck of the included studies with those of previous reviews, rule out the exclusion of a compliant study.

Our conclusions were drawn from a Youden-indexed classification tree and a four-level reading of statistical reports organized within an evidence table, providing a hierarchical analysis of the accuracy of imaging techniques.

A meta-regression was not performed because of the small number of available studies concerning certain types of cancer and the important heterogeneity in study characteristics. It remains difficult to establish the validity of the distributional assumption on between-study variance, as no random-effect model analysis was performed [182].

CONCLUSION:

Our results suggest that WBMRI is superior to BS for BM detection, independently of the primary cancer. The addition of DWI to WBMRI protocols improves the sensitivity. Still, the need of anatomic sequences is indisputable. Although the diagnostic accuracy of WBMRI and PET-CT appear roughly equivalent, WBMRI is superior in lesion-based analysis. On the other hand PET-CT exceeds WBMRI in patient- based analysis, especially in breast and neuroendocrine tumours. There is a need for new studies comparing WBMRI to PET-CT with new radiotracers as ^{18}NaF, ^{11}C and ^{18}F Choline and labelled PSMA.

Several meta-analyses confirm the performance of MRI and FDG-PET/CT, which are both superior to bone scintigraphy and targeted XRays for the detection of bone metastases in all cancers, on a per-patient and per-lesion basis [168, 183]. Yang et al. found - for all metastatic disease detection on a per-patient basis - that the pooled sensitivity for FDG-PET/CT, CT, MRI and BS were 89.7%, 72.9%, 90.6% and 86.0%, respectively [168]. The pooled specificity for PET/CT, CT, MRI and BS were 96.8%, 94.8%, 95.4% and 81.4%, respectively.

There is a critical need for the future studies to respect the guidelines. There is a lack of multi-center and mono-cancer studies that can help generalize their results.

A considerable advantage of MR imaging is the lack of radiation exposure, contrast injection and its sensitivity to bone marrow infiltration regardless of the primary cancer, when PET-CT relies on the affinity of the cancer for a given tracer.

From a more general perspective, it seems that cancer staging cannot be based on one technique, but it will most likely be shared between WBMRI and PET according to the primary cancer. This scenario is further supported by the perspective offered by both techniques of an all-organ (non-bone limited) screening of metastasis.

The wide variability of anatomic sequences and planes used by different teams led us to the development of a three dimensional WBMRI sequence which could potentially replace the different sequences in the different planes.

VIII. STEP 2

Feasibility and evaluation of Whole body 3D T1 MR imaging

A. Objective

Nowadays and following our critical review of the literature in oncologic imaging, the whole body MRI protocols include two components: the anatomic and the functional. Even though the functional component of the protocol is consistent across teams (Diffusion Weighted Imaging), the anatomic counterpart is highly variable amongst teams. This diversity not only concerns the sequences but also the planes of the acquisition used. ***We developed a three-dimensional whole body T1 Weighted MRI sequence (3D T1) able to study the whole body, in a limited time and with optimized spatial resolution, for bone and node staging of patients with high risk PCa, being sufficient as the only anatomic counterpart of DWI.*** The value of this sequence in terms of image quality (SNR and CNR) was compared to the two dimensional sequence. Finally its diagnostic accuracy for tumoural lesion detection was evaluated.

B. Materials and Methods

Patients

The institutional ethics committee approved this prospective study. Informed consent was obtained from all patients. Thirty consecutive patients with PCa who were considered as high risk for metastases (according to published criteria) were prospectively enrolled between February and December 2012 [39,139,184]. The mean patient age (±standard deviation) was 69 ± 3.3 years. The mean prostate-specific antigen level was 31 ± 28 ng/mL. Three patients were not enrolled because of contra-indications to MR imaging.

MR Imaging

All patients were imaged with a 3.0-T MR unit (Magnetom Verio; Siemens Medical Solutions, Erlangen, Germany). Patients were placed on the imaging table headfirst in the supine position and were covered with a head and neck coil, spine coils, and two six-element body matrix coils. A coronal two-dimensional whole-body T1-weighted MR imaging pulse sequence (2D T1), a sagittal proton density fat suppression sequence of the whole spine (PDFS), a diffusion-weighted MR imaging sequence (DWI), and a three dimensional whole-body T1-weighted pulse sequence (3DT1) were performed. The characteristics of the pulse sequence were the following: a 3D turbo spin-echo SPACE (sampling perfection with application optimized contrast using different flip angle evolutions) pulse sequence

was implemented to get high spatial resolution and high contrast resolution in T1, while limiting both the specific absorption rate and the acquisition time [6]. An elliptic k-space filter was applied. Then, in-plane spatial resolution was chosen so as to be the closest to that of the 2D pulse sequence and to be "as isotropic as possible." As a result, voxel size after acquisition and reconstruction were, respectively, 1.14 × 1.43 × 1.20 mm^3 and 0.57 × 0.57 × 1.20 mm^3 for whole-body 3DT1-weighted imaging, 1.04 × 1.30 × 4.00 mm^3 and 1.04 × 1.04 × 4.00 mm^3 for whole-body T1-weighted imaging, 0.81 × 1.01 × 4.00 mm^3 and 0.81 × 0.81 × 4.00 mm^3 for spine PDFS imaging, and 3.52 × 4.42 × 5.00 mm^3 and 1.76 × 1.76 × 2.70 mm^3 for whole-body diffusion-weighted imaging.

Other imaging parameters are detailed in **Table 13**.

	3DT1	2DT1	2DT1+PDFS	WBDWI
Acquisition time (min)	18.5 (4x4.6)	6 (4x1.5)	5.4 (3x1.8)	15.8
Sequence	3D SPACE (spin echo)	TSE T1	TSE	Diffusion
Plane	CORONAL	CORONAL	SAGITTAL	AXIAL
Slices / Thickness / Gap	176 / 1.2mm / -	50 / 4mm / 0.4mm	13 / 4mm / 0.4mm	25 / 5mm / 0.5mm
FOV / Acquisition matrix	440x307 / 214x384	400x306 / 384x307	260x260 / 256x320	430x366 / 83x122
Phase encoding	Feet-Head	Feet-Head	Feet-Head	Anterior-Posterior
IPAT factor	3	3	2	2
Phase oversampling	0.5	1	1	0
TR / TE / NSA / TF	400 / 13 / 2 / 58	600 / 9.4 / 1 / 4	2600 / 45 / 2 / 13	4500 / 68 / 5 / -
Flip angle	variable	140°	147°	130°
Bandwidth	407 Hz/pixel	260 Hz/pixel	2050 Hz/pixel	255 Hz/pixel
Fat suppression technique	-	-	FAT SAT	SPAIR
Specific parameters	-	-	-	b-values: 0 / 800

Table 13. Specific parameters of 3DT1. IPAT = integrated parallel acquisition techniques, SPACE = sampling perfection with application optimized contrast using different flip angle evolutions, SPAIR = spectral adiabatic inversion recovery, TE = echo time, TR = repetition time, TSE = turbo spin-echo, WBDW = whole-body diffusion-weighted imaging, WB2D = whole-body 2D imaging, WB3D = whole-body 3D imaging.

Image Analysis

Lesion definition

External, internal, common iliac, inguinal, periaortic, and pericaval nodes were defined as abnormal when the short-axis diameter was larger than 10 mm, when there was loss of the normal oblong kidney bean shape and of the fatty hilum, or an irregular outline. In perivisceral (perivesical, perirectal, etc) locations, a node was defined as abnormal when the short-axis size was larger than 8 mm [185,186].

A metastasis was defined as a low signal intensity lesion larger than 8mm on T1WI and as a high signal intensity lesion on PDFS images. The DWI was used as an addition to the anatomic sequences [91,139].

In the absence of a histologic gold standard, as the biopsy of all lesions was neither possible nor ethical, we used the best valuable comparator (BVC) as standard of reference. BVC is a panel of reference, consisting of the CT correlation of equivocal MRI findings, prospective systematic follow-up BS and MRI studies at 6 months, and clinical and biologic follow-up obtained during 6 months of follow-up. All of the material was reviewed afterwards by all of the specialists (radiologists, nuclear medicine physicians and urologists) who concluded in consensus to the final diagnosis for each patient, in terms of bone and node metastasis.

Quantitative image analysis

For the assessment of the image quality of 3D and 2D T1 sequences, both signal-to-noise ratio (SNR) and contrast-to-noise ratio (CNR) in regions of interest (ROIs) within lesions and corresponding reference tissues were calculated by one physicist and one radiologist. The reference ROI for the spine was placed in the bone marrow of an uninvolved lumbar vertebra (L5 or closest uninvolved) (**Figure 13A**). For the pelvis, the reference ROI was chosen in the bone marrow of a non-metastatic ischiopubic ramus (**Figure 13B**). For LNs, a reference ROI was chosen in the local-regional fat. For the calculation of CNR, the largest bone and node lesions from each anatomic area were used and the largest possible ROI that fitted the lesion and/or tissue of interest was chosen (**Figure 13C**), without including the bone cortices and anatomic limits of LNs. The standard deviation of the noise (σ) was estimated from a ROI defined outside the body (a large area that contained only air) (**Figure 13D**). The SNR was then calculated according to the following equation: $\underline{SNR} = 0.66 \times S/\sigma$, where S is the mean signal intensity from the reference region and 0.66 a correction factor that takes into account the fact that the noise is governed by the Rayleigh distribution [187]. The CNR was estimated according to a similar equation, as follows: $\underline{CNR} = 0.66 \times (S^{lesion} - S^{reference})/\sigma$.

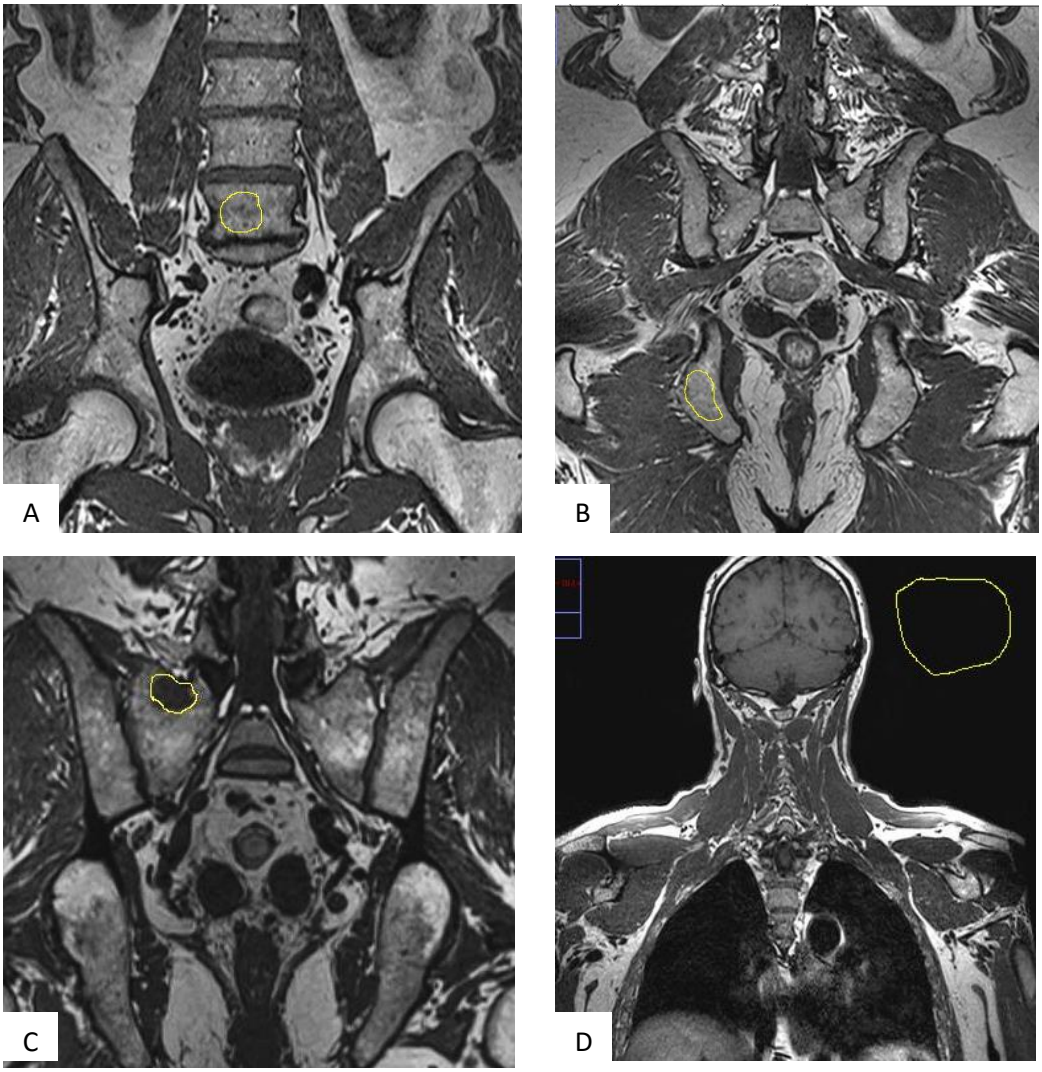

Figure 13. The reference ROI was placed in uninvolved bone marrow of lumbar vertebrae for the spine (A) and in uninvolved bone marrow of an ischiopubic ramus for the pelvis (B). For the calculation of CNR the ROI was positioned in the largest lesion of every region (C). The standard deviation of the noise was calculated by placing a ROI in an area containing only air (D).

Qualitative image analysis

All the sequences were analysed by two radiologists independently and blindly (F.E.L. [observer 1] and V.P. [observer 2], with 15 and 3 years of experience, respectively, in musculoskeletal and oncologic imaging). The whole-body 2DT1 sequence was read during the first reading, the 2DT1 plus PDFS images were read during the second reading, and the 3DT1 images were read during the third reading. Reading of 3D T1 sequence was performed with use of multiplanar reformation. The three readings were performed at 3-week intervals and were randomized. Readings were performed with a picture archiving and communication system workstation (Carestream Vue; Carestream Health, Rochester, NY). The number and location of node and /or BM were recorded for each reading.

Statistical Analysis

The image quality with the 2DT1 and 3DT1 sequences was assessed by comparing the SNR measured in two reference regions (bone and fat) and by comparing the CNR in two common metastatic sites (bone and node). A Wilcoxon rank sum test was performed to assess statistical differences. A Bonferroni-type correction for performing multiple comparisons was then applied. As a result, $P < 0.025$ was regarded as indicative of a statistically significant difference.

For the estimation of the performance of the different MRI sequences, Receiver Operating Characteristic (empirical receiver operating

characteristic) analysis was carried out on a per-patient basis [188]. A pairwise comparison of the areas under the receiver operating characteristic curve (AUCs) was made to rank sequences according to their diagnostic performance [189]. The diagnostic performance of each MR imaging sequence was assessed on a per-lesion basis, followed by a McNemar test to rank sequences according to their sensitivity [190]. Because of the multiple comparisons, $P < 0.0083$ was regarded as indicative of a statistically significant difference.

For each MRI sequence the inter-observer agreement on a per-patient basis was calculated according to the Scott pi and its associated 95% confidence interval (CI) [191]. The per-lesion based inter-observer agreement of the MRI sequences, was evaluated based on the intraclass correlation coefficient on the basis of a two-way model in which systematic differences are relevant and its associated 95% CI . Agreement was interpreted as follows: scores of 0 or less were indicative of poor agreement, 0.01–0.20 slight agreement, 0.21–0.40 fair agreement, 0.41–0.60 moderate agreement, 0.61–0.80 substantial agreement, and 0.81 or greater very good agreement [192]. The sample size was not prospectively planned, as the study was exploratory.

C. Results

Patient Population

Ten patients had BM and thirteen LNM according to the standard of reference. There were forty-one bone lesions and thirty-six node lesions.

Quantitative Image Analysis

3DT1 sequences presented significantly higher SNR and CNR compared to 2D T1 (**Table 14** and **Figure 14**), regardless of the region analysed ($P < 0.025$).

		N	2DT1		3DT1	
			M	IQR	M	IQR
SNR	Ref Bone	42	85	60	234	284
	Ref fat	12	99	50	260	360
CNR	Tum Bone	13	47	41	143	104
	Tum lymph	12	52	33	155	228

Table 14. The number of ROIs represents cases for which SNRs and CNRs could be calculated. In six patients considered for analysis, some thresholding was automatically performed on the saved data, yielding a standard deviation of 0 for the noise ROIs. Hence the number of measured ROIs fell to the number of used ROIs. For the SNR, the number of used ROIs fell from 55 to 45 (reference bone) and from 13 to 12 (reference fat). For the CNR, the numbers fell from 19 to 13 (lesion/bone) and from 13

to 12 (lesion/node). Data are medians and dispersion values (interquartile ranges).

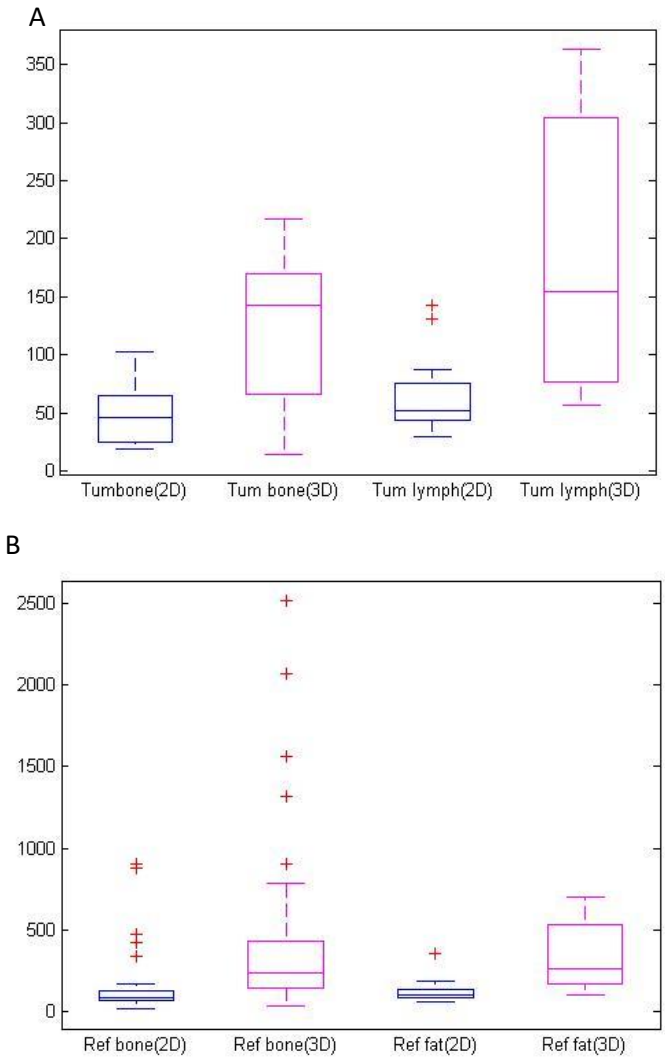

Figure 14. Boxplots for SNR (A) and CNR (B) calculations. 3DT1 sequences presented significantly higher SNR and CNR compared to 2D T1.

3DT1 had a significantly higher performance compared to 2DT1 and 2DT1+ PDFS for the detection of node metastases on a per-patient basis (observer 1 : AUC = 1.00 for 3DT1, 0.81 for 2DT1 + DPFS imaging, and 0.73 for 2DT 1, with $P < 0.001$ for 2DT1 vs 3DT1 and $P = 0.006$ for 2DT1 +PDFS vs 3DT1; observer 2:AUC = 1.00 for 3DT1, 0.81 2DT1+PDFS, and 0.81 for 2DT1, with $P = 0.006$ for 2DT1 vs 3DT1 and $P = 0.006$ for 2DT1+PDFS vs 3DT1), whereas no significant difference was observed between sequences for detecting patients with bone metastases ($P \geq 0.317$ for all) (**Table 15**, **Figures 15** and **16**).

Observer	Per-patient Analysis*		Per-lesion Analysis†	
	Bone Metastasis	Node Metastasis	Bone Metastasis	Node Metastasis
1	2D T1-weighted imaging, 2D T1-weighted imaging + PDFS, 3D T1-weighted imaging	3D T1-weighted imaging	2D T1-weighted imaging + PDFS, 3D T1-weighted imaging	3D T1-weighted imaging
2	2D T1-weighted imaging, 2D T1-weighted imaging + PDFS, 3D T1-weighted imaging	3D T1-weighted imaging	2D T1-weighted imaging + PDFS, 3D T1-weighted imaging	3D T1-weighted imaging

Table 15. Pairwise Comparisons of Diagnostic Performance of MR Imaging Sequences.

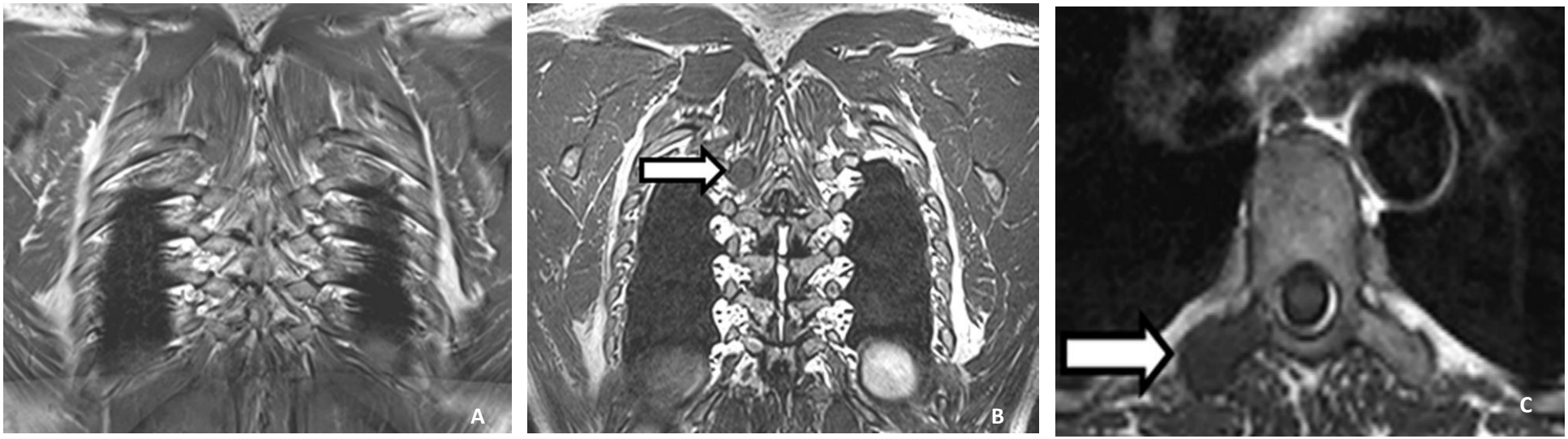

Figure 15. Detection of a BM in a 63 year old PCa patient. The lesion was not seen on 2DT1 sequence (A) but correctly identified by 3DT1 sequence (B). Axial reconstruction obtained with multiplanar reformation at same level confirms the presence of a BM (C).

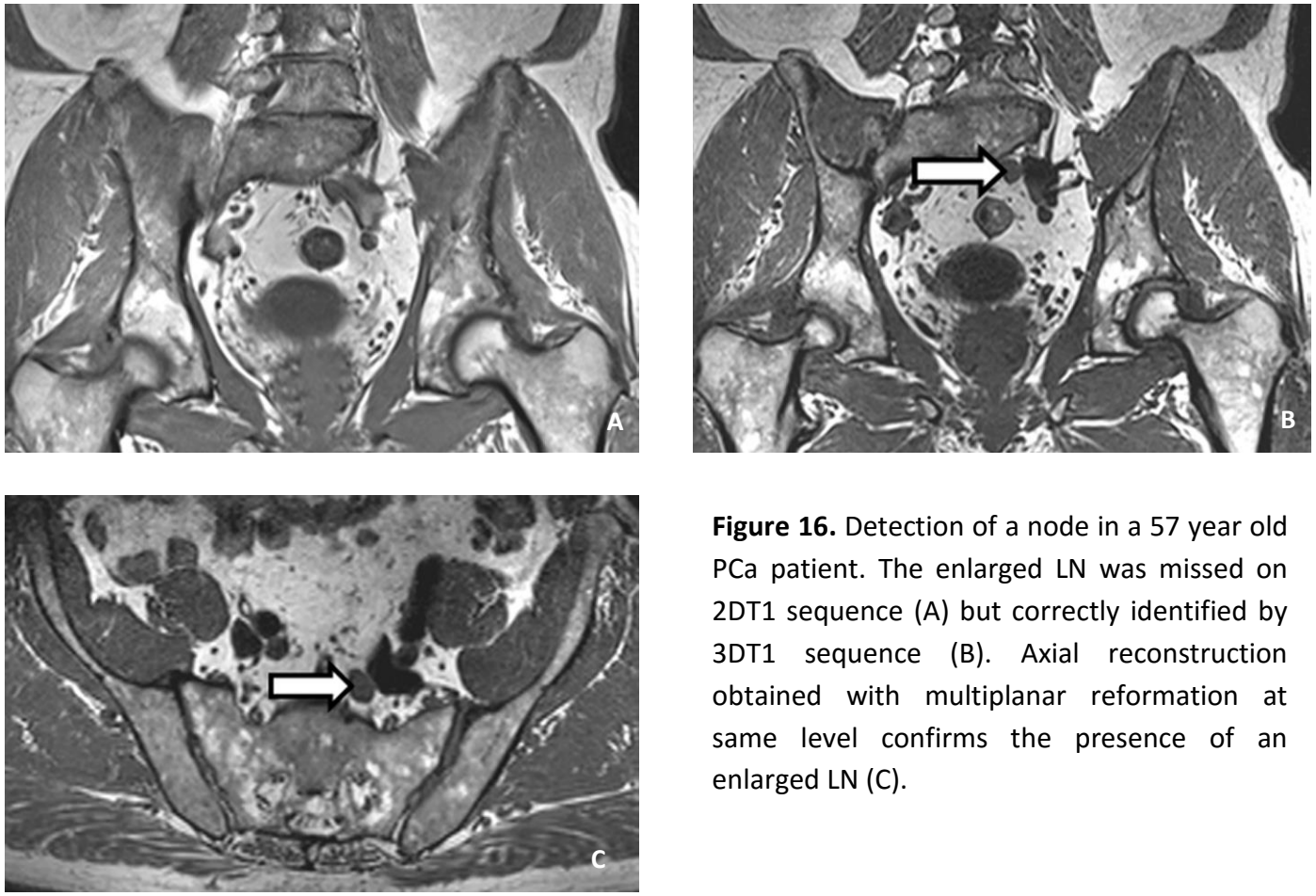

Figure 16. Detection of a node in a 57 year old PCa patient. The enlarged LN was missed on 2DT1 sequence (A) but correctly identified by 3DT1 sequence (B). Axial reconstruction obtained with multiplanar reformation at same level confirms the presence of an enlarged LN (C).

On a per-lesion basis, whole-body 3DT1 had a significantly higher sensitivity than 2DT 1 and 2DT1+PDFS for detecting LNM (observer 1: sensitivity = 100% for 3DT1, 44% for 2DT1+PDFS , and 33% for 2DT1, with *P* < .0001 for 2DT 1vs 3DT1 and *P* < 0.001 for 2DT1+PDFS vs 3DT1; observer 2: sensitivity = 92% for 3DT 1, 39% for 2DT1+PDFS, and 39% for 2DT 1, with *P* < 0.001 for 2DT 1 vas 3DT1 and *P* < 0.001 for 2DT1+PDFS vs 3DT1), while whole-body 2DT1 had a significantly lower sensitivity than 3DT1 and 2DT1+PDFS for detecting BM (observer 1: sensitivity = 98% for 3DT1, 83% for 2DT1+PDFS, and 63% for 2DT1, with *P* < 0.001 for 2DT1 vs 2DT1+PDFS and *P* < 0.001 for 2DT1vs 3DT1 ; observer 2: sensitivity = 100% for 3DT1, 85% for 2DT1+PDFS, and 68% for 2DT1, with *P* = 0.008 for 2DT1 vs 2DT1+PDFS and *P* < 0.001 for 2DT 1 vs 3DT1).

Inter-observer Agreement

For the detection of patients with BM, inter-observer agreement was very good for all the sequences (**Table 16**). On a per-lesion basis, inter-observer agreement in the detection of BM was very good for all the sequences (**Table 17**). For the detection of BM the inter-observer agreement ranged from substantial to very good.

	M lesions		N lesions	
	Disagreement	Scott's pi	Disagreement	Scott's pi
2DT1	0/30	1.00 [0.74 - 1.00]	2/30	0.82 [0.44 - 0.95]
2DT1+DPFS	2/30	0.85 [0.53 - 0.96]	4/30	0.66 [0.28 - 0.86]
3DT1	0/30	1.00 [0.74 - 1.00]	0/30	1.00 [0.77 - 1.00]

95% CI is given in brackets

Table 16. Inter-observer agreement for patient-based analysis.

	M lesions	N lesions
	ICC	ICC
2DT1	0.988 [0.975 - 0.994]	0.876 [0.757 - 0.939]
2DT1+DPFS	0.993 [0.985 - 0.007]	0.639 [0.365 - 0.811]
3DT1	0.993 [0.986 - 0.997]	0.965 [0.928 - 0.983]

95% CI is given in brackets

Table 17. Inter-observer agreement for lesion-based analysis.

D. Discussion

WBMRI is a non-invasive technique free from ionizing radiation and with high resolution for bone marrow and soft tissues. Hence it is a technique which is widely used in oncology. It is known that a precise tumoural staging is crucial for the clinical management of oncologic patients.

It has been demonstrated that MRI is a highly sensitive method for early detection of BM, as it allows the identification of malignant cells in the bone marrow, before bone remodelling. Walker et al. support that WBMRI represents a convenient and cost effective method for the screening of patients with breast cancer [127].

Tc 99m bone scintigraphy is widely used for the detection of metastatic bone disease even though it has been demonstrated by various studies that MRI has a higher specificity and sensitivity [118]. Daldrup-Link et al., demonstrated that WBMRI has a higher sensitivity than BS for the detection of bone marrow metastatic disease in children and young adults [117]. Schmidt et al., showed that in patients with breast cancer and suspicion of recurrence, WBMRI and PET-CT have an overall diagnostic accuracy of 91% for lesion detection [193] .

A wide heterogeneity exists regarding WBMRI protocols between teams, which largely depends on the target cancer. For the examination of the whole skeleton in patients with cancer, a coronal 2D MR imaging pulse sequence and a sagittal pulse sequence on the spine are most commonly used. The sagittal sequence of the spine is strongly recommended to detect small vertebral lesions and potential complications of the metastatic

disease (i.e., fractures and spinal cord or spinal nerve compression) [194]. The use of an axial sequence has been proposed in order to study the skull, the scapula, ribs and sternum [159,195].

The potential to overcome the limitations mentioned above is offered by three-dimensional imaging. The imaging time can be limited by avoiding the repetition of the same sequence in different planes. The use of 3D imaging offers the possibility of multiplanar reconstruction and reduces partial volume effects from section thickness and intersection gaps, therefore provides both high-spatial-resolution images and multiplanar reformation capability [196,197]. The available 3D reconstruction softwares offer various image post-processing algorithms such as multiplanar reconstruction (MPR) maximum intensity projection (MIP), minimum intensity projection (MinIP), volume rendering and shaded surface display. It takes a senior reader almost 15 minutes for the interpretation of the WBMRI protocol with the 3DT1 sequence, while the same reading takes a junior reader approximately 18-20 minutes.

The long acquisition and post-processing times had, until recently, as a result the limited use of 3D sequences; however, the development of more effective imaging techniques and high-performance MR imaging workstations has allowed the overcoming of these problems. The hardware used mainly depends, on one hand on the kind of radiofrequency (RF) receiving coils and the availability to combine them together and on the other hand on the patient table characteristics and performance. The MR signal is received either by the transmitter body coil, or by a combination

of a set of only receiver multi-channel surface coils. In order to optimize the signal-to-noise ratio (S/N) and to minimize the imaging time, the second solution is the optimal, because it allows the simultaneous coverage of the whole body using local coils, which produce a high SNR, and enables excellent image quality as well as fast imaging. Additionally, regarding the table, an important point resides in the possibility to connect several receiving multi-channel coils together, in order to optimize the patient anatomy coverage. Another important feature is the efficient control of the patient table movement.

The reduction of the duration of the sequence is crucial. Increasing the slices' thickness from 1 to 1.5mm can reduce the time of the acquisition but with subsequent loss in isotropy and quality of image. Another way to reduce the duration of the sequence is to increase the PI (parallel imaging) acceleration factor (we already operate in parallel imaging with an acceleration factor 3). Most modern MR systems are built in a parallel architecture, consisting of a body transmit coil and set of local receiver coils that feed into parallel channels for signal amplification and processing. In PI, information about coil positions and sensitivities can be used to reduce the number of phase-encoding steps and speed up imaging. This is quantified by the PI acceleration factor (typically between 2 and 6). The temporal and spatial resolution requirements - the field strength at which the study is performed and the object of interest - all lead to the decision to use PI acceleration.

The major advantages of PI:

-Significant reduction of image acquisition time. This is inversely related to the acceleration factor (R). If R=2 then image acquisition time is cut in half.

-Reduction in susceptibility artefacts. The PI acquisition and reconstruction process lessens phase-related distortions in the MR signal. This is especially advantageous in echo-planar sequences.

It has to be noted that our goal was to optimize the morphological sequence that should complement the functional DWI sequences, rather than directly comparing the two types of sequences. Morphological and functional sequences have indeed shown their complementarity in previous works and we did not intend to confirm those previous findings. Of course we did take into account findings from the DWI sequences in defining the gold standard used to compare the diagnostic performance of the morphological sequences. A future goal will be to study the accuracy of DWI sequence alone, to compare it with individual anatomic sequences (T1, STIR, etc), and its added value over WBMRI protocols using solely anatomic sequences.

Our study had several limitations. First, the enrolment of a larger number of patients is mandatory to validate the present results. The inclusion of patients is still on-going in our department as part of this project, and multicenter acquisitions and readings are planned for large-scale validation. Another limitation is the limited body coverage (top of head to

upper thighs), although the risk of missing significant peripheral metastasis is very low [91]. Finally, the relatively short follow-up period and the use of a "best valuable comparator" as a standard of reference must be underlined. This standard of reference represents the best achievable "truth" in the absence of systematic histologic proof and is used in many studies evaluating metastasis detection [177] .

E. CONCLUSION

We developed and introduced to clinical practice a -to the best of our knowledge- original 3D approach of WB coverage using a 3D T1 weighted MRI sequence. Our goal was to combine the advantages of 3D and WB imaging in one sequence. According to our results, 3DT1 sequence can potentially replace the anatomic sequences currently used for the M and N staging of PCa.

With the use of 3D T1, which can be reconstructed interactively in every plane, we tried to simplify the MRI protocol of oncologic patients by eliminating the use of additional planes as sagittal and axial.

Our results confirm that SNR and CNR are significantly higher on 3DT1 than 2DT1 images. On 3DT1 reading, significantly more patients with node metastasis are detected than on 2D T1 with or without PDFS. Concerning the number of metastatic lesions detected by the observers, we observe that less metastatic bone or node lesions are missed on 3D T1 readings

than on 2D T1, but this result is not statistically significant. This could be explained by the small sample size.

Our study also showed that the inter-observer agreement with the 3DT1 sequence was higher than that with 2DT1 for the detection of node metastasis on a per-patient and a per-lesion basis. Only limited discrepancies were noted between observers with 3DT1 in the detection of LNs, which may be difficult on 2DT1. The agreement was also very good for detecting BM.

Our next objective will be the amelioration of the resolution of this sequence to 1mm slice thickness, in order to improve even more the quality of image and its diagnostic accuracy for BM and LNM detection. Also we could expand the field of view to cover the whole body and not only from head to thighs, even though the vast majority of BM is limited to the axial skeleton. Last but not least, our next goal will be the limitation of the duration of the sequence to less than 15 minutes. It is known that in order to reduce the acquisition time the quality of image has to be compromised. In order to reduce the time we can increase the slice thickness. Also the TR, TE and NSA can be reduced but this reduces the SNR. By reducing the matrix size the spatial resolution will be lowered. A trick to achieve high spatial resolution in a reasonable time is by reducing the field of view only in the phase encoding direction. This is possible because spatial resolution is determined by the matrix size in the

frequency encoding direction while scan time is determined by the matrix size in the phase encoding direction.

For our next step, we combined this new sequence with a whole body DWI and with a multiparametric MRI of the prostate in order to evaluate the feasibility of a TNM staging of PCa in one single MRI session.

IX. STEP 3

One-step TNM staging of high-risk PCa during a unique MRI session

A. Objective

MpMRI is the standard for local (T) PCa staging. WBMRI is effective for the metastatic screening. ***This study assesses the feasibility and value of an "All-in-one" TNM staging combining mpMRI of the prostate and WBMRI including DWI and an optimized 3DT1 sequence described in previous step.***

B. Materials and Methods:

Patients' characteristics

This study was approved by the institutional ethics committee. Informed consent was obtained from all patients. We enrolled 30 newly diagnosed patients with "high-risk" PCa (PSA>20 ng/ml, Gleason≥ 8, or T stage≥ 3a [39]. Median age was 63 years (range: 51-92). Median baseline PSA was 30 ng/ml (range: 1.7–4612). Gleason sum was ≤7 in 13 patients, 7 in 12 and ≥8 in 17 patients. 3 patients were treated by radical prostatectomy, 16 by a combination of EBRT and ADT and 11 by ADT alone, after staging. AJCC clinical stage was cT2 in 7 patients, cT3 in 14 patients, and cT4 in 9 patients (**Table 18**).

	Treatment			
	ADT (N = 11)	EBRT + ADT (N = 16)	(N = 3)	Total (N=30)
Age (years)				
Median	62.0	63.5	58.0	62.5
Range	53.0–92.0	54.0–80.0	51.0–66.0	51.0–92.0
50%range	55.0–66.0	57.5–69.0	51.0–66.0	56.0–69.0
Mean (SD)	64.18 (11.02)	64.06(7.25)	58.33(7.51)	63.53 (8.72)
PSA (ng/ml)				
Median	21.7	37.9	72.7	30.0
Range	1.7–4612.0	4.7–206.0	9.0–126.0	1.7–4612.0
50%range	6.8–60.5	15.9–134.5	9.0–126.0	12.0–99.0
Mean (SD)	470.73 (1,377.31)	70.01 (72.82)	69.24 (58.58)	216.87 (834.09)
Gleason sum				
6	1 (9.1)	0 (0.0)	0 (0.0)	1 (3.3)
7	2 (18.2)	7 (43.8)	3 (100.0)	12 (40.0)
8	4 (36.4)	5 (31.3)	0 (0.0)	9 (30.0)
9	4 (36.4)	4 (25.0)	0 (0.0)	8 (26.7)

Table 18. Patient demographics: 30 PCa patients at high risk of metastasis.

Imaging

All patients were imaged with a 3.0-T MR unit (Magnetom Verio; Siemens Medical Solutions, Erlangen, Germany). The mpMRI of the prostate consisted of high resolution T2 weighted images (T2WI) in three planes (axial, sagittal and coronal) for the analysis of the prostate's zonal anatomy and capsule, dynamic contrast-enhanced MRI (DCE MRI), diffusion weighted imaging (DWI) and apparent diffusion coefficient (ADC) maps,

and post-contrast axial T1 weighted images of the pelvis for the study of regional LNs. At the same time and during the course of the same imaging session, the patients underwent a WBMRI exam consisting of anatomical T1-weighted MR images and DWI sequences (**Table 19**).

Image analysis

Figure 17 demonstrates an example of the reporting sheet of ''All-in-one'' protocol.

Local staging:

Two radiologists using the published PI-RADS criteria from the European Society of European Urology (ESUR) interpreted the mpMRI of the prostate[18] (**Figure 18**). The ADC values of every suspect lesion, as well as the maximum diameter of the largest lesion were recorded. As described in the literature, DCE curves were classified into one of three enhancements: type one with persistent increase of the enhancement; type two with no change in enhancement over time (plateau); type three, the most typical pattern for cancer, with fast enhancement and early wash-out [198].

Distant staging

WBMRI studies were read by two radiologists, recording BM and enlarged LNs according to previously published criteria [185,186].

TARGET	ACQUISITION	ACQUISITION TIME (MIN:SEC)	SEQUENCE TYPE	PLANE	SLICES, THICKNESS, GAP
PROSTATE	T2	02:24	TSE	SAGITTAL	21x 3mm, 0.3mm
		03:35	TSE	TRANSVERSE	30x3mm, 0.9mm
		02:00	TSE	CORONAL	18x3mm, 0.9
	DWI	03:14	Diffusion	AXIAL	20x5mm, 0.5mm
	DCE	04:07	3D FLASH	AXIAL	24x3mm
	VIBE	00:18	3D FLASH	AXIAL	72x3mm
WHOLE BODY	T1WI 3D (body)	18:28 (4x 4:37)	3D SPACE (spin echo)	CORONAL	176x1.2mm
	DWI (body)	15:45	Diffusion	AXIAL	25x5mm, 0.5mm
	PROTON DENSITY (spine)	05:24 (3x1:48)	TSE	SAGITTAL	13x4mm, 0.4mm

TARGET	FOV, ACQUISITION MATRIX	TR, TE, NSA, TF	FAT SATURATION	SPECIFIC PARAMETERS
PROSTATE	130x130, 192x192	3560, 127,1, 21	/	/
	240x240, 304x384	3200, 136, 2, 19	/	/
	240x240, 304x384	4790, 136, 2, 19	/	/
	380x326, 110x128	5500, 69, 3	SPAIR	b-values: 0, 50, 600, 1200
	400x300, 173x256	4.04, 1.35, 1	Q FAT SATURATION	Measurements 45
	400x300, 202x384	4.04, 1.45, 1	Q FAT SATURATION	/
WHOLE BODY	440x307, 214x384	400, 13, 2, 58	/	/
	430x366, 83x122	4500, 68, 5	SPAIR	b-values: 0, 800
	260x260, 256x320	2600, 45, 2, 13	FAT SAT	/

Table 19. Characteristics of “All-in-one” protocol.

ALL IN ONE MRI Pca STAGING report sheet

PATIENT NAME: DOB : ID :

LOCAL STATUS (T STAGING)

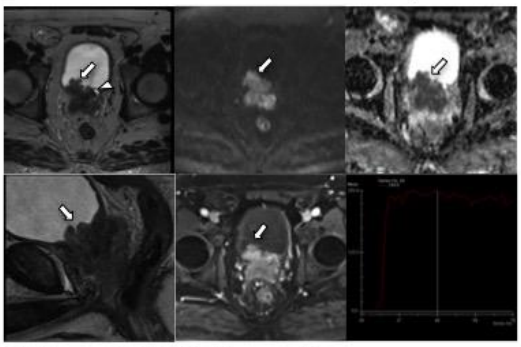

	ESUR Score
Extra capsular	5
Seminal vesicles	4
Distal sphincter	4
Bladder neck	4
Other organ	rectum

Multiparametric MRI of the prostate : summary.
Cancer location: Diffuse infiltration of the prostate
Extracapsular spread: 17

GENERAL STATUS (N AND M STAGING)

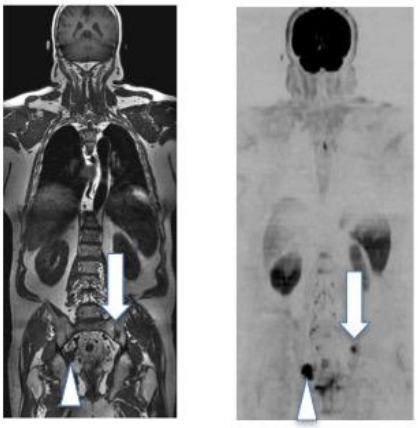

	0/1
Bone mets	1
Node mets	1

Whole body MRI T1 and DWI : summary (Arrow=bone met; arrowhead=node met)
Nodes:
Bone metastasis:

CONCLUSION: T4 N1 M1

Figure 17. An example of an "All-in-one" sheet, for the clinician with the summary of local, nodal and bone status of the patient.

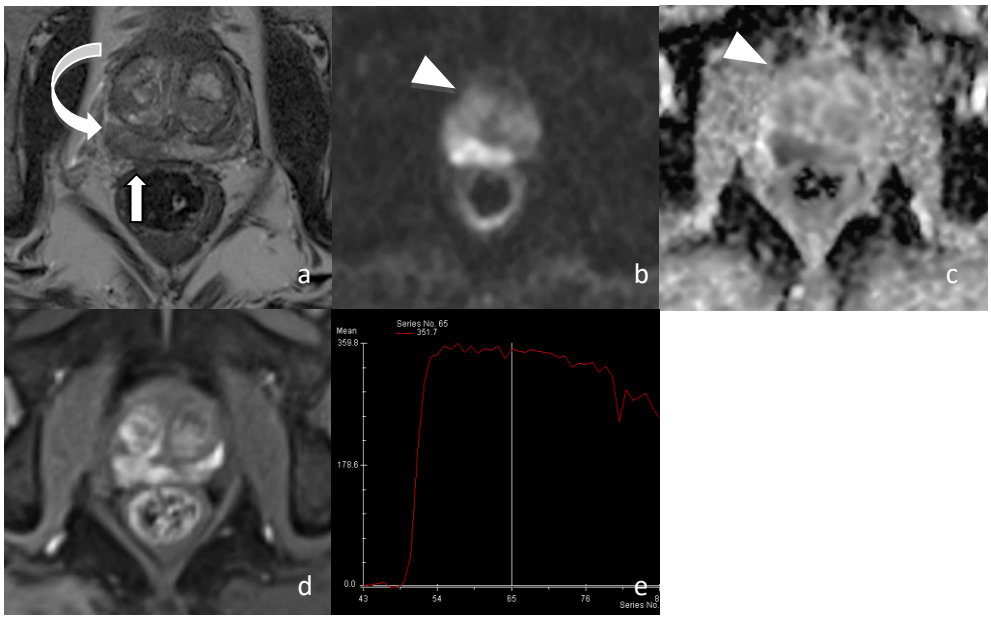

Figure 18. An example of Multiparametric MR of the prostate. Axial (a) T2 weighted MR image shows a contact between the tumour (curved arrow) and the anterior rectal wall (arrow). The normal low signal of the anterior rectal wall (arrow) has disappeared suggesting an invasion. DW MR image (b, with b value = 1200) shows high signal of the tumoural tissue (arrowhead) with low ADC values on the apparent diffusion coefficient (ADC) map (c) (660mm^2/sec) (arrowhead). Post-contrast image and DCE curve within the lesion (e, f) show type 3 curve (f).

Gold standard:

All patients underwent a routine work up for the M and N screening, consisting of Tc 99m BS for the detection of BM, followed by targeted XRays (BS ± TXR) on equivocal foci of increased uptake if the BS was deemed non-diagnostic and an abdomino-pelvic CT for N staging.

The imaging studies were read independently and blindly. Final determination of T, N, and M stage was performed in a consensus session during which all available data - clinical and biological - were analysed by radiologists, nuclear medicine physicians and urologists (BVC). In case of discrepancies between Tc 99m BS or CT and WBMRI, follow-up imaging studies were obtained after 6 months of treatment.

Statistics:

The receiver-operating curve (ROC) characteristics with their 95% exact confidence interval (CI) were calculated for each imaging method.

The comparison of the areas under ROC curve (AUC) effectuated by the Wald test from logistic regression models at the two-sided 5% significance level. The statistical analysis software, version 9.2 (SAS®, Bethesda, MD), was used. The study is exploratory and the sample size was not prospectively planned.

C. Results

Local Staging (T staging)

The T-staging of our patients is summarized in **Table 20** according to the ESUR guidelines.

	PI-RADS SCORE						
	0	1	2	3	4	5	TOTAL
Extra capsular extension T3a	6	0	NA	0	20	4	30
Seminal vesicles (T3b)	12	0	0	1	17	NA	30
Distal sphincter (T4)	21	NA	NA	4	5	NA	30
Bladder neck (T4)	17	0	0		13	NA	30
	YES	NO	TOTAL				
Adjacent organ extension	7	23	30				
	PI-RADS SCORE						
	0	1	2	3	4	5	TOTAL
Extra capsular extension T3a	6	0	NA	0	20	4	30
Seminal vesicles (T3b)	12	0	0	1	17	NA	30
Distal sphincter (T4)	21	NA	NA	4	5	NA	30
Bladder neck (T4)	17	0	0		13	NA	30
	YES	NO	TOTAL				
Adjacent organ extension	7	23	30				

Table 20. Local staging of the patients.

N and M Staging Using WBMRI

According to the BVC, 13/30 patients had metastases (9 BM, 11 LNM). There were no patients with visceral metastasis.

Comparison of the Diagnostic Performance of WBMRI and Tc 99m BS+/- TXR for BM Detection (Figure 18, Table 21,)

Sensitivity of Tc 99m BS ± TXR and WBMRI for detecting bone metastases was 89% and 100%, respectively, and specificity was 90% and 100%, respectively. One patient with BM and with negative BS was correctly identified as metastatic by WBMRI. WBMRI correctly identified the absence of BM in two patients with false positive BS. There was no significant difference between WBMRI and BS +/- TXR for the detection of BM according to the comparison of AUC with a mean increase in AUC with WBMRI.

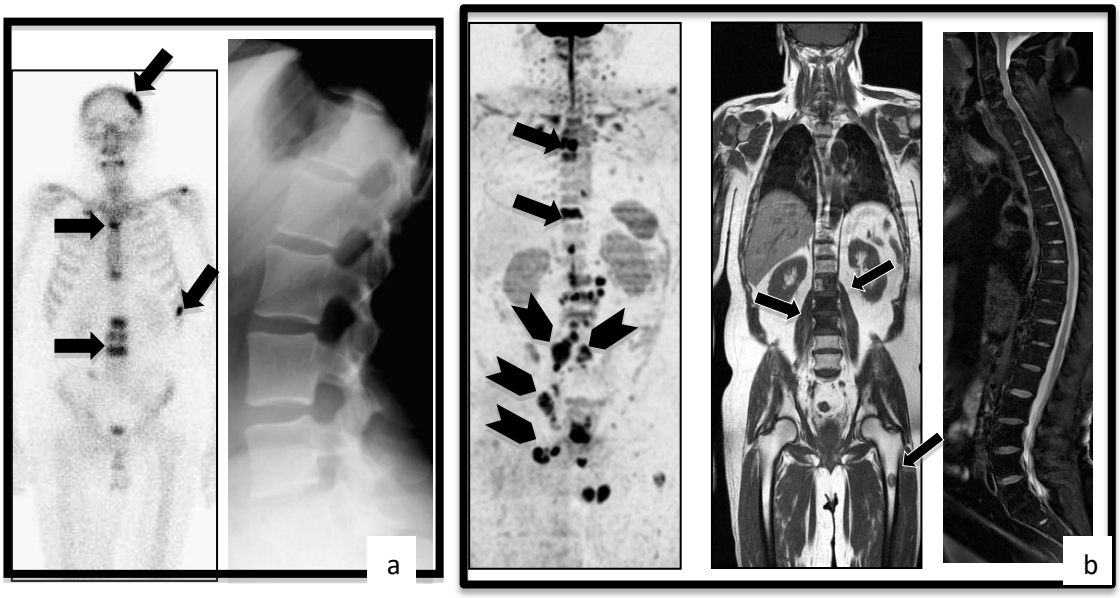

Figure 18.

a. BS +/- TXR demonstrating multiple bone metastasis (arrows)

b. WBMRI (DWI, T1 of the whole body and PDFS of the spine) demonstrating multiple bone (arrows) and node metastasis (arrowheads).

Comparison of the Diagnostic Performance of WBMRI and CT to Detect LNs Enlargement (N Staging) (Figure 19, Table 22)

Sensitivities of CT and WBMRI for LNM were 82% and 100%, respectively; specificities were 100% for both. One patient with positive LN was correctly detected by WBMRI, while missed by CT. There was no significant difference between WBMRI and CT for the detection of LNM according to the comparison of AUC. There was a mean increase in AUC of +9.1% (CI: −2.9% to +21.0%) with WBMRI compared to CT (*P* = 0.136).

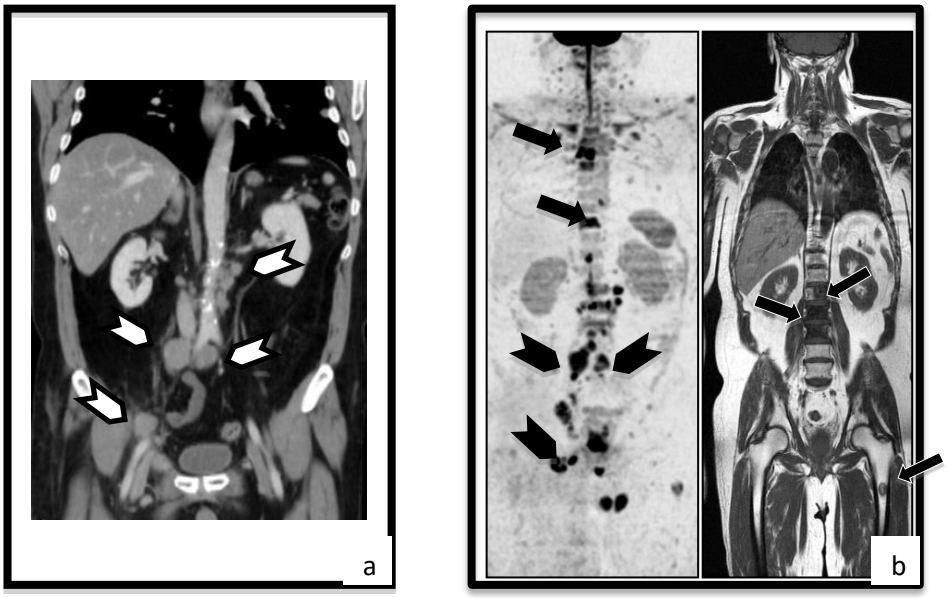

Figure 19.

a. CT demonstrating multiple node metastases (arrowheads)

b. WBMRI (DWI and T1 anatomic sequences) demonstrating bone (arrows) and bone metastases (arrowheads).

Comparison of WBMRI and routine work-up (Combination of BS ± TXR and CT) for for Assessing Global Metastatic Status (N and M Staging) (Table 23)

For each combination of LNs and bone metastases assessment, the patients were classified negative if both exams were negative, and positive if the one or both assessments were positive. On the basis of BVC, 13 patients were adjudicated metastatic. While WBMRI was in perfect agreement with the BVC, combined BS ± TXR and CT readings disagreed with the BVC in four cases (two false positive and two false negative observations). For the detection of bone or node metastasis, sensitivities of BS ± TXR combined with CT and of WBMRI were 85% and 100% respectively and specificities were 88% and 100%, respectively. WBMRI was also superior when it comes to the overall staging of the patients as being either N0M0 or having disease extension beyond the prostate (any metastases). WBMRI was superior to the combination of BS ±TXR and CT (improvement in all ROC characteristics and of AUC by 13.6% [95% CI: +0.7% to +26.5%, $P = 0.039$]).

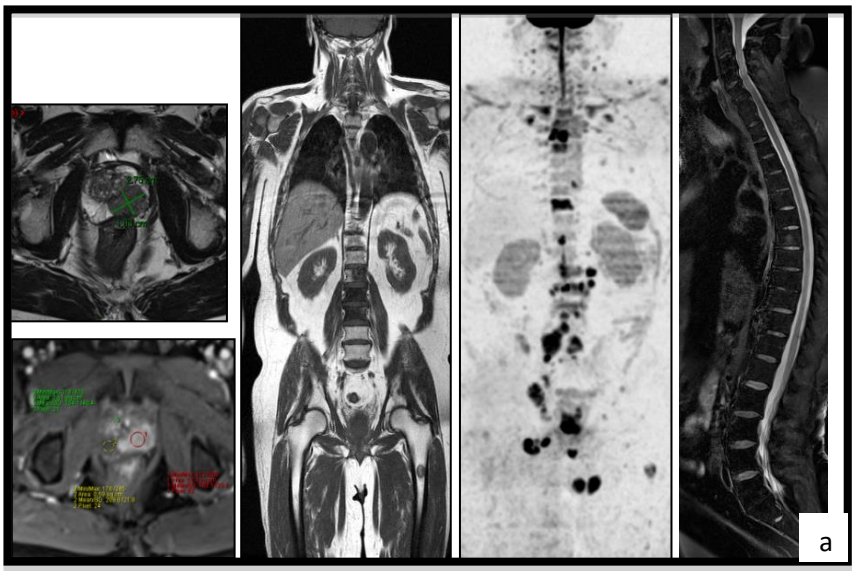

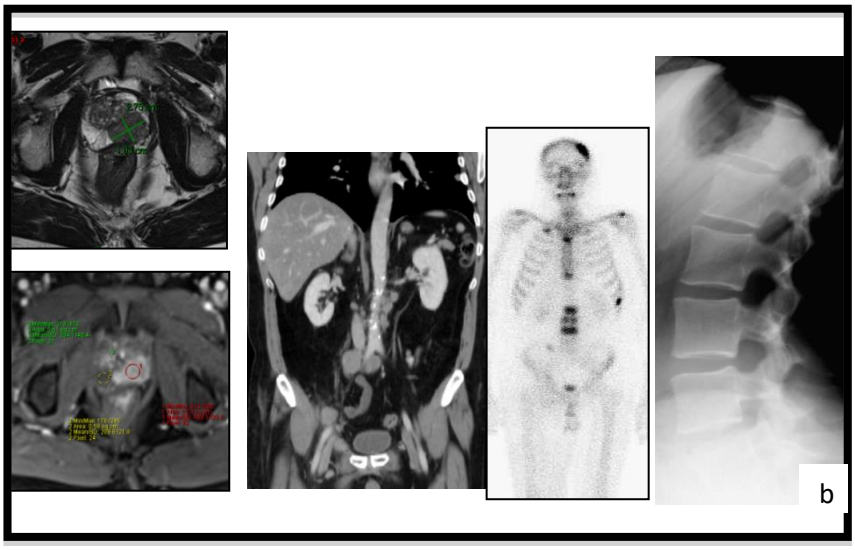

Figure 19.

a. All-in-one

b. Standard work up (mpMRI+CT+BS+/-TXR)

	BVC for BM								
	Neg.	Pos.	Tot.	Se % (95%CI)	Sp% (95%CI)	PPV % (95%CI)	NPV% (95%CI)	AUC % (95%CI)	Overall agreement% (95%CI)
Total	21	9	30						
BS									
Neg.	19	1	20	89 (52-100)	90 (70-99)	80 (44-97)	95 (75-100)	90 (77-100)	90 (74-98%)
Pos.	2	8	10						
WBMRI									
Neg.	21	0	21	100 (94-100)	100 (94-100)	100 (66-100)	100 (94-100)	100 (100-100)	100% (NA)
Pos.	0	9	9						
	Neg. : Negative, Pos. :Positive, Tot.: Total Comparison of ROC AUCs: +10,3% (95% CI: -2,3 to + 23%), P= 0,110. Not statistically significant improvement for MRI compared to standard assessement								

Table 21. Imaging Results and Receiver Operating Characteristic for BM according to the gold standard (BVC).

	BVC for LN metastasis								
	Neg.	Pos.	Tot.	Se % (95%CI)	Sp% (95%CI)	PPV % (95%CI)	NPV% (95%CI)	AUC % (95%CI)	Overall agreement % (95%CI)
Total	19	11	30						
CT									
Neg.	19	2	21	80(48-98)	100 (82-100)	100 (66-100)	90 (70-99)	91 (79-100)	93 (78-99)
Pos.	0	9	9						
WBMRI									
Neg.	19	0	19	100 (71-100)	100 (82-100)	100 (72-100)	100 (82-100)	100 (100-100)	10% (NA)
Pos.	0	11	11						
	Neg. : Negative, Pos. :Positive, Tot.: Total Comparison of ROC AUCs: +9,1% (95% CI: -2,9 to + 21%), P= 0,136. Not statistically significant improvement for MRI compared to standard assessement								

Table 22. Imaging Results and Receiver Operating Characteristic for LNM according to the gold standard (BVC).

	BVC for metastasis								
	Neg.	Pos.	Tot.	Se % (95%CI)	Sp% (95%CI)	PPV % (95%CI)	NPV% (95%CI)	AUC % (95%CI)	Overall agreement% (95%CI)
Total	17	13	30						
Standard									
Neg.	15	2	17	85 (55-98)	88 (64-99)	84 (55-98)	88 (64-99)	86 (74-99)	87 (69-96)
Pos.	2	11	13						
WBMRI									
Neg.	17	0	17	100 (75-100)	100 (80-100)	100 (75-100)	100 (80-100)	100 (100-100)	100% (NA)
Pos.	0	13	13						
	Neg. : Negative, Pos. :Positive, Tot.: Total Comparison of ROC AUCs: +13,6% (95% CI:+0,7% to + 26,5%), P= 0,039. Statistically significant improvement for MRI compared to standard assessement								

Table 23. Imaging Results and Receiver Operating Characteristic for Global staging according to the gold standard (BVC).

D. Discussion

We evaluated a one-step non-irradiating imaging strategy for a complete TNM staging of PCa, with evaluation of local disease by mpMRI and of metastatic spread by WBMRI. MpMRI is essential for the local staging in intermediate and high-risk PCa, as it demonstrates higher accuracy for the assessment of extra-capsular extension, seminal vesical and adjacent structures extension [199,200]. The average sensitivity and specificity of mpMRI for detecting LNs range around 71% [43].

Based on current guidelines, patients with high-risk PCa also require assessment for distant metastases. In most PCa, the usual sites of metastases are the pelvic LNs and/or the hematopoietic red marrow of the axial skeleton [201,202,203.] Visceral metastases are rare and usually appear in later stages of the disease [203].

Besides detecting the metastatic spread, WBMRI is a very promising technique for monitoring of BM under therapy.

Most international guidelines still recognize contrast-enhanced CT or MRI of the abdomen and pelvis and Tc 99m BS, completed with plain XRays if necessary, as standard diagnostic techniques to assess initial and follow-up metastatic status [39] . It has been shown that these techniques demonstrate severe limitations. CT and conventional MRI perform similarly bad compared to extended pelvic node dissection (ePLND), the unchallenged gold standard to perform accurate LN staging, with an average specificity of ±80% and reported sensitivity of ±40% [51,204]. A recent study has demonstrated, in a series of 100 consecutive high-risk PCa patients, that WBMRI performed similarly to CT to detect enlarged LNs [90]. Sensitivity of

CT and WBMRI was 77–82% for both, while specificity was 95–96% and 96–98%, respectively. MRI is superior to Tc 99m BS-based algorithm for the detection of BM [91,139,160]. Lecouvet et al. demonstrated that in 100 high-risk patients, the sensitivity of BS ± TXR and WBMRI for detecting BM was 86% and 98–100%, respectively ($p < 0.04$); specificity was 98% and 98–100%, respectively [90]. Furthermore, Tc 99m BS and abdomino-pelvic CT/MRI metastatic assessment require at least two separate visits to the hospital, injection of iodine contrast agent, nuclear waste handling and a significant radiation exposure (between 3.5 and 25 mSv for CT; 6.3 mSv for Tc 99m BS) [205].

It has to be noted that our study had several limitations including a limited number of patients. The inter- and intra-observer agreement of WBMRI for bone and LN lesion detection were not evaluated. Our study was mainly focused on the feasibility of an ''All-in-one'' prostate, node and bone staging MRI. The current gold standard is not perfect, since not all patients were followed up and radical prostatectomy was only performed in three patients.

This protocol acquires a contrast injection for the mpMRI of the prostate and the patient to stay in the MRI machine for 56 minutes. This could be a problem for older patients or patients with claustrophobia. Furthermore we did not address the cost effectiveness of this protocol compared to the sum of current used studies. Finally, a minimum of two different radiologists is required for the interpretation of this ''All-in-one'' protocol (genito-urinary and musculoskeletal radiologists).

E. CONCLUSION

We reported the first attempt to perform during a single MR imaging session the concurrent assessment of local and distant staging of cancer in high-risk PCa patients.

TNM staging of PCa is feasible in less than one hour in an MRI session combining mpMRI and WBMRI, outperforming BS±Targeted XRays and CT for discriminating patients, with or without metastasis.

The reduction of the duration of the different sequences is crucial in order to introduce this ''All-in-one'' protocol in clinical practice.

X. SUMMARY OF RESULTS

The current PhD thesis was set to explore the role of WBMRI in the staging of PCa patients and to maximize the information on disease stage in one single MRI session.

To test the first hypothesis, in Step 1 we have conducted a review of the literature on the subject of WBMRI and BM, in order to clarify the current evidence on the comparison between WBMRI and BS, CT and PET-CT. WBMRI is superior to BS for BM detection, independently of the primary cancer and the addition of DWI improves the sensitivity. Results are less clear regarding the comparison between WBMRI and PET-CT. WBMRI seems superior in lesion-based analysis when PET-CT exceeds WBMRI in patient-based analysis, especially in breast and neuroendocrine tumours. Undeniably, current cancer staging cannot be based on one sole technique but it will most likely be shared between WBMRI and PET according to the primary cancer. In PCa, in patient-based analysis, WBMRI+DWI is more accurate than FDG PET-CT and BS.

To test the second hypothesis in Step 2 we developed 3D T1 whole body sequence for the bone and node staging of high-risk PCa patients. We have optimized Contrast-to-Noise and Signal-to-Noise ratios, in order to ameliorate the quality of image in comparison to the standard two-dimensional sequence. After several tests and modifications, the duration of this new sequence was shortened / minimized down to 18 minutes. We introduced this sequence in clinical practice and compared it with current

MRI anatomic protocol, which includes 2D T1 WBMRI, with or without Sagittal Fat suppression sequence of the spine. Our results demonstrated that 3DT1 is feasible and provides better SNR and CNR compared with 2D sequences, with a diagnostic performance that is as good or better than the sum of 2D sequences for the detection of bone metastases and better for the detection of LNM.

To test the third hypothesis, in Step 3 we created a single step ''All-in-one'' protocol for the staging of high risk PCa patients consisting of a WBMRI anatomic sequence including diffusion weighted imaging (DWI) and prostate mpMRI. This new protocol was compared to the routine bone and node work up [BS ± targeted XRays if necessary (BS±TXR) and contrast CT]. Our results demonstrated that TNM staging of PCa is feasible in less than one hour in an MRI session combining mpMRI and WBMRI, outperforming the routine screening for discriminating patients with or without metastasis.

XI. FUTURE PERSPECTIVES AND QUESTIONS TO BE ANSWERED

Our findings create new perspectives and open opportunities in the staging and management of cancer patients.

A major future goal is to optimize the 3D T1 acquisition by reducing duration and ameliorating the quality of image (reduce slice thickness). Another objective is the refinement of the WB DWI sequence. The addition of DWI to the anatomic sequences provides a better sensitivity, but is generally noisy, of low spatial resolution and may suffer from spatial distortion. It is also time-consuming, which is seen as a major limitation by many end-users. The reduction of the acquisition time of 3DT1 and DWI sequence will result in a higher level of patient comfort, a reduction of movement artefacts and a considerable lowering of the cost. Thus, there is room to shorten the duration of the ‘’All-in-one” protocol (56 minutes), achieve a most efficient workflow, and minimize the operational costs. In order to reach this goal, a series of modifications and tests are taking place for the moment with our physicists and technicians, always taking into consideration not to compromise the quality of the sequences.

We have evaluated the sensitivity and specificity of the protocol 3DT1+WB DWI regarding the detection of Bone and Node metastasis. The next experimental step will be the evaluation of this protocol for the response

assessment of PCa patients during treatment. Even though bone lesions are considered non-measurable by BS or plain films, WBMRI could change this perception. It is common knowledge that the assessment of any change in tumour burden, tumour shrinkage and disease progression, are of crucial importance for the clinical evaluation of cancer therapeutics. Our new 3D sequence could help transpose the concept of **R**esponse **E**valuation **C**riteria **I**n **S**olid **Tumours** (RECIST) to the measurement of BM. The 3DT1 sequence has great potential to be used for the follow-up of metastatic patients, as it allows an accurate size - even volume - measurement of the metastatic lesions. This anatomic approach has to be compared or summed with the information on global tumour burden and viability which can be derived from WBDWI sequences, as demonstrated by other teams. Assessment of the change in tumour burden is an important feature of the clinical evaluation of cancer therapeutics. Tumour shrinkage (objective response) and time to the development of disease progression are important endpoints. A working group consisting of clinicians with expertise in prostate cancer management, along with imaging specialists and statisticians has to be assembled. A database of prospective documented tumour measurement data has to be created in order to investigate the impact of a variety of questions (ex: number of target lesions required, the need for response confirmation, and lymph node measurement rules) on response and progression-free survival outcomes.

The task of radiologists can be facilitated by the development of automatic volume measurement systems, which give a numerical value of the measured volume.

The 3DT1 sequence could be combined with DWI, which is able to calculate the total diffusion volumes (tDV) and the associated global median Apparent Diffusion Coefficient (gADC). Changes in tumour volume in tDV and gADC may be used to assess the response of metastatic disease and thus to provide three quantitative metrics from a single radiologic investigation. Radiologist can now try new commercial software allowing manual definition of Volumes Of Interest (VOI). However, in patients with an important number of bone metastasis this could be impractical to use. Trials testing new software for automatic calculation of the metastatic volume are ongoing.

We compared the 3DT1 sequence to the combination 2DT1 with a PDFS sequence of the spine. The comparison of 3DT1 to other protocols - including STIR sequence of the WB or T2 sequence of the spine - was beyond the scope of this thesis and is a question to be explored.

The number of patients included in our study was limited to thirty. A larger scale and - if possible - a multicenter study will provide a better insight into the subject.

A solid cost analysis of the 3DT1 sequence and the ‘’All-in-one’’ protocol has to be effectuated. The cost of this single step protocol has to be compared to one of the multimodal staging (BS +/- XRays, CT, mpMRI).

There is an urgent need for standardization of WBMRI protocols between centers. Which are the best sequences for the study of the bone marrow in oncologic patients? Could this depend on the cancer type? The best way to standardize WBMRI protocols is to carry out multicenter monocancer studies. It can also be accomplished by using a ‘’consensus’’ group of WBMRI experts, based on literature evidence and consensus expert opinion. True evidence-based guidelines will not be formulated, but a compromise, reflected by “minimal” and “optimal” requirements can be established.

Further comparison of WBMRI with PET-CT using new promising radiotracers such as ^{11}C, ^{18}F choline and mainly PSMA is crucial, in order to answer which technique is superior for the detection of PCa and metastatic disease. Furthermore, the success of combining PET with CT has sparked the interest in trying to combine PET and MRI. The excellent soft tissue contrast of MRI and its applications of functional imaging (DWI, dynamic contrast enhancement) in combination with the molecular information obtained by PET, result in a new hybrid technique, which provides good anatomic, metabolic, and functional information. Software that provides fusion of PET and MRI images has been in use for many years in neurology. The fusion of WBMRI with PET data is more challenging due to the non-

rigid patient motion between the scans and lack of stable landmarks (such as in the case of the skull).

XII. REFERENCES

1. Koh DM, Blackledge M, Padhani AR, et al. Whole-body diffusion-weighted MRI: tips, tricks, and pitfalls. *AJR American journal of roentgenology* 2012;199:252-262
2. Siegel R, Ward E, Brawley O, et al. Cancer statistics, 2011: the impact of eliminating socioeconomic and racial disparities on premature cancer deaths. *CA: a cancer journal for clinicians* 2011;61:212-236
3. Gronberg H. Prostate cancer epidemiology. *Lancet* 2003;361:859-864
4. Feuer EJ, Merrill RM, Hankey BF. Cancer surveillance series: interpreting trends in prostate cancer--part II: Cause of death misclassification and the recent rise and fall in prostate cancer mortality. *Journal of the National Cancer Institute* 1999;91:1025-1032
5. Hankey BF, Feuer EJ, Clegg LX, et al. Cancer surveillance series: interpreting trends in prostate cancer--part I: Evidence of the effects of screening in recent prostate cancer incidence, mortality, and survival rates. *Journal of the National Cancer Institute* 1999;91:1017-1024
6. Ferlay J SI, Ervik M, Dikshit R, Eser S, Mathers C, Rebelo M, Parkin DM, Forman D, Bray, F. GLOBOCAN 2012 v1.0, Cancer Incidence and Mortality Worldwide: IARC CancerBase No. 11 Lyon, France: International Agency for Research on Cancer; 2013. ; 2012
7. National Cancer Institute S, Epidemiology, and End Results Program.
8. Whittemore AS, Wu AH, Kolonel LN, et al. Family history and prostate cancer risk in black, white, and Asian men in the United States and Canada. *American journal of epidemiology* 1995;141:732-740
9. Monroe KR, Yu MC, Kolonel LN, et al. Evidence of an X-linked or recessive genetic component to prostate cancer risk. *Nature medicine* 1995;1:827-829
10. Nadji M, Tabei SZ, Castro A, et al. Prostatic-specific antigen: an immunohistologic marker for prostatic neoplasms. *Cancer* 1981;48:1229-1232
11. Thomson V, Pialat JB, Gay F, et al. Whole-body MRI for metastases screening: a preliminary study using 3D VIBE sequences with automatic subtraction between noncontrast and contrast enhanced images. *American journal of clinical oncology* 2008;31:285-292

12. Thompson IM, Pauler DK, Goodman PJ, et al. Prevalence of prostate cancer among men with a prostate-specific antigen level < or =4.0 ng per milliliter. *The New England journal of medicine* 2004;350:2239-2246
13. Schroder FH, Hugosson J, Roobol MJ, et al. Screening and prostate-cancer mortality in a randomized European study. *The New England journal of medicine* 2009;360:1320-1328
14. Andriole GL, Crawford ED, Grubb RL, 3rd, et al. Mortality results from a randomized prostate-cancer screening trial. *The New England journal of medicine* 2009;360:1310-1319
15. Djulbegovic M, Beyth RJ, Neuberger MM, et al. Screening for prostate cancer: systematic review and meta-analysis of randomised controlled trials. *Bmj* 2010;341:c4543
16. Oliver SE, May MT, Gunnell D. International trends in prostate-cancer mortality in the "PSA ERA". *International journal of cancer Journal international du cancer* 2001;92:893-898
17. Aus G, Bergdahl S, Lodding P, et al. Prostate cancer screening decreases the absolute risk of being diagnosed with advanced prostate cancer--results from a prospective, population-based randomized controlled trial. *European urology* 2007;51:659-664
18. Barentsz JO, Richenberg J, Clements R, et al. ESUR prostate MR guidelines 2012. *European radiology* 2012;22:746-757
19. Loeb S, Carter HB. Limitations and use of PSA derivatives in the screening and risk stratification of prostate cancer. *Urologic oncology* 2009;27:583-584
20. Heidenreich A, Bastian PJ, Bellmunt J, et al. EAU guidelines on prostate cancer. Part II: Treatment of advanced, relapsing, and castration-resistant prostate cancer. *European urology* 2014;65:467-479
21. Hodges TM. Eloise C. Foster, President, Medical Library Association 1988/1989. *Bulletin of the Medical Library Association* 1988;76:273-276
22. Keetch DW, Catalona WJ, Smith DS. Serial prostatic biopsies in men with persistently elevated serum prostate specific antigen values. *The Journal of urology* 1994;151:1571-1574
23. Rabbani F, Stroumbakis N, Kava BR, et al. Incidence and clinical significance of false-negative sextant prostate biopsies. *The Journal of urology* 1998;159:1247-1250

24. Babaian RJ, Toi A, Kamoi K, et al. A comparative analysis of sextant and an extended 11-core multisite directed biopsy strategy. *The Journal of urology* 2000;163:152-157
25. Naughton CK, Miller DC, Mager DE, et al. A prospective randomized trial comparing 6 versus 12 prostate biopsy cores: impact on cancer detection. *The Journal of urology* 2000;164:388-392
26. Presti JC, Jr., Chang JJ, Bhargava V, et al. The optimal systematic prostate biopsy scheme should include 8 rather than 6 biopsies: results of a prospective clinical trial. *The Journal of urology* 2000;163:163-166; discussion 166-167
27. Petrylak DP, Ankerst DP, Jiang CS, et al. Evaluation of prostate-specific antigen declines for surrogacy in patients treated on SWOG 99-16. *Journal of the National Cancer Institute* 2006;98:516-521
28. Smith DC, Dunn RL, Strawderman MS, et al. Change in serum prostate-specific antigen as a marker of response to cytotoxic therapy for hormone-refractory prostate cancer. *Journal of clinical oncology : official journal of the American Society of Clinical Oncology* 1998;16:1835-1843
29. Eskew LA, Bare RL, McCullough DL. Systematic 5 region prostate biopsy is superior to sextant method for diagnosing carcinoma of the prostate. *The Journal of urology* 1997;157:199-202; discussion 202-193
30. Bubendorf L, Schopfer A, Wagner U, et al. Metastatic patterns of prostate cancer: an autopsy study of 1,589 patients. *Human pathology* 2000;31:578-583
31. Hull GW, Rabbani F, Abbas F, et al. Cancer control with radical prostatectomy alone in 1,000 consecutive patients. *The Journal of urology* 2002;167:528-534
32. Epstein JI, Partin AW, Potter SR, et al. Adenocarcinoma of the prostate invading the seminal vesicle: prognostic stratification based on pathologic parameters. *Urology* 2000;56:283-288
33. Heidenreich A. Identification of high-risk prostate cancer: role of prostate-specific antigen, PSA doubling time, and PSA velocity. *European urology* 2008;54:976-977; discussion 978-979
34. Heidenreich A, Aus G, Bolla M, et al. EAU guidelines on prostate cancer. *European urology* 2008;53:68-80

35. D'Amico AV, Whittington R, Malkowicz SB, et al. Biochemical outcome after radical prostatectomy, external beam radiation therapy, or interstitial radiation therapy for clinically localized prostate cancer. *Jama* 1998;280:969-974
36. Boorjian SA, Karnes RJ, Rangel LJ, et al. Impact of prostate-specific antigen testing on the clinical and pathological outcomes after radical prostatectomy for Gleason 8-10 cancers. *BJU international* 2008;101:299-304
37. Cooperberg MR, Broering JM, Carroll PR. Time trends and local variation in primary treatment of localized prostate cancer. *Journal of clinical oncology : official journal of the American Society of Clinical Oncology* 2010;28:1117-1123
38. Thompson I, Thrasher JB, Aus G, et al. Guideline for the management of clinically localized prostate cancer: 2007 update. *The Journal of urology* 2007;177:2106-2131
39. Heidenreich A, Bellmunt J, Bolla M, et al. EAU guidelines on prostate cancer. Part 1: screening, diagnosis, and treatment of clinically localised disease. *European urology* 2011;59:61-71
40. Roach M, Lu J, Pilepich MV, et al. Four prognostic groups predict long-term survival from prostate cancer following radiotherapy alone on Radiation Therapy Oncology Group clinical trials. *International journal of radiation oncology, biology, physics* 2000;47:609-615
41. Cooperberg MR, Pasta DJ, Elkin EP, et al. The University of California, San Francisco Cancer of the Prostate Risk Assessment score: a straightforward and reliable preoperative predictor of disease recurrence after radical prostatectomy. *The Journal of urology* 2005;173:1938-1942
42. Dickinson L, Ahmed HU, Allen C, et al. Magnetic resonance imaging for the detection, localisation, and characterisation of prostate cancer: recommendations from a European consensus meeting. *European urology* 2011;59:477-494
43. Engelbrecht MR, Jager GJ, Laheij RJ, et al. Local staging of prostate cancer using magnetic resonance imaging: a meta-analysis. *European radiology* 2002;12:2294-2302
44. Kahn T, Burrig K, Schmitz-Drager B, et al. Prostatic carcinoma and benign prostatic hyperplasia: MR imaging with histopathologic correlation. *Radiology* 1989;173:847-851

45. McSherry SA, Levy F, Schiebler ML, et al. Preoperative prediction of pathological tumour volume and stage in clinically localized prostate cancer: comparison of digital rectal examination, transrectal ultrasonography and magnetic resonance imaging. *The Journal of urology* 1991;146:85-89
46. Bezzi M, Kressel HY, Allen KS, et al. Prostatic carcinoma: staging with MR imaging at 1.5 T. *Radiology* 1988;169:339-346
47. Cai T, Nesi G, Tinacci G, et al. Clinical importance of lymph node density in predicting outcome of prostate cancer patients. *The Journal of surgical research* 2011;167:267-272
48. Malmstrom PU. Lymph node staging in prostatic carcinoma revisited. *Acta oncologica* 2005;44:593-598
49. Cheng L, Zincke H, Blute ML, et al. Risk of prostate carcinoma death in patients with lymph node metastasis. *Cancer* 2001;91:66-73
50. Wolf JS, Jr., Cher M, Dall'era M, et al. The use and accuracy of cross-sectional imaging and fine needle aspiration cytology for detection of pelvic lymph node metastases before radical prostatectomy. *The Journal of urology* 1995;153:993-999
51. Hovels AM, Heesakkers RA, Adang EM, et al. The diagnostic accuracy of CT and MRI in the staging of pelvic lymph nodes in patients with prostate cancer: a meta-analysis. *Clinical radiology* 2008;63:387-395
52. Lee JK, Stanley RJ, Sagel SS, et al. Accuracy of CT in detecting intraabdominal and pelvic lymph node metastases from pelvic cancers. *AJR American journal of roentgenology* 1978;131:675-679
53. Jing B, Wallace S, Zornoza J. Metastases to retroperitoneal and pelvic lymph nodes: computed tomography and lymphangiography. *Radiologic clinics of North America* 1982;20:511-530
54. Walsh JW, Amendola MA, Konerding KF, et al. Computed tomographic detection of pelvic and inguinal lymph-node metastases from primary and recurrent pelvic malignant disease. *Radiology* 1980;137:157-166
55. Rifkin MD, Ehrlich SM, Marks G. Staging of rectal carcinoma: prospective comparison of endorectal US and CT. *Radiology* 1989;170:319-322
56. McLoud TC, Bourgouin PM, Greenberg RW, et al. Bronchogenic carcinoma: analysis of staging in the mediastinum with CT by correlative lymph node mapping and sampling. *Radiology* 1992;182:319-323

57. Gross BH, Glazer GM, Orringer MB, et al. Bronchogenic carcinoma metastatic to normal-sized lymph nodes: frequency and significance. *Radiology* 1988;166:71-74
58. Kayser K, Bach S, Bulzebruck H, et al. Site, size, and tumour involvement of resected extrapulmonary lymph nodes in lung cancer. *Journal of surgical oncology* 1990;43:45-49
59. Matsuyama T, Tsukamoto N, Matsukuma K, et al. Malignant ovarian tumours associated with pregnancy: report of six cases. *International journal of gynaecology and obstetrics: the official organ of the International Federation of Gynaecology and Obstetrics* 1989;28:61-66
60. Heesakkers RA, Hovels AM, Jager GJ, et al. MRI with a lymph-node-specific contrast agent as an alternative to CT scan and lymph-node dissection in patients with prostate cancer: a prospective multicohort study. *The Lancet Oncology* 2008;9:850-856
61. Kwak JY, Kim JS, Kim HJ, et al. Diagnostic value of FDG-PET/CT for lymph node metastasis of colorectal cancer. *World journal of surgery* 2012;36:1898-1905
62. Helyar V, Mohan HK, Barwick T, et al. The added value of multislice SPECT/CT in patients with equivocal bony metastasis from carcinoma of the prostate. *European journal of nuclear medicine and molecular imaging* 2010;37:706-713
63. Wang C, Shen Y. Study on the distribution features of bone metastases in prostate cancer. *Nuclear medicine communications* 2012;33:379-383
64. Rybak LD, Rosenthal DI. Radiological imaging for the diagnosis of bone metastases. *The quarterly journal of nuclear medicine : official publication of the Italian Association of Nuclear Medicine* 2001;45:53-64
65. Helms CA, Cann CE, Brunelle FO, et al. Detection of bone-marrow metastases using quantitative computed tomography. *Radiology* 1981;140:745-750
66. Genant HK, Bautovich GJ, Singh M, et al. Bone-seeking radionuclides: an in vivo study of factors affecting skeletal uptake. *Radiology* 1974;113:373-382
67. Galasko CS. The pathological basis for skeletal scintigraphy. *The Journal of bone and joint surgery British volume* 1975;57:353-359

68. Wu PS, Chiu NT, Lee BF, et al. Clinical significance of solitary rib hot spots on bone scans in patients with extraskeletal cancer: correlation with other clinical manifestations. *Clinical nuclear medicine* 2002;27:567-571
69. Soloway MS, Hardeman SW, Hickey D, et al. Stratification of patients with metastatic prostate cancer based on extent of disease on initial bone scan. *Cancer* 1988;61:195-202
70. Jacobson AF, Fogelman I. Bone scanning in clinical oncology: does it have a future? *European journal of nuclear medicine* 1998;25:1219-1223
71. Schirrmeister H, Guhlmann A, Kotzerke J, et al. Early detection and accurate description of extent of metastatic bone disease in breast cancer with fluoride ion and positron emission tomography. *Journal of clinical oncology : official journal of the American Society of Clinical Oncology* 1999;17:2381-2389
72. Even-Sapir E, Lerman H, Gutman M, et al. The presentation of malignant tumours and pre-malignant lesions incidentally found on PET-CT. *European journal of nuclear medicine and molecular imaging* 2006;33:541-552
73. Even-Sapir E, Metser U, Mishani E, et al. The detection of bone metastases in patients with high-risk prostate cancer: 99mTc-MDP Planar bone scintigraphy, single- and multi-field-of-view SPECT, 18F-fluoride PET, and 18F-fluoride PET/CT. *Journal of nuclear medicine : official publication, Society of Nuclear Medicine* 2006;47:287-297
74. Schirrmeister H, Glatting G, Hetzel J, et al. Prospective evaluation of the clinical value of planar bone scans, SPECT, and (18)F-labeled NaF PET in newly diagnosed lung cancer. *Journal of nuclear medicine : official publication, Society of Nuclear Medicine* 2001;42:1800-1804
75. Kukekov VG, Fadeev NP. [Positron emission tomography (physico-technical aspects)]. *Meditsinskaia radiologiia* 1986;31:67-76
76. Jadvar H, Tatlidil R, Garcia AA, et al. Evaluation of recurrent gastric malignancy with [F-18]-FDG positron emission tomography. *Clinical radiology* 2003;58:215-221
77. Jadvar H, Kherbache HM, Pinski JK, et al. Diagnostic role of [F-18]-FDG positron emission tomography in restaging renal cell carcinoma. *Clinical nephrology* 2003;60:395-400
78. Hara T, Kosaka N, Kishi H. PET imaging of prostate cancer using carbon-11-choline. *Journal of nuclear medicine : official publication, Society of Nuclear Medicine* 1998;39:990-995

79. A. G. *Positron Emission Tomography*. 2013
80. Ghosh A, Heston WD. Tumour target prostate specific membrane antigen (PSMA) and its regulation in prostate cancer. *Journal of cellular biochemistry* 2004;91:528-539
81. Afshar-Oromieh A, Zechmann CM, Malcher A, et al. Comparison of PET imaging with a (68)Ga-labelled PSMA ligand and (18)F-choline-based PET/CT for the diagnosis of recurrent prostate cancer. *European journal of nuclear medicine and molecular imaging* 2014;41:11-20
82. Afshar-Oromieh A, Haberkorn U, Schlemmer HP, et al. Comparison of PET/CT and PET/MRI hybrid systems using a 68Ga-labelled PSMA ligand for the diagnosis of recurrent prostate cancer: initial experience. *European journal of nuclear medicine and molecular imaging* 2014;41:887-897
83. Afshar-Oromieh A, Haberkorn U, Hadaschik B, et al. PET/MRI with a 68Ga-PSMA ligand for the detection of prostate cancer. *European journal of nuclear medicine and molecular imaging* 2013;40:1629-1630
84. Afshar-Oromieh A, Malcher A, Eder M, et al. PET imaging with a [68Ga]gallium-labelled PSMA ligand for the diagnosis of prostate cancer: biodistribution in humans and first evaluation of tumour lesions. *European journal of nuclear medicine and molecular imaging* 2013;40:486-495
85. Afshar-Oromieh A, Avtzi E, Giesel FL, et al. The diagnostic value of PET/CT imaging with the (68)Ga-labelled PSMA ligand HBED-CC in the diagnosis of recurrent prostate cancer. *European journal of nuclear medicine and molecular imaging* 2015;42:197-209
86. Daffner RH, Lupetin AR, Dash N, et al. MRI in the detection of malignant infiltration of bone marrow. *AJR American journal of roentgenology* 1986;146:353-358
87. Gosfield E, 3rd, Alavi A, Kneeland B. Comparison of radionuclide bone scans and magnetic resonance imaging in detecting spinal metastases. *Journal of nuclear medicine : official publication, Society of Nuclear Medicine* 1993;34:2191-2198
88. Engelhard K, Hollenbach HP, Wohlfart K, et al. Comparison of whole-body MRI with automatic moving table technique and bone scintigraphy for screening for bone metastases in patients with breast cancer. *European radiology* 2004;14:99-105

89. Nakanishi K, Kobayashi M, Takahashi S, et al. Whole body MRI for detecting metastatic bone tumour: comparison with bone scintigrams. *Magnetic resonance in medical sciences : MRMS : an official journal of Japan Society of Magnetic Resonance in Medicine* 2005;4:11-17
90. Lecouvet FE, El Mouedden J, Collette L, et al. Can whole-body magnetic resonance imaging with diffusion-weighted imaging replace Tc 99m bone scanning and computed tomography for single-step detection of metastases in patients with high-risk prostate cancer? *European urology* 2012;62:68-75
91. Lecouvet FE, Simon M, Tombal B, et al. Whole-body MRI (WBMRI) versus axial skeleton MRI (AS-MRI) to detect and measure bone metastases in prostate cancer (PCa). *European radiology* 2010;20:2973-2982
92. Weber M-A. *Magnetic Resonance Imaging of the Skeletal Musculature*. Heidelberg: Springer Heidelberg New York Dordrecht London; 2014
93. Mirowitz SA, Apicella P, Reinus WR, et al. MR imaging of bone marrow lesions: relative conspicuousness on T1-weighted, fat-suppressed T2-weighted, and STIR images. *AJR American journal of roentgenology* 1994;162:215-221
94. Schick F, Bongers H, Aicher K, et al. Subtle bone marrow edema assessed by frequency selective chemical shift MRI. *Journal of computer assisted tomography* 1992;16:454-460
95. Wehrli FW, Perkins TG, Shimakawa A, et al. Chemical shift-induced amplitude modulations in images obtained with gradient refocusing. *Magnetic resonance imaging* 1987;5:157-158
96. Hagmann P, Jonasson L, Maeder P, et al. Understanding diffusion MR imaging techniques: from scalar diffusion-weighted imaging to diffusion tensor imaging and beyond. *Radiographics : a review publication of the Radiological Society of North America, Inc* 2006;26 Suppl 1:S205-223
97. Koh DM, Collins DJ. Diffusion-weighted MRI in the body: applications and challenges in oncology. *AJR American journal of roentgenology* 2007;188:1622-1635
98. Muller MF, Prasad P, Siewert B, et al. Abdominal diffusion mapping with use of a whole-body echo-planar system. *Radiology* 1994;190:475-478

99. Ichikawa T, Haradome H, Hachiya J, et al. Diffusion-weighted MR imaging with single-shot echo-planar imaging in the upper abdomen: preliminary clinical experience in 61 patients. *Abdominal imaging* 1999;24:456-461
100. Bammer R. Basic principles of diffusion-weighted imaging. *European journal of radiology* 2003;45:169-184
101. Bammer R, Acar B, Moseley ME. In vivo MR tractography using diffusion imaging. *European journal of radiology* 2003;45:223-234
102. Glockner JF, Hu HH, Stanley DW, et al. Parallel MR imaging: a user's guide. *Radiographics : a review publication of the Radiological Society of North America, Inc* 2005;25:1279-1297
103. Takahara T, Imai Y, Yamashita T, et al. Diffusion weighted whole body imaging with background body signal suppression (DWIBS): technical improvement using free breathing, STIR and high resolution 3D display. *Radiation medicine* 2004;22:275-282
104. Fischer MA, Nanz D, Hany T, et al. Diagnostic accuracy of whole-body MRI/DWI image fusion for detection of malignant tumours: a comparison with PET/CT. *European radiology* 2011;21:246-255
105. Wu LM, Gu HY, Zheng J, et al. Diagnostic value of whole-body magnetic resonance imaging for bone metastases: a systematic review and meta-analysis. *Journal of magnetic resonance imaging : JMRI* 2011;34:128-135
106. Messiou C, Collins DJ, Morgan VA, et al. Optimising diffusion weighted MRI for imaging metastatic and myeloma bone disease and assessing reproducibility. *European radiology* 2011;21:1713-1718
107. Kwee TC, Takahara T, Vermoolen MA, et al. Whole-body diffusion-weighted imaging for staging malignant lymphoma in children. *Pediatric radiology* 2010;40:1592-1602; quiz 1720-1591
108. Vermoolen MA, Kwee TC, Nievelstein RA. Whole-body MRI for staging Hodgkin lymphoma in a pregnant patient. *American journal of hematology* 2010;85:443
109. Chen W, Jian W, Li HT, et al. Whole-body diffusion-weighted imaging vs. FDG-PET for the detection of non-small-cell lung cancer. How do they measure up? *Magnetic resonance imaging* 2010;28:613-620
110. Sandrasegaran K, Sundaram CP, Ramaswamy R, et al. Usefulness of diffusion-weighted imaging in the evaluation of renal masses. *AJR American journal of roentgenology* 2010;194:438-445

111. Padhani AR, Koh DM, Collins DJ. Whole-body diffusion-weighted MR imaging in cancer: current status and research directions. *Radiology* 2011;261:700-718
112. Khanna R. *Surgical Techniques for Prostate Cancer*
113. Geinitz H. *Radiotherapy in Prostate Cancer : Innovative Techniques and Current Controversies*
114. Ehrenpreis ED. *Radiation therapy pelvic malignancy and its consequences*. 2015
115. Barret E. *Technical Aspects of Focal Therapy in Localized Prostate Cancer* 2015
116. Barkhausen J, Quick HH, Lauenstein T, et al. Whole-body MR imaging in 30 seconds with real-time true FISP and a continuously rolling table platform: feasibility study. *Radiology* 2001;220:252-256
117. Daldrup-Link HE, Franzius C, Link TM, et al. Whole-body MR imaging for detection of bone metastases in children and young adults: comparison with skeletal scintigraphy and FDG PET. *AJR American journal of roentgenology* 2001;177:229-236
118. Steinborn MM, Heuck AF, Tiling R, et al. Whole-body bone marrow MRI in patients with metastatic disease to the skeletal system. *Journal of computer assisted tomography* 1999;23:123-129
119. Lauenstein TC, Freudenberg LS, Goehde SC, et al. Whole-body MRI using a rolling table platform for the detection of bone metastases. *European radiology* 2002;12:2091-2099
120. Larkman DJ, Nunes RG. Parallel magnetic resonance imaging. *Physics in medicine and biology* 2007;52:R15-55
121. Griswold MA, Jakob PM, Heidemann RM, et al. Generalized autocalibrating partially parallel acquisitions (GRAPPA). *Magnetic resonance in medicine* 2002;47:1202-1210
122. Sodickson DK, Manning WJ. Simultaneous acquisition of spatial harmonics (SMASH): fast imaging with radiofrequency coil arrays. *Magnetic resonance in medicine* 1997;38:591-603
123. Busch HP, Hoffmann HG, Rock J, et al. [MR angiography of pelvic and leg vessels with automatic table movement technique ("Mobi-Trak")--clinical experience with 450 studies]. *RoFo : Fortschritte auf dem Gebiete der Rontgenstrahlen und der Nuklearmedizin* 2001;173:405-409

124. Ho KY, Leiner T, de Haan MW, et al. Peripheral vascular tree stenoses: evaluation with moving-bed infusion-tracking MR angiography. *Radiology* 1998;206:683-692
125. Lauenstein TC, Goehde SC, Herborn CU, et al. Whole-body MR imaging: evaluation of patients for metastases. *Radiology* 2004;233:139-148
126. Schmidt GP, Haug AR, Schoenberg SO, et al. Whole-body MRI and PET-CT in the management of cancer patients. *European radiology* 2006;16:1216-1225
127. Walker R, Kessar P, Blanchard R, et al. Turbo STIR magnetic resonance imaging as a whole-body screening tool for metastases in patients with breast carcinoma: preliminary clinical experience. *Journal of magnetic resonance imaging : JMRI* 2000;11:343-350
128. Flickinger FW, Sanal SM. Bone marrow MRI: techniques and accuracy for detecting breast cancer metastases. *Magnetic resonance imaging* 1994;12:829-835
129. Eustace S, Tello R, DeCarvalho V, et al. A comparison of whole-body turboSTIR MR imaging and planar 99mTc-methylene diphosphonate scintigraphy in the examination of patients with suspected skeletal metastases. *AJR American journal of roentgenology* 1997;169:1655-1661
130. Antoch G, Vogt FM, Freudenberg LS, et al. Whole-body dual-modality PET/CT and whole-body MRI for tumour staging in oncology. *Jama* 2003;290:3199-3206
131. Ohno Y, Koyama H, Nogami M, et al. Whole-body MR imaging vs. FDG-PET: comparison of accuracy of M-stage diagnosis for lung cancer patients. *Journal of magnetic resonance imaging : JMRI* 2007;26:498-509
132. Schmidt GP, Baur-Melnyk A, Herzog P, et al. High-resolution whole-body magnetic resonance image tumour staging with the use of parallel imaging versus dual-modality positron emission tomography-computed tomography: experience on a 32-channel system. *Investigative radiology* 2005;40:743-753
133. Schmidt GP, Baur-Melnyk A, Haug A, et al. Whole-body MRI at 1.5 T and 3 T compared with FDG-PET-CT for the detection of tumour recurrence in patients with colorectal cancer. *European radiology* 2009;19:1366-1378

134. Berkovic P, De Meerleer G, Delrue L, et al. Salvage stereotactic body radiotherapy for patients with limited prostate cancer metastases: deferring androgen deprivation therapy. *Clinical genitourinary cancer* 2013;11:27-32
135. Jilg CA, Rischke HC, Reske SN, et al. Salvage lymph node dissection with adjuvant radiotherapy for nodal recurrence of prostate cancer. *The Journal of urology* 2012;188:2190-2197
136. Soylu FN, Peng Y, Jiang Y, et al. Seminal vesicle invasion in prostate cancer: evaluation by using multiparametric endorectal MR imaging. *Radiology* 2013;267:797-806
137. Heidenreich A. Consensus criteria for the use of magnetic resonance imaging in the diagnosis and staging of prostate cancer: not ready for routine use. *European urology* 2011;59:495-497
138. Hanvey S, Sadozye AH, McJury M, et al. The influence of MRI scan position on image registration accuracy, target delineation and calculated dose in prostatic radiotherapy. *The British journal of radiology* 2012;85:e1256-1262
139. Lecouvet FE, Geukens D, Stainier A, et al. Magnetic resonance imaging of the axial skeleton for detecting bone metastases in patients with high-risk prostate cancer: diagnostic and cost-effectiveness and comparison with current detection strategies. *Journal of clinical oncology : official journal of the American Society of Clinical Oncology* 2007;25:3281-3287
140. Savelli S, Di Maurizio M, Perrone A, et al. MRI with diffusion-weighted imaging (DWI) and apparent diffusion coefficient (ADC) assessment in the evaluation of normal and abnormal fetal kidneys: preliminary experience. *Prenatal diagnosis* 2007;27:1104-1111
141. Tudor GR, Finlay D, Taub N. An assessment of inter-observer agreement and accuracy when reporting plain radiographs. *Clinical radiology* 1997;52:235-238
142. Shreve PD, Grossman HB, Gross MD, et al. Metastatic prostate cancer: initial findings of PET with 2-deoxy-2-[F-18]fluoro-D-glucose. *Radiology* 1996;199:751-756
143. Bossuyt PM, Reitsma JB, Standards for Reporting of Diagnostic A. The STARD initiative. *Lancet* 2003;361:71

144. Whiting P, Rutjes AW, Reitsma JB, et al. The development of QUADAS: a tool for the quality assessment of studies of diagnostic accuracy included in systematic reviews. *BMC medical research methodology* 2003;3:25
145. Costelloe CM, Kundra V, Ma J, et al. Fast Dixon whole-body MRI for detecting distant cancer metastasis: a preliminary clinical study. *Journal of magnetic resonance imaging : JMRI* 2012;35:399-408
146. Balliu E, Boada M, Pelaez I, et al. Comparative study of whole-body MRI and bone scintigraphy for the detection of bone metastases. *Clinical radiology* 2010;65:989-996
147. Goo HW, Choi SH, Ghim T, et al. Whole-body MRI of paediatric malignant tumours: comparison with conventional oncological imaging methods. *Pediatric radiology* 2005;35:766-773
148. Gutzeit A, Doert A, Froehlich JM, et al. Comparison of diffusion-weighted whole body MRI and skeletal scintigraphy for the detection of bone metastases in patients with prostate or breast carcinoma. *Skeletal radiology* 2010;39:333-343
149. Heusner TA, Kuemmel S, Koeninger A, et al. Diagnostic value of diffusion-weighted magnetic resonance imaging (DWI) compared to FDG PET/CT for whole-body breast cancer staging. *European journal of nuclear medicine and molecular imaging* 2010;37:1077-1086
150. Heusner T, Golitz P, Hamami M, et al. "One-stop-shop" staging: should we prefer FDG-PET/CT or MRI for the detection of bone metastases? *European journal of radiology* 2011;78:430-435
151. Jouvet JC, Thomas L, Thomson V, et al. Whole-body MRI with diffusion-weighted sequences compared with 18 FDG PET-CT, CT and superficial lymph node ultrasonography in the staging of advanced cutaneous melanoma: a prospective study. *Journal of the European Academy of Dermatology and Venereology : JEADV* 2013
152. Kembhavi SA, Rangarajan V, Shah S, et al. Prospective observational study on diagnostic accuracy of whole-body MRI in solid small round cell tumours. *Clinical radiology* 2014;69:900-908
153. Kumar J, Seith A, Kumar A, et al. Whole-body MR imaging with the use of parallel imaging for detection of skeletal metastases in pediatric patients with small-cell neoplasms: comparison with skeletal scintigraphy and FDG PET/CT. *Pediatric radiology* 2008;38:953-962

154. Laurent V, Trausch G, Bruot O, et al. Comparative study of two whole-body imaging techniques in the case of melanoma metastases: advantages of multi-contrast MRI examination including a diffusion-weighted sequence in comparison with PET-CT. *European journal of radiology* 2010;75:376-383
155. Pfannenberg C, Aschoff P, Schanz S, et al. Prospective comparison of 18F-fluorodeoxyglucose positron emission tomography/computed tomography and whole-body magnetic resonance imaging in staging of advanced malignant melanoma. *European journal of cancer* 2007;43:557-564
156. Sakurai Y, Kawai H, Iwano S, et al. Supplemental value of diffusion-weighted whole-body imaging with background body signal suppression (DWIBS) technique to whole-body magnetic resonance imaging in detection of bone metastases from thyroid cancer. *Journal of medical imaging and radiation oncology* 2013;57:297-305
157. Schmidt GP, Schoenberg SO, Schmid R, et al. Screening for bone metastases: whole-body MRI using a 32-channel system versus dual-modality PET-CT. *European radiology* 2007;17:939-949
158. Schraml C, Schwenzer NF, Sperling O, et al. Staging of neuroendocrine tumours: comparison of [(6)(8)Ga]DOTATOC multiphase PET/CT and whole-body MRI. *Cancer imaging : the official publication of the International Cancer Imaging Society* 2013;13:63-72
159. Sohaib SA, Cook G, Allen SD, et al. Comparison of whole-body MRI and bone scintigraphy in the detection of bone metastases in renal cancer. *The British journal of radiology* 2009;82:632-639
160. Venkitaraman R, Cook GJ, Dearnaley DP, et al. Whole-body magnetic resonance imaging in the detection of skeletal metastases in patients with prostate cancer. *Journal of medical imaging and radiation oncology* 2009;53:241-247
161. Leboulleux S, Dromain C, Vataire AL, et al. Prediction and diagnosis of bone metastases in well-differentiated gastro-entero-pancreatic endocrine cancer: a prospective comparison of whole body magnetic resonance imaging and somatostatin receptor scintigraphy. *The Journal of clinical endocrinology and metabolism* 2008;93:3021-3028

162. Takenaka D, Ohno Y, Matsumoto K, et al. Detection of bone metastases in non-small cell lung cancer patients: comparison of whole-body diffusion-weighted imaging (DWI), whole-body MR imaging without and with DWI, whole-body FDG-PET/CT, and bone scintigraphy. *Journal of magnetic resonance imaging : JMRI* 2009;30:298-308
163. Heusner TA, Antoch G, Wittkowski-Sterczewski A, et al. Transarterial hepatic chemoperfusion of uveal melanoma metastases: survival and response to treatment. *RoFo : Fortschritte auf dem Gebiete der Rontgenstrahlen und der Nuklearmedizin* 2011;183:1151-1160
164. Roberts CC, Daffner RH, Weissman BN, et al. ACR appropriateness criteria on metastatic bone disease. *Journal of the American College of Radiology : JACR* 2010;7:400-409
165. Khatcheressian JL, Wolff AC, Smith TJ, et al. American Society of Clinical Oncology 2006 update of the breast cancer follow-up and management guidelines in the adjuvant setting. *Journal of clinical oncology : official journal of the American Society of Clinical Oncology* 2006;24:5091-5097
166. Briganti A, Passoni N, Ferrari M, et al. When to perform bone scan in patients with newly diagnosed prostate cancer: external validation of the currently available guidelines and proposal of a novel risk stratification tool. *European urology* 2010;57:551-558
167. Erturan S, Yaman M, Aydin G, et al. The role of whole-body bone scanning and clinical factors in detecting bone metastases in patients with non-small cell lung cancer. *Chest* 2005;127:449-454
168. Yang HL, Liu T, Wang XM, et al. Diagnosis of bone metastases: a meta-analysis comparing (1)(8)FDG PET, CT, MRI and bone scintigraphy. *European radiology* 2011;21:2604-2617
169. Shen G, Deng H, Hu S, et al. Comparison of choline-PET/CT, MRI, SPECT, and bone scintigraphy in the diagnosis of bone metastases in patients with prostate cancer: a meta-analysis. *Skeletal radiology* 2014;43:1503-1513
170. Houssami N, Costelloe CM. Imaging bone metastases in breast cancer: evidence on comparative test accuracy. *Annals of oncology : official journal of the European Society for Medical Oncology / ESMO* 2012;23:834-843

171. Duo J, Han X, Zhang L, et al. Comparison of FDG PET/CT and gadolinium-enhanced MRI for the detection of bone metastases in patients with cancer: a meta-analysis. *Clinical nuclear medicine* 2013;38:343-348
172. Khoo MM, Tyler PA, Saifuddin A, et al. Diffusion-weighted imaging (DWI) in musculoskeletal MRI: a critical review. *Skeletal radiology* 2011;40:665-681
173. Even-Sapir E, Metser U, Flusser G, et al. Assessment of malignant skeletal disease: initial experience with 18F-fluoride PET/CT and comparison between 18F-fluoride PET and 18F-fluoride PET/CT. *Journal of nuclear medicine : official publication, Society of Nuclear Medicine* 2004;45:272-278
174. Schiepers C, Nuyts J, Bormans G, et al. Fluoride kinetics of the axial skeleton measured in vivo with fluorine-18-fluoride PET. *Journal of nuclear medicine : official publication, Society of Nuclear Medicine* 1997;38:1970-1976
175. Li W, Ma L, Wang X, et al. C-choline PET/CT tumour recurrence detection and survival prediction in post-treatment patients with high-grade gliomas. *Tumour biology : the journal of the International Society for Oncodevelopmental Biology and Medicine* 2014
176. Luboldt W, Kufer R, Blumstein N, et al. Prostate carcinoma: diffusion-weighted imaging as potential alternative to conventional MR and 11C-choline PET/CT for detection of bone metastases. *Radiology* 2008;249:1017-1025
177. Mosavi F, Johansson S, Sandberg DT, et al. Whole-body diffusion-weighted MRI compared with (18)F-NaF PET/CT for detection of bone metastases in patients with high-risk prostate carcinoma. *AJR American journal of roentgenology* 2012;199:1114-1120
178. Carrio I. *PET/MRI Methodology and Clinical Applications*. Berlin, Heidelberg : Springer Berlin Heidelberg : Imprint: Springer; 2014
179. Peller P. *PET-CT and PET-MRI in Oncology A Practical Guide*. Berlin, Heidelberg : Springer Berlin Heidelberg : Imprint: Springer,; 2012
180. Walter SD, Macaskill P, Lord SJ, et al. Effect of dependent errors in the assessment of diagnostic or screening test accuracy when the reference standard is imperfect. *Statistics in medicine* 2012;31:1129-1138
181. Pasoglou V, Michoux N, Peeters F, et al. Whole-Body 3D T1-weighted MR Imaging in Patients with Prostate Cancer: Feasibility and Evaluation in Screening for Metastatic Disease. *Radiology* 2014:141242

182. Higgins JP, Thompson SG, Spiegelhalter DJ. A re-evaluation of random-effects meta-analysis. *Journal of the Royal Statistical Society Series A* 2009;172:137-159
183. Li B, Li Q, Nie W, et al. Diagnostic value of whole-body diffusion-weighted magnetic resonance imaging for detection of primary and metastatic malignancies: a meta-analysis. *European journal of radiology* 2014;83:338-344
184. Tombal B, Alcaraz A, James N, et al. Can we improve the definition of high-risk, hormone naive, non-metastatic prostate cancer? *BJU international* 2014;113:189-199
185. Eisenhauer EA, Therasse P, Bogaerts J, et al. New response evaluation criteria in solid tumours: revised RECIST guideline (version 1.1). *European journal of cancer* 2009;45:228-247
186. Koh DM, Hughes M, Husband JE. Cross-sectional imaging of nodal metastases in the abdomen and pelvis. *Abdominal imaging* 2006;31:632-643
187. Gudbjartsson H, Patz S. The Rician distribution of noisy MRI data. *Magnetic resonance in medicine* 1995;34:910-914
188. Zweig MH, Campbell G. Receiver-operating characteristic (ROC) plots: a fundamental evaluation tool in clinical medicine. *Clinical chemistry* 1993;39:561-577
189. DeLong ER, DeLong DM, Clarke-Pearson DL. Comparing the areas under two or more correlated receiver operating characteristic curves: a nonparametric approach. *Biometrics* 1988;44:837-845
190. Liddell FD. Simplified exact analysis of case-referent studies: matched pairs; dichotomous exposure. *Journal of epidemiology and community health* 1983;37:82-84
191. WA S. Reliability of content analysis: the case of nominal scale codin. *Public Opinion Quarterly* 1955;19:321-325.
192. Landis JR, Koch GG. The measurement of observer agreement for categorical data. *Biometrics* 1977;33:159-174
193. Schmidt GP, Baur-Melnyk A, Haug A, et al. Comprehensive imaging of tumour recurrence in breast cancer patients using whole-body MRI at 1.5 and 3 T compared to FDG-PET-CT. *European journal of radiology* 2008;65:47-58

194. Dutoit JC, Vanderkerken MA, Verstraete KL. Value of whole body MRI and dynamic contrast enhanced MRI in the diagnosis, follow-up and evaluation of disease activity and extent in multiple myeloma. *European journal of radiology* 2013;82:1444-1452
195. Ghanem N, Altehoefer C, Kelly T, et al. Whole-body MRI in comparison to skeletal scintigraphy in detection of skeletal metastases in patients with solid tumours. *In vivo* 2006;20:173-182
196. Kwon JW, Yoon YC, Choi SH. Three-dimensional isotropic T2-weighted cervical MRI at 3T: comparison with two-dimensional T2-weighted sequences. *Clinical radiology* 2012;67:106-113
197. Hori M, Kim T, Onishi H, et al. Uterine tumours: comparison of 3D versus 2D T2-weighted turbo spin-echo MR imaging at 3.0 T--initial experience. *Radiology* 2011;258:154-163
198. Verma S, Turkbey B, Muradyan N, et al. Overview of dynamic contrast-enhanced MRI in prostate cancer diagnosis and management. *AJR American journal of roentgenology* 2012;198:1277-1288
199. Bloch BN, Genega EM, Costa DN, et al. Prediction of prostate cancer extracapsular extension with high spatial resolution dynamic contrast-enhanced 3-T MRI. *European radiology* 2012;22:2201-2210
200. Preston MA, Harisinghani MG, Mucci L, et al. Diagnostic tests in urology: magnetic resonance imaging (MRI) for the staging of prostate cancer. *BJU international* 2013;111:514-517
201. Hansen J, Rink M, Bianchi M, et al. External validation of the updated Briganti nomogram to predict lymph node invasion in prostate cancer patients undergoing extended lymph node dissection. *The Prostate* 2013;73:211-218
202. Nelson JB, Love W, Chin JL, et al. Phase 3, randomized, controlled trial of atrasentan in patients with nonmetastatic, hormone-refractory prostate cancer. *Cancer* 2008;113:2478-2487
203. Scher HI, Fizazi K, Saad F, et al. Increased survival with enzalutamide in prostate cancer after chemotherapy. *The New England journal of medicine* 2012;367:1187-1197
204. Budiharto T, Joniau S, Lerut E, et al. Prospective evaluation of 11C-choline positron emission tomography/computed tomography and diffusion-weighted magnetic resonance imaging for the nodal staging of prostate cancer with a high risk of lymph node metastases. *European urology* 2011;60:125-130

205. Mettler FA, Jr., Huda W, Yoshizumi TT, et al. Effective doses in radiology and diagnostic nuclear medicine: a catalog. *Radiology* 2008;248:254-263

XIII. APPENDIX

Clin Transl Imaging (2015) 3:141–157
DOI 10.1007/s40336-015-0120-4

REVIEW ARTICLE

wbMRI to detect bone metastases: critical review on diagnostic accuracy and comparison to other imaging modalities

Vasiliki Pasoglou[1] · Nicolas Michoux[1] · Bertrand Tombal[2] · François Jamar[3] · Frédéric E. Lecouvet[1]

Received: 2 February 2015 / Accepted: 12 March 2015 / Published online: 9 April 2015

Abstract Numerous imaging modalities are available for the diagnosis of bone metastases (BM) in patients with cancer. This paper reviews published studies comparing whole-body (wb) MRI to BS, PET or PET-CT to provide up-to-date evaluation of the diagnostic accuracy of wbMRI to detect BM. This review is based on a systematic search of the literature of studies evaluating the diagnostic performance of wbMRI for BM detection. Evidence synthesis was achieved via a classification tree, which provides an overview of the performance of the different imaging techniques and of the context in which these are assessed, and an evidence table to seek confirmation of the diagnostic value of the imaging techniques. Eligible studies ($n = 23/301$) included patients with cancer who underwent wbMRI for suspicion of BM or for systematic cancer staging, compared with at least one other imaging tool. The evidence supporting the superiority of wbMRI over BS for BM screening is strong. wbMRI with diffusion-weighted imaging (DWI) sequence has higher sensitivity than wbMRI alone. The respective accuracies of wbMRI and FDG PET-CT differ depending both on the type of analysis (lesion, region or patient-based) and primary cancer. wbMRI and PET-CT emerge as the techniques of choice for the diagnosis of BM. The inclusion of DWI in wbMRI protocols is of value to optimize the sensitivity but does not add in specificity. This indicates the importance of the anatomical sequences in those protocols. Further comparisons between wbMRI and DWI alone, ^{18}F-NaF, ^{11}C-Choline, PSMA PET-CT and PET-MRI systems remain necessary.

Keywords Cancer · Bone · Metastasis · Imaging · MRI · PET · Meta-analysis

Abbreviations

Se	Sensitivity
Sp	Specificity
CT	Computed tomography
MRI	Magnetic resonance imaging
wbMRI	Whole-body magnetic resonance imaging
DWI	Diffusion-weighted imaging
STIR	Short tau inversion recovery
PET	Positron emission tomography
SPECT	Single photon emission computed tomography
BS	Bone scintigraphy
BM	Bone metastases
SD	Statistical difference between capability (Se/Sp) values assessed at a standard p value <0.05
bSD	Statistical difference between capability values assessed at a p value compliant with Bonferroni's correction
nsSD	Statistical difference between capability values superior or equal to 5 % assessed qualitatively or reported to be statistically non-significant ($p > 0.05$)

V. Pasoglou and N. Michoux contributed equally to this work.

✉ Nicolas Michoux
nicolas.michoux@uclouvain.be

Frédéric E. Lecouvet
frederic.lecouvet@uclouvain.be

[1] Department of Radiology, Institut de Recherche Expérimentale et Clinique (IREC – IMAG), Brussels, Belgium

[2] Department of Urology, Cliniques Universitaires Saint-Luc, Université Catholique de Louvain, Hippocrate Avenue 10/2942, 1200 Brussels, Belgium

[3] Department of Nuclear Medicine, Cliniques Universitaires Saint-Luc, Université Catholique de Louvain, Hippocrate Avenue 10/2942, 1200 Brussels, Belgium

Eq Statistical difference between capability values inferior to 5 % assessed qualitatively or reported to be statistically non-significant ($p > 0.05$)

Introduction

In adults, bone metastases (BM) are more common than primary bone cancers. Skeletal metastatic disease occurs in 30–70 % of all cancers. Breast cancer is the first cause of BM in women and prostate cancer in men, followed by lung cancer [1]. In many patients, bone involvement is diagnosed after a complication such as pain, pathological fracture or compression of adjacent structures. Early and reliable detection of bone involvement is essential to plan the most appropriate therapy given the disease stage and to prevent complications.

Numerous imaging modalities are used to detect bone involvement. X-rays require extensive bone destruction before a metastasis can be detected; as a result the diagnosis of a metastasis is delayed [2].

Although computed tomography (CT) has better anatomical resolution and soft tissue contrast than X-rays, it only detects cortical and trabecular destruction and not bone marrow involvement with subsequent delay in diagnosis of BM. A disadvantage of CT is the use of ionizing radiation, which may become critical as the survival rates of patients with cancer are notably increased [2].

Bone scintigraphy (BS) is widely used for the assessment of bone disease and remains the first line imaging modality for cancer patients with a significant risk for BM. The results of studies using more recent imaging techniques, i.e., MRI and PET, have underlined its limited specificity and sensitivity [3, 4]. Single photon emission computed tomography (SPECT) and CT improve the specificity of the examination but remain limited in terms of sensitivity [4, 5].

Positron emission tomography (PET)-CT is used for staging of a large variety of cancers. The most widely used tracer ^{18}F-FDG is a non-specific tumor-marker, which relies on the heightened glycolysis in tumor cells. Functional data from PET are often combined with the anatomical information provided by CT in one single examination, bringing together the strength of each technique [6].

Magnetic resonance imaging (MRI) is a sensitive method for the early detection of BM as it allows the identification of metastatic lesions in the bone marrow before bone remodeling occurs. Its effectiveness relies on the high contrast between normal bone marrow and the metastatic deposits [7, 8]. Axial skeleton MRI, which covers the spine, pelvis and proximal femurs, has already proven to be powerful to detect lesions, with higher sensitivity and specificity than BS [9–11].

Several early studies using a whole-body (wb) MRI approach have confirmed that wbMRI is superior to BS for the detection of skeletal metastases [12, 13]. The lack of ionizing radiation makes it especially promising for the imaging of pediatric and pregnant patients. Diffusion-weighted imaging (DWI) pulse sequences have been more recently included in MRI studies with the hope to improve the detection of tumoral lesions, characterized by impeded water diffusivity in tissues [14–16]. Normal structures as brain, salivary glands, tonsils, spleen, lymph nodes, prostate, and gonads may demonstrate high signal on high b values DWI, and should not be considered as pathologic findings [17, 18].

Because of the limitations of older imaging modalities [19, 20] and thanks to the latest advances in MRI (TNM staging in a single session [21], shorter examination times without compromises in spatial resolution [22], 3D whole-body sequences [23], diffusion-weighted sequences [24]), the imaging choice for BM screening is progressively shifting to wbMRI and/or PET-CT. To substantiate this evolution, the current paper draws up a review of the literature focusing on wbMRI and compares it to BS, PET or PET-CT for BM screening, and updates the information on their respective diagnostic accuracy for BM detection.

Methods

A systematic search of the literature was undertaken to identify studies using wbMRI for BM screening. A sequential search based on keywords was performed under PubMed as indicated in Table 1.

Following the systematic search, an evaluation of the abstract content was undertaken to identify articles assessing wbMRI accuracy for BM detection and compares it to other BM screening imaging modalities. Therefore, abstracts of all articles identified upstream were independently reviewed by two authors (V. Pasoglou and F. Lecouvet). Disagreement on study eligibility was resolved by discussion and consensus. The eligibility criteria of a study were defined as follows: (i) report on the diagnostic value of wbMRI in the detection of BM, (ii) comparison of wbMRI (anatomical sequences) with or without DWI to BS and/or PET and/or PET-CT, (iii) explicit report on the comparison of imaging technique capabilities Se (sensitivity) and/or Sp (specificity) in the same group of subjects, (iv) study of subjects with known primary malignant solid tumors, (v) whole-body imaging study in which at least the area from the neck to the pelvis was imaged, (vi) study where the reference standard did not consist of only one of the tests under comparison, and (vii) study including at

Table 1 Design of the systematic search of the literature pertaining to whole-body MRI of bone metastases

Sequence of the search	Keywords delimiting the search	PubMed references
1	MRI OR MR imaging OR magnetic resonance imaging	408479
2	Search 1 AND Bone	51448
3	Metastases OR Metastasis	320240
4	Search 2 AND Search 3	3084
5	Whole-body OR Whole body OR wb OR wbMRI OR wbMRI	76167
6	Search 4 AND Search 5	301

Search performed with the PubMed Advanced Search Builder on 11/20/2014. A set of 301 articles potentially relevant to the quantitative assessment of wbMRI accuracy was identified

least 10 patients. Only English or French language studies were considered because the investigators were familiar with these languages. Animal studies, opinion or update articles, case reports, feasibility studies, review studies and meta-analyses, and retrospective studies were not included. Articles dealing with the diagnostic accuracy of wbMRI in haematological cancers, particularly lymphoma and myeloma, were not considered.

Eligible studies identified after the evaluation based on abstract content were independently reviewed by the authors. Because quality scores remain difficult to assign objectively to studies design, are subjects of debate in their proper use [25, 26], and are essentially dedicated to meta-regression (which is not performed in this review), no formal quantitative appraisal was performed. The quality of a study was assessed by checking the compliance in its implementation with items 3, 4, 5, 7, 10, and 11 listed in STARD (STAndards for the Reporting of Diagnostic accuracy studies) [27, 28] as well as with questions 1, 2, 3, 6, 7, 10 and 11 listed in QUADAS (QUality Assessment tool for Diagnostic Accuracy Studies) [28]. Issues on one or more items, and thus on the exploitability of a study in this review, were resolved in consensus.

Then, a three-step assessment of the elected studies was undertaken. Firstly, a review of the reference standard and patient selection methodology was performed with two aims: (i) to check whether the reference was independent, consistently applied and adequate to correctly classify the target conditions (lesion or patient), (ii) to identify studies with a potential selection bias, which would motivate a subgroup analysis of imaging techniques capabilities (Se/Sp). The outcome of this first step is a collection of studies being close enough in their reference and population to ensure a meaningful cross-analysis of the diagnostic performances.

Secondly, information on the main study characteristics (i.e. primary cancer, scoring system, imaging modalities being compared, reference standard) and conclusions were listed in Table 2 in order to provide a comprehensive overview before evaluation. The sample size of the individual studies, as well as the various MR sequences composing the wbMRI protocols were reviewed in detail.

Thirdly, the comparative evaluation of imaging techniques was performed, starting with the assessment of the repeatability of the readings from wbMRI (with or without DWI), BS, PET and PET-CT when possible.

A classification tree, i.e., a visual and analytical decision support tool, of imaging techniques performance for BM screening, was built. This tree-shaped overview addresses the following questions: (i) interventional or observational prospective study, (ii) multi- or a mono-centric study, (iii) reference standard consisting in histology for all patients, (iv) multiple or a unique primary cancer, (v) DWI sequence included or not in addition to the anatomical MRI, (vi) the type of primary tumor, (vii) lesion, region or patient-based analysis (Fig. 1a). A color-coded Youden index scale measuring the diagnostic accuracy of imaging techniques was computed and superimposed on the tree, with the aim to rank imaging techniques and to identify the primary cancers for which the screening of BM using wbMRI was the most effective.

An evidence table was computed to seek confirmation of the superiority of an imaging technique by reviewing the frequency of significance levels with which its capabilities (Se/Sp) differed from those of other techniques (Table 3). Four levels of significance were considered to reflect the following facts: the capabilities of the imaging techniques may be compared qualitatively (without statistical tests), the significance level is rarely adjusted to the number of hypotheses tested, and/or the actual p value of a test is not always reported. From superior to inferior quality ranking, a red level was given when differences between capability values were assessed at a p value compliant with Bonferroni's correction (bSD), a black level when differences between capability values were assessed at a standard p value <0.05 (SD), a green level when differences between capability values were superior or equal to 5 % and were assessed qualitatively, or were reported to be statistically non-significant (nsSD), and a blue level when differences between capability values were inferior to 5 %

Table 2 Study characteristics and main results reported by authors

Study	Cancer	Patients (PP/BM)	Analysis	Modality	Reference standards	Reported conclusions
Antoch[a]	Multiple origins	98 (11/87)	L	MRI PET-CT	Histology and clinical/radiological follow-up	PET CT > wbMRI for TNM staging
Balliu*	Multiple origins	38 (18/–)	P	MRI BS	Clinical follow-up, additional imaging tests and/or biopsy	wbMRI > BS (Se, Sp, Acc) Detects lesions in tissues other than bone
Costelloe	Breast 29 (29/862)		R	MRI BS	Biopsy or imaging studies other than wbMRI and BS	wbMRI > BS (Se) for BM Detects lesions of the liver
Daldrup-Link*	Multiple origins	39 (21/51)	P + L	MRI PET BS	Histopathology for 22 of the 51 BM All BM: clinical and imaging follow-up	WbMRI > BS (Se) for BM WBMRI < PET-CT (Se) for BM
Engelhard[a]	Breast	22 (12/–)	P	MRI BS	Unclear primary origin cross-checked by at least one follow-up study (MRI, BS, CT and X-Rays)	wbMRI tends to have a higher accuracy It should be preferred in patients with high suspicion of metastasis
Eustace	Multiple origins	25 (25/–)	R	MRI BS	Clinical outcome (≥12 months) Additional imaging (CT, 11 patients; MRI, 6 patients) Biopsy (13 patients), Autopsy (1 patient)	wbMRI > BS (Se) for BM
Gutzeit[a]	Prostate (11), breast (25)	36 (7/45)	L	$DWI^{0/1000}$ BS	Consensus reading of all available imaging (DWIBS, CT, MRI, Scintigraphy, PET, PET-CT,US, X-Rays) Oncological follow-up (≥6 months)	DWIBS is not superior to BS for staging More BM are detected with DWIBS
Heusner[a]	Breast	20 (7/268)	P	PET-CT $DWI^{50/600/800}$	BS + other MR sequences + DWI (all patients)	DWI sensitive but unspecific for locoregional or metastatic breast cancer staging
Heusner	Melanoma, NSCLC	109 (11/–)	P	MRI PET-CT	Radiological and clinical follow-up	PET-CT and MRI are equally effective for BM
Jouvet[a]	Melanoma	37 (16/–)	L	MRI + $DWI^{0/800}$ DWI PET-CT CT US	Histology or sequential imaging during clinical follow-up (≥9 months)	wbMRI equivalent to combined CT + PET-CT + lymph node US in diagnostic performance
Kembhavi[a]	Solid small round cell tumors	34 (6/124)	L	PET-CT MRI	Conventional staging and clinical evaluation For BM: PET-CT and BMA/B (30/34 patients) BS with biopsy (4/34 patients)	wbMRI has high diagnostic accuracy
Kumar	Multiple origins	26 (26/–)	R	MRI PET-CT BS	Discordant findings evaluated by Clinical outcome (≥11 months), MRI, Iliac crest biopsy	wbMRI and PET-CT>BS (Se, Sp) for BM
Laurent[a]	melanoma	35 (–/14)	L	MRI PET-CT	Histology or imaging or clinical follow-up	wbMRI with DWI is the most accurate method for detecting secondary lesions

Table 2 continued

Study	Cancer	Patients (PP/BM)	Analysis	Modality	Reference standards	Reported conclusions
Leboulleux	Multiple origins	79 (36/333)	P + R + L	MRI BS	Discordant findings evaluated by second examination and/or MRI with contrast focused on the skeletal segment involved	Bone staging is recommended with Somatostatin Receptor BS and spine MRI
Lecouvet*	Prostate	100 (100/–)	P	MRI + $DWI^{0/1000}$ BS BS/TXRBS/TXR/CT	Consensus review of available imaging tests (BS/TXR and wbMRI), follow-up ≥6 months	wbMRI outperforms BS and BS/TXR for BM wbMRI performs as well as CT for LM
Ohno*	NSCLC	90 (25/–)	P	MRI PET-CT	Standard imaging, Biopsy, follow-up (≥20 months)	wbMRI as effective as FDG-PET for M-staging of lung cancer patients
Pfannenberg[a]	Melanoma	64 (–/50)	L	MRI PET-CT PET CT	Histology Imaging follow-up (PET-CT, CT, dedicated MRI, US, BS or X-Rays) Clinical follow-up	Whole-body staging is most accurate by combining PET-CT and organ-specific wbMRI
Sakurai*	Thyroid	23 (20/–)	R	MRI + $DWI^{0/800}$ PET-CT MRI	Minimum of 2 imaging modalities (BS, wbMRI, PET, and CT)	Adding DWI improved sensitivity and the overall accuracy of wbMRI for BM
Schmidt	Multiple origins	30 (23/102)	P + L	MRI PET-CT	Radiological follow-up (≥6 months)	wbMRI and PET-CT may improve the detection of BM
Schraml*	Neuroendocrine tumors	51 (41/131)	P + L	PET-CT PET CT MRI	Correlation of radiological, histologic and surgical data Radiologic follow-up (≥12 months)	PET-CT and wbMRI have comparable overall lesion-based but different organ-based detection rates wbMRI > PET-CT (detection rate) for BM and liver M PET-CT > wbMRI (Se) for LM and lung M
Sohaib	renal	47 (15/34)	P + L	MRI BS	Consensus review by 2 radiologists, further imaging and follow-up	wbMRI > BS (Se) for BM
Takenaka*	NSCLC	115 (25/67)	P + L	MRI + $DWI^{0/1000}$ MRI DWI PET-CT BS	Results of initial and follow-up imaging (BS, FDG-PET/CT, wbMRI) Biopsy ($n = 52$ sites), follow-up	wbMRI with DWI is as accurate as BS and/or PET-CT for BM
Venkitaraman	Prostate	39 (10/–)	P	MRI BS	Initial study of the MRI and BS, other imaging (X-rays, CT) and follow-up	wbMRI did not show a significant advantage over BS

Patients PP number of patients positive to bone metastases, *BM* number of bone metastases, *Analysis P* patient-based, *R* region-based, *L* lesion-based. *MRI* magnetic resonance imaging, *DWI* (*DWIBS*) diffusion-weighted imaging (*b* values when specified are given in s/mm^2 in uppercase), *PET* positron emission tomography. *CT* computed tomography, *US* ultrasound, *BS* bone scintigraphy, *TXR* targeted X-rays, *M* metastasis, *BM* bone metastasis, *LM* lymph node metastasis *Se* sensitivity, *Sp* specificity, *Acc* accuracy

* Statistical significance assessed at $p < 0.05$ with no adjustment for performing multiple comparisons

[a] Qualitative comparison (reported or performed) of techniques capabilities

and were assessed qualitatively, or were reported to be statistically non-significant (Eq).

Results

Literature search

Three hundred and one studies pertaining to wbMRI of BM were identified following the systematic search on PubMed (Table 1). Twenty-four studies [12, 20, 22, 29–49] met the eligibility criteria of the refined evaluation by abstract content, among which twenty-three presented data in sufficient detail to permit a statistical analysis (rejection of [31]).

Reference standard

Certain limitations, heterogeneity and inconsistency appeared in the implementation of the best achievable method for establishing the presence or absence of BM. All studies used as reference standard the clinical and imaging follow-up of the patients, which included the imaging modalities under evaluation. Hence, the reference standard was never completely independent, leading to a potential bias for the definition of true negative and for the assessment of Sp [34]. Certain authors did not use the same reference standard for all patients or/and lesions, or performed various additional examinations when disagreement was present between imaging modalities [12, 31, 38, 39, 49]. Histological examination of certain lesions was performed in five studies [29–32, 37]. Though deviations from a quality design (relying in particular on positive answers to questions 5, 6 and 7 in QUADAS) were observed, the reference standards achieved by the 23 studies were considered as correctly classifying the target conditions (lesion or patient). The characteristics and conclusions of these studies are reported in Table 2.

Patient selection

All studies included cancer patients who underwent imaging for staging or evaluation of suspected BM due to symptoms, clinical findings or high levels of tumor markers. Two studies included patients with known bone metastasis [32, 49]. Engelhard et al. [12] studied patients with suspected BM on X-rays or inconclusive findings in BS. Costelloe et al. [22] studied only patients with known BM and admitted a favorable bias towards BS, as the selection of the patients was based on a previous positive BS. In these studies, the measurement of the capabilities Se/Sp may be influenced by the selection of the patients based on positive findings of one imaging modality. In spite of this selection bias, reported performances were against the favored modality (see Fig. 1a, b). Therefore, these study results were not submitted to a subgroup analysis. Balliu et al. [30] pointed out that patients with known BM were excluded. Five studies mention that the patients were newly diagnosed without specifying how [31, 35, 36, 38, 48]. The other 13 studies did not specify whether the presence of BM was an exclusion criterion or if patient selection was made at the initial staging. As a result, it was not possible to check whether a selection bias was present in these studies.

Fig. 1 **a** Classification tree of mono-cancer versus multi-cancer studies assessing the performance of imaging modalities in bone metastases. Each node of the tree shows the number of studies performed and includes a descriptive analysis of the technique capabilities (median value and range of capabilities Se, Sp, and Accuracy). As the diagnostic accuracy of a test is known to be dependent on prevalence of the disease in the population studied, the Youden index, a measure of the overall discriminative power of a test that is not affected by prevalence, is calculated from available data. Capabilities and performance are given for lesion, region and patient-based analyses. According to the following arbitrary rule (a *red color code* and/or at least a 0.1 difference in Youden index with other imaging techniques), wbMRI is superior to other imaging modalities for BM detection. **b** Classification tree of mono-cancer studies assessing the performance of imaging modalities in bone metastases. Capabilities and performance are given for lesion, region and patient-based analyses. According to the following arbitrary rule (a *red color code* and/or at least a 0.1 difference in Youden index with other imaging techniques), wbMRI appears superior for BM detection in kidney and melanoma [38, 42], while this superiority is challenged by PET-CT in breast cancer [12, 35]. wbMRI+DWI appears superior to other imaging modalities in prostate cancer [20, 34], while this superiority is challenged by PET-CT in lung, melanoma and thyroid cancers [43–45]

Study characteristics

Sample size

The strength of the statistical evaluation of the diagnostic performance of imaging techniques depends on the size of the data samples. A large heterogeneity across studies was observed with regard to this characteristic. Based on values that are reported, the median number of patients recruited in performance studies was 38 [range: 22; 115]; the median number of patients with confirmed BM was 19 [range: 6; 41]; and the median number of BM was 87 [range: 14; 862].

wbMRI planes and sequences

For the detection of BM, the majority of research teams used a whole-body STIR- or T1-weighted imaging in the coronal plane ($n = 12/23$ for T1 [12, 20, 22, 30, 31, 38, 41,

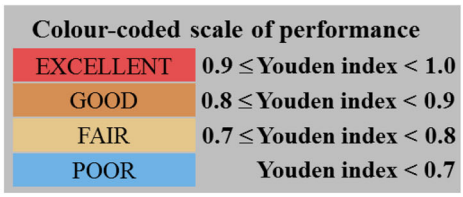

ELIGIBLE STUDIES

23

All studies are observational prospective and mono-centric, with a reference standard that does not rely on biopsy.

MONO-CANCER 13

without DWI 7

with DWI 6

MULTI-CANCER 10

without DWI 9*

with DWI 1 Gutzeit [32]

Lesion

	Se	Sp	Acc	Youden
DWI	98 [96; 100]	71 [47; 94]	83 [71; 94]	0.69 [0.47; 0.90]
MRI	94 [73; 100]	97 [73; 100]	94 [92; 95]	0.82 [0.69; 0.91]
MRI+DWI	98 [96; 100]	86 [76; 96]	91 [85; 96]	0.84 [0.76; 0.92]
PET-CT	99 [71; 97]	95 [80; 100]	91 [88; 95]	0.71 [0.71; 0.92]
PET	70 [69; 71]	73	72	0.44
CT	63 [62; 67]	90 [80; 100]	77 [68; 86]	0.55 [0.43; 0.67]
BS	80 [64; 96]	95 [94; 95]	95	0.75 [0.58; 0.91]

Region

	Se	Sp	Acc	Youden
DWI	-	-	-	-
MRI	64	100	90	0.64
MRI+DWI	77 [71; 82]	94 [89; 99]	94	0.71 [0.60; 0.81]
PET-CT	79	99	94	0.78
PET	-	-	-	-
CT	-	-	-	-
BS	60	99	-	0.59

Patient

	Se	Sp	Acc	Youden
DWI	91 [86; 96]	44 [8; 79]	59 [35; 83]	0.35 [-0.06; 0.75]
MRI	82 [64; 92]	95 [90; 100]	88 [84; 95]	0.76 [0.54; 0.87]
MRI+DWI	98 [96; 99]	95 [90; 99]	-	0.92 [0.86; 0.98]
PET-CT	100 [96; 100]	100 [86; 100]	100 [88; 100]	1.00 [0.82; 1.00]
PET	85 [82; 88]	94 [88-100]	91 [88; 94]	0.84 [0.82; 0.86]
CT	76	100	92	0.76
BS	78 [70; 96]	92 [80; 100]	88	0.73 [0.63; 0.79]

Lesion

	Se	Sp	Acc	Youden
DWI	94 [91; 97]	99	-	0.93 [0.89; 0.96]
MRI	89 [73; 98]	99 [76; 100]	91 [91; 96]	0.93 [0.70; 0.97]
PET-CT	84 [62; 90]	98 [80; 100]	91 [78; 96]	0.74 [0.39; 0.99]
PET	90	-	-	-
BS	57 [30; 76]	98 [97; 99]	-	0.42 [0.29; 0.70]

* Daldrup-Link [29]
Balliu [28]
Eustace [30]
Kumar [37]
Leboulleux [47]
Heusner [34]
Kembhavi [36]
Schmidt [42]
Antoch [27]

Patient

	Se	Sp	Acc	Youden
MRI	86 [64; 94]	92 [90; 100]	92 [91; 93]	0.78 [0.58; 0.76]
PET-CT	68 [45; 91]	100 [99; 100]	94 [93; 94]	0.68 [0.44; 0.91]
PET	86	89	-	0.75
BS	76 [72; 81]	88 [75; 100]	74	0.63 [0.47; 0.79]

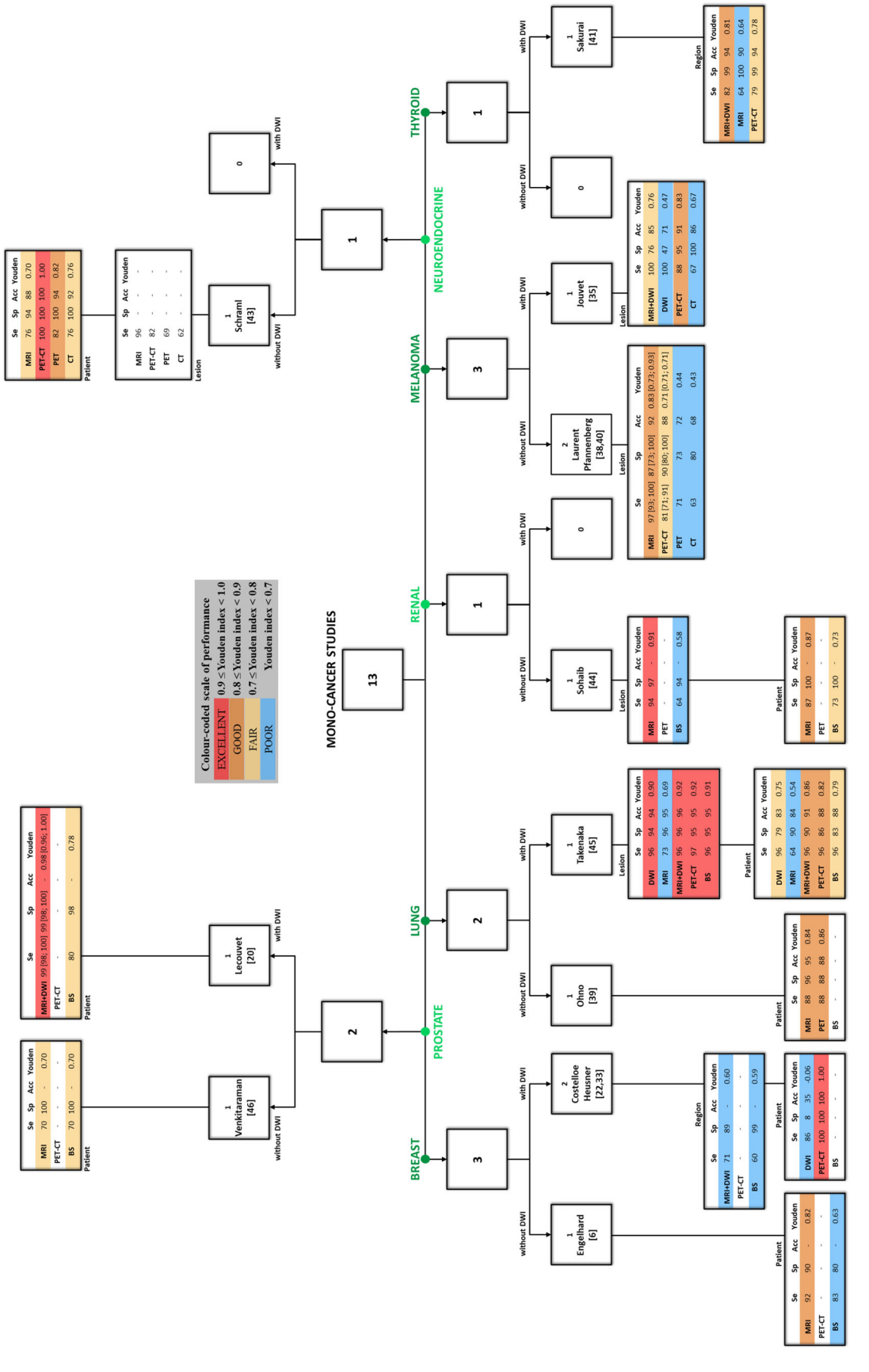

Fig. 1 continued

Table 3 Evidence table providing the following information: (i) the number and references of comparative studies available, (ii) the number of comparisons of Se/Sp available (which can be different from the number of studies when a particular study includes multiple analyses, such as analyses on a per-patient and a per-lesion-basis of the diagnostic capability Se/Sp), (iii) the frequency of significance levels with which the capabilities Se/Sp differed between imaging techniques. Four levels of significance are considered

	MRI superiority	PET superiority	Equivalence
Se	**2 (1)**	**1 + 1**	**1**
Sp	**1 + 1**	**1**	**1**
4 studies: Schraml, Pfannenberg, Daldrup, Ohno.			
5 Se comparisons and 4 Sp comparisons.			

	MRI superiority	PET-CT superiority	Equivalence
Se	**3 (2) + 7**	**3**	_
Sp	_	**1 + 3**	**7**
10 studies: Kumar, Heusner, Schmidt, Antoch, Sakurai, Schraml, Laurent, Kembhavi, Takenaka, Pfannenberg.			
13 Se comparisons and 11 Sp comparisons.			

	MRI+DWI superiority	PET-CT superiority	Equivalence
Se	**1**	_	**3**
Sp	**1**	**1**	**2**
3 studies: Jouvet, Sakurai, Takenaka.			
4 Se comparisons and 4 Sp comparisons.			

	MRI+DWI superiority	MRI superiority	Equivalence
Se	**3 (1)**	_	**1**
Sp	**1**	_	**3**
3 studies: Sakurai, Takenaka, Jouvet.			
4 Se comparisons and 4 Sp comparisons.			

	MRI superiority	BS superiority	Equivalence
Se	**5 (4) + 3**	**2**	**3**
Sp	**3 + 1**	_	**6**
9 studies:Balliu, Eustace, Kumar, Leboulleux, Engelhard, Sohaib, Daldrup, Venkitaraman, Takenaka.			
13 Se comparisons and 10 Sp comparisons.			

	MRI+DWI superiority	BS superiority	Equivalence
Se	**2 (1)**	_	**2**
Sp	**2**	**1 (1)**	**1**
3 studies: Takenaka, Costelloe, Lecouvet.			
4 Se comparisons and 4 Sp comparisons.			

	DWI superiority	PET-CT superiority	Equivalence
Se	**1**	**1**	**2**
Sp	_	**3 + 1**	_
3 studies: Jouvet, Takenaka, Heusner.			
4 Se comparisons and 5 Sp comparisons.			

	DWI superiority	BS superiority	Equivalence
Se	**1**	_	**2**
Sp	_	**1**	**2**
2 studies: Takenaka, Gutzeit.			
3 Se comparisons and 3 Sp comparisons.			

From superior to inferior quality ranking, a red level is given when differences between capability values are assessed at a p value compliant with Bonferroni's correction (bSD), a black level when differences between capability values are assessed at a standard p value <0.05 (SD), a green level when differences between capability values are superior or equal to 5 % and are assessed qualitatively, or are reported to be statistically non-significant (nsSD), and a blue level when differences between capability values are inferior to 5 % and are assessed qualitatively, or are reported to be statistically non-significant (Eq). The table can be read as follows: when comparing wbMRI to PET, there is some evidence, based on one Bonferroni-corrected statistical difference (1 bSD, in red) among two statistical differences (2 SD, in black) against one SD plus one non-significant statistical difference (1 nsSD, in green) and one equivalence (1 Eq, in blue), that MRI is more sensitive than PET

43, 46–49] and $n = 13/23$ for STIR [12, 20, 30, 32, 38–44, 46, 48]). Axial sequences were not systematically used for the detection of BM. A single study, the oldest one published [32], performed coronal STIR sequences only. Seven teams added dedicated sequences in the sagittal plane [12, 20, 22, 31, 39, 44, 48], and all teams used a T1-weighted SE sequence. Two teams did not use the same imaging protocol for all patients [31, 38]. Daldrup-Link et al. [31] did not perform STIR in all patients, assuming that the T1 sequence had higher spatial resolution, a comparable sensitivity and a higher specificity than STIR in children. Kembhavi et al. [38] added more sequences when a metastatic lesion was detected. Eight studies included DWI in their MRI protocol [20, 22, 34, 35, 37, 40, 43, 47] and seven of these studies quantitatively compared the diagnostic value of DWI alone or in combination with wbMRI.

Comparative evaluation of the imaging techniques

Repeatability

Over the 23 studies, 4 reported inter-observer agreement analysis on a per-lesion basis [34, 37, 41, 47], 2 reported inter-observer agreement analysis on a per-patient basis [20, 30] and 1 reported intra-observer agreement analysis [30, 37]. The visual detection of BM was assessed according to different scoring scales, using either a 2-point scale (presence or absence of lesion) [37], a 3-point scale [34], a 4-point scale [30], or even a 5-point scale (1 = lesion definitely absent, 2 = lesion probably absent, 3 = lesion equivocal, 4 = lesion probably present, 5 = lesion definitely present) [41, 47]. A consequence of this is a limitation of the pertinence of aggregating the results, as the measurement of agreement based on Kappa statistics may be negatively affected by the complexity of the scale.

Inter-observer agreement was reported to be very good for wbMRI + DWI ($K = 0.87$ [0.66; 1.00] based on three studies [20, 37, 47]); substantial for PET-CT ($K = 0.75$, one study [47]); substantial for wbMRI ($K = 0.73$ [0.66; 0.90], three studies [30, 41, 47]); substantial for PET ($K = 0.70$, one study [41]); substantial for DWI ($K = 0.66$ [0.64; 0.80], three studies [34, 37, 47]); and moderate for BS ($K = 0.60$ [0.26; 0.78], three studies [30, 34, 47]). Intra-observer agreement for wbMRI + DWI was reported to be very good ($K = 0.93$ [0.90; 0.95], on two readers [37]) and moderate for DWI ($K = 0.60$ [0.50; 0.70], on two readers [37]).

Context

The classification tree provides a global overview of the diagnostic accuracy of wbMRI in comparison with other imaging techniques used for BM screening, and of the context in which the accuracy was evaluated (Fig. 1a, b).

Quite typically, all studies consisted of observational prospective series and were performed in a single center. Studies did not use histopathology in all patients or did not use histopathology at all as reference standard. Half of the teams studied a single cancer and the remaining half addressed several primary cancers. In mono cancer studies, the performance of the imaging techniques was assessed by a single study, except in breast cancer (three studies [12, 22, 35]), melanoma (three studies [37, 40, 42]), prostate (two studies [20, 48]) and NSCLC (two studies [41, 47]). The performance was assessed either on a per-patient-basis, a per-region basis or on a per-lesion-basis. A single study assessed the imaging techniques on the three bases [49]. Five studies assessed imaging techniques on both a per-patient and a per-lesion-basis [31, 44–47].

Diagnostic accuracy

The color-coded scale of performance superimposed to the classification tree leads to the following observations. In mono-cancer studies (Fig. 1b), the most accurate imaging techniques for BM screening are PET-CT ([^{68}Ga] DOTA-TOC) in neuroendocrine tumors [45], wbMRI + DWI or PET-CT in thyroid [43], wbMRI in renal tumors [46], wbMRI or PET-CT in melanoma [37, 40, 42] and wbMRI + DWI or PET-CT or BS in lung [41, 47]. In prostate and breast cancers, trends differed for lesion, region and patient-based analysis. In prostate cancer, in patient-based analysis, wbMRI + DWI is more accurate [20] (Fig. 2), while wbMRI and BS are reported to be equivalent [48]. In breast cancer, wbMRI + DWI is more accurate in region-based analysis [22], while PET-CT is more accurate in patient-based analysis [50].

The cumulative analysis of the color codes shows that wbMRI + DWI is superior or equal to other techniques in 5/6 analyses [22, 43, 47], PET-CT is superior or equal to other techniques in 5/8 analyses [37, 45, 47, 50], wbMRI is superior or equal to other techniques in 7/11 analyses [12, 40–42, 46, 48], DWI alone is superior or equal to BS or PET-CT in 3/6 analyses [34, 47], BS is superior to wbMRI in 2/6 analyses [47], and BS is superior to wbMRI + DWI in 0/3 analyses [20, 22, 47].

When performances reported in mono-cancer studies are pooled together (Fig. 1a), the observation of the color codes suggests that wbMRI + DWI and PET-CT have similar diagnostic accuracy in region and patient-based analysis, while wbMRI (with or without DWI) is superior to other imaging techniques in lesion-based analysis.

In multi-cancer studies (Fig. 1a), wbMRI is superior to other imaging techniques in lesion and patient-based analysis. In prostate and breast cancers conjoint studies,

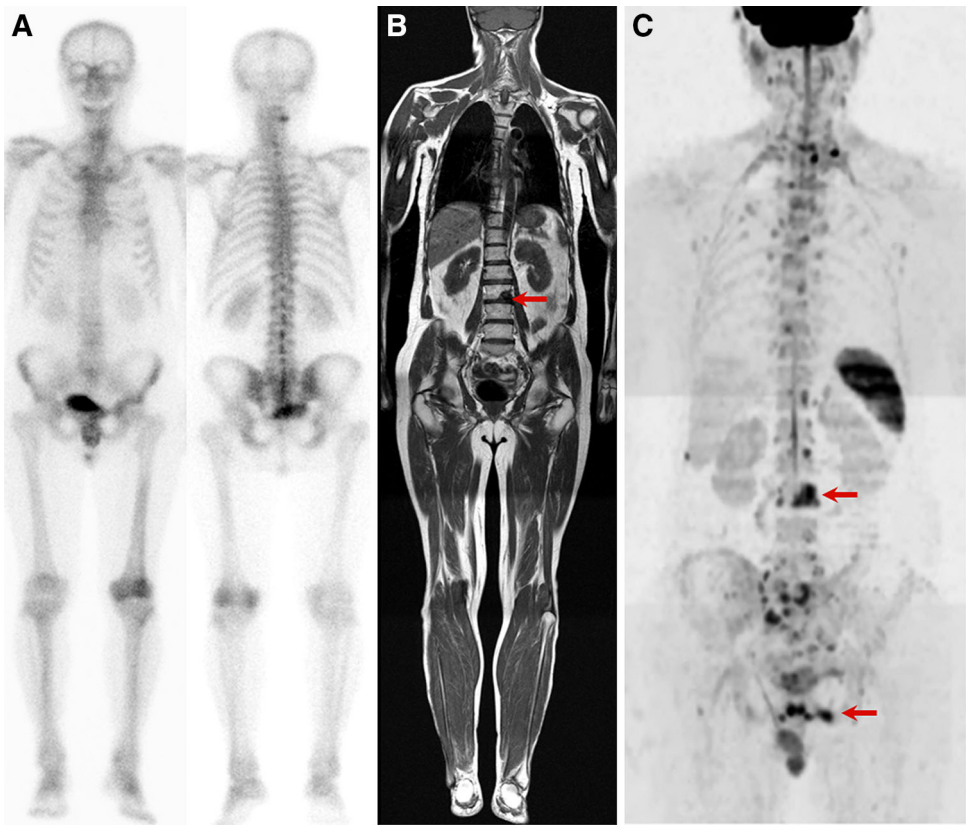

Fig. 2 Whole-body magnetic resonance imaging (MRI) versus false-negative bone scintigraphy (BS) for bone metastasis detection in a 65-year-old patient with newly diagnosed prostate cancer (prostate-specific antigen 18 ng/ml; Gleason score 7 [4 + 3]). **a** BS (anterior-posterior and posterior-anterior views) shows no significant lesion. **b** Coronal T1 and **c** diffusion-weighted MR images of the whole body confirm bone metastases within L3 and the left iliac bone (*arrows*). Reprinted from Eur Urol. 2012 Jul; 62 (1), Lecouvet FE, El Mouedden J, Collette L, Coche E, Danse E, Jamar F, Machiels JP, Vande Berg B, Omoumi P, Tombal B, "Can Whole body Magnetic Resonance Imaging with Diffusion-weighted Imaging Replace Tc 99m Bone Scanning and Computed Tomography for Single-Step Detection of Metastases in Patients with High-risk Prostate Cancer?" with permission from Elsevier

DWI is more accurate than BS in lesion-based analysis [34].

Capabilities Se and Sp

The evidence table leads to the following observations on the diagnostic value of imaging techniques (Table 3). There is strong evidence that wbMRI is more sensitive than BS (4 bSD among 5 SD) [32, 39, 46, 49] but less evidence concerning the superiority of wbMRI in terms of Sp (3 SD against 6 Eq). The superiority of MRI compared to BS in terms of Se is confirmed when DWI is added (1 bSD among 2 SD) [20, 22], while evidence on Sp is balanced. Very limited data exist on the comparison of DWI alone to BS; DWI may be more sensitive [34] but less specific [47]. Finally, there is strong evidence that DWI is less specific than PET-CT (3 SD) [37, 47], while difference in Se is not evident [37].

There is some evidence that wbMRI is more sensitive than PET (1 bSD among 2 SD) [42, 45] but evidence that wbMRI is more specific (1 SD) is limited. There is some evidence that wbMRI is more sensitive than PET-CT (2 bSD) [45, 51] and little evidence that PET-CT is more specific than wbMRI (1 SD against 7 Eq). There is insufficient (statistically demonstrated) evidence that adding DWI to wbMRI improves its Se compared to PET-CT and very little evidence that it improves its Sp (1 SD against 1 nsSD + 2 Eq). These results are to some extent consistent with the strong evidence that wbMRI + DWI is more sensitive than wbMRI alone (1 bSD among 3 SD) [43, 47], and with the lack of improvement in Sp by adding DWI to wbMRI (1 nsSD against 3 Eq) [43, 47].

Discussion

Background and current approach

The guidelines and consensus recommendations for bone staging in cancer differ substantially depending on the primary tumor, the local stage, the age and the symptoms of the patients [52]. For breast cancer, a plethora of imaging

methods is available for the detection of BM, although the use of BS is the most consistent [53, 54]. Unless multiple foci are detected, a positive BS should be confirmed by targeted radiographs or/and CT and MRI. For prostate cancer, staging BS is recommended in patients with a biopsy Gleason score >7 or with a prostate-specific antigen >10 ng/ml and palpable disease (cT2/T3) prior to treatment [55]. Regarding the follow-up of patients, BS is not necessary unless the prostate-specific antigen (PSA) level is ≥20 ng/mL, the Gleason sum is ≥8, the clinical stage is ≥T3a or the primary tumor is poorly differentiated [56–58]. In non-small cell lung cancer, the literature is not clear regarding the necessity of BS in every patient, even though the presence of BM radically changes the treatment and the prognosis [52, 59].

Such guidelines have to be updated in parallel to technical advances. This process requires a careful comparison of the newer techniques with the previous standards, in strong studies of diagnostic performance. Reviews are also helpful in this evaluation process. This study provides a critical review of the performance of wbMRI for BM screening versus other nuclear medicine or radiologic modalities, and derives conclusions from a classification tree and an evidence table for contrasting and combining results from studies implemented in different contexts.

Performance of wbMRI

In terms of self-consistency of the readings, the available data suggest that wbMRI + DWI has a high repeatability, while this repeatability is only moderate for DWI alone. wbMRI + DWI also demonstrates a high reproducibility, which is higher than that of PET-CT, wbMRI without DWI, and BS. The latter tends to be the less reproducible imaging technique, also when compared to DWI alone.

In terms of capability, there is some evidence that wbMRI is a more sensitive imaging technique compared to PET-CT, PET and BS. Adding DWI to wbMRI, the sensitivity of the whole-body examination is improved, without noticeably improving its specificity. DWI appears as a very promising detection tool for BM [35, 43]. However, this observation cannot be validated because of the currently limited number of studies assessing its Se and Sp. DWI may be more sensitive but less specific than BS. There is strong evidence that DWI is less specific than PET-CT, suggesting that the use of anatomical sequences remains essential in wbMRI protocols.

The review of "mono-cancer" studies shows that wbMRI with DWI has higher or equal diagnostic accuracy than PET-CT in lesion, region and patient-based analyses. BS is found to be inferior or equal to these two techniques in the three analyses. Adding DWI to conventional wbMRI sequences improves the accuracy (especially the Se) of wbMRI in region-based and patient-based analyses. However, DWI alone does not demonstrate a sufficiently high accuracy as false positive findings occur.

Multi-cancer studies constitute a heterogeneous framework for assessing the capabilities of the different techniques, and should be considered with caution if they are used for nuancing conclusions made from mono-cancers studies. Though DWI alone is found equivalent to wbMRI in lesion-based analysis, this report is based on a single study [34]. Adding DWI to wbMRI is not assessed in multi-cancer studies. BS is found to be inferior to wbMRI and PET-CT in lesion-based and patient-based analyses.

Comparison with other reviews

Five reviews exploring the diagnostic accuracy of MRI for BM screening were identified among which, three provide additional contextual information [60–62] and two may appear redundant (i.e., including studies discussed in this review) [63] or redundant and potentially biased (4/9 of elected studies coming from the same team on the same type of cancer) [64]. Based on 67 multi-cancer studies (anterior to January 2010 and including 7 studies on MRI and 15 on wbMRI), Yang et al. reported that ^{18}FDG PET and MRI were equivalent and both significantly more accurate than CT and BS for BM screening [61]. Based on 16 prostate cancer studies (anterior to November 2012 and including 3 studies on MRI, 1 on wbMRI and 2 on wbMRI + DWI), Shen et al. reported that MRI was superior to choline PET-CT and BS in patient-based analysis, though choline PET-CT had the highest specificity [62]. In the latter two reviews, MRI and wbMRI were not assessed separately. Based on 11 multi-cancer studies (anterior to Sept. 2010 and including 5 wbMRI studies discussed in our review), Wu et al. [60] reported that DWI had a high sensitivity but limited specificity for the detection of whole-body tumor involvement; a report consistent with previous observations showing that DWI excels at detecting bony lesions but is less capable in soft tissue metastases [65].

New techniques non-assessed because not meeting inclusion criteria

It has to be noted that when it comes to PET-CT, FDG was the only tracer used in the eligible studies. There is currently a lack of studies of diagnostic accuracies comparing wbMRI with PET-CT based on newer tracers such as ^{18}F sodium fluoride [66, 67], ^{11}C-Choline [65, 68, 69] or Prostate-Specific Membrane Antigen (PSMA) [70–72].

Luboldt et al. [73] compared the effectiveness of a fast DWI to anatomic MR sequences and to ^{11}C-Choline PET-CT. This team suggested that DWI is equivalent to, if not more sensitive than, the STIR and T1-weighted SE MR sequences and as effective as ^{11}C-Choline PET-CT for the

detection of prostate cancer BM. The need for anatomic sequences to avoid false positive observations must be emphasized [74]. Mosavi et al. [75] evaluated the accuracy of DWI versus NaF PET-CT for the detection of BM in patients with PCa, concluding that DWI has higher Sp but lower Se. Afshar-Oromieh et al. [72] demonstrated that suspicious PCa lesions present excellent contrast as early as 1 h post-injection of PSMA tracer. In a retrospective analysis of 319 patients who underwent ^{68}Ga-PSMA-ligand PET-CT, the same team found that PSMA is highly specific for PCa and can detect the disease in a high percentage of patients (82.8 %) [76].

PET-MRI is an innovative diagnostic imaging modality that combines the anatomical information given by MRI and the functional data from PET. Even though there has been great progress in this field, there are some problems that have to be resolved. The main pitfalls relate to imaging bias and artifacts due to image distortion [77, 78]. The technique is recent and will hopefully help in the comparison of MRI and PET, and in the identification of the necessary and sufficient images to obtain, which may differ according to the primary cancer.

Weaknesses of performance studies

No multicentre studies were identified during this review, which are however crucial before generalization. These studies allow enlarged and homogeneous enrolment of patients for each cancer type. The participation of investigators from different horizons offers the guarantee of an objective evaluation, not restricted by local habits, and facilitates evaluation of the inter-center repeatability and reproducibility of the technique [79].

There were different sources of heterogeneity affecting the reviewed performance studies, starting with the study design. Patients' inclusion criteria may affect Se/Sp, and also the prevalence of lesions. Following more strictly guidelines such as those summarized by Sardanelli et al. [80] may limit the different sources of bias (including those affecting the selection of patients) related to the implementation of performance studies.

A substantial heterogeneity regarding the "gold standard" is observed between studies and sometimes within the same study. It is known that when the reference standard does not correspond to the true target disease status, measurement of Se/Sp and Accuracy can be biased [81]. In patients with multiple BM, the histopathological confirmation after biopsy is neither feasible nor ethical, and probably unnecessary for all lesions. The majority of studies used the consensus reading of all clinical, biological and radiological results, along with a clinical and imaging follow up as gold standard. Thus, the need for standardization of the gold standard emerges. This general problem, common to any evaluation of a new diagnostic imaging tool, has to be addressed by a working group of clinicians with experience in the field of oncology in order to construct a consensus document which, like the STARD initiative, would include a list of criteria that have to be fulfilled (minimum follow-up period, appropriate and necessary imaging modalities, scoring system, reading methodology, relevant clinical or/and biological information, etc.

Furthermore, there was substantial heterogeneity in wbMRI sequences that vary depending on the team, the hospital, the country, the primary cancer. In recent studies, DWI was only used as a complement to the anatomical sequences. There is an urgent need to determine which sequences are the most appropriate, "necessary and sufficient" and cost/time effective in order to set a global guideline. Combining whole-body anatomic 3D sequences to DWI is a potential solution [23].

This review reveals certain methodological limitations in current performance studies and in turn, suggests how future studies should be built. The use of a tool such as STARD would help improve the quality of research on diagnostic performance of new technology [27]. Especially, quantities TP/FP/TN/FN, Se/Sp/Acc with their 95 % CI, the actual level of significance of a test, estimates of uncertainty, inconclusive tests and outliers, sources of bias, and gage repeatability and reproducibility analyses (allowing assessing whether a technique is capable or not) should be systematically reported to deliver a study of high quality (reproducible and exploitable).

Limitations of the review

As wbMRI and PET technology for BM detection represent a really « hot topic », with results of new studies published each month, our work is as a « snapshot » with conclusions that will show evolution very soon.

Only a PubMed search based on English and French language was undertaken, while other knowledge databases (EMBASE, Scopus, ScienceDirect, SpringerLink) and languages could have been considered to search for relevant performance studies. The search was updated until mid-November 2014. The review process did not include unpublished data or studies with unclear or incomplete reporting of technique capabilities Se/Sp. Hence, a publication bias remains possible. Funnel plot analysis was not performed. However, crosscheck of our elected studies with those of previously published reviews [60–64] confirms that no study compliant with our inclusion criteria was omitted.

We did not apply all of the criteria in STARD [27] and QUADAS [28] for assessing the quality of performance studies. Information on implementation (items 1 and 2 in

QUADAS) and on results (items 12, 13, 19, 20 and 21 to 24 in STARD) in primary studies was often reported in insufficient details or unclear. Therefore, potential for bias (internal validity) and lack of generalizability (external validity) were not studied and heterogeneity between studies was not measured in figures [80]. Twenty-three studies, respecting 6 questions in STARD and 7 questions in the QUADAS tool as far as can be ascertained, and fitting our own inclusion criteria, were considered of adequate quality for review. Our conclusions were drawn from a Youden-indexed classification tree and a four-level reading of statistical reports organized within an evidence table, providing a hierarchical analysis of the accuracy of imaging techniques. Hence, these conclusions can be extended or limited depending on whether new studies are performed or more conservative eligibility/quality criteria are applied.

Statistical approaches other than a decision tree and descriptive statistics from raw capability measurements reported in individual studies could be chosen for evidence synthesis, though this choice ultimately depends on the availability and accuracy of key data such as capabilities values, confidence intervals, and sources of bias. Due to the limited number of available studies in certain types of cancer and the heterogeneity in study characteristics (and their reporting), the search for characteristics significantly affecting the assessment of Se/Sp was considered of little relevance and no meta-regression was performed. Furthermore, as it remains difficult to establish the validity of the distributional assumption on between-study variance, no random effect model analysis was performed [82].

Conclusion

After previous reviews reporting on the performance of wbMRI compared to other imaging modalities for the screening of BM, our study confirms that there is still a critical need for multicentric and mono-cancer studies respecting more accurately the guidelines for implementing performance studies to enhance knowledge on the field. Studies assessing DWI and comparing wbMRI to PET with new promising radiotracers such as ^{18}NaF, ^{11}C and ^{18}F Choline and labeled PSMA are still missing, preventing to reach a definitive conclusion on which of these emerging methods will become the standard of choice in each primary cancer for BM screening.

Nevertheless, recently published performance studies bring additional information on the diagnostic accuracy of wbMRI. The evidence supporting the superiority of wbMRI over BS for BM detection, independently of the primary cancer, is today very robust. DWI alone does not demonstrate a sufficiently high diagnostic accuracy. DWI must be embedded in wbMRI as it improves the sensitivity of the examination.

Regarding the practical issue of the imaging pathway, i.e. when considering wbMRI instead of PET-CT for BM screening, this review provides some additional answers. Although their diagnostic accuracy appears roughly equivalent, it appears that wbMRI is superior in lesion-based analysis, while PET-CT seems to keep some advantage in patient-based analysis, especially in breast and neuroendocrine tumors. Notwithstanding this advantage and apart from all other considerations (radiation exposure, local availability of the techniques, availability of dedicated/tumor specific PET tracers, local experience, cost), wbMRI might be a more "universal" solution as it is sensitive to bone marrow infiltration by any metastasis regardless of the primary cancer, while PET-CT definitively relies on the affinity of the cancer and its metastases for a given tracer [83].

From a more general standpoint, the comprehensive review of the diagnostic performances suggests that the work-up of metastases will not remain "mono-technique" as it has been the historical case for BS; it will most likely be shared between wbMRI and PET according to the primary cancer [9, 83]. This scenario is further supported by the perspective offered by both techniques of an all-organ (non-bone limited) screening of metastasis [41, 51, 84].

Acknowledgments Supported by Grants from the Belgian non-profit organizations FRS-FNRS Télévie, Fondation Contre le Cancer and Fondation Saint Luc to VP and FEL

Conflict of interest V. Pasoglou, N. Michoux, B. Tombal, F. Jamar, F.E. Lecouvet declare no conflict of interest.

Compliance with ethics guidelines Critical review of human study.

References

1. Padhani AHJ (1998) Imaging in oncology/bone metastases. Isis Medical Media, Oxford, pp 765–787
2. Bronner F (2009) Bone and cancer. Springer, London
3. Schirrmeister H, Guhlmann A, Kotzerke J et al (1999) Early detection and accurate description of extent of metastatic bone disease in breast cancer with fluoride ion and positron emission tomography. J Clin Oncol 17:2381–2389
4. Even-Sapir E, Metser U, Mishani E et al (2006) The detection of bone metastases in patients with high-risk prostate cancer: 99mTc-MDP Planar bone scintigraphy, single- and multi-field-of-view SPECT, 18F-fluoride PET, and 18F-fluoride PET/CT. J Nucl Med 47:287–297
5. Savelli G, Maffioli L, Maccauro M et al (2001) Bone scintigraphy and the added value of SPECT (single photon emission tomography) in detecting skeletal lesions. Q J Nucl Med 45:27–37
6. Kim EE (2013) Clinical PET and PET/CT principles and applications. Springer, New York
7. Walker R, Kessar P, Blanchard R et al (2000) Turbo STIR magnetic resonance imaging as a whole-body screening tool for

metastases in patients with breast carcinoma: preliminary clinical experience. J Magn Reson Imaging 11:343–350
8. Lauenstein TC, Freudenberg LS, Goehde SC et al (2002) Whole-body MRI using a rolling table platform for the detection of bone metastases. Eur Radiol 12:2091–2099
9. Lecouvet FE, Geukens D, Stainier A et al (2007) Magnetic resonance imaging of the axial skeleton for detecting bone metastases in patients with high-risk prostate cancer: diagnostic and cost-effectiveness and comparison with current detection strategies. J Clin Oncol 25:3281–3287
10. Freedman GM, Negendank WG, Hudes GR et al (1999) Preliminary results of a bone marrow magnetic resonance imaging protocol for patients with high-risk prostate cancer. Urology 54:118–123
11. Ghanem N, Altehoefer C, Hogerle S et al (2002) Comparative diagnostic value and therapeutic relevance of magnetic resonance imaging and bone marrow scintigraphy in patients with metastatic solid tumors of the axial skeleton. Eur J Radiol 43:256–261
12. Engelhard K, Hollenbach HP, Wohlfart K et al (2004) Comparison of whole-body MRI with automatic moving table technique and bone scintigraphy for screening for bone metastases in patients with breast cancer. Eur Radiol 14:99–105
13. Nakanishi K, Kobayashi M, Nakaguchi K et al (2007) Whole-body MRI for detecting metastatic bone tumor: diagnostic value of diffusion-weighted images. Magn Reson Med Sci 6:147–155
14. Kwee TC, Takahara T, Ochiai R et al (2008) Diffusion-weighted whole-body imaging with background body signal suppression (DWIBS): features and potential applications in oncology. Eur Radiol 18:1937–1952
15. Pearce T, Philip S, Brown J et al (2012) Bone metastases from prostate, breast and multiple myeloma: differences in lesion conspicuity at short-tau inversion recovery and diffusion-weighted MRI. Br J Radiol 85:1102–1106
16. Thoeny HC, De Keyzer F (2007) Extracranial applications of diffusion-weighted magnetic resonance imaging. Eur Radiol 17:1385–1393
17. Muller MF, Prasad P, Siewert B et al (1994) Abdominal diffusion mapping with use of a whole-body echo-planar system. Radiology 190:475–478
18. Muller MF, Prasad PV, Bimmler D et al (1994) Functional imaging of the kidney by means of measurement of the apparent diffusion coefficient. Radiology 193:711–715
19. Hovels AM, Heesakkers RA, Adang EM et al (2008) The diagnostic accuracy of CT and MRI in the staging of pelvic lymph nodes in patients with prostate cancer: a meta-analysis. Clin Radiol 63:387–395
20. Lecouvet FE, El Mouedden J, Collette L et al (2012) Can whole-body magnetic resonance imaging with diffusion-weighted imaging replace Tc 99m bone scanning and computed tomography for single-step detection of metastases in patients with high-risk prostate cancer? Eur Urol 62:68–75
21. Pasoglou V, Larbi A, Collette L et al (2014) One-step TNM staging of high-risk prostate cancer using magnetic resonance imaging (MRI): toward an upfront simplified "all-in-one" imaging approach? Prostate 74:469–477
22. Costelloe CM, Kundra V, Ma J et al (2012) Fast Dixon whole-body MRI for detecting distant cancer metastasis: a preliminary clinical study. J Magn Reson Imaging 35:399–408
23. Pasoglou V, Michoux N, Peeters F et al. (2014) Whole-body 3D T1-weighted MR imaging in patients with prostate cancer: feasibility and evaluation in screening for metastatic disease. Radiology 275(1):155–166
24. Takahara TIY, Yamashita T, Yasuda S, Nasu S, Van Cauteren M (2004) Diffusion weighted whole body imaging with backgraound body signal suppression (DWIBS): technical impovement using free breathing STIR and high resolution 3D display. Radiat Med 22:275–282
25. Berlin JA, Rennie D (1999) Measuring the quality of trials: the quality of quality scales. JAMA 282:1083–1085
26. Greenland S (1994) Invited commentary: a critical look at some popular meta-analytic methods. Am J Epidemiol 140:290–296
27. Bossuyt PM, Reitsma JB (2003) Standards for reporting of diagnostic A: the STARD initiative. Lancet 361:71
28. Whiting P, Rutjes AW, Reitsma JB et al (2003) The development of QUADAS: a tool for the quality assessment of studies of diagnostic accuracy included in systematic reviews. BMC Med Res Methodol 3:25
29. Antoch G, Vogt FM, Freudenberg LS et al (2003) Whole-body dual-modality PET/CT and whole-body MRI for tumor staging in oncology. JAMA 290:3199–3206
30. Balliu E, Boada M, Pelaez I et al (2010) Comparative study of whole-body MRI and bone scintigraphy for the detection of bone metastases. Clin Radiol 65:989–996
31. Daldrup-Link HE, Franzius C, Link TM et al (2001) Whole-body MR imaging for detection of bone metastases in children and young adults: comparison with skeletal scintigraphy and FDG PET. AJR Am J Roentgenol 177:229–236
32. Eustace S, Tello R, DeCarvalho V et al (1997) A comparison of whole-body turboSTIR MR imaging and planar 99mTc-methylene diphosphonate scintigraphy in the examination of patients with suspected skeletal metastases. AJR Am J Roentgenol 169:1655–1661
33. Goo HW, Choi SH, Ghim T et al (2005) Whole-body MRI of paediatric malignant tumours: comparison with conventional oncological imaging methods. Pediatr Radiol 35:766–773
34. Gutzeit A, Doert A, Froehlich JM et al (2010) Comparison of diffusion-weighted whole body MRI and skeletal scintigraphy for the detection of bone metastases in patients with prostate or breast carcinoma. Skeletal Radiol 39:333–343
35. Heusner TA, Kuemmel S, Koeninger A et al (2010) Diagnostic value of diffusion-weighted magnetic resonance imaging (DWI) compared to FDG PET/CT for whole-body breast cancer staging. Eur J Nucl Med Mol Imaging 37:1077–1086
36. Heusner T, Golitz P, Hamami M et al (2011) "One-stop-shop" staging: should we prefer FDG-PET/CT or MRI for the detection of bone metastases? Eur J Radiol 78:430–435
37. Jouvet JC, Thomas L, Thomson V et al (2013) Whole-body MRI with diffusion-weighted sequences compared with 18 FDG PET-CT: CT and superficial lymph node ultrasonography in the staging of advanced cutaneous melanoma: a prospective study. J Eur Acad Dermatol Venereol. doi:10.1111/jdv.12078
38. Kembhavi SA, Rangarajan V, Shah S et al (2014) Prospective observational study on diagnostic accuracy of whole-body MRI in solid small round cell tumours. Clin Radiol 69:900–908
39. Kumar J, Seith A, Kumar A et al (2008) Whole-body MR imaging with the use of parallel imaging for detection of skeletal metastases in pediatric patients with small-cell neoplasms: comparison with skeletal scintigraphy and FDG PET/CT. Pediatr Radiol 38:953–962
40. Laurent V, Trausch G, Bruot O et al (2010) Comparative study of two whole-body imaging techniques in the case of melanoma metastases: advantages of multi-contrast MRI examination including a diffusion-weighted sequence in comparison with PET-CT. Eur J Radiol 75:376–383
41. Ohno Y, Koyama H, Nogami M et al (2007) Whole-body MR imaging vs. FDG-PET: comparison of accuracy of M-stage diagnosis for lung cancer patients. J Magn Reson Imaging 26:498–509
42. Pfannenberg C, Aschoff P, Schanz S et al (2007) Prospective comparison of 18F-fluorodeoxyglucose positron emission tomography/computed tomography and whole-body magnetic

resonance imaging in staging of advanced malignant melanoma. Eur J Cancer 43:557–564
43. Sakurai Y, Kawai H, Iwano S et al (2013) Supplemental value of diffusion-weighted whole-body imaging with background body signal suppression (DWIBS) technique to whole-body magnetic resonance imaging in detection of bone metastases from thyroid cancer. J Med Imaging Radiat Oncol 57:297–305
44. Schmidt GP, Schoenberg SO, Schmid R et al (2007) Screening for bone metastases: whole-body MRI using a 32-channel system versus dual-modality PET-CT. Eur Radiol 17:939–949
45. Schraml C, Schwenzer NF, Sperling O et al (2013) Staging of neuroendocrine tumours: comparison of [(6)(8)Ga]DOTATOC multiphase PET/CT and whole-body MRI. Cancer Imaging 13:63–72
46. Sohaib SA, Cook G, Allen SD et al (2009) Comparison of whole-body MRI and bone scintigraphy in the detection of bone metastases in renal cancer. Br J Radiol 82:632–639
47. Takenaka D, Ohno Y, Matsumoto K et al (2009) Detection of bone metastases in non-small cell lung cancer patients: comparison of whole-body diffusion-weighted imaging (DWI), whole-body MR imaging without and with DWI, whole-body FDG-PET/CT, and bone scintigraphy. J Magn Reson Imaging 30:298–308
48. Venkitaraman R, Cook GJ, Dearnaley DP et al (2009) Whole-body magnetic resonance imaging in the detection of skeletal metastases in patients with prostate cancer. J Med Imaging Radiat Oncol 53:241–247
49. Leboulleux S, Dromain C, Vataire AL et al (2008) Prediction and diagnosis of bone metastases in well-differentiated gastro-entero-pancreatic endocrine cancer: a prospective comparison of whole body magnetic resonance imaging and somatostatin receptor scintigraphy. J Clin Endocrinol Metab 93:3021–3028
50. Heusner TA, Antoch G, Wittkowski-Sterczewski A et al (2011) Transarterial hepatic chemoperfusion of uveal melanoma metastases: survival and response to treatment. RoFo 183:1151–1160
51. Schmidt GP, Baur-Melnyk A, Haug A et al (2009) Whole-body MRI at 1.5 T and 3 T compared with FDG-PET-CT for the detection of tumour recurrence in patients with colorectal cancer. Eur Radiol 19:1366–1378
52. Roberts CC, Daffner RH, Weissman BN et al (2010) ACR appropriateness criteria on metastatic bone disease. J Am Coll Radiol 7:400–409
53. Cardoso F, Senkus-Konefka E, Fallowfield L et al (2010) Locally recurrent or metastatic breast cancer: ESMO Clinical Practice Guidelines for diagnosis, treatment and follow-up. Ann Oncol 21(Suppl 5):v15–v19
54. Khatcheressian JL, Wolff AC, Smith TJ et al (2006) American Society of Clinical Oncology 2006 update of the breast cancer follow-up and management guidelines in the adjuvant setting. J Clin Oncol 24:5091–5097
55. Briganti A, Passoni N, Ferrari M et al (2010) When to perform bone scan in patients with newly diagnosed prostate cancer: external validation of the currently available guidelines and proposal of a novel risk stratification tool. Eur Urol 57:551–558
56. Horwich A, Parker C, de Reijke T et al (2013) Prostate cancer: ESMO Clinical Practice Guidelines for diagnosis, treatment and follow up. Ann Oncol 24(5):1141–1162
57. Leibovici D, Spiess PE, Agarwal PK et al (2007) Prostate cancer progression in the presence of undetectable or low serum prostate-specific antigen level. Cancer 109:198–204
58. Kosuda S, Yoshimura I, Aizawa T et al (2002) Can initial prostate specific antigen determinations eliminate the need for bone scans in patients with newly diagnosed prostate carcinoma? A multicenter retrospective study in Japan. Cancer 94:964–972
59. Erturan S, Yaman M, Aydin G et al (2005) The role of whole-body bone scanning and clinical factors in detecting bone metastases in patients with non-small cell lung cancer. Chest 127:449–454
60. Wu LM, Gu HY, Zheng J et al (2011) Diagnostic value of whole-body magnetic resonance imaging for bone metastases: a systematic review and meta-analysis. J Magn Reson Imaging 34:128–135
61. Yang HL, Liu T, Wang XM et al (2011) Diagnosis of bone metastases: a meta-analysis comparing (1)(8)FDG PET, CT, MRI and bone scintigraphy. Eur Radiol 21:2604–2617
62. Shen G, Deng H, Hu S et al (2014) Comparison of choline-PET/CT, MRI, SPECT, and bone scintigraphy in the diagnosis of bone metastases in patients with prostate cancer: a meta-analysis. Skeletal Radiol 43:1503–1513
63. Houssami N, Costelloe CM (2012) Imaging bone metastases in breast cancer: evidence on comparative test accuracy. Ann Oncol 23:834–843
64. Duo J, Han X, Zhang L et al (2013) Comparison of FDG PET/CT and gadolinium-enhanced MRI for the detection of bone metastases in patients with cancer: a meta-analysis. Clin Nucl Med 38:343–348
65. Khoo MM, Tyler PA, Saifuddin A et al (2011) Diffusion-weighted imaging (DWI) in musculoskeletal MRI: a critical review. Skeletal Radiol 40:665–681
66. Schiepers C, Nuyts J, Bormans G et al (1997) Fluoride kinetics of the axial skeleton measured in vivo with fluorine-18-fluoride PET. J Nucl Med 38:1970–1976
67. Even-Sapir E, Metser U, Flusser G et al (2004) Assessment of malignant skeletal disease: initial experience with 18F-fluoride PET/CT and comparison between 18F-fluoride PET and 18F-fluoride PET/CT. J Nucl Med 45:272–278
68. Li W, Ma L, Wang X et al (2014) C-choline PET/CT tumor recurrence detection and survival prediction in post-treatment patients with high-grade gliomas. Tumour Biol 35:12353–12360
69. Granov A (2013) Positron emission tomography. Springer, Berlin
70. Ghosh A, Heston WD (2004) Tumor target prostate specific membrane antigen (PSMA) and its regulation in prostate cancer. J Cell Biochem 91:528–539
71. Bacich DJ, Pinto JT, Tong WP et al (2001) Cloning, expression, genomic localization, and enzymatic activities of the mouse homolog of prostate-specific membrane antigen/NAALADase/folate hydrolase. Mamm Genome 12:117–123
72. Afshar-Oromieh A, Malcher A, Eder M et al (2013) PET imaging with a [68 Ga]gallium-labelled PSMA ligand for the diagnosis of prostate cancer: biodistribution in humans and first evaluation of tumour lesions. Eur J Nucl Med Mol Imaging 40:486–495
73. Luboldt W, Kufer R, Blumstein N et al (2008) Prostate carcinoma: diffusion-weighted imaging as potential alternative to conventional MR and 11C-choline PET/CT for detection of bone metastases. Radiology 249:1017–1025
74. Lecouvet FE, Vande Berg BC, Malghem J et al (2009) Diffusion-weighted MR imaging: adjunct or alternative to T1-weighted MR imaging for prostate carcinoma bone metastases? Radiology 252:624
75. Mosavi F, Johansson S, Sandberg DT et al (2012) Whole-body diffusion-weighted MRI compared with (18)F-NaF PET/CT for detection of bone metastases in patients with high-risk prostate carcinoma. AJR Am J Roentgenol 199:1114–1120
76. Afshar-Oromieh A, Avtzi E, Giesel FL et al (2014) The diagnostic value of PET/CT imaging with the Ga-labelled PSMA ligand HBED-CC in the diagnosis of recurrent prostate cancer. Eur J Nucl Med Mol Imaging 42:197–209
77. Carrio I (2014) PET/MRI methodology and clinical applications. Springer, Berlin
78. Peller P (2012) PET-CT and PET-MRI in oncology: a practical guide. Springer, Berlin
79. ClinicalTrials.gov. In: Health USNIo, ed. (2014)

80. Sardanelli F, Di Leo G (2009) Biostatistics for radiologists: planning, performing, and writing a radiologic study. Springer, Italy
81. Walter SD, Macaskill P, Lord SJ et al (2012) Effect of dependent errors in the assessment of diagnostic or screening test accuracy when the reference standard is imperfect. Stat Med 31:1129–1138
82. Higgins JP, Thompson SG, Spiegelhalter DJ (2009) A re-evaluation of random-effects meta-analysis. J R Stat Soc Ser A Stat Soc 172:137–159
83. Lecouvet FE, Talbot JN, Messiou C et al (2014) Monitoring the response of bone metastases to treatment with magnetic resonance imaging and nuclear medicine techniques: a review and position statement by the European Organisation for Research and Treatment of Cancer imaging group. Eur J Cancer 50:2519–2531
84. Schmidt GP, Baur-Melnyk A, Herzog P et al (2005) High-resolution whole-body magnetic resonance image tumor staging with the use of parallel imaging versus dual-modality positron emission tomography-computed tomography: experience on a 32-channel system. Invest Radiol 40:743–753

Whole-Body 3D T1-weighted MR Imaging in Patients with Prostate Cancer: Feasibility and Evaluation in Screening for Metastatic Disease[1]

Vasiliki Pasoglou, MD
Nicolas Michoux, PhD
Frank Peeters, PhD
Ahmed Larbi, MD
Bertrand Tombal, MD, PhD
Tom Selleslagh, RT
Patrick Omoumi, MD
Bruno C. Vande Berg, MD, PhD
Frédéric E. Lecouvet, MD, PhD

Purpose: To develop and assess the diagnostic performance of a three-dimensional (3D) whole-body T1-weighted magnetic resonance (MR) imaging pulse sequence at 3.0 T for bone and node staging in patients with prostate cancer.

Materials and Methods: This prospective study was approved by the institutional ethics committee; informed consent was obtained from all patients. Thirty patients with prostate cancer at high risk for metastases underwent whole-body 3D T1-weighted imaging in addition to the routine MR imaging protocol for node and/or bone metastasis screening, which included coronal two-dimensional (2D) whole-body T1-weighted MR imaging, sagittal proton-density fat-saturated (PDFS) imaging of the spine, and whole-body diffusion-weighted MR imaging. Two observers read the 2D and 3D images separately in a blinded manner for bone and node screening. Images were read in random order. The consensus review of MR images and the findings at prospective clinical and MR imaging follow-up at 6 months were used as the standard of reference. The interobserver agreement and diagnostic performance of each sequence were assessed on per-patient and per-lesion bases.

Results: The signal-to-noise ratio (SNR) and contrast-to-noise ratio (CNR) were significantly higher with whole-body 3D T1-weighted imaging than with whole-body 2D T1-weighted imaging regardless of the reference region (bone or fat) and lesion location (bone or node) ($P < .003$ for all). For node metastasis, diagnostic performance (area under the receiver operating characteristic curve) was higher for whole-body 3D T1-weighted imaging (per-patient analysis; observer 1: $P < .001$ for 2D T1-weighted imaging vs 3D T1-weighted imaging, $P = .006$ for 2D T1-weighted imaging + PDFS imaging vs 3D T1-weighted imaging; observer 2: $P = .006$ for 2D T1-weighted imaging vs 3D T1-weighted imaging, $P = .006$ for 2D T1-weighted imaging + PDFS imaging vs 3D T1-weighted imaging), as was sensitivity (per-lesion analysis; observer 1: $P < .001$ for 2D T1-weighted imaging vs 3D T1-weighted imaging, $P < .001$ for 2D T1-weighted imaging + PDFS imaging vs 3D T1-weighted imaging; observer 2: $P < .001$ for 2D T1-weighted imaging vs 3D T1-weighted imaging, $P < .001$ for 2D T1-weighted imaging + PDFS imaging vs 3D T1-weighted imaging).

Conclusion: Whole-body MR imaging is feasible with a 3D T1-weighted sequence and provides better SNR and CNR compared with 2D sequences, with a diagnostic performance that is as good or better for the detection of bone metastases and better for the detection of lymph node metastases.

Online supplemental material is available for this article.

[1] From the Department of Radiology, Centre du Cancer and Institut de Recherche Expérimentale et Clinique, Cliniques Universitaires Saint-Luc, Université Catholique de Louvain, Avenue Hippocrate 10/2942, B-1200 Brussels, Belgium (V.P., N.M., F.P., A.L., T.S., B.C.V.B., F.E.L.); Department of Urology, Cliniques Universitaires Saint-Luc, Brussels, Belgium (B.T.); and Department of Radiology, Centre Hospitalier Universitaire Vaudois, Lausanne, Switzerland (P.O.). Received May 28, 2014; revision requested July 16; revision received August 4; accepted September 8; final version accepted September 19. V.P., B.T., and F.E.L. supported by grants from FRS-FNRS Télévie, Fondation Contre le Cancer, and Fondation Saint Luc. **Address correspondence to** F.E.L. (e-mail: *frederic.lecouvet@uclouvain.be*).

Whole-body magnetic resonance (MR) imaging studies have been increasingly used for more than 10 years to screen for bone and soft-tissue metastases (1–3). The conventional whole-body MR imaging protocol for the screening of bone and soft-tissue metastases consists of morphologic two-dimensional (2D) images of the whole body with use of T1-weighted and fat-suppressed fluid-sensitive (proton-density fat-saturated [PDFS] or short inversion time inversion-recovery) sequences generally performed in the coronal plane, in sequential acquisitions of limited fields of view that are then fused by using postprocessing software (4–6). Although 2D pulse sequences provide an acceptable in-plane spatial resolution, the section thickness is relatively large, with intersection gaps, which can lead to partial volume effects. These pulse sequences perform quite well for the detection of lesions, but the concurrent use of multiple planes is mandatory—especially for the study of the spine (7–9). This repetition of morphologic pulse sequences in multiple planes is time consuming. More recently, the addition of a functional diffusion-weighted imaging sequence to this conventional morphologic whole-body MR imaging protocol was shown to be useful for the screening of node and bone metastases from solid cancers or hematologic malignancies (8–10).

Three-dimensional (3D) imaging is playing an increasingly important role in modern MR imaging. Three-dimensional MR imaging acquisitions are routinely performed in head and neck, abdominal, thoracic, vascular, obstetric and/or gynecologic, and musculoskeletal indications (11–14). Three-dimensional MR imaging may provide high-spatial-resolution images that can be reconstructed in any spatial direction (coronal, sagittal, oblique, or curvilinear planes), leading to a shorter image acquisition time and/or better diagnostic performance (12,14–16).

There is a consensus on the need to combine anatomic and functional sequences to achieve optimal diagnostic effectiveness in oncologic applications of whole-body MR imaging. In practice, metastases screening in patients with cancer is usually performed with a set of 2D anatomic sequences, in combination with diffusion-weighted functional sequences (17–20). Herein, we hypothesized that an optimized 3D pulse sequence designed to cover the whole body could replace the set of conventional 2D sequences that are performed for the anatomic part of screening.

The purpose of this study was to develop and assess the diagnostic performance of a 3D whole-body T1-weighted MR imaging pulse sequence at 3.0 T for bone and node staging in patients with prostate cancer. This sequence was compared with a conventional 2D whole-body T1-weighted MR pulse sequence used alone or in combination with a sagittal spine PDFS MR pulse sequence. Prostate cancer was chosen because of its "concurrent" tropism for bone and lymph nodes in metastatic spread.

Advances in Knowledge

- Whole-body coverage with a high-spatial-resolution three-dimensional (3D) T1-weighted MR pulse sequence is feasible in clinical practice in less than 18 minutes (voxel size at acquisition: $1.14 \times 1.43 \times 1.20$ mm^3; voxel size after reconstruction: $0.57 \times 0.57 \times 1.20$ mm^3).
- Whole-body 3D T1-weighted imaging has a higher signal-to-noise ratio and contrast-to-noise ratio compared with two-dimensional (2D) sequences.
- Compared with whole-body 2D T1-weighted sequences, the whole-body 3D T1-weighted sequence performs equally well for the detection of bone metastases (sensitivity = 90% vs 100%, respectively; $P = .317$) and better for the detection of abnormal lymph nodes (sensitivity = 46% vs 100%, respectively; $P < .001$).

Implications for Patient Care

- Volumic acquisition of T1-weighted MR images is feasible at the scale of the whole body, with subsequent multiplanar reformation for reading, paralleling multidetector CT scan acquisition and reading.
- This sequence could be used as a single morphologic complement to functional diffusion-weighted imaging sequences for the screening of metastases in patients with prostate cancer.

Materials and Methods

Patients

This prospective study was approved by the institutional ethics committee. Informed consent was obtained from all patients. Thirty consecutive patients with prostate cancer who were considered at high risk for metastases according to published criteria (21,22) were prospectively enrolled between February and December 2012. Patients were considered at high risk for metastases whenever they had one of the following features: clinical stage

Published online before print
10.1148/radiol.14141242 **Content code:** GU

Radiology 2015; 275:155–166

Abbreviations:
AUC = area under the receiver operating characteristic curve
CI = confidence interval
CNR = contrast-to-noise ratio
PDFS = proton density fat saturated
ROI = region of interest
SNR = signal-to-noise ratio
3D = three-dimensional
2D = two-dimensional

Author contributions:
Guarantors of integrity of entire study, V.P., N.M., B.T., F.E.L.; study concepts/study design or data acquisition or data analysis/interpretation, all authors; manuscript drafting or manuscript revision for important intellectual content, all authors; manuscript final version approval, all authors; agrees to ensure any questions related to the work are appropriately resolved, all authors; literature research, V.P., F.P., A.L., T.S., B.C.V.B., F.E.L.; clinical studies, V.P., A.L., B.T., T.S., B.C.V.B., F.E.L.; statistical analysis, N.M., F.P., T.S., F.E.L.; and manuscript editing, V.P., N.M., F.P., A.L., T.S., P.O., B.C.V.B., F.E.L.

Conflicts of interest are listed at the end of this article.

Table 1

Imaging Parameters

Parameter	Morphologic Sequences			
	T1-weighted WB3D	T1-weighted WB2D	Spine PDFS	WBDW*
Acquisition time (min)	17.2 (4 × 4.3)	7.2 (4 × 1.8)	5.4 (3 × 1.8)	15.8
Sequence	3D SPACE (spin echo)	TSE	TSE	Diffusion
Plane	Coronal	Coronal	Sagittal	Axial
No. of sections	176	50	13	25
Section thickness (mm)	1.2	4	4	5
Gap (mm)	…	0.4	0.4	0.5
Field of view	440 × 307	400 × 306	260 × 260	430 × 366
Acquisition matrix	214 × 384	384 × 307	256 × 320	83 × 122
No. of stations	4	4	4	5
Coverage in z-axis (mm)	1024	1024	1024	968
Phase-encoding direction	Feet-head	Feet-head	Feet-head	Anterior-posterior
IPAT factor	3	3	2	2
Phase oversampling	0.5	1	1	0
TR/TE (msec)	400/13	600/9.4	2600/45	4500/68
No. of signals acquired	2	1	2	5
Turbo factor	58	4	13	…
Flip angle (degrees)	Variable	140	147	130
Bandwidth (Hz/pixel)	407	260	2050	255
Fat suppression technique	…	…	Fat saturation	SPAIR
Specific parameters	…	…	…	*b* values: 0, 800

Note.—IPAT = integrated parallel acquisition techniques, SPACE = sampling perfecton with application optimized contrast using different flip angle evolutions, SPAIR = spectral adiabatic inversion recovery, TE = echo time, TR = repetition time, TSE = turbo spin-echo, WBDW = whole-body diffusion-weighted imaging, WB2D = whole-body 2D imaging, WB3D = whole-body 3D imaging.

* Functional sequence.

greater than T3a or at least N1 (n = 19), Gleason score of at least 8 (n = 12), prostate-specific antigen level of at least 20 ng/mL (n = 5), increasing prostate-specific antigen level after local treatment with a doubling time of 12 months or less (n = 8), and increasing prostate-specific antigen level while receiving androgen deprivation therapy with a doubling time of 12 months or less (n = 5). The mean patient age (±standard deviation) was 69 years ± 3.3. The mean prostate-specific antigen level was 31 ng/mL ± 28. Three patients were not enrolled because of contraindications to MR imaging.

MR Imaging

All patients were imaged with a 3.0-T MR unit (Magnetom Verio; Siemens Medical Solutions, Erlangen, Germany). Patients were placed on the imaging table headfirst in the supine position and were covered with a head and neck coil, spine coils, and two six-element body matrix coils. A coronal 2D whole-body T1-weighted MR imaging pulse sequence, a sagittal PDFS sequence of the whole spine, a diffusion-weighted MR imaging sequence, and a 3D whole-body T1-weighted pulse sequence were performed. The latter pulse sequence was designed as follows: A 3D turbo spin-echo SPACE (sampling perfection with application optimized contrast using different flip angle evolutions) pulse sequence was implemented to get both high spatial resolution and high contrast resolution in T1 while limiting both the specific absorption rate and the acquisition time (23). An elliptic k-space filter was applied. Then, in-plane spatial resolution was chosen so as to be the closest to that of the 2D pulse sequence and to be "as isotropic as possible." As a result, voxel size after acquisition and reconstruction were, respectively, 1.14 × 1.43 × 1.20 mm^3 and 0.57 × 0.57 × 1.20 mm^3 for whole-body 3D T1-weighted imaging, 1.04 × 1.30 × 4.00 mm^3 and 1.04 × 1.04 × 4.00 mm^3 for whole-body 2D T1-weighted imaging, 0.81 × 1.01 × 4.00 mm^3 and 0.81 × 0.81 × 4.00 mm^3 for spine PDFS imaging, and 3.52 × 4.42 × 5.00 mm^3 and 1.76 × 1.76 × 2.70 mm^3 for whole-body diffusion-weighted imaging. Other imaging parameters are detailed in Table 1. Example images are shown in Figure 1 and in the Movies (online).

Image Analysis

Lesion definition.—For lymph node staging, external, internal, common iliac, inguinal, periaortic, and pericaval nodes were defined as abnormal when the short-axis diameter was larger than 10 mm, when there was loss of the normal oblong kidney bean shape and of the fatty hilum, or an irregular outline. In perivisceral (perivesical, perirectal, etc) locations, a node was defined as abnormal when the short-axis size was larger than 8 mm (24,25).

Figure 1

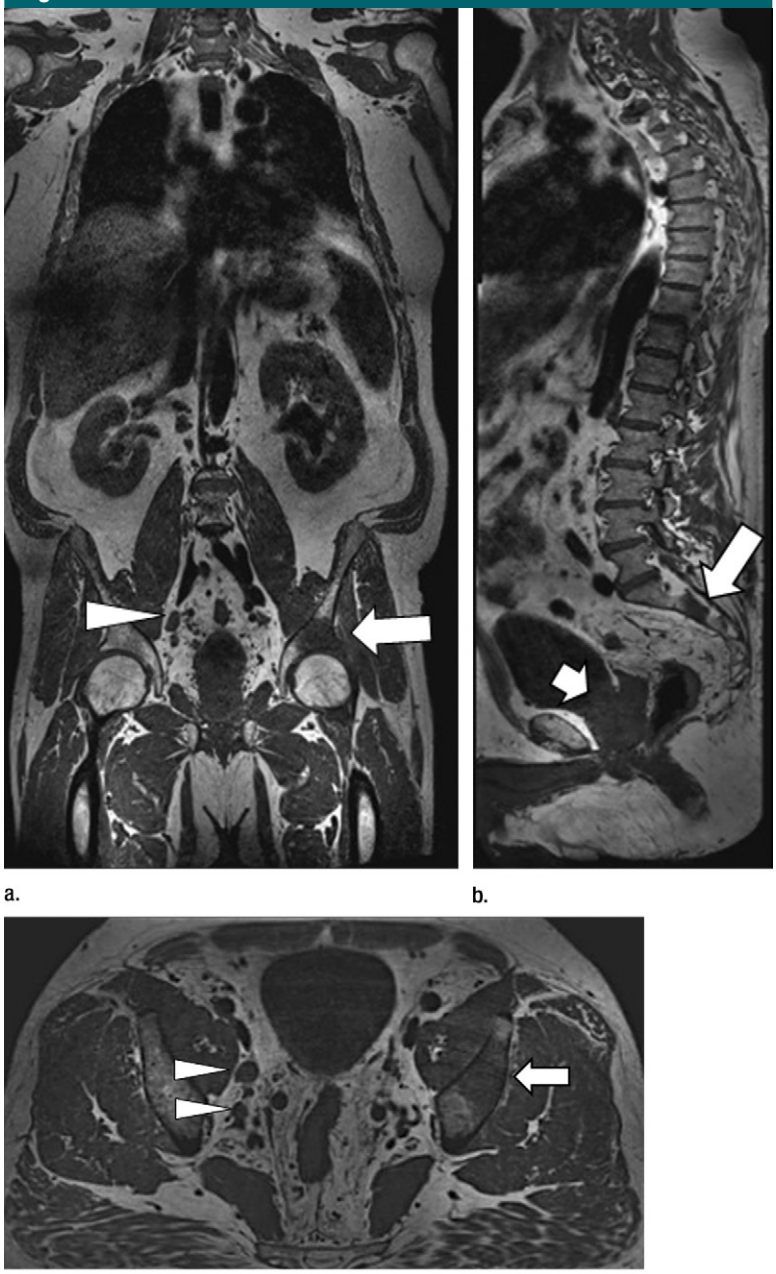

Figure 1: Whole-body 3D MR images in 46-year-old man with prostate cancer. **(a)** Coronal reconstructed image shows bone marrow metastasis of left acetabulum (arrow) and right common iliac pathologic lymph node (arrowhead). **(b)** Sagittal reconstructed image shows bone marrow metastasis of second sacral vertebra (large arrow). Invasion of bladder neck by prostate cancer is seen (small arrow). **(c)** Axial reconstructed image shows bone marrow metastasis at level of left ilium (arrow) and two right obturator lymph node metastases (arrowheads). This case is also illustrated in the Movies (online), which cover the whole body in the three planes.

For bone lesions, a metastasis was defined according to the following criteria: rounded focus larger than 8 mm with low signal intensity on T1-weighted images, high signal intensity on PDFS images, and high *b* values on diffusion-weighted images (4,21).

The standard of reference for bone and lymph node lesions was based on a consensus session of all available morphologic and functional MR images by three radiologists (V.P., A.L., and F.E.L., with 3, 8, and 15 years of experience in reading MR images, respectively), prospective clinical and biologic follow-up by an uro-oncologist (B.T., with 20 years of experience), and imaging follow-up at 6 months.

Quantitative image analysis.—Image quality was assessed for whole-body 2D T1-weighted imaging and whole-body 3D T1-weighted imaging by measuring both signal-to-noise ratio (SNR) and contrast-to-noise ratio (CNR) in regions of interest (ROIs) within lesions and corresponding reference tissues. The measurements were performed by one physicist (F.P., with 25 years of experience in MR imaging) and one radiologist (V.P.). For spine lesions, the reference ROI was chosen in the bone marrow of an uninvolved lumbar vertebra (L5 or the closest uninvolved area). For pelvic lesions, the reference ROI was chosen in the bone marrow of a nonmetastatic ischiopubic ramus. For lymph nodes, a reference ROI was chosen in the local-regional fat. The largest bone and node lesions from each anatomic area were used for this analysis. Each time the largest possible ROI that fitted the lesion and/or tissue of interest was chosen, without including the bone cortices and anatomic limits of lymph nodes. The standard deviation of the noise (σ) was estimated from an ROI defined outside the body (a large area that contained only air). The SNR was then calculated according to the following equation: $SNR = 0.66 \times S/\sigma$, where S is the mean signal intensity from the reference region and 0.66 a correction factor that takes into account the fact that the noise is governed by the Rayleigh distribution

(26). The CNR was estimated according to a similar equation, as follows: $CNR = 0.66 \times (S^{lesion} - S^{reference})/\sigma$.

Qualitative image analysis.—Morphologic images from the whole-body 2D T1-weighted sequence, the whole-body 2D T1-weighted plus PDFS sequence, and the whole-body 3D T1-weighted sequence were consecutively analyzed by two radiologists independently (F.E.L. [observer 1] and V.P. [observer 2], with 15 and 3 years of experience, respectively, in musculoskeletal and oncologic imaging). The whole-body 2D T1-weighted images were read during the first reading, the whole-body 2D T1-weighted plus PDFS images were read during the second reading, and the whole-body 3D T1-weighted images were read during the third reading. The radiologists were blinded to the patient's clinical information. To prevent recall bias, the three readings were performed at 3-week intervals and were randomized. Readings were performed with a picture archiving and communication system workstation (Carestream Vue; Carestream Health, Rochester, NY). Readings of images from whole-body 3D T1-weighted pulse sequences were performed by each reader separately with use of multiplanar reformation. For each reading, we recorded the number and location of node and/or bone metastases and the metastatic status of the patient for bone and for node metastasis.

Statistical Analysis

The image quality with the 2D T1-weighted and 3D T1-weighted pulse sequences was assessed by comparing the SNR measured in two reference regions (bone and fat) and by comparing the CNR in two common metastatic sites (bone and node). A Wilcoxon rank sum test was performed to assess statistical differences. This nonparametric test was chosen because the normality of the data distribution was not verified (on the basis of the D'Agostino-Pearson test). A Bonferroni-type correction for performing multiple comparisons was then applied. As a result, $P < .025$ was regarded as indicative of a statistically significant difference.

Receiver operating characteristic (empirical receiver operating characteristic) analysis was performed to assess the performance of each MR imaging sequence on a per-patient basis (27). A pairwise comparison of the areas under the receiver operating characteristic curve (AUCs) was made to rank sequences according to their diagnostic performance (28). Then, the diagnostic performance of each MR imaging sequence was calculated on a per-lesion basis, followed by a McNemar test to rank sequences according to their sensitivity (29). Because of the multiple comparisons, $P < .0083$ was regarded as indicative of a statistically significant difference.

Interobserver agreement on a per-patient basis was evaluated for each MR imaging sequence according to the Scott pi and its associated 95% confidence interval (CI) (30). Interobserver agreement on a per-lesion basis was evaluated for each MR sequence according to the intraclass correlation coefficient on the basis of a two-way model in which systematic differences are relevant and its associated 95% CI (31). Agreement was interpreted as follows: scores of 0 or less were indicative of poor agreement, 0.01–0.20 slight agreement, 0.21–0.40 fair agreement, 0.41–0.60 moderate agreement, 0.61–0.80 substantial agreement, and 0.81 or greater very good agreement (32).

Because the study is exploratory, the sample size was not prospectively planned. Calculations were done with software (Statsdirect Statistical Software, version 2.7.8 [*http://www.statsdirect.com/*] and Matlab [Matlab R2011b, MathWorks, Natick, Mass]). Image J software (*http://rsbweb.nih.gov/ij/*) was used for the segmentation of the ROIs.

Table 2

SNRs for Reference ROIs and CNRs for ROIs in Tumors of Interest at Whole-Body 2D and 3D T1-weighted Imaging

Parameter	No. of ROIs	2D T1-weighted Imaging*	3D T1-weighted Imaging*	*P* Value†
SNR				
Reference bone	45	85 (60)	234 (284)	< .001
Reference fat	12	99 (50)	260 (360)	< .001
CNR				
Lesion-bone	13	47 (41)	143 (104)	.003
Lesion-node	12	52 (33)	155 (228)	< .001

Note.—The number of ROIs represents cases for which SNRs and CNRs could be calculated. In six patients considered for analysis, some thresholding was automatically performed on the saved data, yielding a standard deviation of 0 for the noise ROIs. As a result, SNR and CNR could not be estimated in these ROIs. Therefore, the number of measured ROIs fell to the number of used ROIs. For the SNR, the number of used ROIs fell from 55 to 45 (reference bone) and from 13 to 12 (reference fat). For the CNR, the numbers fell from 19 to 13 (lesion/bone) and from 13 to 12 (lesion/node).

* Data are medians and dispersion values (interquartile ranges. in parentheses).

† Statistical differences (Wilcoxon rank-sum test) between T1-weighted 2D imaging and T1-weighted 3D imaging.

Results

Patient Population

On the basis of the standard of reference (ie, the combination of imaging findings and clinical information provided for every patient at baseline and 6-month follow-up), 10 patients had bone metastasis and 13 had node metastasis. There were 41 bone lesions and 36 node lesions (Fig 1, Movies [online]).

Quantitative Image Analysis

SNR and CNR measurements are summarized in Table 2. SNR and CNR were significantly higher with whole-body 3D T1-weighted imaging than with whole-body 2D T1-weighted imaging, regardless of the region analyzed ($P < .025$).

Sensitivity, specificity, positive predictive value, negative predictive value,

and 2 × 2 contingency tables were estimated for each MR imaging sequence on a per-patient (Table 3) and per-lesion (Table 4) basis.

On a per-patient basis, whole-body 3D T1-weighted imaging had a significantly higher performance compared with whole-body 2D T1-weighted imaging and whole-body 2D T1-weighted imaging plus PDFS imaging for detecting patients with node metastases (observer 1: AUC = 1.00 for 3D T1-weighted imaging, 0.81 for 2D T1-weighted imaging + DPFS imaging, and 0.73 for 2D T1-weighted imaging, with $P < .001$ for 2D T1-weighted imaging vs 3D T1-weighted imaging and $P = .006$ for 2D T1-weighted imaging + PDFS imaging vs 3D T1-weighted imaging; observer 2: AUC = 1.00 for 3D T1-weighted imaging, 0.81 for 2D T1-weighted imaging + DPFS imaging, and 0.81 for 2D T1-weighted imaging, with $P = .006$ for 2D T1-weighted imaging vs 3D T1-weighted imaging and $P = .006$ for 2D T1-weighted imaging + PDFS imaging vs 3D T1-weighted imaging), whereas no significant difference was observed between sequences for detecting patients with bone metastases ($P \geq .317$ for all) (Table E1 [online]; Figs 2, 3).

On a per-lesion basis, whole-body 3D T1-weighted imaging had a significantly higher sensitivity than whole-body 2D T1-weighted imaging and whole-body 2D T1-weighted imaging plus PDFS for detecting node metastases (observer 1: sensitivity = 100% for 3D T1-weighted imaging, 44% for 2D T1-weighted imaging + PDFS imaging, and 33% for 2D T1-weighted imaging, with $P < .001$ for 2D T1-weighted imaging vs 3D T1-weighted imaging and $P < .001$ for 2D T1-weighted imaging + PDFS imaging vs 3D T1-weighted imaging; observer 2: sensitivity = 92% for 3D T1-weighted imaging, 39% for 2D T1-weighted imaging + PDFS imaging, and 39% for 2D T1-weighted imaging, with $P < .001$ for 2D T1-weighted imaging vs 3D T1-weighted imaging and $P < .001$ for 2D T1-weighted imaging + PDFS imaging vs 3D T1-weighted imaging), whereas whole-body 2D T1-weighted imaging had a significantly

Table 3

Per-Patient Analysis: Diagnostic Performance of MR Imaging Sequences in Comparison to the Standard of Reference

Parameter	2D T1-weighted Imaging	2D T1-weighted Imaging + PDFS	3D T1-weighted Imaging
Bone-positive patients			
TP findings			
Observer 1	9	9	10
Observer 2	9	10	10
TN findings			
Observer 1	20	20	20
Observer 2	20	19	20
FP findings			
Observer 1	0	0	0
Observer 2	0	1	0
FN findings			
Observer 1	1	1	0
Observer 2	1	0	0
Sensitivity (%)			
Observer 1	90 (56, 100)	90 (56, 100)	100 (69, 100)
Observer 2	90 (56, 100)	100 (69, 100)	100 (69, 100)
Specificity (%)			
Observer 1	100 (83, 100)	100 (83, 100)	100 (83, 100)
Observer 2	100 (83, 100)	95 (75, 100)	100 (83, 100)
AUC			
Observer 1	0.95 (0.80, 1.00)*	0.95 (0.80, 1.00)*	1.00 (0.88, 1.00)*
Observer 2	0.95 ((0.80, 1.00)*	0.98 (0.84, 1.00)*	1.00 (0.88, 1.00)*
PPV (%)			
Observer 1	100 (66, 100)	100 (66, 100)	100 (69, 100)
Observer 2	100 (66, 100)	91 (59, 100)	100 (69, 100)
NPV (%)			
Observer 1	95 (76, 100)	95 (76, 100)	100 (83, 100)
Observer 2	95 (76, 100)	100 (82, 100)	100 (83, 100)
Node-positive patients			
TP findings			
Observer 1	6	8	13
Observer 2	8	8	19
TN findings			
Observer 1	17	17	17
Observer 2	17	17	17
FP findings			
Observer 1	0	0	0
Observer 2	0	0	0
FN findings			
Observer 1	7	5	0
Observer 2	5	5	0
Sensitivity (%)			
Observer 1	46 (19, 75)	62 (32, 86)	100 (75, 100)
Observer 2	62 (32, 86)	62 (32, 86)	100 (75, 100)
Specificity (%)			
Observer 1	100 (81, 100)	100 (81, 100)	100 (81, 100)
Observer 2	100 (81, 100)	100 (81, 100)	100 (81, 100)
AUC			
Observer 1	0.73 (0.54, 0.88)†	0.81 (0.62, 0.93)*	1.00 (0.88, 1.00)*

Table 3 (continues)

Table 3 (continued)

Per-Patient Analysis: Diagnostic Performance of MR Imaging Sequences in Comparison to the Standard of Reference

Parameter	2D T1-weighted Imaging	2D T1-weighted Imaging + PDFS	3D T1-weighted Imaging
Observer 2	0.81 ((0.62, 0.93)*	0.81 (0.62, 0.93)*	1.00 (0.88, 1.00)*
PPV (%)			
Observer 1	100 (54, 100)	100 (63, 100)	100 (75, 100)
Observer 2	100 (63, 100)	100 (63, 100)	100 (75, 100)
NPV (%)			
Observer 1	71 (49, 87)	77 (55, 92)	100 (81, 100)
Observer 2	77 (55, 92)	77 (55, 92)	100 (81, 100)
Node- or bone-positive patients			
TP findings			
Observer 1	14	15	15
Observer 2	13	14	16
TN findings			
Observer 1	14	14	14
Observer 2	14	13	14
FP findings			
Observer 1	0	0	0
Observer 2	0	1	0
FN findings			
Observer 1	2	1	1
Observer 2	3	2	0
Sensitivity (%)			
Observer 1	88 (62, 98)	94 (70, 100)	94 (70, 100)
Observer 2	81 (54, 96)	88 (62, 98)	100 (79, 100)
Specificity (%)			
Observer 1	100 (77, 100)	100 (77, 100)	100 (77, 100)
Observer 2	100 (77, 100)	93 (66, 100)	100 (77, 100)
AUC			
Observer 1	0.94 (0.79, 0.99)*	0.97 (0.83, 1.00)*	0.97 (0.83, 1.00)*
Observer 2	0.91 (0.74, 0.98)*	0.90 (0.74, 0.98)*	1.00 (0.88, 1.00)*
PPV (%)			
Observer 1	100 (77, 100)	100 (78, 100)	100 (78, 100)
Observer 2	100 (75, 100)	93 (68, 100)	100 (79, 100)
NPV (%)			
Observer 1	88 (62, 98)	93 (68, 100)	93 (68, 100)
Observer 2	82 (57, 96)	87 (60, 98)	100 (77, 100)

Note.—FN = false negative, FP = false positive, NPV = negative predictive value, PPV = positive predictive value, TN = true negative, TP = true positive. Numbers in parentheses are the 95% CI.

* The sequence performed better than a random classifier ($P < .0001$).

† The sequence performed better than a random classifier ($P = .0013$).

lower sensitivity than whole-body 3D T1-weighted imaging and whole-body 2D T1-weighted imaging plus PDFS imaging for detecting bone metastasis (observer 1: sensitivity = 98% for 3D T1-weighted imaging, 83% for 2D T1-weighted imaging + PDFS imaging, and 63% for 2D T1-weighted imaging, with $P < .001$ for 2D T1-weighted imaging vs 2D T1-weighted imaging + PDFS imaging and $P < .001$ for 2D T1-weighted imaging vs 3D T1-weighted imaging; observer 2: sensitivity = 100% for 3D T1-weighted imaging, 85% for 2D T1-weighted imaging + PDFS imaging, and 68% for 2D T1-weighted imaging, with $P = .008$ for 2D T1-weighted imaging vs 2D T1-weighted imaging + PDFS imaging and $P < .001$ for 2D T1-weighted imaging vs 3D T1-weighted imaging).

Interobserver Agreement

On a per-patient basis, interobserver agreement in the detection of patients with bone metastasis was very good, regardless of the MR sequence used (Table 5). Interobserver agreement ranged from substantial (2D T1-weighted imaging + PDFS imaging: Scott pi = 0.66 [95% CI: 0.28, 0.86]) to very good (whole-body 2D T1-weighted imaging: Scott pi = 0.82 [95% CI: 0.44, 0.95], whole-body 3D T1-weighted imaging: Scott pi = 1.00 [95% CI: 0.77, 1.00]) for detecting patients with node metastasis. On a per-lesion basis, interobserver agreement in the detection of bone metastasis was very good, regardless of the MR sequence used (Table 6). Interobserver agreement in the detection of node metastasis ranged from substantial (whole-body 2D T1-weighted imaging + PDFS imaging: intraclass correlation coefficient = 0.64 [95% CI: 0.37, 0.81]) to very good (whole-body 2D T1-weighted imaging: intraclass correlation coefficient = 0.88 [95% CI: 0.76, 0.94]; whole-body 3D T1-weighted imaging: intraclass correlation coefficient = 0.97 [95% CI: 0.93, 0.98]).

Discussion

Numerous musculoskeletal applications of whole-body MR imaging have been developed during the past decade, mainly in the fields of oncologic imaging and rheumatology.

In patients with cancer, precise and complete tumor staging is crucial for adequate treatment planning. MR imaging is a highly sensitive method for the early detection of bone metastasis because it is sensitive to the infiltration of the bone marrow by malignant cells before bone remodeling occurs (33–35). Whole-body MR imaging has been proved an efficient and cost-effective tool for the screening of bone metastasis in patients with breast or prostate cancer (4,36). This technique represents an alternative to other diagnostic methods, that is, bone scintigraphy

with targeted radiographys, which lack specificity and sensitivity in the detection of bone metastasis (9,37). More recently, the performance of whole-body MR imaging has been highlighted for the concurrent evaluation of bone and visceral—in particular nodal—metastases, in large part thanks to the development of diffusion-weighted imaging that complements morphologic MR imaging pulse sequences (5,20,36). In patients with high-risk prostate cancer, whole-body MR imaging outperforms the current multimodality work-up used for the evaluation of bones and lymph nodes (bone scintigraphy with targeted radiographs and thoracoabdominal computed tomography) (8,10,20,38–41).

A review of the literature shows a wide heterogeneity in whole-body MR imaging protocols used in different centers or according to the target cancer and metastases, with a lack of standardization. Although most examinations are performed in the coronal plane, a second plane is used in most cases. For the examination of the whole skeleton in patients with cancer, a coronal 2D whole-body MR imaging pulse sequence and a sagittal pulse sequence on the spine are most commonly used. The sagittal pulse sequence on the spine is strongly recommended to detect small vertebral lesions and potential complications of the metastatic disease (ie, fractures and spinal cord or spinal nerve compression) (7,9). The study of the skull, scapula, ribs, and sternum may be limited in the coronal plane, and the potential benefit of acquisition in the axial plane has been suggested (5,42).

Three-dimensional imaging has the potential to overcome many of the limitations mentioned earlier. Three-dimensional acquisition may shorten the imaging time by avoiding the repetition of imaging planes and reduces the partial volume effects resulting from section thickness and intersection gaps, therefore providing both high-spatial-resolution images and multiplanar reformation capability (12–14).

In this study, we developed an original high-spatial-resolution 3D

Table 4

Per-Lesion Analysis: Diagnostic Performance of MR Imaging Sequences in Comparison with the Reference Standard

Parameter	2D T1-weighted Imaging	2D T1-weighted Imaging + PDFS	3D T1-weighted Imaging
Bone lesions			
TP findings			
Observer 1	26	34	40
Observer 2	28	35	41
TN findings			
Observer 1	21	21	21
Observer 2	21	20	21
FP findings			
Observer 1	0	0	0
Observer 2	0	1	2
FN findings			
Observer 1	15	7	1
Observer 2	13	6	0
Sensitivity (%)			
Observer 1	63 (47, 78)	83 (68, 93)	98 (87, 100)
Observer 2	68 (52, 82)	85 (71, 94)	100 (91, 100)
Specificity			
Observer 1	100 (84, 100)	100 (84, 100)	100 (84, 100)
Observer 2	100 (84, 100)	95 (76, 100)	91 (72, 99)
PPV (%)			
Observer 1	100 (87, 100)	100 (90, 100)	100 (91, 100)
Observer 2	100 (88, 100)	97 (85, 100)	95 (84, 99)
NPV (%)			
Observer 1	58 (41, 74)	75 (55, 89)	95 (77, 100)
Observer 2	62 (44, 78)	77 (56, 91)	100 (83, 100)
Node lesions			
TP findings			
Observer 1	12	16	36
Observer 2	14	14	33
TN findings			
Observer 1	17	17	17
Observer 2	17	17	17
FP findings			
Observer 1	0	0	0
Observer 2	0	1	1
FN findings			
Observer 1	24	20	0
Observer 2	22	22	3
Sensitivity (%)			
Observer 1	33 (19, 51)	44 (28, 62)	100 (90, 100)
Observer 2	39 (23, 57)	39 (23, 57)	92 (78, 98)
Specificity (%)			
Observer 1	100 (80, 100)	100 (80, 100)	100 (80, 100)
Observer 2	100 (80, 100)	94 (73, 100)	94 (73, 100)
PPV (%)			
Observer 1	100 (74, 100)	100 (79, 100)	100 (90, 100)
Observer 2	100 (79, 100)	93 (68, 100)	97 (85, 100)
NPV (%)			

Table 4 (continues)

Table 4 (continued)

Per-Lesion Analysis: Diagnostic Performance of MR Imaging Sequences in Comparison with the Reference Standard

Parameter	2D T1-weighted Imaging	2D T1-weighted Imaging + PDFS	3D T1-weighted Imaging
Observer 1	41 (26, 58)	46 (29, 63)	100 (80, 100)
Observer 2	44 (28, 60)	44 (28, 60)	85 (62, 97)

Note.—FN = false negative, FP = false positive, NPV = negative predictive value, PPV = positive predictive value, TN = true negative, TP = true positive. Numbers in parentheses are the 95% CI.

Figure 2

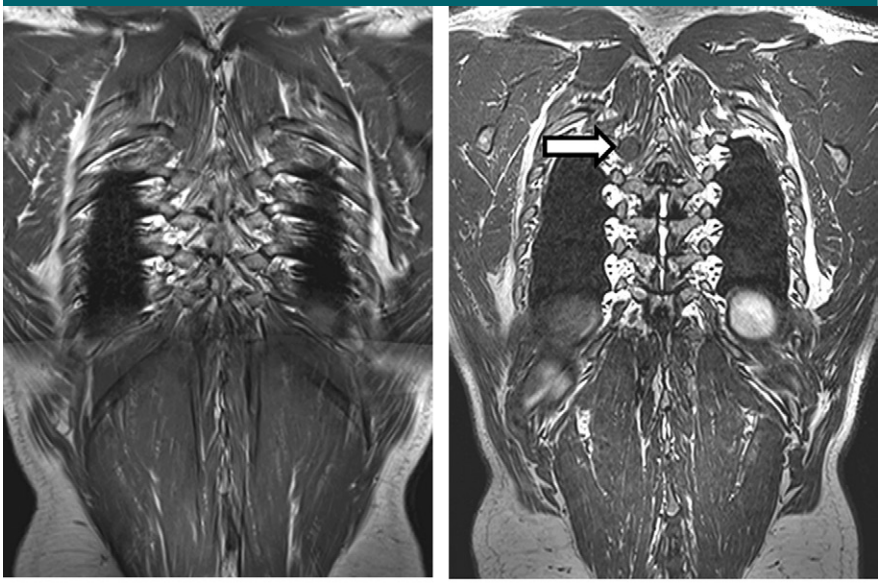

a. b.

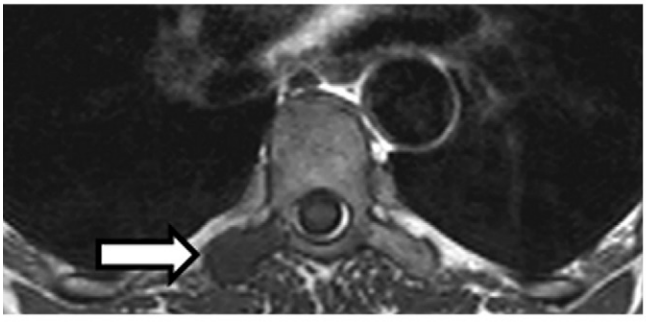

c.

Figure 2: Bone lesion detection in 63-year-old man with prostate cancer. The lesion was missed on whole-body 2D image but correctly identified on whole-body 3D image. **(a)** Whole-body 2D coronal image. No lesion is visible. **(b)** Whole-body 3D image shows low-signal-intensity lesion in right transverse process of T4 (arrow). **(c)** Transverse image obtained with multiplanar reformation at same level confirms the presence of lesion (arrow).

T1-weighted MR imaging pulse sequence for whole-body coverage and assessed its diagnostic performance in a definite clinical setting. We showed that the whole-body 3D T1-weighted pulse sequence helped detect significantly more node metastases as well as significantly more node-positive patients compared with whole-body 2D T1-weighted or whole-body 2D T1-weighted plus spine PDFS morphologic pulse sequences. No significant superiority of whole-body 3D T1-weighted imaging was observed for the detection of bone-positive patients, although whole-body 3D T1-weighted imaging depicted more bone lesions than whole-body 2D T1-weighted pulse sequences. The gain of performance is explained by the fact that more nodes and more bone lesions were detected on whole-body 3D T1-weighted images in general and in regions of difficult analysis, such as the posterior vertebral elements and pelvis. Indeed, consistent with MR imaging physics, the whole-body 3D T1-weighted pulse significantly outperformed 2D sequences in terms of SNR and CNR. The increase in SNR and CNR (resulting from the additional phase-encoding step in the z direction and the higher number of signals acquired) combined with the high spatial resolution and the multiplanar reformation capability of whole-body 3D T1-weighted imaging facilitated the study of regions that otherwise were difficult to study with conventional pulse sequences, such as the skull, ribs, sternum, posterior vertebral elements, and abdominopelvic content.

Our study also showed that the interobserver agreement with the whole-body 3D T1-weighted pulse sequence was higher than that with 2D pulse sequences when studying node metastasis on a per-patient and a per-lesion basis. Only limited discrepancies were noted between observers with whole-body 3D T1-weighted imaging in the detection of lymph nodes, which may be difficult on 2D images. The agreement was also very good for detecting bone metastasis. The difference between the readers' experience allowed the evaluation of the dependence of reading whole-body 3D T1-weighted images on the observer, which, according to agreement measurements, was inferior or equal to that with 2D pulse sequences. The blinded randomized readings were performed

Figure 3

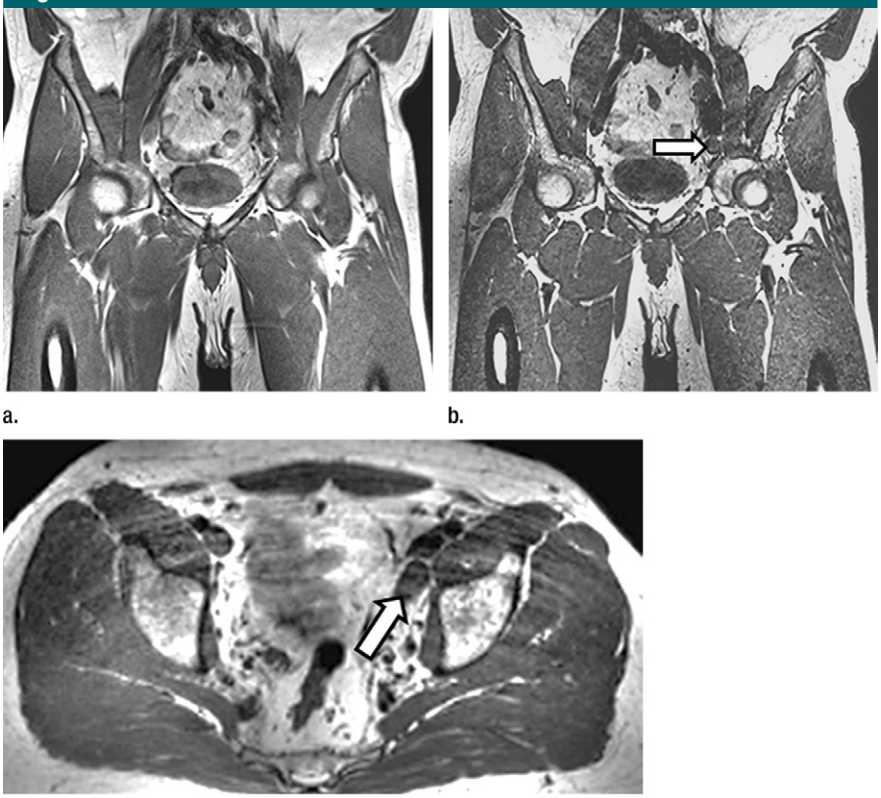

Figure 3: Images in 57-year-old man with prostate cancer and nodal metastasis. Lesion was missed on whole-body 2D image but correctly identified on whole-body 3D image. **(a)** Coronal whole-body 2D image. No abnormal lymph node is identified. **(b)** Whole-body 3D image shows enlarged left external iliac lymph node (arrow). **(c)** Transverse image obtained with multiplanar reformation helps confirm the presence of enlarged lymph node (arrow).

Table 5

Patient-based Analysis: Interobserver Agreement in 30 Patients

	Bone Lesions		Node Lesions	
Sequence	Disagreement*	Scott Pi†	Disagreement*	Scott Pi†
2D T1 weighted	0	1.00 (0.74, 1.00)	2	0.82 (0.44, 0.95)
2D T1 weighted + PDFS	2	0.85 (0.53, 0.96)	4	0.66 (0.28, 0.86)
3D T1 weighted	0	1.00 (0.74, 1.00)	0	1.00 (0.77, 1.00)

* Numbers of patients.

† Numbers in parentheses are the 95% CI.

3 weeks apart, which suggests that the high interobserver agreement obtained with whole-body 3D T1-weighted imaging is related to the higher sensitivity and multiplanar reformation capability of the pulse sequence and not to recall bias.

Our study has several limitations. First, the enrollment of a larger number of patients is mandatory to validate the present results. The inclusion of patients is still ongoing in our department as part of this project, and multicentric acquisitions and readings are planned for large-scale validation. Second, in most institutions like ours, staging cancer with whole-body MR imaging is performed with coronal whole-body 2D T1-weighted imaging and a sagittal short inversion time inversion-recovery and/or PDFS pulse sequence of the spine combined with a whole-body diffusion-weighted imaging pulse sequence, which has gained widespread interest (40). This combination of morphologic (whole-body 2D T1-weighted imaging + PDFS imaging) and functional (diffusion-weighted imaging) sequences is advocated for optimal lesion detection because the specificity provided with morphologic pulse sequences complements the sensitivity provided by diffusion-weighted imaging (17,19,25,43,44). This complementarity explains the lack of comparison between the pulse sequences used with whole-body 3D T1-weighted imaging and whole-body diffusion-weighted imaging in our study, as the question of replacing this functional sequence was not considered. Another limitation is the limited body coverage (top of head to upper thighs), although the risk of missing significant peripheral metastasis is very low (4). Finally, the relatively short follow-up period and the use of a "best valuable comparator" as a standard of reference must be underlined. This standard of reference represents the best achievable "truth" in the absence of systematic histologic proof and is used in many studies evaluating metastasis detection (10).

Future studies should evaluate the feasibility and diagnostic value of whole-body 3D T1-weighted imaging for metastatic bone and node screening in other cancers, such as breast cancer, myeloma, and lymphoma, for which whole-body 2D pulse sequences have been shown useful (36,45,46). The value of the same whole-body 3D T1-weighted pulse sequence used with contrast material injection to screen other frequent metastatic sites such as the brain and liver could also be studied (6,47).

In conclusion, we evaluated a high-spatial-resolution 3D T1-weighted MR imaging pulse sequence developed for

Table 6

Lesion-based Analysis: Interobserver Agreement in 30 Patients

Sequence	Bone Lesions	Node Lesions
2D T1 weighted	0.988 (0.975, 0.994)	0.876 (0.757, 0.939)
2D T1 weighted + PDFS	0.993 (0.985, 0.007)	0.639 (0.365, 0.811)
3D T1 weighted	0.993 (0.986, 0.997)	0.965 (0.928, 0.983)

Note.—Data are intraclass correlation coefficients. Numbers in parentheses are the 95% CI.

whole-body coverage. This sequence offers better CNR and SNR compared with classic 2D sequences. Compared with 2D T1-weighted whole-body MR imaging used alone or in combination with sagittal spine sequences, a 3D T1-weighted whole-body MR imaging pulse sequence is highly effective for bone metastases screening and superior for abnormal lymph node screening in prostate cancer; in future practice, 3D T1-weighted whole-body MR imaging could be the single morphologic complement to functional diffusion-weighted imaging sequences for metastasis screening.

Disclosures of Conflicts of Interest: V.P. disclosed no relevant relationships. **N.M.** disclosed no relevant relationships. **F.P.** disclosed no relevant relationships. **A.L.** disclosed no relevant relationships. **B.T.** Activities related to the present article: disclosed no relevant relationships. Activities not related to the present article: received personal fees from Amgen, Astellas, Bayer, Ferring, and Sanofi; received a grant from Amgen and Bayer; received nonfinancial support from Astellas. Other relationships: disclosed no relevant relationships. **T.S.** disclosed no relevant relationships. **P.O.** disclosed no relevant relationships. **B.C.V.B.** disclosed no relevant relationships. **F.E.L.** disclosed no relevant relationships. Activities not related to the present article: received an honorarium for lectures from Amgen and Johnson & Johnson. Other relationships: none to disclose.

References

1. Antoch G, Vogt FM, Freudenberg LS, et al. Whole-body dual-modality PET/CT and whole-body MRI for tumor staging in oncology. JAMA 2003;290(24):3199–3206.
2. Daldrup-Link HE, Franzius C, Link TM, et al. Whole-body MR imaging for detection of bone metastases in children and young adults: comparison with skeletal scintigraphy and FDG PET. AJR Am J Roentgenol 2001;177(1):229–236.
3. Lauenstein TC, Goehde SC, Herborn CU, et al. Whole-body MR imaging: evaluation of patients for metastases. Radiology 2004; 233(1):139–148.
4. Lecouvet FE, Simon M, Tombal B, Jamart J, Vande Berg BC, Simoni P. Whole-body MRI (WB-MRI) versus axial skeleton MRI (AS-MRI) to detect and measure bone metastases in prostate cancer (PCa). Eur Radiol 2010;20(12):2973–2982.
5. Sohaib SA, Cook G, Allen SD, Hughes M, Eisen T, Gore M. Comparison of whole-body MRI and bone scintigraphy in the detection of bone metastases in renal cancer. Br J Radiol 2009;82(980):632–639.
6. Weckbach S, Michaely HJ, Stemmer A, Schoenberg SO, Dinter DJ. Comparison of a new whole-body continuous-table-movement protocol versus a standard whole-body MR protocol for the assessment of multiple myeloma. Eur Radiol 2010;20(12):2907–2916.
7. Dutoit JC, Vanderkerken MA, Verstraete KL. Value of whole body MRI and dynamic contrast enhanced MRI in the diagnosis, follow-up and evaluation of disease activity and extent in multiple myeloma. Eur J Radiol 2013; 82(9):1444–1452.
8. Lecouvet FE, El Mouedden J, Collette L, et al. Can whole-body magnetic resonance imaging with diffusion-weighted imaging replace Tc 99m bone scanning and computed tomography for single-step detection of metastases in patients with high-risk prostate cancer? Eur Urol 2012;62(1):68–75.
9. Nakanishi K, Kobayashi M, Nakaguchi K, et al. Whole-body MRI for detecting metastatic bone tumor: diagnostic value of diffusion-weighted images. Magn Reson Med Sci 2007;6(3):147–155.
10. Mosavi F, Johansson S, Sandberg DT, Turesson I, Sörensen J, Ahlström H. Whole-body diffusion-weighted MRI compared with (18)F-NaF PET/CT for detection of bone metastases in patients with high-risk prostate carcinoma. AJR Am J Roentgenol 2012;199(5):1114–1120.
11. Choi JY, Kim MJ, Lee JM, et al. Magnetic resonance cholangiography: comparison of two- and three-dimensional sequences for assessment of malignant biliary obstruction. Eur Radiol 2008;18(1):78–86.
12. Hori M, Kim T, Onishi H, et al. Uterine tumors: comparison of 3D versus 2D T2-weighted turbo spin-echo MR imaging at 3.0 T—initial experience. Radiology 2011; 258(1):154–163.
13. Kijowski R, Davis KW, Woods MA, et al. Knee joint: comprehensive assessment with 3D isotropic resolution fast spin-echo MR imaging—diagnostic performance compared with that of conventional MR imaging at 3.0 T. Radiology 2009;252(2):486–495.
14. Kwon JW, Yoon YC, Choi SH. Three-dimensional isotropic T2-weighted cervical MRI at 3T: comparison with two-dimensional T2-weighted sequences. Clin Radiol 2012;67(2):106–113.
15. Hecht EM, Yitta S, Lim RP, et al. Preliminary clinical experience at 3 T with a 3D T2-weighted sequence compared with multiplanar 2D for evaluation of the female pelvis. AJR Am J Roentgenol 2011;197(2):W346–W352.
16. Jung JY, Yoon YC, Choi SH, Kwon JW, Yoo J, Choe BK. Three-dimensional isotropic shoulder MR arthrography: comparison with two-dimensional MR arthrography for the diagnosis of labral lesions at 3.0 T. Radiology 2009;250(2):498–505.
17. Heusner TA, Kuemmel S, Koeninger A, et al. Diagnostic value of diffusion-weighted magnetic resonance imaging (DWI) compared to FDG PET/CT for whole-body breast cancer staging. Eur J Nucl Med Mol Imaging 2010;37(6):1077–1086.
18. Koh DM, Blackledge M, Padhani AR, et al. Whole-body diffusion-weighted MRI: tips, tricks, and pitfalls. AJR Am J Roentgenol 2012;199(2):252–262.
19. Lecouvet FE, Vande Berg BC, Malghem J, Omoumi P, Simoni P. Diffusion-weighted MR imaging: adjunct or alternative to T1-weighted MR imaging for prostate carcinoma bone metastases? Radiology 2009;252(2):624.
20. Ohno Y, Koyama H, Onishi Y, et al. Non–small cell lung cancer: whole-body MR examination for M-stage assessment—utility for whole-body diffusion-weighted imaging compared with integrated FDG PET/CT. Radiology 2008;248(2):643–654.
21. Lecouvet FE, Geukens D, Stainier A, et al. Magnetic resonance imaging of the axial skeleton for detecting bone metastases in patients with high-risk prostate cancer: diagnostic and cost-effectiveness and comparison with current detection strategies. J Clin Oncol 2007;25(22):3281–3287.
22. Tombal B, Alcaraz A, James N, Valdagni R, Irani J. Can we improve the definition of high-

risk, hormone naïve, non-metastatic prostate cancer? BJU Int 2014;113(2):189–199.

23. Park J, Mugler JP 3rd, Horger W, Kiefer B. Optimized T1-weighted contrast for single-slab 3D turbo spin-echo imaging with long echo trains: application to whole-brain imaging. Magn Reson Med 2007;58(5):982–992.

24. Eisenhauer EA, Therasse P, Bogaerts J, et al. New response evaluation criteria in solid tumours: revised RECIST guideline (version 1.1). Eur J Cancer 2009;45(2):228–247.

25. Koh DM, Hughes M, Husband JE. Cross-sectional imaging of nodal metastases in the abdomen and pelvis. Abdom Imaging 2006;31(6):632–643.

26. Gudbjartsson H, Patz S. The Rician distribution of noisy MRI data. Magn Reson Med 1995;34(6):910–914.

27. Zweig MH, Campbell G. Receiver-operating characteristic (ROC) plots: a fundamental evaluation tool in clinical medicine. Clin Chem 1993;39(4):561–577.

28. DeLong ER, DeLong DM, Clarke-Pearson DL. Comparing the areas under two or more correlated receiver operating characteristic curves: a nonparametric approach. Biometrics 1988;44(3):837–845.

29. Liddell FD. Simplified exact analysis of case-referent studies: matched pairs; dichotomous exposure. J Epidemiol Community Health 1983;37(1):82–84.

30. Scott WA. Reliability of content analysis: the case of nominal scale coding. Public Opin Q 1955;19(3):321–325.

31. McGraw KO, Wong SP. Forming inferences about some intraclass correlation coefficients. Psychol Methods 1996;1(1):30–46.

32. Landis JR, Koch GG. The measurement of observer agreement for categorical data. Biometrics 1977;33(1):159–174.

33. Avrahami E, Tadmor R, Dally O, Hadar H. Early MR demonstration of spinal metastases in patients with normal radiographs and CT and radionuclide bone scans. J Comput Assist Tomogr 1989;13(4):598–602.

34. Sanal SM, Flickinger FW, Caudell MJ, Sherry RM. Detection of bone marrow involvement in breast cancer with magnetic resonance imaging. J Clin Oncol 1994;12(7):1415–1421.

35. Vogler JB 3rd, Murphy WA. Bone marrow imaging. Radiology 1988;168(3):679–693.

36. Schmidt GP, Baur-Melnyk A, Haug A, et al. Comprehensive imaging of tumor recurrence in breast cancer patients using whole-body MRI at 1.5 and 3 T compared to FDG-PET-CT. Eur J Radiol 2008;65(1):47–58.

37. Gutzeit A, Doert A, Froehlich JM, et al. Comparison of diffusion-weighted whole body MRI and skeletal scintigraphy for the detection of bone metastases in patients with prostate or breast carcinoma. Skeletal Radiol 2010;39(4):333–343.

38. Giles SL, Messiou C, Collins DJ, et al. Whole-body diffusion-weighted MR imaging for assessment of treatment response in myeloma. Radiology 2014;271(3):785–794.

39. Kwee TC, Fijnheer R, Ludwig I, et al. Whole-body magnetic resonance imaging, including diffusion-weighted imaging, for diagnosing bone marrow involvement in malignant lymphoma. Br J Haematol 2010;149(4):628–630.

40. Padhani AR, Koh DM, Collins DJ. Whole-body diffusion-weighted MR imaging in cancer: current status and research directions. Radiology 2011;261(3):700–718.

41. Takenaka D, Ohno Y, Matsumoto K, et al. Detection of bone metastases in non–small cell lung cancer patients: comparison of whole-body diffusion-weighted imaging (DWI), whole-body MR imaging without and with DWI, whole-body FDG-PET/CT, and bone scintigraphy. J Magn Reson Imaging 2009;30(2):298–308.

42. Ghanem N, Altehoefer C, Kelly T, et al. Whole-body MRI in comparison to skeletal scintigraphy in detection of skeletal metastases in patients with solid tumors. In Vivo 2006;20(1):173–182.

43. Fischer MA, Nanz D, Hany T, et al. Diagnostic accuracy of whole-body MRI/DWI image fusion for detection of malignant tumours: a comparison with PET/CT. Eur Radiol 2011;21(2):246–255.

44. Manenti G, Cicciò C, Squillaci E, et al. Role of combined DWIBS/3D-CE-T1w whole-body MRI in tumor staging: comparison with PET-CT. Eur J Radiol 2012;81(8):1917–1925.

45. Fechtner K, Hillengass J, Delorme S, et al. Staging monoclonal plasma cell disease: comparison of the Durie-Salmon and the Durie-Salmon PLUS staging systems. Radiology 2010;257(1):195–204.

46. Punwani S, Prakash V, Bainbridge A, et al. Quantitative diffusion weighted MRI: a functional biomarker of nodal disease in Hodgkin lymphoma? Cancer Biomark 2010;7(4):249–259.

47. Cai W, Kassarjian A, Bredella MA, et al. Tumor burden in patients with neurofibromatosis types 1 and 2 and schwannomatosis: determination on whole-body MR images. Radiology 2009;250(3):665–673.

The Prostate 74:469–477 (2014)

One-StepTNM Staging of High-Risk Prostate Cancer using Magnetic Resonance Imaging (MRI): Toward an Upfront Simplified "all-in-one" Imaging Approach?

Vasiliki Pasoglou,[1] Ahmed Larbi,[1] Laurence Collette,[2] Laurence Annet,[1] François Jamar,[3] Jean-Pascal Machiels,[4] Nicolas Michoux,[1] Bruno C. Vande Berg,[1] Bertrand Tombal,[5] and Frederic E. Lecouvet[1]*

[1]*Department of Radiology, Centre du Cancer et Institut de Recherche Expérimentale et Clinique (IREC), Cliniques Universitaires Saint Luc, Université Catholique de Louvain, Brussels, Belgium*
[2]*Statistics Department, EORTC Headquarters, Brussels, Belgium*
[3]*Division of Nuclear Medicine, Centre du Cancer et Institut de Recherche Expérimentale et Clinique (IREC), Cliniques Universitaires Saint Luc, Université Catholique de Louvain, Brussels, Belgium*
[4]*Division of Medical Oncology, Centre du Cancer et Institut de Recherche Expérimentale et Clinique (IREC), Cliniques Universitaires Saint Luc, Université Catholique de Louvain, Brussels, Belgium*
[5]*Division of Urology, Centre du Cancer et Institut de Recherche Expérimentale et Clinique (IREC), Cliniques Universitaires Saint Luc, Université Catholique de Louvain, Brussels, Belgium*

BACKGROUND. Multiparametric magnetic resonance imaging (mpMRI) is the standard for local prostate cancer (PCa) staging. Whole-body MRI (wbMRI) has shown capabilities for metastatic screening. This study assesses the feasibility and value of an all-in-one AJCC TNM staging of PCa during a unique MRI session combining mpMRI and wbMRI.

METHODS. Thirty consecutive patients with "high-risk" PCa prospectively underwent mpMRI of the prostate and wbMRI, in addition to ^{99m}Tc bone scan (BS), completed with standard X-rays (±TXR) and contrast enhanced CT for distant staging. For the statistical analysis, a "best valuable comparator" (BVC) combining a panel review of all available baseline and follow-up imaging, biological, and clinical data was used to adjudicate lymph node and bone metastatic status.

RESULTS. Prostate mpMRI was analyzed using ESUR guidelines. Sensitivity of BS ± TXR combined with CT and of wbMRI for detecting metastases (bones or nodes) was 85% and 100%, respectively, and specificity was 88% and 100%, respectively. For the overall staging of the patients as being either N0M0 or having disease extension beyond the prostate, wbMRI was superior to the combination of BS and CT (improvement in all ROC characteristics and of AUC by 13.6% (95% CI: +0.7% to +26.5%, $P = 0.039$)). The main limitation is the limited number of patients.

CONCLUSIONS. AJCC M and N staging using wbMRI is feasible during the same imaging session as mpMRI performed for T staging, in less then one hour. wbMRI outperforms BS ± TXR and abdomino-pelvic CT work up for discriminating subsets of patients with or without distant spread of the cancer. *Prostate 74:469–477, 2014.* © 2013 Wiley Periodicals, Inc.

KEY WORDS: **prostate cancer; lymph nodes; bone metastases; magnetic resonance imaging**

Abbreviations: AJCC, American Joint Committee on Cancer; CT, computed tomography; MRI, magnetic resonance imaging; PCa, prostate cancer; PSA, prostate specific antigen; TNM, tumor, node, metastasis.

Grant sponsor: FRS-FNRS Télévie; Grant sponsor: Fondation Saint Luc; Grant sponsor: Fondation Contre le Cancer.

Bertrand Tombal and Frederic E. Lecouvet contributed equally to this work.

*Correspondence to: Frédéric E. Lecouvet, MD, PhD, Department of Radiology, Cliniques Universitaires Saint Luc, Hippocrate Avenue, 10/2942, B-1200 Brussels, Belgium. E-mail: frederic.lecouvet@uclouvain.be
Received 25 October 2013; Accepted 25 November 2013
DOI 10.1002/pros.22764
Published online 24 December 2013 in Wiley Online Library (wileyonlinelibrary.com).

INTRODUCTION

Prostate cancers (PCa) with a prostate specific antigen (PSA) > 20 ng/dl, a Gleason Score ≥ 8, or a cT stage ≥ 3, carry a high-risk of biochemical recurrence after local treatment, of metastatic spread, and of cancer death [1]. Initially intended for low or intermediate risk PCa, external beam radiation therapy (EBRT) and radical prostatectomy are nowadays the standard of care for high-risk PCa [1]. These strategies require a precise evaluation of metastatic spread, especially with the development of clinical trials evaluating novel compounds and local treatment in oligo-metastatic patients [2,3].

The standard assessment of tumor stage is based on the system established by the American Joint Committee on Cancer (AJCC) [4]. Local staging of high-risk PCa implies assessment of extra-capsular extension, seminal vesicles and adjacent organ extension [5]. This is critical for surgery planning in order to avoid surgical margins and for EBRT planning to optimize the delineation of target organs. Multi-parametric magnetic resonance imaging (mpMRI) has been shown to increase the staging accuracy and most treatment guidelines recognize that local (T) staging of PCa should be based on mpMRI [6,7]. In addition, mpMRI has become an essential adjunct for target delineation in radiotherapy [8].

Most treatment guidelines recommend computed tomography (CT) and/or abdominal MRI and ^{99m}Tc bone scanning (BS) with targeted X-rays if necessary for the early assessment of metastatic spread, that is, for N and M staging [6,7]. Recently, whole body MRI with diffusion imaging (wbMRI/DWI) has positioned itself as an accurate alternative to CT and ^{99m}Tc BS for the concurrent evaluation of LN and bone metastases [9,10].

In the present study, we assessed whether a same imaging session combining mpMRI and wbMRI is suitable for single step local (T) and distant (N and M) staging in high-risk PCa patients.

MATERIALS AND METHODS

Patients Demographics

The study has enrolled 30 consecutive patients with newly diagnosed high-risk PCa, that is, those with PSA > 20 ng/ml, Gleason sum ≥ 8, or clinical stage ≥T3a [6]. Median age was 63 years (range: 51–92). Median baseline PSA was 30 ng/ml (range: 1.7–4612). Gleason sum was ≤7 in 13 patients, 7 in 12 and ≥8 in 17 patients. After final staging, 3 patients were treated by radical prostatectomy, 16 by a combination of EBRT and ADT and 11 by ADT alone. AJCC clinical stage [4] was cT2 in 7 patients, cT3 in 14 patients, and cT4 in 9 patients. The local ethical committee approved the study and written informed consent was obtained from all patients (Table I).

Imaging

Three Tesla (3T) mpMRI study of the prostate consisted of high resolution T2 weighted images (T2WI) in three planes (axial, sagittal and coronal) for the analysis of the prostate's zonal anatomy and

TABLE I. Patients Characteristics

	Treatment			
	ADT (N = 11)	EBRT + ADT (N = 16)	(N = 3)	Total (N = 30)
Age (years)				
Median	62.0	63.5	58.0	62.5
Range	53.0–92.0	54.0–80.0	51.0–66.0	51.0–92.0
50%range	55.0–66.0	57.5–69.0	51.0–66.0	56.0–69.0
Mean (SD)	64.18 (11.02)	64.06(7.25)	58.33(7.51)	63.53 (8.72)
PSA (ng/ml)				
Median	21.7	37.9	72.7	30.0
Range	1.7–4612.0	4.7–206.0	9.0–126.0	1.7–4612.0
50%range	6.8–60.5	15.9–134.5	9.0–126.0	12.0–99.0
Mean (SD)	470.73 (1,377.31)	70.01 (72.82)	69.24 (58.58)	216.87 (834.09)
Gleason sum				
6	1 (9.1)	0 (0.0)	0 (0.0)	1 (3.3)
7	2 (18.2)	7 (43.8)	3 (100.0)	12 (40.0)
8	4 (36.4)	5 (31.3)	0 (0.0)	9 (30.0)
9	4 (36.4)	4 (25.0)	0 (0.0)	8 (26.7)

ADT, androgen deprivation therapy; EBRT, external beam radiation therapy.

capsule, dynamic contrast-enhanced MRI (DCE MRI), diffusion weighted imaging (DWI) and apparent diffusion coefficient (ADC) maps, and post-contrast axial T1 weighted images of the pelvis for the study of regional lymph nodes. MR spectroscopic imaging was not performed. During the same imaging session, each patient underwent an MRI study of the whole body (wbMRI) consisting of anatomical T1-weighted MR images and DWI sequences. Imaging times and parameters are detailed in Table II. All images were read on PACS workstations allowing multi-planar reformations.

Local staging, including extra-capsular extension, seminal vesicles and adjacent organ invasion, was performed by two radiologists specialized in uroradiology using the published criteria from the European Society of European Urology (ESUR) [11]. The ADC values of every suspect lesion, as well as the maximum diameter of the largest lesion were recorded. DCE curves were classified into one of three enhancement patterns as reported in the literature: type one with persistent increase of the enhancement; type two with no change in enhancement over time (plateau); type three, the most typical pattern for cancer, with fast enhancement and early wash-out [12].

wbMRI studies were read by two radiologists, recording bone metastasis and enlarged lymph nodes according to previously published criteria [9].

Comparison With Current Standards and Best Valuable Comparator (BVC)

All patients underwent routine M and N screening of high risk PCa, consisting for the assessment of bone metastases of ^{99m}Tc BS study followed by targeted X-Rays (BS $\pm$ TXR) on equivocal foci of increased uptake if the BS was deemed non-diagnostic, and assessment of enlarged lymph nodes by contrast enhanced abdomino-pelvic CT.

Each imaging study was read without knowledge of the results of the other modalities. Final adjudication of T, N, and M stage was done in a consensus session during which all initial imaging studies were reviewed by radiologists and nuclear medicine physicians, using all available clinical and biological data (BVC). In case of discrepancy between ^{99m}Tc BS or CT and wbMRI, follow-up imaging studies were obtained after 6 months of treatment and included in the adjudication process [9,13].

Statistical Methods

For each imaging method, we estimated the receiver-operating characteristic (ROC) characteristics with their 95% exact confidence interval (CI). Areas under ROC

TABLE II. Imaging Parameters

Target	Acquisition	Time (min/sec)	Sequence type	Plane	Slice thickness, gap	FOV, matrix	TR, TE, NSA, TF	Fat saturation	Specific parameters
Prostate	T2	02:24	TSE	Sagittal	21 × 3 mm, 0.3 mm	130 × 130, 192 × 192	3560, 127, 1, 21		
		03:35	TSE	Axial	30 × 3 mm, 0.9 mm	240 × 240, 304 × 384	3200, 136, 2, 19		
		02:00	TSE	Coronal	18 × 3 mm, 0.9 mm	240 × 240, 304 × 384	4790, 136, 2, 19		
	DWI	03:14	Diffusion	Axial	20 × 5 mm, 0.5 mm	380 × 326, 110 × 128	5500, 69, 3	Spair	b-values: 0, 50, 600, 1200
	DCE	04:07	3D flash	Axial	24 × 3 mm	400 × 300, 173 × 256	4.04, 1.35, 1	Q FAT	Measurements 45
	VIBE	00:18	3D flash	Axial	72 × 3 mm	400 × 300, 202 × 384	4.04, 1.45, 1	Q FAT	
Whole Body (WB)	T1WI (body)	18:28 (4 × 4:37)	3D space	Coronal	176 × 1.2 mm	440 × 307, 214 × 384	400, 13, 2, 58	/	
	DWI (body)	15:45	Diffusion	Axial	25 × 5 mm, 0.5 mm	430 × 366, 83 × 122	4500, 68, 5	SPAIR	b-value: 0, 800
	PDFS (spine)	05:24 (3 × 1:48)	TSE	Sagittal	13 × 4 mm, 0.4 mm	260 × 260, 256 × 320	2600, 45, 2, 13	FAT SAT	
		56 minutes							

DWI = diffusion weighted imaging; PDFS = proton density with fat signal suppression; TSE = turbo spin echo; FOV = field of view; TR = relaxation time; TE = echo time; NSA = number of signals averaged; TF = turbo factor.

curve (AUC) were compared by Wald test from logistic regression models at the two-sided 5% significance level. The statistical analysis software, version 9.2 (SAS®, Bethesda, MD), was used. The study is exploratory and the sample size was not prospectively planned.

RESULTS

Figures 1 and 2 illustrate an example of report of an "all-in-one MRI study" combining mpMRI and wbMRI.

Local Staging of Prostate Cancer Using mpMRI (T Staging)

Results of the local staging, that is, extra-prostatic involvement, performed by mpMRI following the ESUR guidelines are summarized in Table III [11].

N and M Staging Using wbMRI

Based on the BVC, 13/30 patients had metastases (9 had bone metastases, 11 had lymph nodes). None had visceral metastases.

Comparison of the Diagnostic Performance of wbMRI and ^{99m}Tc BS ± TXR to Detect Bone Metastases (M Staging)

Table IV illustrates the performance of BS ± TXR and wbMRI for predicting bone metastases, using BVC as reference. Based on the BVC, nine patients had bone metastases. Sensitivity of ^{99m}Tc BS ± TXR and wbMRI for detecting bone metastases was 89% and 100%, respectively, and specificity was 90% and 100%, respectively. wbMRI correctly identified bone metastases in one patient with negative BS, and correctly identified the absence of bone metastases in two patients with false positive BS. Comparison of AUC showed no significant difference between wbMRI and BS ± TXR for the detection of bone metastases with a mean increase in AUC with wbMRI compared to BS ± TXR of 10.3% (CI: −2.3% to +23%, $P = 0.110$).

Comparison of the Diagnostic Performance of wbMRI and CT to Detect Lymph Nodes Enlargement (N Staging)

Table V illustrates the performance of CT and wbMRI for predicting lymph nodes metastases, using BVC as reference. Based on the BVC, 11 patients had enlarged lymph nodes. Sensitivities of CT and wbMRI for detecting lymph nodes were 82% and 100%, respectively; specificities were 100% for both. wbMRI correctly identified lymph nodes in one patient with negative CT. Comparison of AUC showed no significant difference between wbMRI and CT for the detection of enlarged lymph nodes with mean increase in AUC of +9.1% (CI: −2.9% to +21.0%) with wbMRI compared to CT ($P = 0.136$).

Comparison of wbMRI and of the Combination of BS ± TXR and CT for Assessing Global Metastatic Status (N and M Staging)

The performance of wbMRI to define lymph nodes and bone status was compared to the results of BS ± TXR and CT, taking BVC as reference (Table VI). For each combination of lymph nodes and bone metastases assessment, the patients were classified negative if both exams were negative, and positive if

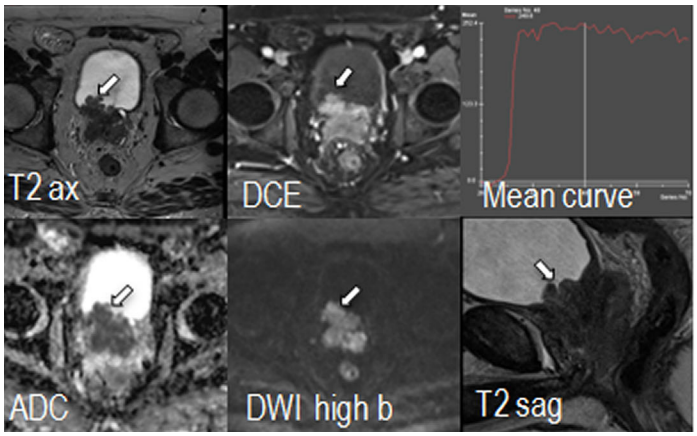

	ESUR Score
Extra capsular	5
Seminal vesicles	4
Distal sphincter	4
Bladder neck	4
Other organ	rectum

Fig. 1. Example of multiparametric (mpMRI) T staging: tumor diffusely infiltrates the prostate, showing low signal intensity on T2 images, high signal intensity on DWI with low ADC values, type 3 enhancement curve. There is non-ambiguous extension to the bladder wall (arrows) and other organs (extraprostatic spread scored I7 according to ESUR criteria).

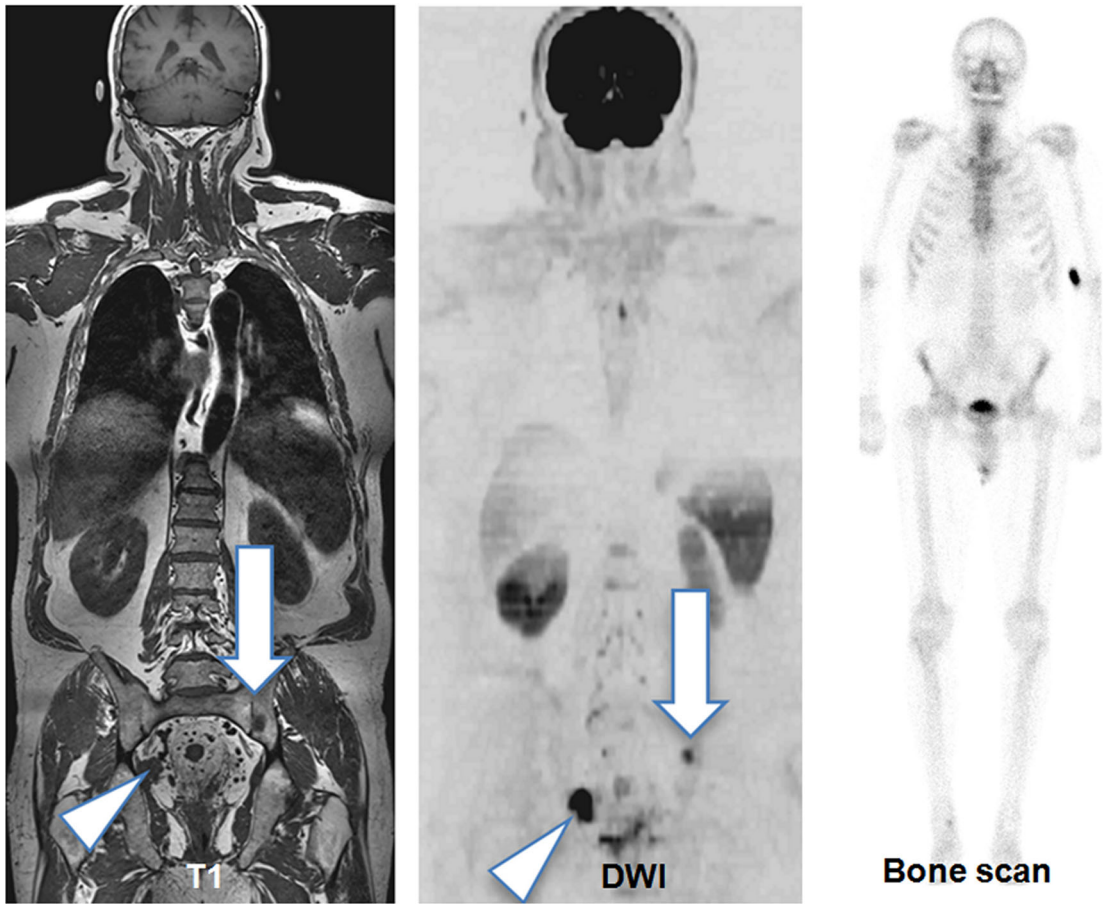

Fig. 2. Illustration of the N and M staging, and of the superiority of wbMRI over bone scintigraphy: coronal T1 (left) and diffusion (center) weighted MR images of the whole body obtained in the same patient as Figure I show pathologic right iliac node (arrowhead) and bone metastasis within the left iliac bone (arrow). This bone metastasis was not detected on the bone scintigraphy (right).

the one or both assessment was positive. On the basis of BVC, 13 patients were adjudicated metastatic. wbMRI readings were in perfect agreement with the BVC whereas combined BS ± TXR and CT readings disagreed with the BVC in four cases (two false positive and two false negative observations). Sensitivities of BS ± TXR combined with CT and of wbMRI for detecting bone or lymph node metastases were 85% and 100% respectively and specificities were 88% and 100%, respectively (Table VI). For the overall staging of the patients as being either N0M0 or having disease extension beyond the prostate (any metastases), wbMRI was superior to the combination of BS ± TXR and CT (improvement in all ROC characteristics and of AUC by 13.6% (95% CI: +0.7% to +26.5%, $P = 0.039$)).

DISCUSSION

To our knowledge, this is the first work evaluating a single-step non-irradiating imaging strategy for tumor, node, metastasis (TNM) staging of PCa, incorporating evaluation of local disease by mpMRI and of metastatic spread by whole-body MRI. Such integrated evaluation is critical in case of high-risk PCa, since the decision to perform a local treatment, either by radical prostatectomy or EBRT, and the final planning of these treatments, largely depend on the local extension of the cancer [1]. In the last few years, mpMRI has positioned itself as an essential adjunct to clinical staging for tumor localization in intermediate and high-risk PCa [14,15]. Based on a published meta analysis, the average sensitivity and specificity of mpMRI for detecting lymph nodes range around 71% [16]. In addition, mpMRI may help planning local treatment [8,17]. The EAU guidelines recognize that, in comparison with clinical staging, MRI demonstrates higher accuracy for the assessment of extracapsular extension (stage T3a), seminal vesicle invasion (stage T3b) and invasion of adjacent structures (stage T4) [6]. To reduce the inter-observer variability and standardize reporting, the European Society of Urological

TABLE III. Local (T) Staging at mpMRI According to ESUR Guidelines (Extraprostatic Disease According to PIRADS Scoring [11])

	PI-RAD score						
Sign	0	1	2	3	4	5	Total
Extra capsular extension (T3a)	6	0	NA	0	20	4	30
Invasion of seminal vesicles (T3b)	12	0	0	1	17	NA	30
Invasion of apical sphincter (T4)	21	NA	NA	4	5	NA	30
Invasion of bladder neck (T4)	17	0	0	0	13	NA	30
Adjacent organ extension	Yes, 7	No 23					30

Radiology has recently produced a set of guidelines that is based on a consensus of experts [11,18].

Based on current guidelines, patients with high-risk PCa also require assessment for distant metastases. In most PCa, the initial seeding of metastatic deposits occurs in pelvic lymph nodes and/or the hematopoietic red marrow of the axial skeleton [19–21]. Extranodal visceral metastases are rare at presentation and appear usually in later stages of the disease [21]. wbMRI enhances diagnosis of bone metastases but also allows their monitoring under therapy. wbMRI will therefore potentially help tackling an important unmet need, considering the arrival of many new drugs in advanced PCa and the necessity to assess their efficacy in a disease that is almost exclusively metastatic to the bone [10,22,23].

In contrast to what is happening in the therapeutic arena, there has been no recent major evolution in the diagnostic techniques. Most international guidelines still recognize contrast-enhanced CT or MRI of the abdomen and pelvis, and ^{99m}Tc BS, completed with plain X-rays if necessary, as standard diagnostic techniques to assess initial and follow-up metastatic status [6,7]. These techniques carry severe limitations and, ultimately, provide more of a best guess than a robust diagnosis. CT and conventional MRI perform similarly bad compared to extended pelvic node dissection (ePLND), the unchallenged gold standard to perform accurate lymph node staging, with an average specificity of ±80% and reported sensitivity of ±40% [24,25]. However, ePLND is not routinely performed in every patient. A recent study has demonstrated, in a series of 100 consecutive high-risk PCa patients, that wbMRI performed similarly to CT to detect enlarged lymph nodes [9]. Sensitivity of CT and wbMRI was 77–82% for both, while specificity was 95–96% and 96–98%, respectively. MRI has been proven superior to ^{99m}Tc-based algorithm for the detection of bone metastases, because it detects cancer cells in the bone marrow before bone remodeling has occurred [10,13,26]. In the aforementioned study on 100 high-risk patients, the sensitivity of BS ± TXR and wbMRI for detecting bone metastases was 86% and 98–100%, respectively ($p < 0.04$); specificity was 98% and 98–100%, respectively [9]. Two independent wbMRI readers identified bone metastases in 7 and 8 of 55 patients with negative BS ± TXR, therefore inducing significant changes in treatment strategy.

TABLE IV. Imaging Results and Receiver Operating Characteristic for Predicting Bone Metastasis on Best Valuable Comparator (BVC)

	BVC (N) for bone metastasis[a]							
	Neg.	Pos.	Tot.	Sensitivity % (95% CI)	Specificity % (95% CI)	PPV % (95% CI)	NPV % (95% CI)	AUC[a] % (95% CI)	Overall agreement % (95% CI)
Total	21	9	30						
BS									
Neg.	19	1	20	89 (52–100)	90 (70–99)	80 (44–97)	95 (75–100)	90 (77–100)	90 (74–98%)
Pos.	2	8	10						
wbMRI									
Neg.	21	0	21	100 (66–100)	100 (94–100)	100 (66–100)	100 (94–100)	100 (100–100)	100% (NA)
Pos.	0	9	9						

Neg, negative; Pos, positive; Tot, total.
[a]Comparison of ROC AUCs: +10.3% (95% CI: −2.3% to +23.0%), $P = 0.110$. Not statistically significant improvement for MRI compared to standard assessment.

TABLE V. Imaging Results and Receiver Operating Characteristic for Predicting Node Metastasis on best Valuable Comparator (BVC)

	BVC (N) for nodal metastasis			Sensitivity % (95% CI)	Specificity % (95% CI)	PPV % (95% CI)	NPV % (95% CI)	AUC[a] % (95% CI)	Overall agreement % (95% CI)
	Neg.	Pos.	Tot.						
Total	19	11	30						
CT									
Neg.	19	2	21	82 (48–98)	100 (82–100)	100 (66–100)	90 (70–99)	91 (79–100)	93 (78–99)
Pos.	0	9	9						
wbMRI									
Neg.	19	0	19	100 (71–100)	100 (82–100)	100 (72–100)	100 (82–100)	100 (100–100)	100% (NA)
Pos.	0	11	11						

Neg, negative; Pos, positive; Tot, total.
[a]Comparison of ROC AUCs: +9.1% (95% CI: −2.9% to +21.0%), $P = 0.136$. Not statistically significant improvement for MRI compared to CT.

In addition of a low sensitivity and specificity, ^{99m}Tc BS and abdomino-pelvic CT/MRI metastatic assessment require—at least—two separate visits to the hospital, injection of iodine contrast agent, nuclear waste handling and a significant radiation exposure (between 3.5 and 25 mSv for CT; 6.3 mSv for 99mTC BS) [27]. The ideal test for the future should be straightforward and single-step, provide high diagnostic performance for local staging, lymph nodes, (rare) visceral, and bone metastases' screening, and allow monitoring of response under treatment. It should minimize or avoid radiation exposure and the need for contrast agents. wbMRI with DWI and PET/CT compete for single step whole body assessment of metastases and imaging of response to therapy in solid cancers, but PET has limited value compared to MRI for local staging [22].

Here we report the first attempt to perform during a single imaging session the concurrent assessment of local and distant staging of cancer in high-risk PCa patients, that is, a one-step T, N, M staging of these patients. A 3 T mpMRI study of the prostate was performed in all 30 patients, consisting of high resolution T2 weighted images (T2WI) in three planes (axial, sagittal and coronal) for the analysis of the prostate's zonal anatomy and capsule, dynamic contrast enhanced MRI (DCE MRI) for the study of the angiogenesis, DWI and ADC maps for the study of the cellularity. wbMRI with diffusion was performed during the same imaging session to detect enlarged lymph nodes and bone metastases, as reported previously [9]. In line with previous works, the sensitivity and specificity of wbMRI for detecting any metastases (bone or lymph node) were significantly superior than those of BS ± TXR combined with CT.

This "all-in-one T, N, M" assessment using mpMRI and wbMRI was done in less than one hour, during a single visit to the imaging department, and was non-

TABLE VI. Imaging Results and Receiver Operating Characteristic for Global Diagnosis on Best Valuable Comparator (BVC)

	BVC (N) for metastasis			Sensitivity % (95% CI)	Specificity % (95% CI)	PPV % (95% CI)	NPV % (95% CI)	AUC[a] % (95% CI)	Overall agreement % (95% CI)
	Neg.	Pos.	Tot.						
Total	17	13	30						
Standard									
Neg.	15	2	17	85 (55–98)	88 (64–99)	84 (55–98)	88 (64–99)	86 (74–99)	87 (69–96)
Pos.	2	11	13						
wbMRI									
Neg.	17	0	17	100 (75–100)	100 (80–100)	100 (75–100)	100 (80–100)	100 (100–100)	100% (NA)
Pos.	0	13	13						

Neg, negative; Pos, positive; Tot, total.
[a]Comparison of ROC AUCs: +13.6% (95% CI: +0.7% to +26.5%), $P = 0.039$. Statistically significant improvement for MRI compared to standard assessment.

irradiating. This duration could be reduced even more if the injection of gadolinium can be avoided, which would save 4.25 min. DCE sequences, however, are useful to detect extracapsular extension and seminal vesicles invasion [28,29].

There are several limitations to this preliminary study, including a limited number of patients. We have not evaluated the inter- and intra-observer agreement of wbMRI for bone and lymph node lesion detection, as this definite question has been addressed in previous studies [9], and as the current study mainly focused on the feasibility of a concurrent, one step, prostate, node, and bone staging using MRI.

In a meta-analysis published in 2002, Engelbrecht et al. [16] suggested that the staging performance of MRI is influenced by the experience of the reader. Integrating TNM staging in an all-in-one single step assessment will require specific training of "prostate" radiologists, and/or collaboration of "genito-urinary" and "musculoskeletal" radiologists as done in this study.

The present gold standard is not perfect, since not all patients were followed up and radical prostatectomy was only performed in three patients. However, we used a consensus evaluation of all imaging modalities, by imaging experts, and prospective follow-up of those patients with any discrepancy between imaging modalities, showing that initial bone and node evaluation using MRI was correct.

Finally, this study has been conducted on a 3T MRI magnet, without endorectal coil and spectroscopic imaging. MR spectroscopic imaging provides information about lesion aggressiveness, but does not give staging information owing to its poor spatial resolution [30]. In addition, although the data on 3 T mpMRI are still debated, it benefits from higher signal to noise ratio, thus enabling high quality imaging within a short time and without the use of an endorectal coil [31]. With regard to body imaging, the use of 3 T has been challenging compared to results obtained on 1.5 T magnets; however, this challenge has been addressed and results are now (at least) similar to those obtained at lower magnetic fields [32]. This preference for high field MRI parallels the increasing availability of 3 T magnets in most centers.

The present study did not address precisely the cost-effectiveness of the all-in-one MRI work-up compared to the current sum of imaging studies. The difficulty of such an analysis has been pinpointed in a European Urology editorial on our primary publication on whole-body MRI [33]. Indeed differences in health care reimbursements, billing arrangements, and resource allocation across health care providers make that analysis difficult. In contrast to the conventional wisdom, the editorial by Linton and Catto concluded that wbMRI is not that much more expensive than current staging tools.

CONCLUSION

In conclusion, this preliminary work suggests that a "all in one MRI session" combining wbMRI and mpMRI of the prostate positions itself as a single-step, non-irradiating technique to perform TNM staging in high-risk PCa.

ACKNOWLEDGMENTS

This work was supported by Grants from FRS-FNRS Télévie, Fondation Saint Luc, and Fondation Contre le Cancer, non-profit organizations, to Pasoglou, Lecouvet, and Tombal.

REFERENCES

1. Bastian PJ, Boorjian SA, Bossi A, Briganti A, Heidenreich A, Freedland SJ, Montorsi F, Roach M III, Schroder F, van Poppel H, Stief CG, Stephenson AJ, Zelefsky MJ. High-risk prostate cancer: From definition to contemporary management. Eur Urol 2012;61(6):1096–1106.
2. Berkovic P, De Meerleer G, Delrue L, Lambert B, Fonteyne V, Lumen N, Decaestecker K, Villeirs G, Vuye P, Ost P. Salvage stereotactic body radiotherapy for patients with limited prostate cancer metastases: Deferring androgen deprivation therapy. Clin Genitourin Cancer 2013;11(1):27–32.
3. Jilg CA, Rischke HC, Reske SN, Henne K, Grosu AL, Weber W, Drendel V, Schwardt M, Jandausch A, Schultze-Seemann W. Salvage lymph node dissection with adjuvant radiotherapy for nodal recurrence of prostate cancer. J Urol 2012;188(6):2190–2197.
4. Genitourinary Cancers. In: Edge S, Byrd DR, Compton CC, Fritz AG, Greene FL, Trotti A, Editors. AJCC Cancer Staging Manual. 7th ed. 2010. XV, 649 pp.
5. Soylu FN, Peng Y, Jiang Y, Wang S, Schmid-Tannwald C, Sethi I, Eggener S, Antic T, Oto A. Seminal vesicle invasion in prostate cancer: Evaluation by using multiparametric endorectal MR imaging. Radiology 2013;267(3):797–806.
6. Heidenreich A, Bellmunt J, Bolla M, Joniau S, Mason M, Matveev V, Mottet N, Schmid HP, van der Kwast T, Wiegel T, Zattoni F. EAU guidelines on prostate cancer. Part 1: Screening, diagnosis, and treatment of clinically localised disease. Eur Urol 2011; 59(1):61–71.
7. Network NCC. Prostate cancer. In: Network NCC, editor. NCCN Clinical Practice Guidelines in Oncology (NCCN Guidelines), Volume 2013; 2013.
8. Hanvey S, Sadozye AH, McJury M, Glegg M, Foster J. The influence of MRI scan position on image registration accuracy, target delineation and calculated dose in prostatic radiotherapy. Br J Radiol 2012;85(1020):e1256–e1262.
9. Lecouvet FE, El Mouedden J, Collette L, Coche E, Danse E, Jamar F, Machiels JP, Vande Berg B, Omoumi P, Tombal B. Can whole-body magnetic resonance imaging with diffusion-weighted imaging replace Tc 99m bone scanning and computed

tomography for single-step detection of metastases in patients with high-risk prostate cancer? Eur Urol 2012;62(1):68–75.

10. Lecouvet FE, Simon M, Tombal B, Jamart J, Vande Berg BC, Simoni P. Whole-body MRI (WB-MRI) versus axial skeleton MRI (AS-MRI) to detect and measure bone metastases in prostate cancer (PCa). Eur Radiol 2010;20(12):2973–2982.
11. Barentsz JO, Richenberg J, Clements R, Choyke P, Verma S, Villeirs G, Rouviere O, Logager V, Futterer JJ. ESUR prostate MR guidelines 2012. Eur Radiol 2012;22(4):746–757.
12. Verma S, Turkbey B, Muradyan N, Rajesh A, Cornud F, Haider MA, Choyke PL, Harisinghani M. Overview of dynamic contrast-enhanced MRI in prostate cancer diagnosis and management. Am J Roentgenol 2012;198(6):1277–1288.
13. Lecouvet FE, Geukens D, Stainier A, Jamar F, Jamart J, d'Othee BJ, Therasse P, Berg BV, Tombal B. Magnetic resonance imaging of the axial skeleton for detecting bone metastases in patients with high-risk prostate cancer: Diagnostic and cost-effectiveness and comparison with current detection strategies. J Clin Oncol 2007;25(22):3281–3287.
14. Bloch BN, Genega EM, Costa DN, Pedrosa I, Smith MP, Kressel HY, Ngo L, Sanda MG, Dewolf WC, Rofsky NM. Prediction of prostate cancer extracapsular extension with high spatial resolution dynamic contrast-enhanced 3-T MRI. Eur Radiol 2012; 22(10):2201–2210.
15. Preston MA, Harisinghani MG, Mucci L, Witiuk K, Breau RH. Diagnostic tests in urology: Magnetic resonance imaging (MRI) for the staging of prostate cancer. BJU Int 2013;111(3):514–517.
16. Engelbrecht MR, Jager GJ, Laheij RJ, Verbeek AL, van Lier HJ, Barentsz JO. Local staging of prostate cancer using magnetic resonance imaging: A meta-analysis. Eur Radiol 2002;12(9): 2294–2302.
17. Kapanen M, Collan J, Beule A, Seppala T, Saarilahti K, Tenhunen M. Commissioning of MRI-only based treatment planning procedure for external beam radiotherapy of prostate. Magn Reson Med 2013;70(1):127–135.
18. Dickinson L, Ahmed HU, Allen C, Barentsz JO, Carey B, Futterer JJ, Heijmink SW, Hoskin PJ, Kirkham A, Padhani AR, Persad R, Puech P, Punwani S, Sohaib AS, Tombal B, Villers A, van der Meulen J, Emberton M. Magnetic resonance imaging for the detection, localisation, and characterisation of prostate cancer: Recommendations from a European consensus meeting. Eur Urol 2011;59(4):477–494.
19. Hansen J, Rink M, Bianchi M, Kluth LA, Tian Z, Ahyai SA, Shariat SF, Briganti A, Steuber T, Fisch M, Graefen M, Karakiewicz PI, Chun FK. External validation of the updated briganti nomogram to predict lymph node invasion in prostate cancer patients undergoing extended lymph node dissection. Prostate 2013;73(2):211–218.
20. Nelson JB, Love W, Chin JL, Saad F, Schulman CC, Sleep DJ, Qian J, Steinberg J, Carducci M. Phase 3, randomized, controlled trial of atrasentan in patients with nonmetastatic, hormone-refractory prostate cancer. Cancer 2008;113(9):2478–2487.
21. Scher HI, Fizazi K, Saad F, Taplin ME, Sternberg CN, Miller K, de Wit R, Mulders P, Chi KN, Shore ND, Armstrong AJ, Flaig TW, Flechon A, Mainwaring P, Fleming M, Hainsworth JD, Hirmand M, Selby B, Seely L, de Bono JS. Increased survival with enzalutamide in prostate cancer after chemotherapy. N Engl J Med 2012;367(13):1187–1197.
22. Lecouvet FE, Lhommel R, Pasoglou V, Larbi A, Jamar F, Tombal B. Novel imaging techniques reshape the landscape in high-risk prostate cancers. Curr Opin Urol 2013;23(4):323–330.
23. Tombal B, Rezazadeh A, Therasse P, Van Cangh PJ, Vande Berg B, Lecouvet FE. Magnetic resonance imaging of the axial skeleton enables objective measurement of tumor response on prostate cancer bone metastases. Prostate 2005;65(2):178–187.
24. Hovels AM, Heesakkers RA, Adang EM, Jager GJ, Strum S, Hoogeveen YL, Severens JL, Barentsz JO. The diagnostic accuracy of CT and MRI in the staging of pelvic lymph nodes in patients with prostate cancer: A meta-analysis. Clin Radiol 2008;63(4):387–395.
25. Budiharto T, Joniau S, Lerut E, Van den Bergh L, Mottaghy F, Deroose CM, Oyen R, Ameye F, Bogaerts K, Haustermans K, Van Poppel H. Prospective evaluation of 11C-choline positron emission tomography/computed tomography and diffusion-weighted magnetic resonance imaging for the nodal staging of prostate cancer with a high risk of lymph node metastases. Eur Urol 2011;60(1):125–130.
26. Venkitaraman R, Cook GJ, Dearnaley DP, Parker CC, Khoo V, Eeles R, Huddart RA, Horwich A, Sohaib SA. Whole-body magnetic resonance imaging in the detection of skeletal metastases in patients with prostate cancer. J Med Imaging Radiat Oncol 2009;53(3):241–247.
27. Mettler FA Jr, Huda W, Yoshizumi TT, Mahesh M. Effective doses in radiology and diagnostic nuclear medicine: A catalog. Radiology 2008;248(1):254–263.
28. Futterer JJ, Engelbrecht MR, Huisman HJ, Jager GJ, Hulsbergen-van De Kaa CA, Witjes JA, Barentsz JO. Staging prostate cancer with dynamic contrast-enhanced endorectal MR imaging prior to radical prostatectomy: Experienced versus less experienced readers. Radiology 2005;237(2):541–549.
29. Bloch BN, Furman-Haran E, Helbich TH, Lenkinski RE, Degani H, Kratzik C, Susani M, Haitel A, Jaromi S, Ngo L, Rofsky NM. Prostate cancer: Accurate determination of extracapsular extension with high-spatial-resolution dynamic contrast-enhanced and T2-weighted MR imaging–initial results. Radiology 2007; 245(1):176–185.
30. Villeirs GM, De Meerleer GO, De Visschere PJ, Fonteyne VH, Verbaeys AC, Oosterlinck W. Combined magnetic resonance imaging and spectroscopy in the assessment of high grade prostate carcinoma in patients with elevated PSA: A single-institution experience of 356 patients. Eur J Radiol 2011; 77(2):340–345.
31. Kim CK, Park BK, Kim B. Diffusion-weighted MRI at 3 T for the evaluation of prostate cancer. Am J Roentgenol 2010;194(6): 1461–1469.
32. Rosenkrantz AB, Oei M, Babb JS, Niver BE, Taouli B. Diffusion-weighted imaging of the abdomen at 3.0 Tesla: Image quality and apparent diffusion coefficient reproducibility compared with 1.5 Tesla. J Magn Reson Imaging 2011;33(1):128–135.
33. Linton KD, Catto JW. Whole-body magnetic resonance imaging and prostate cancer metastases: A new gold standard of detection, but does it help us and at what cost? Eur Urol 2012;62(1):76–77.